

Biomass Estimation in Indonesian Tropical Forests using Active Remote Sensing Systems



Dissertation der Fakultät für Biologie
der Ludwig-Maximilians-Universität München

vorgelegt von
Anna Luisa Berninger

München, 08. Juni 2020

Erstgutachter: Prof. Dr. Florian Siegert

Zweitgutachter: Prof. Dr. Martin Heß

Tag der Abgabe: 08. Juni 2020

Tag der mündlichen Prüfung: 18. November 2020

ACKNOWLEDGEMENTS

I would like to thank Prof. Dr. Florian Siegert for giving me the opportunity to realize the dissertation at hand at the Remote Sensing Solutions GmbH, Munich. As my supervisor, he supported me and provided helpful ideas and thoughts to my work. Thank you for the opportunity to take part in summer schools and field trips that have been very helpful for my thesis and my personal development.

I thank Prof. Dr. Christiane Schmullius very much for awakening my interest in radar remote sensing, for her belief in my work and me and for motivating me to graduate. I am thankful that Prof. Schmullius agreed on being the second referee of my thesis.

I also thank Prof. Dr. Haszprunar for being part of my TAC and proof-reading my papers and thesis.

Furthermore, I would like to express my gratitude to my colleagues and former colleagues Sandra, Jonas, Liz, Natalie, Kim, Isabel, Werner, Claudius, Maxi and Yannic for being always helpful and supportive. Thank you all for being the best team over the last years. Especially, I would like to thank Sandra and Liz, who were always helpful with proof-reading, answering all questions about scientific topics as well as non-scientific topics. They motivated and emboldened me during all parts of my thesis, the good and the bad ones.

This dissertation would not have been possible without my family and friends. I want to thank my family for believing in me and supporting me during all the years of my studies. Thank you to all my friends, who accompanied me during my doctoral studies. I am glad to call you my friends. Very special thanks to my boyfriend Axel for his support, motivation and never-ending love. I want to express my great gratitude for his help and patience.

"Nobody said it was easy" (Coldplay – The Scientist)

ABSTRACT

Substantial terrestrial carbon (C) reservoirs on Earth are formed by soil and living vegetation as well as dead plant litter. Carbon dioxide (CO₂) emissions resulting from the conversion of forests into agricultural land and the burning of vegetation are estimated to account for up to 15 % of annual global CO₂ emissions. However, these estimates are currently still highly speculative and show a wide range in the literature. Neither accurate quantifications of the carbon stock stored in the vegetation and soils, nor the resulting emissions through deforestation and fire are available to provide reliable data for global climate models. By accumulating dead plant debris over thousands of years, peat soils form gigantic carbon sinks storing about 1,200 – 2,000 gigatons (Gt) C. Global peatlands are known for being one of the largest terrestrial long-term carbon sinks in relation to their total area. It is estimated that they store carbon in the range of 180 – 700 Gt worldwide, covering only 3 % of the Earth's terrestrial surface. Besides, it is assumed that the carbon stock of living vegetation is between 400 – 800 Gt C.

In particular, tropical rainforest ecosystems, one of the most species-rich habitats on Earth, serve as significant carbon reservoirs. Its vegetation is assumed to store carbon in a range of 200 – 475 Gt. Furthermore, the tropical peatlands act as relevant carbon sinks with an estimated total amount of 80 – 90 Gt C. The world's largest peat areas are located South East Asia, with Indonesia extending over an area of approximately 210,000 km², which accounts for 47 % of the earth's tropical peatland area. Scientists assume that Indonesian peatlands alone hold quantities of 14 – 58 Gt C. Furthermore, Indonesian rainforests are estimated to have a carbon stock ranging from 6 – 40 Gt.

Global population growth, oil palm plantation business, and unsustainable usage of tropical forests increasingly lead to a release of the stored carbon. Deforestation and degradation conducted for selling timber, but also for gaining agricultural land, does not only release considerable quantities of greenhouse gas. Additionally, these interventions encourage further damage: peat domes are disturbed by the loss of vegetation growing on top, and the construction of drainage channels permanently dries out the generally moist soil. These weakened and drained carbon-rich ecosystems are now vulnerable to fire, which is used by the Indonesian population and the timber or oil palm industry to clear forested areas. Consequently the carbon previously retained in the soil is released and contributes to climate change as CO₂. Besides anthropogenic influences, extreme events such as El Niño droughts (1997/1998, 2002/2003, 2006, 2015/2016 and 2019) affect the attenuated ecosystem immensely. Fires spread more rapidly due to the dry and carbon-rich soil, leading to additional loss of forest and peat. Recurrent fires on peatlands have made Indonesia one of the largest emitters of greenhouse gases. As a result, the country

has become a prime target for carbon-related projects, for example REDD+ (Reducing Emissions from Deforestation, forest Degradation, and the role of conservation, sustainable management of forests, and enhancement of forest carbon stocks).

An accurate estimation of the amount of carbon e.g. in the tropical forest or peatlands is complicated and usually achieved by collecting extensive biomass field data. In very large or poorly accessible areas as in tropical forests, however, this is a labor- and time-consuming method. The scientific field of remote sensing has established itself as an economical and fast alternative to large-scale data collection. In tropical regions, which are characterized by a high annual cloud cover, the use of long-wave active remote sensing systems, such as radar, is the first choice. These systems are almost unaffected by clouds and smoke and not dependent on daylight. An additional advantage of active systems is, depending on the wavelength, the radiation's penetration into the vegetation, what enables to gain an insight into the vertical vegetation structure. This allows a more accurate estimation of above-ground biomass (AGB) and, consequently, the carbon content. Nevertheless, field inventory data is essential for calibrating and validating AGB estimations based on remote sensing data.

The main goal of the present thesis was to investigate whether new satellites can be used to estimate the carbon stock in vegetation and peat in carbon-rich Indonesian tropical forest ecosystems more accurately than previous sensors. Furthermore, the insufficient accuracy of current biomass models is to be improved, in order to obtain more accurate and robust input data for carbon and thus climate models.

In the first study, the radar backscatter signals of Sentinel-1 and ALOS PALSAR C- and L-band synthetic aperture radar (SAR) systems of three years (2007, 2009, and 2016) were analyzed. The data were successfully used to robustly model accurate and high-resolution AGB maps of Kalimantan, the Indonesian part of the island Borneo for the first time. A change analysis was carried out to identify areas of forest and thus biomass loss and gain including their uncertainties for a period of ten years. The second study compares the results of the first one to biomass studies in other habitats, which are representative for numerous forest biomes and biomass levels worldwide. As part of a comprehensive international project funded from the European Space Agency (ESA), this work is so far the widest inter-comparison of regional-to-national AGB maps in terms of area, forest types, input datasets, and retrieval methods. In the third study, canopy heights were derived, and AGB was modelled for a smaller area of Kalimantan. In order to test the possibility to overcome the limitation of the saturation effect, a complex Pol-InSAR (polarimetric SAR interferometry) approach based on TerraSAR-X and Radarsat-2 X- and C-band data were used to derive canopy height. Besides the estimation of AGB in

Kalimantan, an analysis of the soil organic carbon content within carbon-rich peatlands in Central Kalimantan was performed using the new and freely available LiDAR satellite ICESat-2 (study four). ICESat-2 terrain height transects were compared with a highly-precise but cost-intensive airborne LiDAR digital terrain model (DTM) and a radar-based WorldDEM DTM. Since the comparison showed a strong correlation between multiple DTM datasets, an interpolation of comprehensive DTMs based on ICESat-2 transects was carried out to model the surface topography of peat domes within the study area. The methodology reflects a cost-effective and robust alternative for deriving the topography of peatlands. Knowing the surface topography of typically curved peat domes allows conclusions to be drawn about the volume of the peat dome and the associated estimation of the stored carbon.

Different remote sensing instruments were investigated and new methods were developed in order to improve current estimations of above-ground biomass and below-ground carbon stocks in tropical forest ecosystems. The results demonstrate that more robust estimations in a higher spatial resolution can be achieved with these new technologies, which can contribute to REDD+ monitoring projects hopefully support the Indonesian government towards a more sustainable development policy.

ZUSAMMENFASSUNG

Die wichtigsten und größten terrestrischen Kohlenstoff (C) -Speicher weltweit werden vom Boden sowie der lebenden Vegetation als auch abgestorbenem Pflanzenstreu gebildet. Die Kohlendioxid- (CO_2) Emissionen die aus der Umwandlung von Wäldern in Agrarflächen sowie der Verbrennung von Vegetation resultieren, tragen bis zu 15 % zu den globalen CO_2 Emissionen bei. Sowohl der Kohlenstoffvorrat, also auch die resultierenden Emissionen sind jedoch noch nicht hinreichend genau bekannt, um verlässliche Daten für globale Klimamodelle bereitzustellen und decken in der Literatur ein breites Spektrum an Angaben zu ihrer Menge ab. So gehen Wissenschaftler davon aus, dass der Kohlenstoffvorrat der lebenden Vegetation zwischen 400 – 800 Gigatonnen (Gt) C liegt. Weitere 1,200 – 2,000 Gt C werden im Boden gebunden. Insbesondere Torfgebiete sind im Verhältnis zu ihrer Gesamtfläche als eine der größten terrestrischen Langzeit-Kohlenstoffsinken bekannt. Nach Schätzungen speichern sie Kohlenstoff in einem Umfang von 180 – 700 Gt weltweit, wobei sie lediglich 3 % der terrestrischen Oberfläche der Erde bedecken.

Insbesondere tropische Ökosysteme dienen aufgrund ihrer dichten Vegetation und der damit einhergehenden hohen Biomasse als signifikante Kohlenstoffspeicher. Jedoch sind auch hier sowohl der Kohlenstoffvorrat, als auch die aus Entwaldung und Degradierung resultierenden Emissionen nicht ausreichend genau bekannt, um zuverlässige Eingangsdaten für globale Klimamodelle zu liefern. Es wird angenommen, dass die Vegetation der Tropenwälder 200 – 475 Gt C speichert. Tropische Torfgebiete fungieren mit einer geschätzten Gesamtmenge von 80 – 90 Gt C als relevante Kohlenstoffsinken. Die größten tropischen Torfgebiete befinden sich dabei in Südost-Asien. Alleine in Indonesien erstrecken sich Torfgebiete über eine Fläche von ca. 207,000 km^2 , was 47 % ihrer weltweiten Fläche ausmacht. Schätzungen zufolge sind allein in indonesischen Torfgebieten 14 – 58 Gt C gebunden. Darüber hinaus wird angenommen, dass die lebende Vegetation der indonesischen Regenwälder einen Kohlenstoffspeicher von 6 – 40 Gt aufweist.

Das globale Bevölkerungswachstum und eine damit einhergehende nicht nachhaltige Nutzung der Tropenwälder führen jedoch zunehmend zu einer Freisetzung des gebundenen Kohlenstoffs. Abholzung zum Zweck des Holzverkaufs, aber auch zur Gewinnung von Agrarflächen für Palmöl Plantagen sowie die Degradierung der Böden setzen nicht nur kurzfristig große Mengen des Treibhausgases CO_2 frei. Zudem begünstigen diese Eingriffe weitere Schäden innerhalb der Ökosysteme. So werden Torfgebiete durch den Verlust der darüber befindlichen Vegetation gestört und der Bau von Entwässerungskanälen trocknet die in der Regel feuchten Böden dauerhaft aus. Diese

geschwächten und trockengelegten Ökosysteme sind nunmehr anfällig für Feuer. Neben den anthropogenen Einflüssen wirken sich auch Extremwetterereignisse wie El Niño Trockenperioden (1997/1998, 2002/2003, 2006, 2015/2016 and 2019) negativ auf die Ökosysteme aus. Brände können sich aufgrund des trockenen und kohlenstoffreichen Bodens rasant ausbreiten, was zu einem zusätzlichen Verlust an Wald und Torf führt. Da Feuer in der Regel von der Bevölkerung und der Palmöl-Industrie genutzt werden, um bewaldete Flächen zu roden, kommt es nicht selten zu erheblichen Bränden. Wiederkehrende Feuer in Torfgebieten machten Indonesien in den letzten Jahrzehnten zu einem der größten Emittenten von Treibhausgasen, was das Land zu einem Hauptziel für kohlenstoffbezogene Projekte wie z.B. REDD+ (Reducing Emissions from Deforestation, forest Degradation, and the role of conservation, sustainable management of forests, and enhancement of forest carbon stocks) werden ließ.

Die Abschätzung des Kohlenstoffgehalts erfolgt in der Regel anhand von Feldmessungen der Biomasse. In sehr großen oder nur schwer zugänglichen Gebieten stellt dies jedoch eine arbeits- und zeitintensive Methode dar. Bis heute gibt es keine genauen Biomasseschätzungen von Wäldern und Torfgebieten in tropischen Regionen wie dem Amazonasraum, dem Kongobecken oder Indonesien. Als wirtschaftliche und zeitsparende Alternative zur großflächigen Datengewinnung hat sich das wissenschaftliche Feld der Fernerkundung etabliert. In tropischen Regionen, die durch eine hohe jährliche Bewölkungsrate geprägt sind, ist der Einsatz von langwelligen aktiven Fernerkundungssystemen wie Radar die geeignetste Methode. Diese Systeme sind aufgrund ihrer systemimmanenten Eigenschaften in der Lage Wolken sowie Rauch, die eine hohe Präsenz in den Tropen haben, zu durchdringen. Darüber hinaus ermöglicht das Eindringen der Strahlung in die Vegetation je nach Wellenlänge einen Einblick in die vertikale Vegetationsstruktur und erlaubt somit eine genauere Abschätzung der oberirdischen Biomasse und einhergehend des Kohlenstoffgehalts. Nichtsdestotrotz werden Feldmessungen benötigt, um die Fernerkundungsdaten zu kalibrieren sowie zu validieren.

Hauptziel der vorliegenden Arbeit ist es zu untersuchen, ob neue Satellitendaten zur besseren sowie robusteren Abschätzung der Kohlenstoffvorräte in Vegetation und Torf in den Ökosystemen der indonesischen Tropenwälder verwendet werden können. Darüber hinaus soll die unzureichende Genauigkeit der derzeitigen Biomasse-Modelle verbessert werden, um akkuratere Eingangsdaten für Kohlenstoff- und Klimamodelle zu generieren.

Das Untersuchungsgebiet befindet sich in Kalimantan, dem indonesischen Teil der Insel Borneo. Dieses Gebiet ist von tropischen Torfsumpfwäldern und Torfgebieten geprägt,

welche aufgrund der stetig wachsenden Nachfrage nach Palmöl seit mehreren Jahrzehnten unter starkem und anhaltendem anthropogenem Einfluss und wirtschaftlichem Druck stehen.

Im Rahmen der ersten Studie dieser Arbeit wurde das Radarrückstreusignal von Sentinel-1 und ALOS PALSAR C- und L-Band Synthetic Aperture Radar (SAR) Systemen erfolgreich eingesetzt, um eine möglichst akkurate, hochauflösende oberirdische Biomassekarte von Kalimantan für drei verschiedene Jahre (2007, 2009, 2016) zu modellieren. Anhand der drei Karten, die für einen Zeitraum von zehn Jahren abgeleitet wurden, konnte zusätzlich eine Veränderungsanalyse durchgeführt werden. Diese ermöglicht die Quantifizierung von Waldflächen- und damit Biomasseverlusten sowie -gewinnen. Die zweite Studie vergleicht die Ergebnisse der ersten mit Biomasseanalysen in anderen Ökosystemen, die für zahlreiche Waldbiome und Biomasseniveaus weltweit repräsentativ sind. Als Teil eines umfassenden internationalen Projekts, das von der Europäischen Weltraumorganisation (ESA) finanziert wurde, ist diese Arbeit der bisher umfangreichste Vergleich von regionalen und nationalen AGB-Karten in Bezug auf Fläche, Waldtypen, Eingabedatensätze und Methoden zur Biomasseabschätzung.

Um die Limitierung der Sättigung der Radarrückstreuintensitäten bezüglich oberirdischer Biomasse zu verbessern, erfolgte im Rahmen einer zweiten Studie die Ableitung der Baumkronenhöhe mit Hilfe des komplexeren Pol-InSAR-Ansatzes (polarimetrische SAR-Interferometrie) auf der Grundlage von hochaufgelösten TerraSAR-X und Radarsat-2 X- und C-Band Daten. Basierend auf der resultierenden Baumkronenhöhe wurde ein AGB-Modellierungsansatz auf Basis der interferometrischen Kohärenz implementiert.

Neben der Abschätzung der oberirdischen Biomasse in Kalimantan erfolgte zudem eine Analyse der Topographie von kohlenstoffreichen Torfgebieten in Zentral-Kalimantan anhand des neuen und frei verfügbaren LiDAR-Satelliten ICESat-2. ICESat-2 Transekte mit Messungen zur Geländehöhe wurden mit einem hochpräzisen, aber kostenintensiven luftgestützten digitalen LiDAR-Geländemodell (Digital Terrain Model, DTM) und einem radargestützten WorldDEM DTM verglichen. Da der Vergleich eine starke Korrelation zwischen den verschiedenen DTM-Datensätzen ergab, konnte eine erfolgreiche Interpolation eines großflächigen DTMs auf der Grundlage von ICESat-2-Transekten durchgeführt werden. Diese Interpolation erlaubt es, die Oberflächentopographie von Torfkuppen innerhalb des Untersuchungsgebiets zu modellieren. Die Ableitung der Oberflächentopographie von typischerweise konvexen Torfkuppen erlaubt Rückschlüsse auf das Volumen der Torfkuppe und die damit verbundene Abschätzung des gespeicherten Kohlenstoffs. Die erstmals vorgestellte Methodik zeigt eine kostengünstige

und robuste Alternative zur Ableitung der Topographie von Torfgebieten und bietet somit ein großes Potential in der Ableitung ihrer Kohlenstoffgehalte.

Verschiedene Fernerkundungsmethoden und -datensätze wurden eingesetzt, um die Abschätzung der oberirdischen und unterirdischen Biomasse in den Tropenwäldern zu verbessern. Die Ergebnisse liefern eine robustere Abschätzung in einer höheren räumlichen Auflösung. Die Ergebnisse können zum einen zu REDD+ Projekten beitragen, helfen zum anderen jedoch auch, die Haltung der indonesischen Regierung zur nachhaltigen Entwicklung des Landes zu verbessern.

LIST OF ORIGINAL ARTICLES

CHAPTER I

Berninger, A., Lohberger, S., Stängel, M. & F. Siegert (2018) SAR-based Estimation of Above-Ground Biomass and Its Changes in Tropical Forests of Kalimantan using L-Band and C-Band. *Remote Sensing*, 10(6), 831-852.

CHAPTER II

Rodríguez-Veiga, P., Quegan, S., Carreiras, J., Persson H.J., Fransson, J.E.S., Hoscilo A., Ziólkowski D., Stereńczak, K., Lohberger S., Stängel, M., **Berninger, A.**, Siegert, F., Avitabile V., Herold, M. Mermoz, S., Bouvet, A., Le Toan, T., Carvalhais N., Santoro, M., Cartus, O., Rauste, Y., Mathieu, R., Asner, G.P., Thiel, C., Pathe, C., Schullius, C., Seifert, F.M., Tansey, K., & H. Balzter (2019) Forest biomass retrieval approaches from Earth Observation in different biomes. *International Journal of Applied Earth Observation and Geoinformation*, 77, 53-68.

CHAPTER III

Berninger, A., Lohberger, S., Zhang, D. & F. Siegert (2019) Forest Height and Above-Ground Biomass retrieval in Tropical Forests Using Multi-Pass X- and C-Band Pol-InSAR Data. *Remote Sensing*, 11(18), 2105-2128.

CHAPTER IV

Berninger, A. & F. Siegert (2020) The potential of ICESat-2 to identify carbon-rich peatlands in Indonesia. *Remote Sensing*. Submitted.

Published after finishing the thesis as: **Berninger, A.** & F. Siegert (2020) The potential of ICESat-2 to identify carbon-rich peatlands in Indonesia. *Remote Sensing*. 12(24), 4175.

CONTRIBUTION OF THE AUTHORS

CHAPTER I

Dr. Sandra Lohberger and Matthias Stängel conceived and designed the experiments. **Anna Berninger** and Matthias Stängel performed the experiments on the remote sensing data and **Anna Berninger** and Dr. Sandra Lohberger analyzed the data. **Anna Berninger**, Dr. Sandra Lohberger and Prof. Dr. Florian Siegert discussed the results and **Anna Berninger** wrote the paper. Prof. Dr. Florian Siegert supervised the project and commented on the manuscript.

CHAPTER II

P. Rodríguez-Veiga drafted the manuscript, and made the overall analysis and interpretation of the data. P. Rodríguez-Veiga and Heiko Balzter made the study conception and design. S. Quegan did the accuracy analysis, supervised the teams, and interpreted the results. Data acquisition, field work, mapping, and accuracy analysis, in each region was performed by the different teams organized as follows: Yucatan peninsula and central Mexico (P. Rodríguez-Veiga, K. Tansey, and H. Balzter), Eastern South Africa (S. Mermoz, A. Bouvet, T. Le Toan, R. Mathieu, and G. P. Asner), Sweden (H. J. Persson, and J.E.S. Fransson), Poland (A. Hoscilo, D. Ziólkowski, and K. Stereńczak), and Kalimantan (S. Lohberger, M. Stängel, **Anna Berninger**, and F. Siegert). V. Avitabile and M. Herold provided support for the teams on standardized definitions, and characterization of the uncertainties. C. Thiel, C. Pathe, and C. Schullius were responsible for the overall coordination of the project. Moreover, C. Pathe assisted in SAR data acquisition and pre-processing. S. Quegan, H. Balzter, C. Schullius, and F. M. Seifert supervised the project, and provided science advice on the work of the regional teams. All authors discussed the results, provided critical feedback, and helped shape the research, analysis and manuscript.

CHAPTER III

Dr. Sandra Lohberger and **Anna Berninger** conceived, designed and performed the experiments on Pol-InSAR data. **Anna Berninger** preprocessed the data. Devin Zhang supported the Pol-InSAR processing and implemented the RVoG and RMoG models. **Anna Berninger** analyzed the data. **Anna Berninger**, Dr. Sandra Lohberger and Prof.

Dr. Florian Siegert discussed the results. **Anna Berninger** wrote the paper. Dr. Sandra Lohberger and Prof. Dr. Florian Siegert supervised the project and commented on the manuscript.

CHAPTER IV

Anna Berninger and Prof. Dr. Florian Siegert conceived and designed the experiments and analyses. **Anna Berninger** collected, processed and analyzed the data. **Anna Berninger** wrote the manuscript. Prof. Dr. Florian Siegert supervised the project and commented on the manuscript.

I hereby confirm the above statements.

Munich, 29 May 2020

Anna Luisa Berninger

Prof. Dr. Florian Siegert

TABLE OF CONTENTS

ACKNOWLEDGEMENTS i

ABSTRACT..... iii

ZUSAMMENFASSUNG vii

LIST OF ORIGINAL ARTICLES xi

CONTRIBUTION OF THE AUTHORS..... xii

TABLE OF CONTENTS..... xv

LIST OF FIGURES xvii

LIST OF TABLES..... xix

LIST OF ACRONYMS xxi

I. Introduction 1

 1. Climate change and carbon dioxide..... 1

 2. Tropical forest ecosystems of Indonesia in the carbon context 3

 2.1. Tropical peatlands..... 3

 2.2. Tropical forests 7

 3. Forest carbon stock monitoring 9

 4. Basics of Remote Sensing..... 10

 4.1. Passive systems..... 12

 4.2. Active systems 14

 4.2.1. Radar (radio detection and ranging) 14

 4.2.2. LiDAR (light detection and ranging)..... 18

 5. Remote sensing for biomass monitoring 18

 5.1. Passive Systems 19

 5.2. Active Systems 20

 5.2.1. Radar 20

 5.2.2. LiDAR 23

 6. Modeling approaches..... 26

 6.1. Canopy height modeling algorithms 26

 6.2. Biomass modeling algorithms 27

 6.3. Peat surface interpolation..... 28

 7. Sources of uncertainty in biomass estimations 29

 8. Objectives and structure of the thesis 30

TABLE OF CONTENTS

II. Biomass estimation in tropical forests using the backscatter approach in Indonesia (Chapter I)	35
III. Biomass estimation in tropical forests using the backscatter approach in different biomes (Chapter II)	59
IV. Biomass estimation in tropical forests based on Pol-InSAR data (Chapter III)	76
V. Peat dome surface modeling using space borne LiDAR (Chapter IV)	101
VI. Synthesis	121
1. General discussion.....	121
2. Benefits and constraints	126
3. Future research	127
REFERENCES.....	129
STATEMENT AND DECLARATION OF HONOR.....	155
CURRICULUM VITAE	clvii

LIST OF FIGURES

Figure I-1: Left side: Annual global anthropogenic CO ₂ emissions 1850 – 2011. Right side: Cumulative emissions and their uncertainties 1750 – 2011 (IPCC 2015).	2
Figure I-2: Schematic overview of the formation of a peat dome in Indonesia. A) Dead plant material accumulates in a water-filled depression that lacks oxygen. B) The accumulation rate is about 1 – 2 mm/y. After thousands of years an up-to a several meters thick convex shaped peat dome is formed. The dome is generally covered by forests such as peat swamp forest (Ballhorn 2012; World Wide Fund for Nature Germany 2009).....	5
Figure I-3: A) Schematic overview of a beginning degradation of a peat dome due to drainage to lower groundwater level (GWL) for new agricultural areas in Indonesia B) The GWL sinks, resulting in carbon emissions from microbiological decomposition. Furthermore, the dry peat is highly susceptibility to fire (Ballhorn 2012; World Wide Fund for Nature Germany 2009).	6
Figure I-4: The electromagnetic spectrum, including wavelength, frequency, and energy (ESA / AOES Medialab 2012).....	11
Figure I-5: Electric (E) and magnetic (H) fields of electromagnetic radiation (Campbell und Wynne 2011).....	11
Figure I-6: Spectral signatures of different land cover types (Eumetrain 2017; Lillesand et al. 2015).....	14
Figure I-7: Schematic overview of the different scattering mechanisms surface scattering, volume scattering and double-bounce, arrows simulate directions of energy (own graphic).	17

LIST OF TABLES

Table I-1: Radar frequencies and wavelengths (European Space Agency 2020).....	16
Table I-2: Main sources of uncertainty for the remote sensing based AGB estimation approach.	30

LIST OF ACRONYMS

3D	Three-dimensional
AGB	Above-ground biomass
ALOS	Advanced Land Observation Satellite
ANN	Artificial neural network
ASAR	Advanced Synthetic Aperture Radar
BGB	Below-ground biomass
C	Carbon
CCI	Climate Change Initiative
CH	Centroid height
CH ₄	Methane
CHM	Canopy height model
CNES	Centre National D'Études Spatiales
CO ₂	Carbon dioxide
CSA	Canadian Space Agency
DBH	Diameter at breast height
DEM	Digital Elevation Model
DLR	Deutsches Zentrum für Luft- und Raumfahrt
DTM	Digital terrain model
dGPS	Differential Global Positioning System
DSM	Digital surface model
ECV	Essential Climate Variable
ENSO	El Niño Southern Oscillation
ENVISAT	Environmental Satellite
ESA	European Space Agency
f-gases	Fluorinated gases
FAO	Food and Agriculture Organization
FIRMS	Fire Information For Resource Management System
GCOS	Global Climate Observing System
GLAS	Geoscience Laser Altimeter System
GLCM	Gray Level Co-occurrence Matrix
GLRM	Gray Level Run-length Matrix
GPS	Global Positioning System
Gt	Giga tons
GWL	Groundwater level
H	Horizontal
ICESat	Ice, Cloud, and land Elevation Satellite
IPCC	Intergovernmental Panel on Climate Change
IW	Interferometric Wide swath
IWCM	Interferometric Water Cloud Model
JAXA	Japan Aerospace Exploration Agency
K-NN	K-Nearest Neighbor
LiDAR	Light Detection and Ranging
MaxEnt	Maximum Entropy
MERIS	Moderate Resolution Imaging Spectrometer
MIR	Mid-wave infrared
MLR	Multivariate linear regression

LIST OF ACRONYMS

MODIS	Moderate Resolution Imaging Spectroradiometer
MRP	Mega Rice Project
NASA	National Aeronautics and Space Administration
NIR	Near-infrared
NOAA	National Oceanic and Atmospheric Administration
NSE	Nash-Sutcliffe Efficiency
PALSAR	Phased Array type L-band Synthetic Aperture Radar
Pol-InSAR	Polarimetric SAR Interferometry
QMCH	Quadratic Mean Canopy Height
R ²	Coefficient of determination
RADAR	Radio Detection and Ranging
REDD	Reducing emissions from deforestation and forest degradation
REDD+	Reducing emissions from deforestation and forest degradation, and the role of conservation, sustainable management of forests, and enhancement of forest carbon stocks
RF	Random Forest
RMoG	Random Motion over Ground
RMSE	Root mean square error
RSE	Residual Standard Error
RVoG	Random Volume over Ground
SAR	Synthetic Aperture Radar
SOC	Soil Organic Carbon
SRTM	Shuttle Radar Topography Mission
SD	Standard deviation
SVM	Support Vector Machine
SVR	Support vector regression
SWIR	Short wave infrared
TIR	Thermal infrared
TRMM	Tropical Rainfall Measuring Mission
UNEP-WCMC	United Nations Environment Programme World Conservation Monitoring Centre
UN	United Nations
USD	United States Dollar
USGS	United States Geological Survey
UV	Ultraviolet
V	Vertical
VIF	Variable Inflation Factor
WCM	Water Cloud Model

I. Introduction

1. Climate change and carbon dioxide

The fact that life was able to develop on our planet as we know it today is partly due to the good climatic conditions on earth. The mild temperatures enable water to appear in its liquid form and provide plants with ideal growing conditions. The optimal climatic conditions are primarily due to the so-called greenhouse effect. This effect ensures that some of the gases the atmosphere contains, the so-called greenhouse gases, absorb thermal radiation. The main components of our atmosphere are nitrogen and oxygen, which together make up 99 % of the atmosphere. However, these elements are not able to absorb infrared radiation. The greenhouse effect is the result of the trace gases water vapor, carbon dioxide (CO₂) and methane (CH₄), which why these elements were termed greenhouse gases (King 2005). Without greenhouse gases, the crucial heat radiation would be reflected into space. The greenhouse effect ensures that the average surface temperature of our planet is 15 °C instead of being -18 °C (King 2005). However, this is a very fragile balance. An increase in the concentration of these greenhouse gases amplifies the greenhouse effect and increases the temperature on our planet. In addition to a rise in global temperature by only a few degrees, global warming has far-reaching effects on the overall climate, and local weather phenomena. The rise in temperature leads to changes in humidity, precipitation rates, solar radiation intensity, wind speed, and evapotranspiration (Hulme 2005). The weather becomes unsteady and entire ecosystems (land and water) change due to changing climatic conditions.

Regarding the climatic history of the earth, climatic fluctuations are regular appearances. Earlier climate changes resulted from small fluctuations in the distance of the earth to the sun or the continuous change in the position of the continental plates and the associated changes in ocean currents (Atwood 2018). A total of eight fluctuation cycles have been identified over the last 750,000 years. Only 12,000 years ago, with the end of the last ice age, the relatively stable climate of our present time began (King 2005). However, these historical climatic changes developed over centuries or even millennia, thus leaving the biosphere enough time to adapt to the changing conditions. In the current climate change, warming and associated changes in the weather are occurring much faster. The main reason for this is considered to be the anthropogenic emissions of recent decades (King

2005). These emissions are dominated by carbon dioxide (CO₂), methane (CH₄), nitrous oxide (N₂O) and fluorinated gases (F-gases) (IPCC 2015).

Figure I-1 shows how significantly CO₂ emissions have increased between 1950 and 2011. According to the IPCC 2015, a cumulative amount of 2040 ± 310 Gt CO₂ was released into the atmosphere between 1750 and 2011. Merely from 1970 to 2011, the emission rates tripled due to the burning of fossil fuels and cement production. In addition, emissions from forestry and other land use increased by about 40 % simultaneously.

In total, 49 Gt of CO₂ and its equivalents (-eq) were emitted in 2010 consisting of 76 % CO₂, 16 % CH₄, 6 % N₂O and 2 % f-gases. 65 % (32 Gt) of the overall emissions for 2010 result from fossil fuel and industrial processes and 11 % (5 Gt) from forestry and other land-use change (IPCC 2015). However, other studies, e. g. van der Werf et al. (2009) discovered high uncertainties in the estimates of deforestation and degradation and preferred to specify a contribution to the total anthropogenic CO₂ emission due to forestry in a range of 6 – 17 %. Combining deforestation and forest degradation with tropical peatland oxidation and fires, this estimate of the contribution of forest and peatland loss amount to approximately 24 % of total the global CO₂ emissions (IPCC 2015).

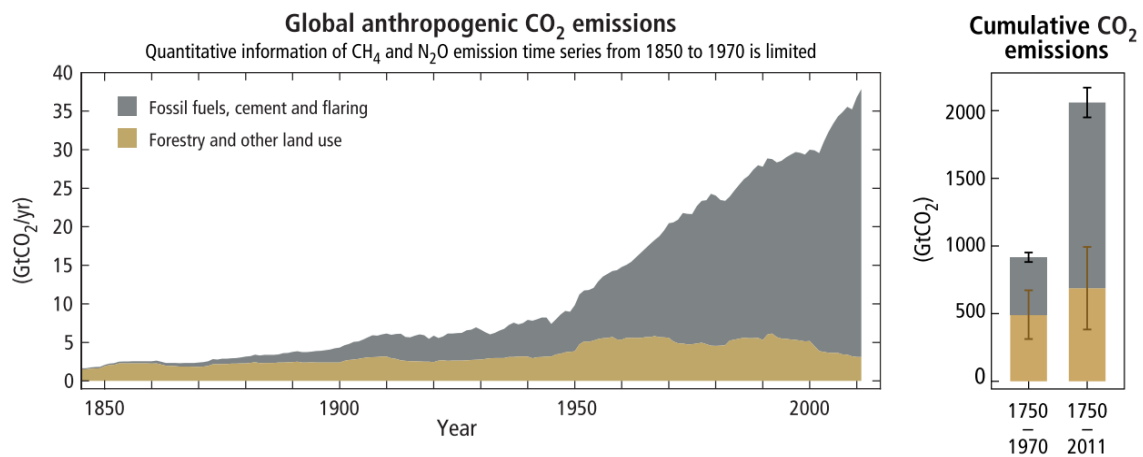


Figure I-1: Left side: Annual global anthropogenic CO₂ emissions 1850 – 2011. Right side: Cumulative emissions and their uncertainties 1750 – 2011 (IPCC 2015).

In 2019, emissions of CO₂ from fossil fuel were reported at 37 Gt (Levin and Lebing 2019; Friedlingstein et al. 2019). The CO₂ emissions from all human activities in 2019,

including forestry and land-use change are estimated between 40 – 46 Gt (Friedlingstein et al. 2019) but are expected to be higher in reality since the emission rate increases annually, even if the increase is diminishing.

From the anthropogenic CO₂ emissions between 1750 and 2011, approximately 40 % (880 ± 35 Gt CO₂) have remained in the atmosphere. The other 60 % were absorbed as carbon (C) by plants, soils and the ocean (IPCC 2015). In order to decrease these high uncertainty ranges, data availability and estimation methods for carbon emissions need to be improved.

2. Tropical forest ecosystems of Indonesia in the carbon context

Tropical ecosystems are among the most carbon-rich ecosystems in the world and are, therefore, an essential element of the global carbon cycle. Indonesia's tropical forests are considered one of the oldest and most species-rich tropical rainforests on earth, storing 6 – 40 Gt C in above-ground biomass (AGB), defined as the living biomass above soil. In addition to the dense vegetation of Indonesian rainforests, underlying tropical peatlands make a vital contribution to terrestrial carbon storage, storing 14 – 58 Gt C (Page et al. 2011; Harrison et al. 2020). An accurate estimation of the amount of C in the forests or soils is complicated and usually achieved by collecting extensive biomass field data. In the following section the characteristics of tropical peatlands and tropical forests are presented.

2.1. Tropical peatlands

Peatland ecosystems are known as the largest terrestrial near-surface long-term carbon sinks, storing 180 – 700 Gt C worldwide while covering no more than 3 % of the earth's surface (Agus et al. 2011; Joosten et al. 2016; Page and Hooijer 2016; Evans et al. 2019; Jurasinski et al. 2020). In comparison to mineral soils, peatlands store 3.5 times more in (sub-)polar, seven times more in boreal and ten times more carbon per ha in tropical regions of the world (Parish et al. 2008). In general, tropical peatlands can be found in the Caribbean, Central America, South America, Southeast Asia and Central Africa, containing an estimated total carbon stock of 80 – 90 Gt (United Nations Environment Programme et al. 2008; Page et al. 2011; Page and Hooijer 2016; Lohberger et al. 2018).

The entire area of tropical peatlands worldwide covers about 441,000 km² of which 248,000 km² and thus 56 % of the world's peatlands, can be found in Southeast Asia (Parish et al. 2008; Page et al. 2011; Jurasinski et al. 2020). The largest peat areas are located in Indonesia, extending over an area of approximately 207,000 km², which account for 83 % of the total peatland area of Southeast Asia and 47 % of worldwide tropical peatland area (Jaenicke et al. 2008; Page et al. 2011; Agus et al. 2011; Baccini et al. 2012; Page and Hooijer 2016).

Peatlands are formed over tens of thousands of years from deposited plant remains, which accumulate in water-filled oxygen-free depressions (Figure I-2) (World Wide Fund for Nature Germany 2009; Warren et al. 2017). Due to the formation being based on organic matter containing 48 – 63 % of carbon, peatlands are one of the largest near-surface storages of terrestrial carbon (IPCC 2015; Joosten et al. 2016). Water prevents the organic substance from reacting with oxygen and thus the decomposition of organic matter by micro-biological processes called oxidation (World Wide Fund for Nature Germany 2009). Two forms of peatlands are distinguished: on the one hand topogenous peat and the other hand ombrogenous peat. Topogenous peatlands were formed from organic matter accumulated in depressions, mainly under the influence of fluctuating water levels of rivers. This type of peat is found near rivers, in floodplains, and flood zones. Ombrogenous peat is formed in low altitudes under the influence of rainfall. This type of peat is the dominant species in Southeast Asia due to the heavy rainfall in the tropics. They are mostly bordered by rivers or the coast (Page et al. 2006).

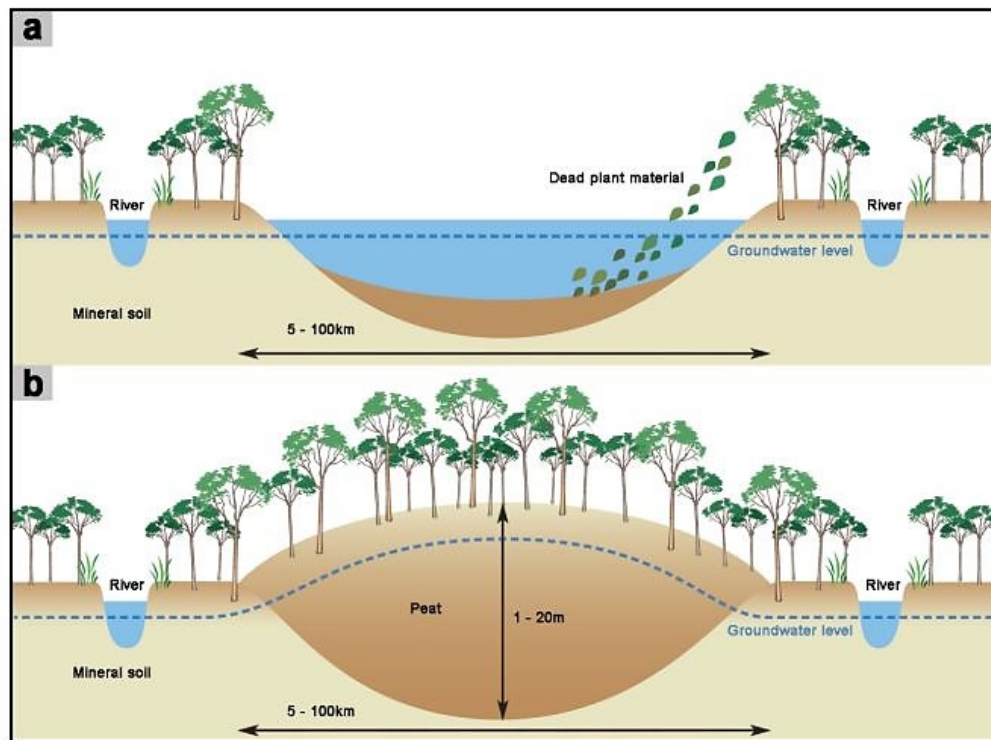


Figure I-2: Schematic overview of the formation of a peat dome in Indonesia. A) Dead plant material accumulates in a water-filled depression that lacks oxygen. B) The accumulation rate is about 1 – 2 mm/y. After thousands of years an up-to a several meters thick convex shaped peat dome is formed. The dome is generally covered by forests such as peat swamp forest (Ballhorn 2012; World Wide Fund for Nature Germany 2009).

Covering about 15 – 21 million ha, Indonesia has the largest area of tropical peatlands (Anshari et al. 2004; Agus et al. 2011; Palamba et al. 2018). The below-ground carbon stock of Indonesia is estimated at approximately 14 – 58 Gt (Agus et al. 2011; Page et al. 2011; Harrison et al. 2020). Indonesian peatlands typically form convex-shaped peat domes up to 20 m thick and up to 100 km wide (Figure I-2) (Agus et al. 2011; Mitchard 2018). Peatlands within Indonesia are covered by evergreen tropical forests which contribute a large amount of organic matter and plant debris to the formation of peatland. The annual accumulation rate is approximately 1 – 2 mm/y in undisturbed peatlands, which is more than twice as much compared to temperate peatlands (0.2 – 1.0 mm/y) or boreal peatlands (0.2 – 0.8 mm/y) (Yule 2010; Ballhorn 2012; Warren et al. 2017). Different peat swamp forest types are an indicator for variations in the pH value, nutrient

and water availability (Page et al. 2006). This can be seen in the number and variety of species.

However, peatlands are under pressure due to anthropogenic influences. In particular, deforestation and drainage to gain land for agricultural use disrupt the hydrological stability of peatlands (Agus et al. 2011; Carlson et al. 2015; Warren et al. 2017). Draining the naturally waterlogged carbon-rich ecosystems leads to peat loss due to oxidation and increases the susceptibility to fire (Figure I-3 (World Wide Fund for Nature Germany 2009; Carlson et al. 2015; Konecny et al. 2016; Palamba et al. 2018)). Since land in Indonesia is traditionally cleared by fire (slash and burn) to make it suitable for oil palms and timber plantations, fires often spread rapidly and erratically on the dried peat soils (Page et al. 2007; Page et al. 2009; Palamba et al. 2018).

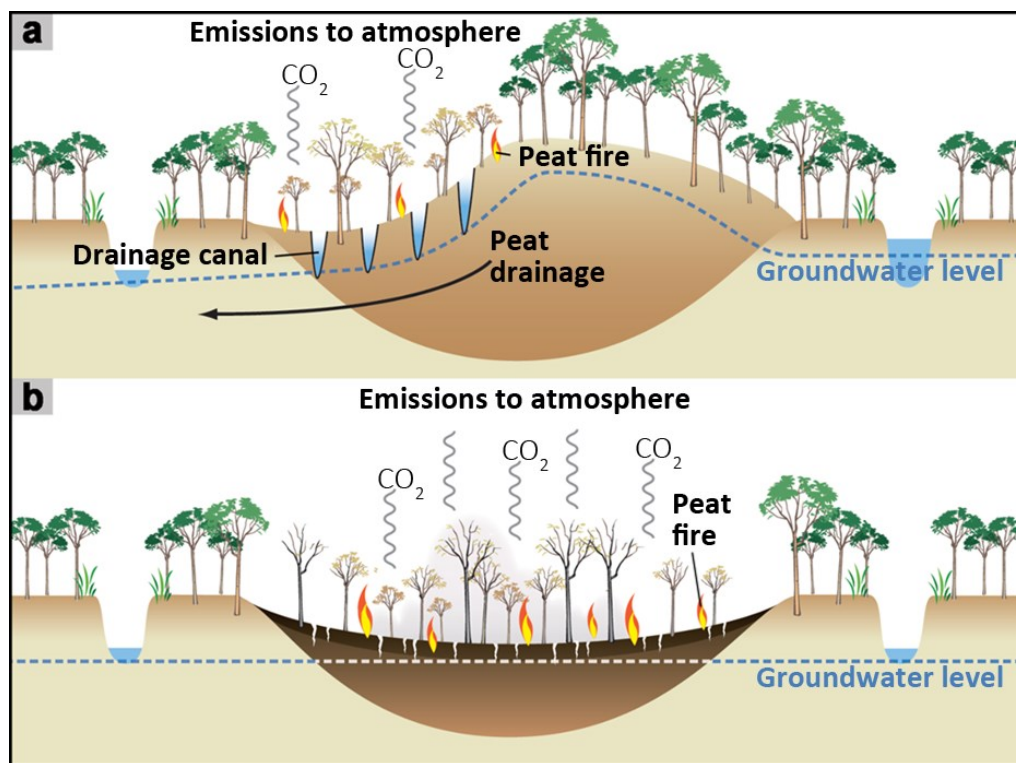


Figure I-3: A) Schematic overview of a beginning degradation of a peat dome due to drainage to lower groundwater level (GWL) for new agricultural areas in Indonesia B) The GWL sinks, resulting in carbon emissions from micro-biological decomposition. Furthermore, the dry peat is highly susceptible to fire (Ballhorn 2012; World Wide Fund for Nature Germany 2009).

Nowadays it is estimated that peatland fires in combination with forest degradation and deforestation contribute 23 % of annual global CO₂ emissions and release of 17 % of anthropogenic greenhouse gases into the atmosphere (van der Werf et al. 2009; Englhart 2012). In the years 2001 – 2010, forest and peat fires released 3.2 Gt CO₂-eq/y into the atmosphere. Furthermore, 0.9 Gt CO₂-eq/y were emitted through peat degradation and drainage (FAO 2013). In the last 20 years, there have been recurrent extreme climate events that have caused large-scale fires in Indonesia and thus a higher carbon release than in other years. There were particularly strong El Niño episodes (1997/1998, 2002/2003, 2006, 2015/2016, 2019) occurring in a higher frequency than previously observed (Ballhorn 2012; Harrison et al. 2016; Setyawati and Suwarsono 2018; Harrison et al. 2020). In 1997/1998, 2.4 – 6.8 million ha of peatlands burned, which released 2.97 – 69.43 Gt CO₂-eq (Agus et al. 2013; Huijnen et al. 2016; Lohberger et al. 2018). In 2015, 4.6 million ha burned, causing emissions of 0.89 – 1.75 Gt CO₂-eq (The World Bank 2015; Huijnen et al. 2016; Lohberger et al. 2018). Due to those strong fires and peat emissions, Indonesia became one of the top five greenhouse gas emitting countries worldwide (Warren et al. 2017).

2.2. Tropical forests

Besides tropical peatland burning, deforestation and degradation contribute further to carbon emissions (van der Werf et al. 2009; IPCC 2015; Mitchard 2018). Forests are one of the most essential carbon sinks since they absorb CO₂ from the atmosphere. It is estimated that tropical forests worldwide store 200 – 300 Gt C (Avitabile et al. 2016; Mitchard 2018). The tropical forests of Indonesia store about 6 – 40 Gt C (FAO 2009; Page et al. 2011; Baccini et al. 2012; Page and Hooijer 2016). Indonesian tropical forests contain different forest ecosystems, mainly dipterocarp forests, freshwater forests, peat swamp forests, heath forests (Kerangas), and along the coast forests dominated by mangroves and *Nypa* palms (MacKinnon et al. 2013; Paoli et al. 2010; Ferraz et al. 2018). The majority of Indonesian carbon emissions stem from the deforestation of peat swamp forests located on waterlogged peatlands and dipterocarp forests on drained mineral soils (Paoli et al. 2010).

Tropical peat swamp forest ecosystems fulfil important ecological and hydrological functions such as protection against seawater intrusion, water retention, and flood

reduction, but they also host endemic species (Parish et al. 2008; Mitchard 2018). The predominant vegetation of Indonesian lowland peat swamp forests are trees with buttress or stilt roots (Posa et al. 2011). These roots allow for good stability on the water-saturated peat soils. In addition, the trees have so-called breathing roots that protrude above the soil. The dominant tree species are assigned to the family of dipterocarps (Takahashi et al. 2017), mainly "Anacardiaceae, Annonaceae, Burseraceae, Clusiaceae, Dipterocarpaceae, Euphorbiaceae, Lauraceae, Leguminosae, Myristicaceae, Myrtaceae, and Rubiaceae" (Page et al. 2006). Due to differences in water and nutrient availability, but also pH characteristics of soils, the forest structure and composition is influenced (Posa et al. 2011; Harrison et al. 2016). In general, the distribution of plants in the peatlands shows a concentric pattern associated with the increase of the thickness of the peat dome. In the peripheral areas, where the peat is relatively flat, up to 240 different tree species per ha can be counted. In the center of the peat domes, where the deepest and thus wettest peat is found, a significant decline in the number of tree species is found. Usually, 30 – 55 tree species per ha can be found in these peat affluent areas. Furthermore, the trees in this area, the center, are most likely smaller compared to the periphery (Page et al. 2006; Harrison et al. 2020).

In ombrotrophic tropical lowland peatlands, species diversity is generally lower than on mineral soils of adjacent ecosystems. Nevertheless, in ombrotrophic ecosystems, due to the extreme hydrological and chemical conditions, the plants are mostly very specialized and often endemic to these areas (Posa et al. 2011; Yule et al. 2018). Tall peat swamp forest sub-types have the most extensive diversity of trees among peat forests and thus the highest canopy stratification. This ecosystem also hosts the greatest diversity of fauna. In addition to the diversity of flora and fauna, differences in terms of biomass can be identified as well (Page et al. 2006). Dipterocarps can reach a height of 45 – 60 m and are a valuable tree species prone to logging (MacKinnon et al. 2013). Lowland dipterocarp forests are more diverse, have taller trees and a more closed canopy than peat swamp forests.

The AGB in Central Kalimantan, Indonesia, varies from 252 t/ha for low pole forest on peat > 7 m to 314 t/ha for mixed swamp forest on shallow peat. AGB up to 395 – 641 t/ha were measured in mixed swamp forest on peat of 3 – 6 m thickness, but only 85 – 177 t/ha for low pole forests on peat thicker than 9 m in eastern Sumatra (Page et al. 2006; Ferraz

et al. 2018). For lowland primary forests, a mean value of 400 t/ha is assumed, varying depending on the forest type (MacKinnon et al. 2013).

In recent decades there has been a significant decline in tropical forests due to illegal logging, deforestation for agricultural development, but also natural and anthropogenic fires (Harrison et al. 2020). However, deforestation not only results in a loss of this vital carbon sink but also increases the emission of CO₂ through the release of carbon stored in the vegetation and underlying soils (Yule et al. 2018; Harrison et al. 2020).

In total, 200 – 300 Gt C is stored in tropical woody vegetation worldwide (Avitabile et al. 2016; Mitchard 2018). Throughout the years 2000 – 2010, Baccini et al. (2012) estimated a total net emission of 1.0 Gt CO₂/y from tropical deforestation in America, Asia and Africa. Mitchard et al. (2018) quantified the release of carbon and equivalents from tropical deforestation and degradation at 0.5 – 3.5 Gt CO₂-eq/y. Pearson et al. (2017) estimated the emissions due to tropical forest degradation between 2005 – 2010 at around 2.1 Gt CO₂-eq/y. Furthermore, the authors summarized that Indonesia has the most substantial forest degradation emissions of all 74 analyzed developing countries within the tropics (0.3 Gt CO₂-eq/y), making climate protection within the country a priority.

In addition to deforestation, forests are nowadays also threatened by global warming itself (Mitchard 2018). The increase in temperature and the accompanying decrease in precipitation will threaten ecosystems by causing drought for which they are not prepared (King 2005). Ecosystems are also becoming more vulnerable to forest fires and pests, which results in a positive feedback.

3. Forest carbon stock monitoring

The carbon content in plants is usually derived from biomass measurements. In literature, the carbon content of dried biomass is estimated at approximately 50 % (Goetz and Dubayah 2011).

The most accurate method to measure tree biomass is to harvest and dry a tree and weigh it (Klinge et al. 1975). Nevertheless, this method does not allow to calculate biomass without felling the tree and is only suitable for small areas (Lu et al. 2015). However, so gained knowledge about the typical biomass values for specific species can be used as

input in allometric models (Pagel et al. 1991). Within allometric models, biomass is calculated as the function of different in situ measurements such as tree height, diameter at breast height (DBH) and/or wood density (Chave et al. 2005). In tropical forests with a high amount of diversity, allometric models for individual species cannot be implemented without losing accuracy. To overcome this limitation, special allometric models for tropical forests (e. g. moist tropical forests) were invented (Chave et al. 2005) and improved (Chave et al. 2014). However, the collection requires a costly and time-consuming field inventory. Tropical forests are often highly inaccessible due to terrain, vegetation and the lack of road networks which complicates field data acquisitions. Remote sensing presents a solution for collecting biomass data without retrieval on-site. Instead, data can be recorded remotely by aircraft or satellite. This allows data acquisitions with extensive spatial and temporal coverage (Mitchard 2018; Goetz et al. 2009). Nevertheless, in-situ data are necessary to calibrate and validate biomass estimations derived from remote sensing signals.

4. Basics of Remote Sensing

The following section gives an introduction to remote sensing to enable a better understanding of its ability to derive AGB.

All objects in the universe emit electromagnetic radiation, except for objects at absolute zero. Remote sensing sensors record the emitted or reflected electromagnetic radiation from earth surface features (Campbell and Wynne 2011). Electromagnetic radiation can be sub-divided in gamma-ray, x-ray, ultraviolet (UV), visible, infrared, microwaves, and radio waves, which together form the electromagnetic spectrum (Figure I-4).

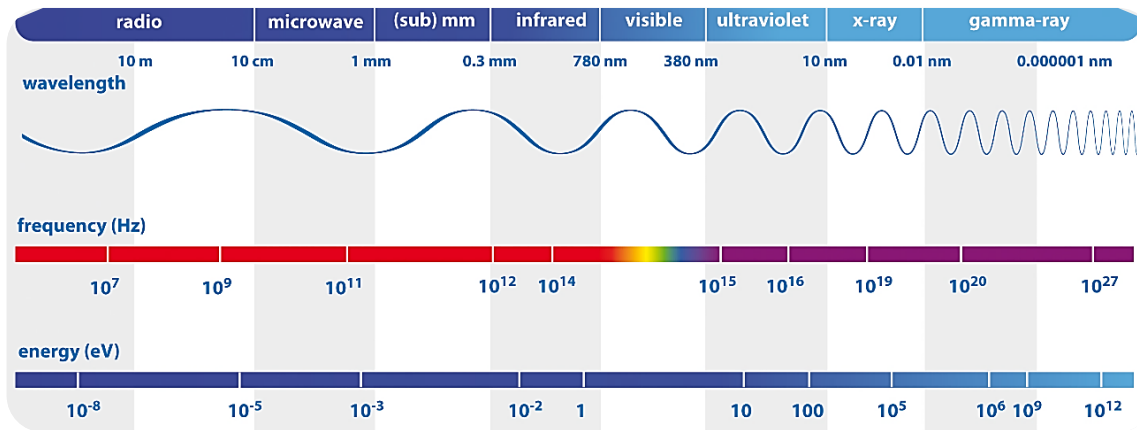


Figure I-4: The electromagnetic spectrum, including wavelength, frequency, and energy (ESA / AOES Medialab 2012).

All parts of the electromagnetic spectrum can be described according to the fundamental wave theory. Electromagnetic radiation consists of an electric field (E) and a magnetic field (H) oriented at right angles and both perpendicular to the axis of dispersion (Campbell and Wynne 2011). A schematic overview of the components of electromagnetic radiation is displayed in Figure I-5.

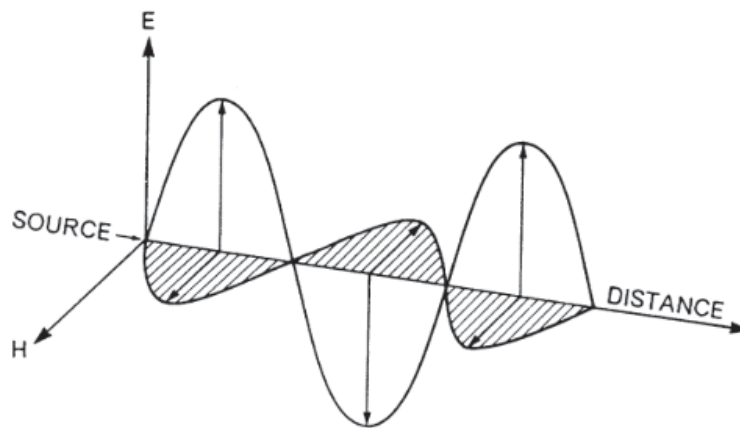


Figure I-5: Electric (E) and magnetic (H) fields of electromagnetic radiation (Campbell and Wynne 2011)

Electromagnetic energy is characterized by the parameters *wavelength*, *frequency*, and *amplitude*. A wavelength (λ) is defined as the distance from one peak to the next and is measured in units of length. The frequency (ν), expressed in hertz (Hz), is the number of waves passing a fixed point per second. The energy level of an electromagnetic wave is

called the amplitude. It is equivalent to the height of each crest, measured as watts per square meter per micrometer ($W * m^2 * \mu m$) (Campbell and Wynne 2011).

Electromagnetic waves travel with the velocity of light (c), a constant of 299,792.458 km/s, expressed by

$$c = \lambda v. \quad (\text{eq. I-1})$$

The relation of frequency and wavelength indicates that frequency and wavelength are inversely proportional, as can be seen also in Figure I-4.

Even if the physical principles are the same, the field of remote sensing distinguishes between active and passive systems. In the following section, the general physics of passive systems is introduced. While different active remote sensing systems and their potential to derive biomass and thus carbon are presented in section I-5.2.

4.1. Passive systems

Passive systems measure the radiation that is reflected or emitted by an object. They are dependent on an external energy source such as the reflected sunlight or thermal infrared signals from fires (Schowengerdt 2007). Passive systems measure wavelength in a range from 0.4 – 14 μm (400 – 14,000 nm), which is the visible (VIS), near-infrared (NIR), mid-infrared (MIR), and thermal infrared (TIR) part of the electromagnetic spectrum (Figure I-4) (Lillesand et al. 2015). The TIR, which is the self-emitted thermal radiation from the earth, is not directly dependent on the sun as an energy source, and, therefore, measurements can be carried out at night (Schowengerdt 2007).

Materials on Earth react differently to the incident radiation because they can reflect, emit, transmit or absorb the sunlight. Reflection refers to the processes that are characterized by a change in the radiation's direction but without absorption or emission of radiation energy. Reflection can be diffuse (diffuse reflectance) or directed (specular reflectance). Absorption, on the other hand, is the intake of part of the energy by an object. In contrast, emission is the radiation of secondary heat radiation and transmission refers to the transit of radiation through an object without any further change in energy (Borengasser et al. 2008). These properties vary depending on material, shape, size, and physical and chemical characteristics, such as the moisture content, of the regarded object. The most important properties that influence reflection are color, structure and surface condition. Since every material on the earth's surface has unique properties in this respect, it is possible to identify the substances by analyzing the spectral signatures in the

same way as a fingerprint (Campbell and Wynne 2011). Figure I-6 displays typical spectral signatures of water, soil, and green (and healthy) vegetation in a spectral range from 500 – 2,500 nm. The figure shows the high separability between the different land cover types using the electromagnetic spectrum. Strong absorption values in the VIS at 490 nm and 650 nm, consequently in the blue and red wavelength range, are typical for vital vegetation (Borengasser et al. 2008; Thenkabail et al. 2012). These features are referred to as chlorophyll absorption bands since the blue and red light is required and absorbed by chloroplasts for photosynthesis. This absorption indicates high chlorophyll a and b contents within healthy leaf cells (Curran et al. 1991). Green light, on the other hand, is reflected by healthy vegetation forming the so-called green peak, a higher reflectance in the green-wave range at 600 nm (Gitelson et al. 1996). Another characteristic feature for green vegetation is the significant increase in range between 680 – 700 nm, referred to as the red edge (Horler et al. 1983). This phenomenon results from the fact that healthy vegetation absorbs red light for photosynthesis, but strongly reflects infrared light at the interfaces of leaf cell walls and intercellular space. Depending on the plant type, reflectance ranges between 30 – 70 % (Borengasser et al. 2008). Furthermore, a decrease of the reflectance in the SWIR (1,300 – 2,500 nm) can be detected in the vegetation signature. The strongest absorption can be identified in the water absorption bands, especially at 1,450 nm and 1,950 nm (Chemura et al. 2017). Water absorption bands originate from the vibrational process of hydrogen bonds (Thenkabail et al. 2012). The spectral signature of vegetation varies according to the vegetation type, which is why it is possible to classify not only vegetation but also different vegetation types.

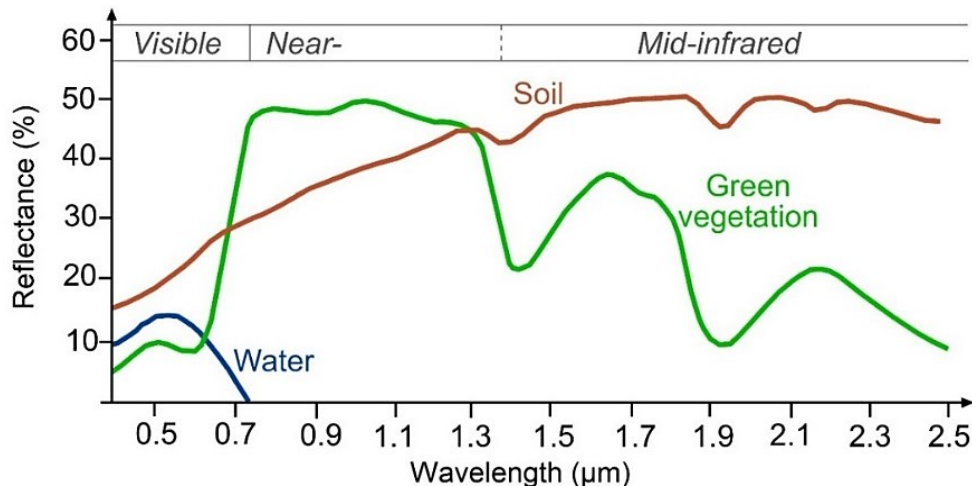


Figure I-6: Spectral signatures of different land cover types (Lillesand et al. 2015; Eumetrain 2017).

4.2. Active systems

Active systems, on the other hand, actively emit energy and detect the energy, which is reflected and backscattered by the objects. This measurement method makes the sensors independent from other energy sources such as the sun-light. In the following section the two active systems radar (radio detection and ranging) and LiDAR (light detection and ranging) are presented and discussed.

4.2.1. Radar (radio detection and ranging)

Synthetic Aperture Radar (SAR) can overcome the limitations of passive remote sensing. It is an active remote sensing technique that transmits microwave pulses at a given frequency to the earth's surface and measures the backscattered energy, which is recorded as magnitude and phase measurements (Campbell and Wynne 2011). Since the system uses its own source of energy, acquisitions can be made independent of the sun at any time of the day. The relatively long wavelengths used by radar (1 mm – 1 m) penetrate through clouds and thus enable imaging under almost all weather conditions (Richards 2009).

A radar system primarily measures time. The antenna sends out pulsed microwaves and detects the time it takes for the echoes to return to the antenna. This measured time determines the accurate distance of the target. Energy is transmitted and received either by one (monostatic) or two (bistatic) antennas (Richards 2009).

The geometrical orientation of the oscillations of a wave is specified by its polarization (Campbell and Wynne 2011). Most radar systems use the simple linear polarization for transmitting and receiving electromagnetic waves. In general, the systems either transmit linear horizontally (H) or linear vertically (V) polarized energy. Since scatterers can change the polarization of the wave, sensors receive both horizontally and vertically polarized energy in different channels of a radar system (Cloude 2010):

- horizontal transmission and horizontal reception = HH
- vertical transmission and vertical reception = VV
- horizontal transmission and vertical reception = HV, and
- vertical transmission and horizontal reception = VH.

HH and VV are called like-polarized or co-polarized since their transmitted and received polarization are identical. With an orthogonal transmitted and received polarization, HV and VH are referred to as cross-polarized (Campbell and Wynne 2011). In general, horizontally polarized waves are more sensitive to objects that are horizontally oriented, and vertically polarized waves are more sensitive to vertically oriented targets. Besides, the cross-polarized waves are influenced more by volume scatterers than the co-polarized waves. However, co-polarization is affected strongly by surface properties such as moisture (Le Toan et al. 1992). Using different polarizations thus allows distinguishing between different land cover types and properties (Campbell and Wynne 2011). Radar systems can be single-polarized, dual-polarized or quad-polarized, depending on the level of polarization used by the sensor. Single-polarized systems are based on one polarization (HH or VV or HV or VH), whereas dual-pol sensors are using two different polarizations as HH and HV or VV and VH. Quad-polarization systems can transmit and receive all four polarizations and thus allow the best separability of land cover classes (Richards 2009).

In addition to different polarizations, SAR systems transmit energy in varying frequencies and wavelengths Figure I-4. The deviation based on bands originates from the military development of radars. Operational radar systems generally use a single band. Table I-1 displays the satellites used during this thesis, their specific band names, wavelength and frequency.

Table I-1: Radar frequencies and wavelengths (European Space Agency 2020).

Band	Frequency [GHz]	Wavelength [cm]	Satellites used in this thesis
P	0.255 – 0.39	133.00 – 76.90	ALOS PALSAR-1 and -2
L	0.39 – 1.55	76.90 – 19.30	
S	1.55 – 4.20	19.30 – 7.10	Sentinel-1, Radarsat-2
C	4.20 – 5.75	7.10 – 5.20	
X	5.75 – 10.90	5.20 – 2.70	TerraSAR-X, Tandem-X
Ku	10.90 – 22.00	2.70 – 1.36	
Ka	22.00 – 36.00	1.36 – 0.83	
Q	36.00 – 46.00	0.83 – 0.65	
V	46.00 – 56.00	0.65 – 0.53	
W	56.00 – 100.00	0.53 – 0.30	

For imaging airborne and space-borne radar remote sensing the most commonly used bands are C-, K-, X-, L- and P-band (Campbell and Wynne 2011). Radar bands and their characteristic wavelength differ in the penetration depth of the signal into the soil or vegetation. Under dry conditions, the penetration depth increases with increasing wavelength. Furthermore, waves are sensitive to objects similar in size to the wavelength. The energy transmitted by the sensor is scattered back from features on the earth's surface. Scattering is defined as the redirection of electromagnetic energy (Campbell and Wynne 2011). Depending on the chemical and physical properties of the target, such as roughness or moisture, radiation is backscattered differently, which influences the received amount of energy backscattered to the sensor. Furthermore, the backscattered signal is influenced by sensor parameters such as the wavelength and the polarization, as mentioned before. The three most common scattering mechanisms are surface scattering, volume scattering and double-bounce as displayed in Figure I-7 (Richards 2009). Surface scattering describes the scattering process where energy is scattered back from an object without interacting with other objects. Depending on the target's roughness, parts of the energy are scattered back to the sensor, where they are measured. The roughness of the surface is relative to the wavelength of the sensor. With increasing wavelength, the surface appears smoother to the sensor (Richards 2009). A very smooth surface behaves similar to a mirror and scatters the radiation away from the sensor. With increasing roughness, more scattered energy reaches the sensor (see Figure I-7). Volume scattering, on the contrary, is influenced by numerous scattering elements. This type of scattering occurs if the radar pulse penetrates a 3D body (Campbell and Wynne 2011). Tree canopies are typical volume scatterers because the energy is scattered between leaves and/or branches.

Double-bounce, or dihedral scattering, occurs when the radar pulse hits two relatively smooth surfaces that are perpendicular to each other. The returned signal is particularly strong since the energy is scattered back into the direction of the sensor (Richards 2009).

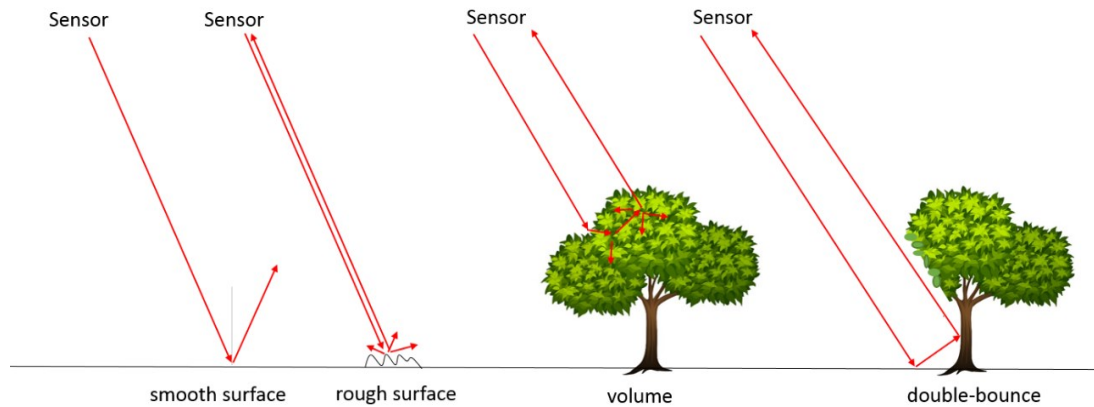


Figure I-7: Schematic overview of the different scattering mechanisms surface scattering, volume scattering and double-bounce, arrows simulate directions of energy (own graphic).

Interferometric SAR (InSAR) refers to the method of correlating two SAR images acquired from slightly different positions of the sensor. Two SAR images can be acquired using either single-pass InSAR (two or more receiving antennas on a platform that collects two images within milliseconds) or repeat-pass InSAR (one receiving antenna that collects two images during two different overpasses of the sensor). The result of correlating the SAR images is called interferogram and consists of two parts, first the coherence, second the phase difference of the backscattered signal (Santoro et al. 2018). Coherence is hereby defined as the amplitude of the complex correlation coefficient between those two SAR acquisitions (Baltzer et al. 2007; Lu et al. 2015). The phase describes the oscillation of an electromagnetic wave, measured as the phase angle.

InSAR can be combined with the so-called polarimetric SAR (PolSAR) approach, during which the SAR imaging process is repeated for all the different polarizations (HH, VV, HV, and VH) and their coherent combination (Cloude 2010; Lavalle and Hensley 2015). The combination of both techniques leads to the complex polarimetric InSAR (Pol-InSAR) technique, which unites the advantages of both SAR techniques and enables the investigation of the structure of volume scatterers, such as forests, based on phase and coherence (Cloude and Papathanassiou 2003; Cloude 2010).

4.2.2. LiDAR (*light detection and ranging*)

LiDAR sensors are active systems that emit pulses of light in the infrared or visible spectrum and measure the time it takes for the pulse to return to the sensor. Depending on the land cover, the pulse can generate one or many returns, for example, in a canopy cover. LiDAR systems can be on board aircrafts or satellites. The area that is illuminated by the sensor is called laser footprint. Its size varies from centimeters (airborne) to several meters (space-borne). The distance between the sensor and the signal reflecting object is defined as the return time (Lillesand et al. 2015). LiDAR can penetrate the tree canopy, enabling the detection of the 3D canopy structure as well as ground information (Lefsky et al. 2002).

LiDAR systems are divided into two recording methods. On the one hand the discrete-return and on the other hand the full-waveform LiDAR systems (Lefsky et al. 2002). The first one uses real-time pulse acquisition of the returned signal. This approach results in a waveform partitioned in discrete time-stamped pulses, from which the individual position of the objects can be derived (Mallet and Bretar 2009). This type of LiDAR system typically only detects the first and last pulses and some intermediate pulses. Therefore, an accurate canopy cover estimation is limited by the small number of echoes (Nie et al. 2017). The newer generation of LiDAR systems, on the other hand, record the entire backscatter energy for equal time intervals (Mallet and Bretar 2009). These so-called full-waveform LiDAR systems enhance the accuracy and resolution of the pulse detection and thus produce more information about the canopy structure. Remote sensing for biomass monitoring

5. Remote sensing for biomass monitoring

The relationships between the biophysical properties of vegetation and remote sensing observations can be used to derive biomass and thus the carbon content (Goetz et al. 2009; Englhart et al. 2011; Goetz and Dubayah 2011; Saatchi et al. 2011; Englhart et al. 2012). Several studies investigated and summarized the derivation of AGB and the carbon content, based on different remote sensing sensors and methods (Goetz et al. 2009; Lu et al. 2015). AGB can be derived by remote sensing in two ways, directly and indirectly (McRoberts et al. 2015). The first method relates the remote sensing data directly to the biomass stock by calibrating it to AGB field measurements using machine learning

algorithms (Goetz et al. 2009; Avitabile et al. 2012). The indirect approach is based on parameters that are first obtained from remote sensing data. These include parameters such as the fraction of forest cover, canopy density or diameter, on the basis of which the biomass is then derived by, e.g. multivariate regressions, K nearest-neighbor, and neural network (Lu 2006; Sousa et al. 2015). The development of robust relationships between forest attributes such as crown height, basal area, DBH, and remote sensing parameters are good examples (Goetz and Dubayah 2011).

5.1. Passive Systems

The wide range of different spatial, spectral, radiometric, and temporal resolutions of optical sensors offers multiple suitable techniques to extract parameters for AGB modeling (Lu 2006; Baccini et al. 2008; Avitabile et al. 2012; Singh et al. 2014).

Via land cover information derived from spectral signatures as described in section I-4.1, indirect estimations of AGB become a possibility. The spectral bands can be used to calculate vegetation indices that minimize solar irradiance and emphasize the vegetation signal (Foody et al. 2003; Sousa et al. 2015; Li et al. 2020). Within this approach, known values for individual land cover types and their density can be used to map different types of forests and estimate AGB over a large area (Bourdeau et al. 2008; Steininger 2010; Goetz and Dubayah 2011; Lu et al. 2015). In addition, the subpixel-based variables can be used as input variables for AGB estimation (Huang et al. 2009; Yan et al. 2015). Information within a pixel originates from the combination of several land coverages in that area. Using spectral unmixing techniques like the spectral mixture analysis (SMA), the reconstruction of the individual components of the pixel, based on pure reference signatures is possible. This approach reveals more comprehensive information about a single pixel and improves the AGB estimation using spectral features (Basuki et al. 2012; Lu et al. 2015; Peroni Venancio et al. 2020). Besides spectral properties, image texture properties can be used to derive AGB estimations from optical data (Lu and Batistella 2005; Sarker and Nichol 2011; Lu et al. 2015; Phua et al. 2017). This approach uses the multi-dimensional variance, which is observed for the image under a moving window (Lu et al. 2015). For complex forest structures, these textures provide better results than the sole use of spectral signatures.

The potential and the limits of applying optical remote sensing for deriving biomass have been sufficiently discussed in many studies (Foody et al. 2003; Lu et al. 2005; Lu et al. 2015; Li et al. 2020). A sensitivity to the structure and density of vegetation, and thus AGB, in the visible and near-infrared wavelength range was demonstrated (Avitabile et al. 2012). However, the methodology has not always proven to be robust for large areas. The spectral variables are influenced by external factors such as soil moisture, vegetation phenology and the atmosphere (Lu et al. 2015). This is often due to the fairly long repetition time of the satellite acquisitions (mostly days to weeks), compared to the rapid changes in weather and surface conditions (Goetz et al. 2009).

Moreover, due to the relatively short wavelengths in which passive sensors record, the sensors are limited in high biomass ranges because the satellite signal is saturated (Lu et al. 2015). The point of saturation primarily depends on the forest density and partly on the forest structure, but also the quality of the reference and remote sensing data (Ghasemi et al. 2011). Scientific literature reports a saturation level for biomass values of 80 – 200 t/ha for optical sensors such as Landsat and Sentinel-2, depending on the forest cover types (Li et al. 2010; Avitabile et al. 2012; Zhao et al. 2016; Pandit et al. 2018; Li et al. 2020). This saturation results in AGB underestimations especially in dense forests such as tropical forests (Lu et al. 2015).

Besides the limitation of the optical satellite signal in dense tropical forests, a central issue in the humid tropical regions is the omnipresent cloud cover (Asner 2010). To overcome these limitations, the thesis at hand is focused on active remote sensing systems.

5.2. Active Systems

5.2.1. Radar

SAR data is often used for AGB estimations since the systems are weather and day light independent. Especially the issue of substantial cloud cover in humid tropical regions can be overcome by SAR systems. Furthermore, and even more importantly, SAR can penetrate vegetation and is sensitive to the water content of vegetation and other objects (Koch 2010; Lu et al. 2015). There are generally three different methods when using SAR for biomass estimations: the backscatter approach, coherence approach and phase-based approach (Baltzer et al. 2007; Koch 2010; Ghasemi et al. 2011; Lu et al. 2015).

a. AGB estimation based on backscatter amplitudes

The relationship of backscatter and AGB has been discussed in several studies so far (Le Toan et al. 1992; Beaudoin et al. 1994; Saatchi et al. 2007; Sandberg et al. 2011; Sandberg et al. 2014; Joshi et al. 2015; Yu and Saatchi 2016; Joshi et al. 2017; Urbazaev et al. 2018; Cartus and Santoro 2019). This approach uses the backscatter, which is the energy received by the sensor after transmission and relates it to reference AGB measurements. The total backscatter from forest areas is composed of a combination of different scattering mechanisms, while the main component results from volume scattering tree canopies. However, surface scattering from the ground and double-bounce scattering originating from the ground and tree trunks also contribute to the overall backscattering intensity. Backscatter typically increases with augmented AGB values. Nevertheless, at a certain point the sensitivity of the backscatter stagnates, which is called the biomass saturation level. This level is dependent on the wavelength of the sensor (Sandberg et al. 2011; Joshi et al. 2017). Longer wavelength radar can penetrate the canopy and thus collect more information on the vertical structure. The relatively short X- and C-bands (3 and 5 cm, respectively) are only able to penetrate through leaves that are about the same size as the wavelength of the bands (Ghasemi et al. 2011). However, the energy can be backscattered from branches located in the higher canopy. In contrast, the L-band with a wavelength of up to 30 cm is mainly scattered on trunks and thick branches. The very long wavelength P-band SAR data, can deeply penetrate the canopy and is backscattered by trunks and the ground and is, therefore, more suitable for relatively high AGB contents (Lu et al. 2015). Besides the wavelength, parameters such as the polarization, incidence angle of the system, terrain properties (e.g. roughness and moisture), and the land cover influence the backscattering amplitude and thus the biomass saturation level (Lu et al. 2015). Cross-polarizations, were found to be more suitable for biomass estimations than co-polarized data (Le Toan et al. 1992). Furthermore, more shallow incident angles are affected by weakened scatter contributions due to longer paths through the canopy (Koyama et al. 2019).

Previous studies showed the sensitivity of long-wave L- and P-band data for biomass estimations using backscatter in parametric (e.g. linear regression, multiple linear regression) and non-parametric models such as K-nearest neighbor (K-NN), artificial neural network (ANN), Random Forest, Support Vector Machine (SVM), and Maximum Entropy (MaxEnt) (Ghasemi et al. 2011; Joshi et al. 2015; Urbazaev et al. 2015; Yu and

Saatchi 2016; Thiel and Schmulius 2016; Kumar et al. 2017; Antropov et al. 2017; Urbazaev et al. 2018; Cartus and Santoro 2019). Since, up to now, P-band is only available on aircrafts, only few studies have been conducted, analyzing small areas (Santos et al. 2003; Saatchi et al. 2019; Liao et al. 2019). AGB estimations based on backscatter from the Advanced Land Observing Satellite's Phased Array-type L-band Synthetic Aperture Radar (ALOS PALSAR) has been successfully performed by several authors (Mermoz et al. 2014; Hamdan et al. 2014; Antropov et al. 2017; Urbazaev et al. 2018). Especially in tropical forests, an AGB estimation is often based on L-band SAR to overcome the limitations of backscatter saturation in dense forests (Wijaya 2009; Hamdan et al. 2011; Mitchard et al. 2011; Hamdan et al. 2015; Wijaya et al. 2015; Mermoz and Le Toan 2016; Chaparro et al. 2019; Koyama et al. 2019). For L-band SAR, the biomass saturation level for tropical forests ranges from 50 to 250 t/ha (Hamdan et al. 2011; Enghart et al. 2011; Saatchi et al. 2011; Chaparro et al. 2019). Using backscatter ratios (Foody et al. 1997) and/or texture, measures (Kuplich et al. 2011) were found to improve the AGB estimations.

b. AGB estimation based on coherence and phase

To overcome the limitations of the radar saturation effect, InSAR and Pol-InSAR are well-known techniques for estimating the AGB (Solberg et al. 2017; Ghasemi et al. 2018; Agrawal et al. 2019).

The coherence approach relies on the assumption that interferometric coherence is related to the vertical distribution of the backscattering elements and thus allows an exact localization of the scattering center of an object and the estimation of the canopy height (Ghasemi et al. 2011; Santoro et al. 2018). Based on the canopy height, AGB can be estimated by e.g. applying allometric equations or regression models (Chave et al. 2005; Koch 2010; Mette et al. 2012). Since coherence based models are sensitive to the vertical structure of trees, they are more suitable for AGB estimations than backscatter based models, especially in tropical forests characterized by dense vegetation (Lu et al. 2015; Santoro et al. 2018). Coherence can be applied to linear regression models (Fransson et al. 2010) or machine learning algorithms, such as Random Forest or Maximum Entropy, to estimate the AGB (Wilhelm et al. 2014; Stelmaszczuk-Górska et al. 2016). A combination of backscatter and coherence increases the value at which the saturation effect occurs, as shown in Thiel and Schmulius 2016; Soja et al. 2017. However, the

coherence based models can be limited by external factors such as wind speed, temperature and humidity causing a decorrelation between two InSAR images.

Besides the coherence, the phase difference between two InSAR images is exploited for canopy height estimations (Thiel and Schmullius 2013; Solberg et al. 2017; Santoro et al. 2018; Hosseini et al. 2019). This technique uses interference patterns, referred to as fringes, to model the "topographic height of the scattering phase center" within a target such as the canopy (Papathanassiou and Cloude 2001; Baltzer et al. 2007). For both, the coherence and the phase-based approach, the height of the center relies on parameters such as the density or canopy structure. Furthermore, the sensor characteristics - frequency, incidence angle, and polarization - affect the scattering processes and thus, the location of the scattering center (Koch 2010). Nevertheless, Ghasemi et al. (2018) showed that the application of Pol-InSAR heights for AGB estimations increases the saturation level compared to the backscatter approach for L-band data to a range from 150 to 300 t/ha.

Since the scattering centers derived from InSAR and Pol-InSAR data usually are not located at the top of the canopy or the ground surface but somewhere in between, the canopy height is not directly derived but can be retrieved with ambitious model-based inversion techniques (Liao et al. 2018; Simard and Denbina 2018). The inversion techniques are described in detail in section I-5.

5.2.2. LiDAR

a. Above-ground biomass estimation using LiDAR

This second active remote sensing system cannot measure AGB directly, but it enables the collection of vegetation structure parameters. LiDAR does not only measure the top of the canopy, but can derive the vertical structure and thus a 3D image of the vegetation instead. This allows the determination of attributes such as the crown diameter or the canopy height (Asner et al. 2012b). Since it is well known that AGB strongly correlates with forest height and the canopy structure, LiDAR-derived height metrics and penetration indices are widely used to model AGB (Ioki et al. 2014; Nie et al. 2017; Wan-Mohd-Jaafar et al. 2017; Pereira et al. 2018; Dong et al. 2019; Tian et al. 2019). It has been shown in several studies that LiDAR metrics, such as the mean canopy height

(MCH) or quadratic mean canopy height (QMCH), are sensitive to vertical forest structures (Asner et al. 2012b; Englhart et al. 2013). Since vertical canopy structures are directly related to the AGB, a linear correlation between LiDAR metrics and the AGB can be found (Drake et al. 2003; Jubanski et al. 2013; Meyer et al. 2013; Asner et al. 2018). AGB can be estimated based on LiDAR metrics with statistical modeling or allometric models (Asner et al. 2012b).

Most LiDAR-related studies use airborne measurements to accurately predict the AGB (Asner et al. 2010; Mascaro et al. 2011; Asner et al. 2012a). Ballhorn et al. (2009), Kronseder et al. (2012), and Englhart et al. (2013) estimated AGB from in-situ data and airborne LiDAR measurements in moist tropical forests in Indonesia. Although airborne sensors provide highly accurate biomass estimates, the high costs involved usually limit their application to small areas or transects (Avitabile et al. 2012; Asner et al. 2012a; Asner et al. 2012b; Ellis et al. 2016; Levick et al. 2016; Asner et al. 2018; Dong et al. 2019). Nevertheless, AGB estimations derived from airborne LiDAR data in combination with field inventory data can be used as an accurate reference data for satellite-based AGB modeling (Asner et al. 2012b; Englhart et al. 2013). The accuracy is thereby dependent on the sensor system (airborne or space-borne, photon-counting, full-waveform or discrete-return LiDAR), the forest type and density but also the field inventory plot size (Frazer et al. 2011).

As a cost-effective alternative for large areas, the full-waveform sensor of the Geoscience Laser Altimeter System (GLAS) on board the Ice, Cloud and Elevation Satellite (ICESat) (2003 – 2010) has already been proven to be valuable for biomass and crown height estimations (Lefsky et al. 2005; Harding and Carabajal 2005; Carabajal and Harding 2006; Baccini et al. 2008; Bourdeau et al. 2008; Lefsky 2010; Chi et al. 2017).

With the launch of the follow-up mission, ICESat-2, in September 2018 carrying the Advanced Topographic Laser Altimeter System (ATLAS), an improvement of previous estimations is possible due to higher data availability and spatial resolution. ATLAS is a photon-counting LiDAR that detects sensitivities at the photon level. The sensor works at the wavelength of green light (532 nm) and a pulse repetition rate of 10 kHz (Neuenschwander and Pitts 2019b). This significantly higher repetition rate compared to GLAS enables a higher resolution in along-track direction. Furthermore, ATLAS uses six beams arranged in three single pairs, separated by 90 m in across-track direction, containing a low-energy and a high-energy beam. This constellation enables the detection

of surfaces with low and high reflectivity (Neuenschwander and Pitts 2019b). The nominal diameter footprint for each beam is about 17 m (Neuenschwander and Pitts 2019b). Within the ICESat-2 product, photons collected by ATLAS are classified as terrain or canopy. All derived terrain and canopy height values are then defined as absolute heights above the WGS84 ellipsoid (Neuenschwander and Pitts 2019a).

Narine et al. (2019) were the first to test a simulated ICESat-2 canopy product in combination with optical data from Landsat for mapping AGB in Texas, US. The results showed potential for biomass estimations, reaching an R^2 of 0.51. Since the analysis is based on simulated data, there is still the possibility that real data would lead to model improvements. Liu et al. (2020) investigated the suitability of ATLAS in combination with optical data from Landsat 8 and Sentinel-2 canopy height data for mapping burned areas in California and New Mexico, obtaining an R^2 of 0.61 with a moderate correlation ($r = 0.78$).

It can be concluded that aircraft data provides an excellent spatial resolution but cannot cost- and time-effectively survey large areas on a continental or even global scale. The use of satellite-based data allows cheaper and more comprehensive long-term data acquisitions but at costs of the spatial resolution (Goetz et al. 2009). A combination of these acquisition methods enables the coverage of large areas with a high accuracy and an excellent spatial resolution.

In general, LiDAR can overcome the saturation limitations of optical and radar data, but the limited availability of LiDAR data and the restricted spatial resolution prevents its comprehensive application (Lu et al. 2015). Nevertheless, LiDAR offers accurate calibration and validation data for large-scale AGB mapping using radar.

In this thesis, AGB reference data, which were extrapolated by relating field data to airborne laser scanning (ALS) point cloud signals, were used. This AGB reference data cover all ranges of AGB, from shrubs to tropical rainforests and presents a highly accurate AGB reference.

b. Below-ground biomass estimation using LiDAR

Besides the estimation of AGB based on space-borne LiDAR data, Ballhorn et al. (2011) used ICESat measurements to identify the topography of carbon-rich peatlands in Indonesia successfully. This indirect approach for below-ground carbon content modeling identifies convex-shaped peat domes beneath the forest vegetation with airborne and

space-borne LiDAR instruments. Jeanicke et al. (2008) identified a strong correlation between the convex peat dome surface derived from a digital terrain model (DTM) and the thickness of the dome-shaped peat layer. An estimation of the carbon stock became possible after modeling the 3D peat layer (Jaenicke et al. 2008). Measurements with airborne LiDAR result in more accurate estimates due to the higher spatial resolution for the surface 3D models. However, this technology is extremely costly for large areas. A satellite-based approach allows screening the whole country. The launch of ICESat-2 presents new possibilities to model carbon-rich peatlands and are analyzed in the fourth paper included in this thesis.

Resulting biomass and carbon local, nationwide or even global maps, derived from remote sensing signals, support forest monitoring or risk managing systems under REDD+ (Reducing Emissions from Deforestation, forest Degradation, and the role of conservation, sustainable management of forests, and enhancement of forest carbon stocks) and other programs and policymakers, protecting forests and analyzing carbon release.

6. Modeling approaches

6.1. Canopy height modeling algorithms

Canopy height is the most crucial single forest variable to model AGB, e.g. by applying allometric equations or regression models (Koch 2010; Chave et al. 2005; Mette et al. 2012). Based on InSAR and Pol-InSAR data, the canopy height can be derived. However, the canopy height cannot directly be measured by InSAR or Pol-InSAR, but can be derived with ambitious model-based inversion techniques. A frequently used model based on coherence is the Interferometric Water Cloud Model (IWCM) developed by Attema and Ulaby (Attema and Ulaby 1978; Soja et al. 2015; Soja et al. 2017; Askne et al. 2017; Santoro et al. 2018; Agrawal et al. 2019). This model exploits the total coherence of a forest and divides it into the individual coherence sums of soil and canopy cover (Lu et al. 2015; Santoro et al. 2018). Cloude and Papathanassiou (2008) presented a new algorithm for quantifying variations in vertical structures based on a new 3D radar imaging technique called polarization coherence tomography (PCT). PCT reconstructs vertical profiles based on measurements of volume height and topographic phase.

Different parameters are defined to characterize an average vertical distribution profile of relative reflectivity with SAR data (Luo et al. 2011; Li et al. 2015; Zhang et al. 2018). Additionally, the coherence based Random Volume over Ground model (RVoG) was successfully applied in multiple studies for estimating canopy heights as it interprets interferometric coherence as a function of vertical backscatter profiles (Papathanassiou and Cloude 2001; Cloude and Papathanassiou 2003; Lavalley et al. 2012; Sun and Song 2015; Olesk et al. 2016; Sportouche et al. 2018; Babu and Kumar 2018; Aghabalaei et al. 2020). Different studies have applied the RVoG model to various forest ecosystems and frequencies, showing that the results are partly dependent on forest density (Garestier et al. 2008; Neumann et al. 2010; Schlund et al. 2014; Chen et al. 2016). Using repeat-pass InSAR data, the RVoG model can be affected by temporal decorrelation. To compensate for errors due to temporal decorrelation and improve the AGB estimation, a model combining the RVoG with a Gaussian-statistic motion model of canopy elements was formulated in 2015 (Lavalley and Hensley 2015). This model is termed Random Motion over Ground (RMoG) model and considers volumetric and temporal decorrelation effects resulting from random motion. Up to date only a few studies have been conducted using the novel RMoG model (Zhang et al. 2017; Jung et al. 2018; Ghasemi et al. 2018; Qi Z. et al. 2019).

6.2. Biomass modeling algorithms

For biomass estimations from remote sensing signals, several types of models such as parametric and non-parametric algorithms can be applied (Lu et al. 2015). Parametric algorithms are models based on the relationship between dependent and independent variables and specified by parameters, as found in linear and multiple linear regression models.

Regression-based models are the most common parametric algorithm for AGB estimations using remote sensing data (Le Toan et al. 1992; Sandberg et al. 2011; Soja et al. 2013; Sinha et al. 2015; Makinano-Santillan et al. 2019). A simple linear regression assumes a linear relationship between a dependent and an independent variable. The approach can be extended to multiple predictors (multiple linear regression). In this case, the remote sensing derived variables show a strong correlation with AGB but not with each other. However, AGB and remote sensing derived variables are usually non-linear,

which is why the linear regression can be transformed logarithmically to be more suitable. Non-linear models, such as logistic regression models (McRoberts et al. 2013) or power models (Næsset et al. 2011), are commonly applied for estimating AGB from purely remote sensing derived variables (Lu et al. 2015).

The physically-based algorithms Water Cloud Model (WCM) and Interferometric Water Cloud Model (IWCM) are built on linear regression models. These models describe the total SAR signal (backscatter intensity or coherence) over vegetation as the sum of ground- and vegetation-scattering (Attema and Ulaby 1978).

Non-parametric algorithms include models such as K-nearest neighbor (K-NN), support vector machine (SVM), artificial neural network (ANN), Random Forest, and Maximum Entropy (MaxEnt). These algorithms do not predefine the model structure and are more flexible. Nevertheless, non-parametric models are often highly complicated, necessitate longer computing times and a high amount of training data. Furthermore, non-parametric algorithms are known to be prone to overfitting. Within this thesis, parametric models were used to derive biomass estimations from earth observation data. However, an extensive summary of major nonparametric algorithms for biomass estimation modeling can be found in Lu et al. (2015).

6.3. Peat surface interpolation

Several interpolation approaches are known. Inverse Distance Weighting (IDW), Nearest Neighbor (NN), Moving Average (MA), and Kriging are probably the best-known ones (Wojciech 2018). To model peat dome surfaces from ICESat-2 point data, the geostatistical interpolation method Kriging, developed by Matheron (1971) was used. Kriging is often described in literature as the method with the best results for modeling terrain (Barton et al. 1999; Jassim and Altaany 2013; Yilmaz and Uysal 2017; Ferreira et al. 2017). In comparison to other interpolation methods, it can handle irregularly spaced data like ICESat-2 measurements. Another advantage is the possibility to simply use the kriging defaults or to adjust the model manually. The method supplies accuracies associated with each prediction (Ferreira et al. 2017), while it is also the most time-consuming approach with a computational time of eight to 20 times longer than other methods (Jassim and Altaany 2013; Wojciech 2018).

Kriging assumes that the direction and distance between points have a spatial correlation. This spatial correlation is used to explain surface variations. The value of a specific

location is predicted by estimating a weighted average of the known values in the location's neighborhood (Wojciech 2018). As a result, the prediction is more accurate at points that are closer to observations and declines with increasing distance. Kriging is defined as:

$$\hat{Z}(s_0) = \sum_{i=1}^N \lambda_i Z(s_i) \quad (\text{Equation I-2})$$

Where $Z(s_i)$ represents the measured values at position i , λ_i is an unknown weight for the $Z(s_i)$, s_0 defines the prediction location, and N is the number of measurements. The approach is more sensitive to measurements than other interpolation methods such as IDW since its weights are determined by a semi-variogram. Furthermore, it provides unbiased estimates (Oliver and Webster 1990).

7. Sources of uncertainty in biomass estimations

An estimate of biomass and carbon as accurate as possible is necessary to develop strategies for reducing carbon emissions. However, estimates of biomass and carbon contents are highly imprecise, including different uncertainties, covering a wide range of estimation values found in literature.

Uncertainty analyses of a product are performed to understand error sources, reduce uncertainties and to guarantee a robust model. However, an internationally standardized approach for the validation of large scale biomass products is not yet available. Uncertainty can result both from random errors and systematic errors. Multiple studies showed that the relative errors of biomass estimates could vary between 5 % and 30 % (Chave et al. 2003; Saatchi et al. 2007; Mascaro et al. 2011; Lu et al. 2015; Avitabile et al. 2016; Rodríguez-Veiga et al. 2019). The level of error depends on factors such as forest type, topographic features, and spatial resolution of the sensors, as well as the applied models.

For carbon estimations, many sources of uncertainty are accumulated and propagated through a modeling or mapping system. Main sources of errors for AGB and carbon estimations were identified, such as inaccuracies within the field inventory design, the allometric models including conversion coefficients from volume to biomass, incorrect regression models relating variables to AGB, sensor errors, atmospheric conditions, and slope. Besides, the spatial accuracy can influence the result of biomass estimations,

mainly due to inappropriate geometric corrections, different spatial resolutions, sample plot locations, shape and size. The temporal difference between acquisitions can furthermore cause inaccuracies, for example, during the model calibration process (Lu et al. 2015). An overview of the sources of uncertainty for earth observation based AGB estimations are displayed in Table I-2.

Table I-2: Main sources of uncertainty for the remote sensing based AGB estimation approach.

Error source	Explanation
In-situ data	<ul style="list-style-type: none"> • Measurement errors while collecting field inventory data • Allometric model prediction uncertainty • Sampling errors due to incomplete representativeness of the biomass range, plot size or plot shape • Geolocation errors on the plot scale
Remote sensing data	<ul style="list-style-type: none"> • Sensor errors (radiometric stability, noise, scanner motions) • Geolocation errors on pixel scale • Spectral errors (due to atmosphere) • Errors due to steep terrain (slope)
Spatial mismatch	<ul style="list-style-type: none"> • Inaccuracies due to alignment and sizes of field plots and remote sensing map units
Temporal mismatch	<ul style="list-style-type: none"> • Inaccuracies due to temporal discrepancies between used datasets (deforestation, degradation, regrowth)
Model errors	<ul style="list-style-type: none"> • Prediction errors of the models applied to transform remote sensing signals in AGB

Providing uncertainty quantifications at pixel level, taking the sources of uncertainties mentioned above into account, helps users understand errors and increases the product's acceptance within the international community. Furthermore, the models can be improved based on the accuracy assessment.

8. Objectives and structure of the thesis

In the context of climate change, monitoring carbon sources is essential. Indonesia contains enormous carbon sinks in the form of tropical forests and underground peatlands. However, the unsustainable management of these ecosystems has led to Indonesia,

especially the regions Kalimantan and Sumatra, becoming one of the largest carbon emitters in the world. Because many areas in Indonesia are still remote and difficult to access, the derivation of biomass values using remote sensing is the only way to monitor carbon sinks and sources reliably. Since optical remote sensing methods in the tropics are limited by the constant cloud cover, but also because the short wavelengths cannot penetrate the dense vegetation, it is necessary to use active remote sensing to derive biomass estimates.

The main goals of this thesis are first the improvement of available AGB estimations, including a lower uncertainty to make more accurate information about carbon storage in moist tropical forests of Indonesia accessible. Second, the realization of a more accurate peatland identification from space in Indonesia, since peatlands are insufficiently well-known and located to date. These goals can be sub-divided in the tasks for the different studies:

A. Above-ground biomass (AGB)

- 1) The robust mapping of high-resolution AGB for extensive areas and reduced uncertainties
 - Improvement of the spatial resolution of existing biomass maps enables the identification of small-scale biomass variability and changes.
- 2) Examination of the potential to overcome the saturation limitations for biomass modeling based on backscatter values with the Pol-InSAR approach, and to provide high-resolution AGB maps of tropical forests
 - Increasing the threshold at which saturation occurs facilitates the AGB estimations in tropical forests containing high biomass values.

B. Below-ground biomass

Testing the possibility of identifying comprehensive carbon-rich ombrogenous peat domes in Indonesia using up to date satellite LiDAR DTM measurements

- Knowledge about the peat dome topography allows the calculation of peat volume and thus, the carbon content of peat domes

This thesis is divided into four chapters based on stand-alone publications. In the context of this thesis, different radar satellite instruments were used in order to analyze their suitability for modeling accurate AGB in Kalimantan, Indonesia.

The first study (Chapter I) is about AGB modeling based on L-band radar data of the ALOS PALSAR satellite of the Japan Aerospace Exploration Agency (JAXA) and its follow up mission ALOS-2. ALOS PALSAR and ALOS-2 PALSAR-2 mosaics with a spatial resolution of 25 m were used to model biomass of tropical forests in Indonesia using backscatter values, polarization ratios and textures for the years 2007, 2009, and 2015. In combination with L-band data, Sentinel-1a and b C-band radar, launched within the Copernicus program by the ESA in 2014 and 2016, respectively, were used for the modeling period of 2015.

Chapter II compares the results of Chapter I to biomass studies in other habitats, which are representative of numerous forest biomes and biomass levels worldwide. As part of a comprehensive international project funded by the European Space Agency (ESA), this work is the so far most expansive inter-comparison of regional-to-national AGB maps in terms of area, forest types, input datasets, and retrieval methods.

In Chapter III, TerraSAR-X (TS-X) and Radarsat-2 (RS-2) single-look complex (SLC) imageries were used to model the canopy heights of tropical forests in Kalimantan, Indonesia, based on Pol-InSAR. The RS-2 SAR satellite operates a C-band with a wavelength of 5.6 cm and a frequency of 5.3 GHz and was launched by the Canadian Space Agency (CSA) in 2007. TS-X was launched in June 2007 by the DLR (German Aerospace Center). It provides different acquisition modes with varying spatial resolutions at X-band wavelength (3.1 cm) with a frequency of 9.65 GHz.

The last chapter, Chapter IV, is based on the space-borne sensor ATLAS onboard the ICESat-2 satellite. ICESat-2 was launched in September 2018 by the National Aeronautics and Space Administration (NASA). The sensor is a photon-counting LiDAR, that works at a wavelength of 532 nm (green) and a pulse repetition rate of 10 kHz. Moreover, the sensor can illuminate the ground and detect terrain heights of the earth because it penetrates sparse vegetation. The data is used to create a digital terrain model product made accessible by NASA.

The results of the studies provide input for more precise carbon modeling, as well as risk managing or forest monitoring systems. The analyses contribute to programs protecting

forests and analyzing carbon releases such as (REDD+), "United Nations Environment Programme World Conservation Monitoring Centre" (UNEP-WCMC), the "Global Canopy Programme", and other similar programs national and subnational level.

II. Biomass estimation in tropical forests using the backscatter approach in Indonesia (Chapter I)

Berninger, A., Lohberger, S., Stängel, M. & F. Siegert (2018) SAR-based Estimation of Above-Ground Biomass and Its Changes in Tropical Forests of Kalimantan using L-Band and C-Band. *Remote Sensing*, 10(6), 831-852.



Article

SAR-Based Estimation of Above-Ground Biomass and Its Changes in Tropical Forests of Kalimantan Using L- and C-Band

Anna Berninger ^{1,2,*}, Sandra Lohberger ¹, Matthias Stängel ¹ and Florian Siegert ^{1,2}

¹ Remote Sensing Solutions GmbH, Isarstr. 3, 82065 Baierbrunn, Germany; lohberger@rsgsbmbh.de (S.L.); matthias_staengel@trimble.com (M.S.); siegert@bio.lmu.de (F.S.)

² Department of Biology, Ludwig-Maximilians-University Munich, Großhaderner Str. 2, 82152 Planegg-Martinsried, Germany

* Correspondence: berninger@rsgsbmbh.de; Tel.: +49-89-489-547-65

Received: 6 April 2018; Accepted: 24 May 2018; Published: 25 May 2018



Abstract: Kalimantan poses one of the highest carbon emissions worldwide since its landscape is strongly endangered by deforestation and degradation and, thus, carbon release. The goal of this study is to conduct large-scale monitoring of above-ground biomass (AGB) from space and create more accurate biomass maps of Kalimantan than currently available. AGB was estimated for 2007, 2009, and 2016 in order to give an overview of ongoing forest loss and to estimate changes between the three time steps in a more precise manner. Extensive field inventory and LiDAR data were used as reference AGB. A multivariate linear regression model (MLR) based on backscatter values, ratios, and Haralick textures derived from Sentinel-1 (C-band), ALOS PALSAR (Advanced Land Observing Satellite's Phased Array-type L-band Synthetic Aperture Radar), and ALOS-2 PALSAR-2 polarizations was used to estimate AGB across the country. The selection of the most suitable model parameters was accomplished considering VIF (variable inflation factor), p -value, R^2 , and RMSE (root mean square error). The final AGB maps were validated by calculating bias, RMSE, R^2 , and NSE (Nash-Sutcliffe efficiency). The results show a correlation (R^2) between the reference biomass and the estimated biomass varying from 0.69 in 2016 to 0.77 in 2007, and a model performance (NSE) in a range of 0.70 in 2016 to 0.76 in 2007. Modelling three different years with a consistent method allows a more accurate estimation of the change than using available biomass maps based on different models. All final biomass products have a resolution of 100 m, which is much finer than other existing maps of this region (>500 m). These high-resolution maps enable identification of even small-scaled biomass variability and changes and can be used for more precise carbon modelling, as well as forest monitoring or risk managing systems under REDD+ (Reducing Emissions from Deforestation, forest Degradation, and the role of conservation, sustainable management of forests, and enhancement of forest carbon stocks) and other programs, protecting forests and analyzing carbon release.

Keywords: above-ground biomass; carbon; SAR; backscatter approach; multivariate linear regression modelling; biomass change mapping; Indonesia; tropical deciduous forest

1. Introduction

The Earth's land surface spans approximately 149.4 million km², of which nearly 30% is characterized by forested areas [1]. Tropical forest ecosystems (forests and soils) alone hold about 40% of terrestrial carbon [2,3]. However, due to unsustainable use and deforestation, the stored carbon can be released into the atmosphere as CO₂ (carbon dioxide) and will contribute significantly to global climate change. According to the Intergovernmental Panel on Climate Change (IPCC),

II. Biomass estimation in tropical forests using the backscatter approach in Indonesia (Chapter I)

the resulting greenhouse gas emissions account for approximately 11% of all anthropogenic emissions worldwide [4,5].

The forests of Indonesia are considered to be one of the oldest and most species-rich tropical rainforests on the planet [6]. Indonesia's forests alone store 18.6 Gt of carbon [7]. Additionally, the country has some of the largest known tropical peat reservoirs on Earth, storing 55–58 Gt of carbon in belowground peatlands [8,9]. At the same time the deforestation and degradation of these tropical ecosystems lead to a considerable release of carbon, making Indonesia, especially Kalimantan and Sumatra, one of the largest carbon emitters worldwide [10]. Digging canals for means of transport is a detrimental form of degradation, as it causes drying in peatlands and encourages the spread of fires and, thus, increases the potential of forest and peatland loss. As a result of the significant emission levels and immense loss of forests and peatlands, Indonesia has become a prime target for REDD+ projects (Reducing Emissions from Deforestation, forest Degradation, and the role of conservation, sustainable management of forests, and enhancement of forest carbon stocks). One of the intentions of REDD+ includes conditional payments to developing countries for reducing their emissions [11]. Within this framework, the most active projects and initiatives worldwide are taking place in Indonesia and its provinces [12]. Nevertheless, Indonesia, especially Kalimantan, the largest isle of Indonesia, is affected by ongoing deforestation and degradation processes.

To perform current REDD+ policies, accurate forest monitoring systems, consistent measurements, and information about carbon emissions at national and subnational scales are necessary for participating countries. Especially, subnational projects require accurate high-resolution maps capturing small-scaled variability and changes in forested areas. Forest carbon stocks are usually calculated using above-ground biomass (AGB) by assuming that typically 50% of AGB is carbon [13]. Biomass, as the fundamental biophysical parameter quantifying the Earth's living vegetation [14], describes the amount of woody matter within a forest. It is defined by the Global Climate Observing System (GCOS) as an essential climate variable (ECV) [15]. Well-known methods for mapping AGB include field-data, airborne and space-borne LiDAR (light detection and ranging) scanning, satellite optical remote sensing, and imaging radar [14]. In contrast to ground-based inventories and LiDAR surveys, Earth observation approaches are able to cover larger areas and in a more cost-effective manner. Additionally, forest inventories are not always comparable, since the definition of national forests and sampling strategies vary between countries [16].

An appropriate compromise represents the upscaling of accurate forest inventories or regional LiDAR-derived biomass estimations with large-scale satellite imagery [17]. Since optical data are limited by clouds, smoke, and lacking illumination, as well as not being able to capture the vertical structures of trees [18], synthetic aperture radar (SAR) is more suitable in this scope of application, as it is daylight- and almost weather-independent [19]. The SAR data-based backscatter approach is well known for forest cover and biomass mapping. This method uses the energy that is received by the sensor after transmission, the so-called backscatter, and relates it to field biomass measurements. The backscatter typically increases with an increasing amount of biomass until a certain value, at which the sensitivity of the backscatter to the AGB stagnates. This biomass saturation level is dependent on the wavelength of the sensor [20]. With regard to the sensitivity of vegetation, wavelengths underlay different physical characteristics. While the C-band is able to penetrate through leaves, but is scattered by small branches, the L-band, with a wavelength of up to 30 cm, is scattered mainly by trunks and tall branches. Since P-band SAR data, which is able to penetrate deeply into the canopy cover and is backscattered by trunks and the ground, has been unavailable to date, the L-band represents the most suitable operational data for biomass estimation [21]. AGB estimation based on Advanced Land Observing Satellite's Phased Array-type L-band Synthetic Aperture Radar (ALOS PALSAR) data has already been successfully performed by [22,23]. AGB studies in tropical forests were also mostly conducted on the basis of L-band SAR data [24–28]. Reported saturation levels using L-band in tropical forests in Indonesia are at approximately 50 t/ha to 200 t/ha [25,29–32]. A combination of C- and

II. Biomass estimation in tropical forests using the backscatter approach in Indonesia (Chapter I)

L-bands has shown better results in tropical forests of Colombia than using a single band [33,34] found a correlation of C-band ENVISAT ASAR backscatter and AGB up to 250 t/ha.

Existing biomass maps of pan-tropical ecosystems by [7,30] exhibit resolutions of 500 m or 1 km, respectively. In Southeast Asia the biomass map of [7] overestimates AGB in the lower biomass ranges and does not identify heterogeneity in forests in detail. In contrast, the map of [30] slightly underestimates high biomass ranges, but captures disturbances in forested areas [35]. Avitabile et al. [36] fuse those two maps in combination with additional data to create an improved pan-tropical biomass map. The results show a smaller RMSE and bias for all continents. Nevertheless, the spatial resolution is about 1 km, which is why the AGB heterogeneity and small-scaled changes cannot be detected as accurate as necessary for most REDD+ projects. Freely available, large-scale biomass maps at national or subnational scales for Indonesia are not available to date.

The aim of the ESA DUE GlobBiomass project is to improve existing AGB estimation products and reduce uncertainties in different ecosystems by developing an innovative synergistic mapping approach. Within the project above-ground biomass is estimated for five regional sites (Sweden, Poland, Mexico, Eastern South Africa, Kalimantan) for the epochs 2005 (2005 ± 2 years), 2010 (2010 ± 2 years), and 2015 (2015 ± 2 years), as well as a global map for the epoch 2010, using different data and methods. Additionally, the change of biomass during the three epochs is estimated per region. As part of the GlobBiomass project, the present study focuses on large-scale monitoring of biomass in Kalimantan, Indonesia, from space. The aim of the study is to estimate AGB with a finer resolution and better accuracy than other existing AGB maps. Therefore, ALOS PALSAR/ALOS-2 PALSAR-2 L-band, and Sentinel-1 C-band data from 2007, 2009, and 2016 were used. A multivariate linear regression model (MLR) based on SAR backscatter values, polarization ratios, and textures was set up in order to increase the biomass saturation level. As the reference biomass for the model calibration and validation from SAR data, a combination of field inventory data and LiDAR data was used in order to provide a more accurate base. Modelling three different years with a consistent method allows a more accurate estimation of changes between the three time steps than using the available biomass maps based on different models. A higher spatial resolution is important in order to make them a promising alternative building a forest monitoring or risk managing system, but also to achieve the objectives of REDD+, the Global Canopy Programme, UNEP-WCMC, and other programs protecting forests or analyzing carbon release at national and subnational levels.

2. Study Area and Data

Kalimantan, which is the Indonesian part of Borneo island, has a size of about 544,000 km² and lies within the geographic coordinates 4°15'41"N to 3°45'44"S latitude and 108°48'0"E to 118°49'41"E longitude (Figure 1). The island's climate is mainly conditioned by the dry southeast monsoon from May to October and the wet northwest monsoon from November to April, and is influenced by frequent rainfall and high temperatures throughout the year. Those conditions are ideal for plant growth, which is why Kalimantan's land cover is characterized mainly by tropical forests covering 301,750 km² and, thus, more than 55% of the country. The forests of Borneo are considered to be one of the oldest and most species-rich tropical rainforests on Earth. The dominating forest ecosystems are mangrove forests, peat swamp and freshwater swamp forests, riparian forests, heath forests, lowland dipterocarp forests, ironwood forests, forests on limestone and ultrabasic soils, hill dipterocarp forests, and various montane formations [6]. In general lowland dipterocarp and peat swamp forests can be well discriminated in the field by means of average tree height, tree crown diameter, canopy closure, and species composition. Lowland dipterocarp forests are more diverse with taller trees and a more closed canopy [6]. Dipterocarps can reach a height of 45–60 m and are a valuable tree species prone to logging. All of the forest types store an extensive amount of carbon [8]. Nevertheless, the most significant carbon sinks in this area are belowground peatlands, which can store up to ten times more carbon than the forests growing on top them, since they were formed over the past millennia, as plant debris accumulated under waterlogged conditions [37]. The last decades witnessed a decrease of

forest due to illegal logging, deforestation for agricultural development but also due to natural and manmade fires. Additionally, the ability of peatlands to store carbon is reduced due to anthropogenic activities like logging and drainage. In particular, draining the normally waterlogged peatlands makes these ecosystems vulnerable to fires. For modelling the reference AGB layer a universal AGB model is used for all different forest types.

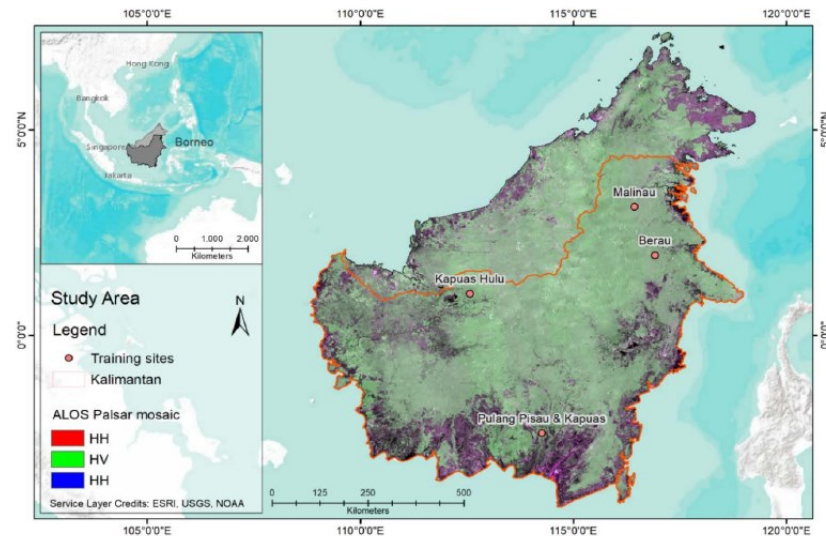


Figure 1. ALOS PALSAR false-color composite of Borneo Island using cross- and co-polarization as RGB (HH; HV; HH). To achieve the full coverage of Borneo 21 images of the year 2009 are mosaicked.

2.1. Above-Ground Data

For the creation of the AGB reference layer existing field inventory data, collected across different forest types using the nested plots method, based on the guidelines provided by [38], were utilized. The methodology varies slightly for the various study sites, since they were processed as part of different research projects. The data was gathered in four test sites across Kalimantan (Figure 1) during 2007, 2009, and 2016 (Table 1). In order to estimate AGB using allometric models after [39], information about forest type, tree species, the diameter at breast height (DBH), and tree height are collected within nested plots based on three or four subplots. Inside the different subplots, trees of a certain diameter at breast height (DBH) were measured, for example, $DBH < 10$ cm (within the 3 m radius), ≥ 10 cm to < 20 cm (10 m radius), ≥ 20 cm to < 50 cm (20 m radius), and ≥ 50 cm (30 m radius). The sum of the measured parameters of the subplots was multiplied by an expansion factor in order to obtain the final values for 1 ha. In Pulang Pisau and Kapuas three circular subplots with radii of 20 m, 14 m, and 4 m, and 16 m, 8 m, and 4 m, and in Berau, Malinau and Kapuas Hulu four subplots with radii of 30/35 m, 20/25 m, 10 m, and 3 m were applied. In addition to circular nested plots, information was collected in rectangular plots of 20×50 m to record saplings and trees in regrowing areas in Pulang Pisau and Kapuas. Moreover, nested rectangular plots with three subplots with sizes of 10×10 m, 20×20 m, and 20×50 m were applied in Kapuas Hulu.

Airborne LiDAR measurements were acquired during the dry seasons in 2007, 2011, and 2012 in the same areas as the field data was collected. In 2007 (May–October) a Riegl LMS-Q560 2D laser scanner by RIEGL Laser Measurement Systems GmbH (Horn, Austria) was flown at a height of 500 m above-ground and a half scan angle of $\pm 30^\circ$ to collect the full-wave LiDAR data. The average point density of the final data 2007 was 1.5 points per m^2 . For the years 2011 and 2012 (August–October) the measurements were acquired using Optech Orion M200 and Optech ALTM 3100 airborne laser

II. Biomass estimation in tropical forests using the backscatter approach in Indonesia (Chapter I)

scanners by Teledyne Optech (Vaughan, Ontario, Canada) at an altitude of 800 m above-ground. A half scan angle of $\pm 11^\circ$ was used and the point density amounted to 10.7 points per m^2 . Since the accuracy of biomass estimations derived from LiDAR metrics increase with a higher point density, a weighting of the plots accordingly to their point density was applied [40]. In total, 8300 km^2 were surveyed in different regions in East, West, and Central Kalimantan (Table 1) representing different ecosystems. Since there was a lack of LiDAR data for 2016 due to vast fires in Kalimantan, adjusted data of 2011 and 2012 was used.

Table 1. Overview of the measured field inventory plots (473) and the acquired LiDAR data (8300 km^2) in Kalimantan.

Test Site	Field Plots		LiDAR		Reference Year
	Acquisition Date	Number of Plots	Acquisition Date	Area [km^2]	
Pulang Pisau & Kapuas	2008	64	2007	300	2007
Kapuas Hulu	2009–2011	82	2012	420	2009
Pulang Pisau & Kapuas	2010–2011	87	2011	7000	2009
Berau	2012–2013	78	2012	340	2009
Malinau	-	-	2012	240	2009
Pulang Pisau & Kapuas	2013–2014	94	2011 *	7000	2016
Malinau	2015	24	2012 *	340	2016
Kapuas Hulu	2014	44	2012 *	240	2016

* adjusted using the MODIS fire hotspot product MDC14DL.

2.2. Earth Observing Datasets

2.2.1. SAR Data

SAR data was acquired in 2007, 2009, and 2016, using years with preferably dry conditions and less active fires. The study is based on L-band radar data of the Phased Array Type L-band Synthetic Aperture Radar (PALSAR), onboard the Advanced Land Observing Satellite (ALOS) of the Japan Aerospace Exploration Agency (JAXA) and ALOS-2 in combination with C-band radar data based on ENVISAT ASAR and Sentinel-1. ALOS PALSAR and ALOS-2 PALSAR-2 mosaics with a spatial resolution of 25 m were provided by the Kyoto and Carbon Initiative. ENVISAT ASAR was launched in 2002 by the European Space Agency (ESA). Sentinel-1a and Sentinel-1b C-band radars were launched within the Copernicus program by the ESA in 2014 and 2016, respectively. ALOS PALSAR (HH, HV) images were used to estimate the biomass in Kalimantan for the years 2007 and 2009. As C-Band radar data for the years 2007 and 2009 imageries of ENVISAT ASAR (VV) data were tested, certainly the data had to be excluded as the study area is not fully covered by scenes acquired in one sensor mode and because of strong moisture effects. In 2016, data of ALOS-2, launched in 2014, in combination with Sentinel-1 GRD data, acquired in interferometric wide (IW) swath and a resolution of $10\text{ m} \times 10\text{ m}$, was used.

2.2.2. SRTM

The Digital Elevation Model (DEM) from the Shuttle Radar Topography mission (SRTM) with a vertical accuracy of $\pm 10\text{ m}$ and a spatial resolution of 30 m is used for topographic analyses. Slope is used to clean up the final AGB map, since extreme overestimation of biomass occurs in steep terrain. Besides, steep terrain can cause layover and shadow effects, decreasing the accuracy of the AGB estimation.

2.2.3. TRMM

Since SAR backscatter is highly sensitive to water content of the surface due to its dielectric properties, daily TRMM (Tropical Rainfall Measuring Mission) of the National Aeronautics and Space Administration (NASA) and JAXA precipitation data with a spatial resolution of 0.25° were incorporated in order to select satellite acquisition dates with dry and comparable conditions [41].

II. Biomass estimation in tropical forests using the backscatter approach in Indonesia (Chapter I)

Remote Sens. 2018, 10, 831

6 of 22

2.2.4. MODIS Active Fire Data (MCD14DL)

MODIS hotspot information (product MCD14DL, provided by NASA) were used as an additional layer to detect thermal anomalies and active fires in Kalimantan. In this layer active fires are represented in the center of a $1 \text{ km} \times 1 \text{ km}$ pixel that is identified by the MODIS MOD14/MYD14 Fire and Thermal Anomalies algorithm as containing one or more fires within the pixel [42,43].

2.2.5. Water Body Mask

ESRI World Water Bodies was used for delineating water bodies within the study area. It provides a base map layer for lakes, seas, oceans and large rivers and as generated on data with a spatial resolution of 100 m [44].

2.2.6. Urban Areas

The ESA CCI land cover map provides three epoch series (2000, 2005, 2010) of global land cover maps at 300 m spatial resolution which were used to evaluate settlement areas. ESA CCI land cover maps were produced used a multi-sensor and multi-temporal strategy based on MERIS Full and Reduced Resolution (FR and RR) archive. The 10-year product has been served as a baseline to derive the 2000, 2005 and 2010 maps using MERIS and SPOT-Vegetation time series specific to each epoch [45].

3. Methods

3.1. Above-Ground Biomass Data

Inventory data and LiDAR data are combined to create more accurate biomass predictions for an area within the SAR images. This upscaling from field inventory to LiDAR transects allows creating a more precise basis for AGB model calibration and validation from SAR backscatter data [40]. An overview of the whole methodology of this study can be found in Figure 2.

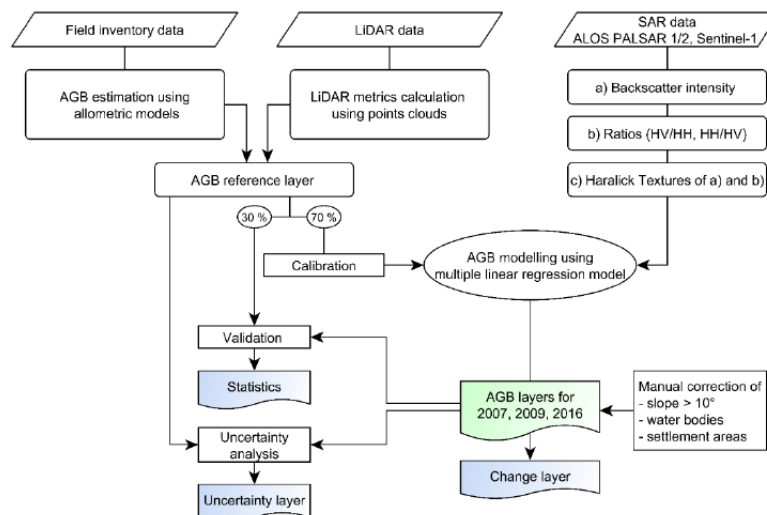


Figure 2. Flow chart of the AGB map processing steps. Blue refers to the results, and green refers to the main result.

The estimation of AGB in t/ha from field inventory data was achieved by using the tree height, diameter at breast height (DBH), and wood specific density of each tree as the input for a combination of different allometric models. Therefore, allometric models from [46] for saplings (if DBH < 5 cm and

II. Biomass estimation in tropical forests using the backscatter approach in Indonesia (Chapter I)

height ≤ 1.3 m) or trees (if DBH < 5 cm and height > 1.3 m) and from [39] for moist tropical forest stands (if DBH ≥ 5 cm and height > 1.3 m) were applied. Those ground-based AGB values were related to LiDAR transects in order to estimate biomass reference data using previously-established regression models for the different study sites, as described in [40].

LiDAR height histograms were calculated by normalizing all points within a grid of, e.g., 30 m (similar to the size of the largest nest of the field inventory plots) to the ground using a DTM as reference, i.e., the height of each LiDAR return was calculated relative to the DTM [47,48]. The number of points within each 0.5 m interval was stored as a histogram. The first (lowest) interval was considered as the ground return and excluded from further processing. The LiDAR data enabled calculating the two LiDAR point cloud metrics quadratic mean canopy height (QMCH) and centroid height (CH), as described more in detail in [40]. Previous studies have shown that those two parameters are able to estimate tropical forests AGB, as they take into account the point distribution of the LiDAR measurements [47,49]. This is why the QMCH and the CH were estimated based on height histograms by weighting each 0.5 m height interval by the fraction of points within the interval. CH and QMCH were related to AGB, estimated by the field inventories using regression models for each particular study site in order to obtain large-scale biomass estimations [29,48]. Furthermore, the point density was included in the regression model, since [47] showed that the accuracy of AGB estimations derived from LiDAR height histograms increased with higher point densities. The coefficient of determination (R^2) of the AGB regression models vary from $R^2 = 0.7$ (Berau and Kapuas Hulu) to $R^2 = 0.8$ (Malinau and Central Kalimantan).

The upscaling from field inventory data to LiDAR transects allows creating numerous biomass reference data for the calibration of SAR images and to upscale AGB across large areas and different ecosystems. It provides AGB estimates over the whole biomass range from woody regrowth to pristine forest, and is able to disclose a spatial variation due to varying growth conditions. In order to estimate AGB based on SAR data the reference AGB was rescaled to a spatial resolution of 100 m.

Since there was a lack of LiDAR data for 2016 due to vast fires in Kalimantan, the data of 2011 and 2012 was used. Differences between the reference AGB and the SAR images over time were detected and excluded using MODIS fire hotspots, as fire is the main reason for deforestation in this area.

3.2. SAR Data

Since SAR backscatter is highly sensitive to water content of the surface due to its dielectric properties, daily TRMM (Tropical Rainfall Measuring Mission) precipitation data with a spatial resolution of 0.25° were used to verify the moisture conditions within the SAR imageries. In order to have dry and comparable conditions images with a high influence of precipitation were excluded. During the pre-processing of the Sentinel-1 (10 m) and ALOS PALSAR (25 m) data a co-registration based on an ALOS PALSAR mosaic with a spatial resolution of 25 m, a radiometric calibration estimating γ^0 backscatter coefficients in dB and a geometric correction were accomplished. Furthermore, a multi-temporal speckle filtering using an enhanced Lee filter with a 7×7 window was applied [50]. The processed data was resampled to a resolution of 100 m resulting in pixels with a spatial resolution of 1 ha.

In order to examine the potential for AGB estimation, ratio images were prepared, using the following equations:

$$R_{hvhh} = HV/HH \quad (1)$$

$$R_{vhvv} = VH/VV \quad (2)$$

where HH, HV, VV, and VH indicate the polarization of the γ^0 backscattering coefficients, depending on available polarizations of ALOS PALSAR and Sentinel-1. An evaluation of ratios and textures can be found in [51].

To improve the model accuracy, Haralick textures [52] and their relationship to AGB were also investigated. Texture describes the properties of objects, such as regularity, smoothness, and tonal variation [51]. Ten simple Haralick textures applying a gray level co-occurrence matrix (GLCM) and eleven higher-order Haralick textures applying a gray level run-length matrix (GLRM) were calculated within the open-source software Orfeo ToolBox by CNES (Centre National D'Études Spatiales) over a moving window with user-defined radius based on single polarized images and the calculated ratios. The radius used for single polarized images had a size of five, while a radius of three was used for calculating textures based on ratios. The relationship between these generated SAR variables and the LiDAR AGB was analyzed and showed an inversely proportional correlation. The variables were linearized in order to use the variables as an input for a multivariate linear regression model (MLR).

3.3. Multivariate Linear Regression Model (MLR)

In Englhart et al. [53] it was found that artificial neural network (ANN) and support vector regression (SVR) were suitable to predict AGB in tropical forests. Nevertheless, in terms of biomass variability and saturation in tropical forest ecosystems, multivariate linear regression models (MLR) are superior to ANN and SVR models [53]. Since very high biomass values are expected in the study area, MLR is used to model the above-ground biomass. Multiple regressions are often affected by overfitting and co-linearity among variables. In order to find a model with the greatest explanatory power, a backward stepwise multiple linear regression was performed to automate the selection of the best explanatory variables. The MLR was first set up with all linearized ratios and textures and run iteratively. To decrease the number of inputs, the p -value and the variable inflation factor (VIF) were investigated for each variable to identify their significance and co-linearity. Regarding literature, parameters with a p -value <0.05 and a VIF >5 were excluded from the model [26,51,54]. After eliminating redundant information, three variables were finally used for 2007 and 2009 and four variables for 2016. However, the extreme fire events in 2015 burned vast forest areas in Kalimantan. Resulting burned and carbonized trunks enhance double bounce effects in this region, which caused higher backscatter values and, thus, an overestimation of the biomass model. To minimize the overestimation in this areas, a second model was set up for 2016 simply based on two variables that were less sensitive to high backscatter. This model was applied only in burned areas, captured by a mask based on high backscatter values. In the remaining parts of the scene the first model, using four inputs, was used.

Settlements and areas with steep terrains cannot be captured correctly by the model. In order to reduce errors due to radar shadow and layover effects, regions with a terrain steeper than 10° were excluded from the biomass estimation using the Shuttle Radar Topography Mission (SRTM) DEM. Mountainous areas in Kalimantan are less influenced by human activity since they are difficult to access and due to a lack of transport routes, like canals. For this reason, the forests in mountainous terrain are mostly unaffected by degradation. Altogether 27.2% of the study area of Kalimantan are influenced by slopes steeper than 10° the main forest type in these regions is the hill- and sub-montane forest which was determined during field inventory campaigns, as well as through detailed forest classification mapping covering the LiDAR areas. The mean value of LiDAR AGB was calculated for the area with a terrain steeper than 10° and resulted in 350 t/ha. Additionally, urban areas and water bodies were excluded from the final results, using an ESRI World Water Body layer and the ESA CCI land cover map of each particular year (2005, 2010, 2015).

3.4. Temporal Change Estimation

The temporal change between 2007–2009, 2009–2016, and 2007–2016 was assessed using the RMSE in order to define a possible biomass range for each estimate at pixel level. The RMSE is calculated for five classes 0–50 t/ha, 50–100 t/ha, 100–150 t/ha, 150–200 t/ha, and >200 t/ha. The specific RMSE of the corresponding AGB range was subtracted from and added to the estimated AGB value at pixel level. The results are two layers consisting of the highest (H) and lowest value (L) of a possible AGB

range per pixel for two comparing time-steps (T1, T2). A change/no-change mask, with discrimination of the increase and decrease, was generated by using threshold values based on the following decisions. If $HT1 > LT2$ or $LT1 < HT2$, an overlap between the ranges exist and, thus, no-change is assumed. In cases where $HT1 < LT2$, we suppose an increase of AGB and if $LT1 > HT2$ a decrease of AGB between the two years, both indicates a change. In order to remove single separated pixel, a minimum change unit of $300\text{ m} \times 300\text{ m}$ was applied.

3.5. Validation and Uncertainty

For the validation of the AGB estimation, field inventory and LiDAR data, was used. The data was randomly split into data used for training (70%) and validation (30%) of the SAR-AGB models. For each map approximately 500 points were randomly set within the reference layer extent. To measure the accuracy of the models different parameters like bias, RMSE, standard deviation (SD) and the R^2 were calculated for each map within an AGB range of 50 t/ha starting from 0 up to >200 t/ha and the overall range. Additionally, the NSE was estimated for the overall biomass range. Regarding [55], the NSE is a dimensionless index measuring the efficiency of a model in a range from $-\infty$ to 1. The closer the NSE is to 1, the more accurate is the model. The NSE is calculated using the following equation:

$$NSE = 1 - \left(\frac{\sum_{i=1}^N (P_i - O_i)^2}{\sum_{i=1}^N (O_i - \bar{O})^2} \right) \quad (3)$$

where N is the number of observations, P_i is the predicted value, O_i is the observed value, and \bar{O} is the mean of the observed value [55].

An uncertainty map at the pixel level is important for the interpretation of AGB maps, as shown in [56,57]. The total uncertainty at the pixel level is composed of different sources of errors which are assumed to be random and independent. These are propagated for each map using the equation proposed by [30], taking into account the errors of measurement, allometry, sampling size, and prediction. Similar to [26], a measurement error supposed to be 10%. In [39] the authors found an error for the estimation of a tree's biomass of approximately $\pm 5\%$. As we mainly used this allometry, an error of 5% is assumed. According to [30,58], a sampling size error of 20% is supposed. The prediction error includes the sampling error associated with the representativeness of the training data of the actual spatial distribution of AGB and the model predictions and is estimated per pixel.

4. Results

4.1. Modelling Results

Using a backward stepwise approach allows to reduce the parameters within in the MLR, resulting in the finally-used variables listed in Table 2. In addition, coefficient of determination and residual standard error are displayed for each model calibration. Model 1 and model 2 of 2016 are used in combination, whereas model 2 is only applied in burned areas. The overall R^2 of the combined models is 0.69. The RP and the Low Grey-Level Run Emphasis (LGRE) showed the best relationship to LiDAR AGB compared to all Haralick textures. Additionally, cross-polarized-based parameters perform significantly better than co-polarized ones.

II. Biomass estimation in tropical forests using the backscatter approach in Indonesia (Chapter I)

Table 2. Overview of the used variables for the different MLR models per year and the R^2 and residual standard error (RSE) for the calibration of the model (RP = higher texture run percentage).

	Predictor	B	Std. Error	Beta	p Value	R^2	RSE
Model 2007	PALSAR-1 HV (dB)	-72.51	44.00	-0.057	0.0996 .	0.75	57.2
	PALSAR-1 HVHH RP	0.61	0.04	0.347	$<2 \times 10^{-16}$ ***		
	PALSAR-1 HV RP	22.35	1.34	0.612	$<2 \times 10^{-16}$ ***		
Model 2009	PALSAR-1 HV (dB)	-105	6.72	0.262	$<2 \times 10^{-16}$ ***	0.77	56.6
	PALSAR-1 HVHH RP	2.86	0.17	0.228	$<2 \times 10^{-16}$ ***		
	PALSAR-1 HV RP	-0.00000236	0.000005127	-0.345	$<2 \times 10^{-16}$ ***		
Model 2016 (1)	PALSAR-1 HV (dB)	8931.00	1445.27	-0.662	8.67×10^{-10} ***	0.63	55.8
	PALSAR-1 HVHH RP	0.47	0.03	0.027	$<2 \times 10^{-16}$ ***		
	PALSAR-1 HV RP	-36.05	2.81	-0.001	$<2 \times 10^{-16}$ ***		
	Sentinel-1 VH (dB)	-3.99	203.88	0.109	0.0503 .		
Model 2016 (2)	PALSAR-2 HVHH RP	-67.18	2.21	-0.664	$<2 \times 10^{-16}$ ***	0.49	73.8
	Sentinel-1 VH (dB)	837.25	222.78	0.082	0.000179 ***		

Signif. codes: 0 '****' 0.001, '***' 0.01, '**' 0.05, '.' 0.1, '' 1.

4.2. Biomass Maps and Temporal Change

The final biomass maps with a resolution of 100 m are presented in Figure 3a–c. Kalimantan is dominated in all years by forests with biomass varying in a range of 50–350 t/ha. However, its land cover is changing in time. Areas close to the coasts and along rivers show low biomass values between 0–50 t/ha. In 2007 15% of Kalimantan was covered by non-forested areas. Certainly, the portion of this class is growing over the years, caused by a decrease of forest and, thus, a loss of biomass. In 2009 the amount of non-forested extents is about 20%, though it reaches the maximum (25%) in 2016. The highest biomass values are reached in areas of mountainous terrain, which can be found in the north and center of Kalimantan. Nevertheless, the extent of forests containing high biomass values is significantly shrinking. In 2007 the model found a percentage of 55% of Kalimantan with biomass values >200 t/ha, while it is 38% in 2016. The biomass variability due to different degradation stages in the forest, as well as different disturbances in contrast to non-disturbed areas or clear-cuts, can be captured in the final maps.

A subset of Kalimantan, showing the change in the south of the island for the period 2009–2016, is displayed in Figure 3d. Red colors show a decrease of biomass, while green colors indicate an increase of AGB. The region is mainly dominated by a loss of biomass with values about -300 to -100 t/ha. In contrast, only few areas show increased biomass. A similar distribution can be observed across the entire coastline of Kalimantan. Mountainous regions in the center of Kalimantan are less influenced by change. Figure 4 is summarizing the percentage of the forest degradation level per year. Highly-degraded areas increase from 15% in 2007 to 20% in 2009 to 25% in 2016. Accordingly, the area covered by natural forest (AGB >200 t/ha) decreases. The coverage of forested areas containing an AGB from 50 to 200 t/ha are rising since areas with natural forest are affected by illegal logging, where single trees are felled. Thus the class of natural forest is slowly converted into degraded forest. Ongoing activities are further converting the degraded forest to highly-degraded areas.

II. Biomass estimation in tropical forests using the backscatter approach in Indonesia (Chapter I)

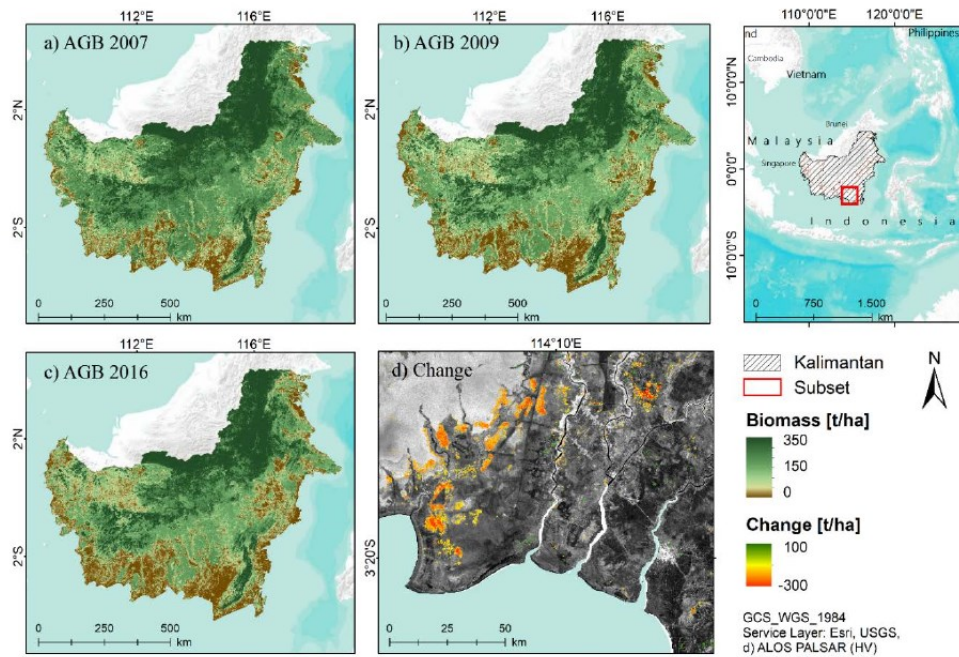


Figure 3. Final biomass maps for Kalimantan, per year and subset of the quantity of change layer for 2009–2016. Biomass ranges from 0–350 t/ha, and the quantity of change ranges from –300–100 t/ha.

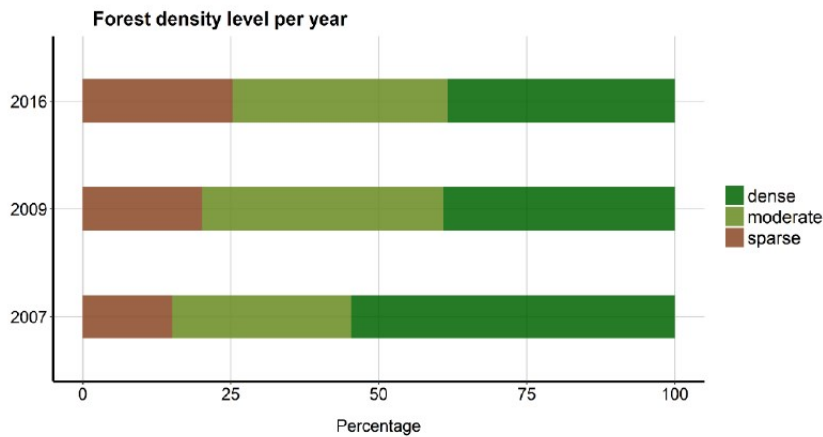


Figure 4. Percentage of the level of forest degradation per year, natural Forest = >200 t/ha, degraded = 50–200 t/ha, and highly-degraded = 0–50 t/ha AGB.

4.3. Comparison with Pan-Tropical Biomass Maps

Figure 5 displays a subset of a degraded peat swamp forest in Central Kalimantan near the capital Palangka Raya. A visual comparison of the estimated AGB map, the LiDAR-derived reference AGB map and other pan-tropical biomass maps [7,30,36] with a resolution of 500 m and 1 km, respectively, points out that the developed MLR model correctly estimates the variability of biomass. The biomass map of [7] overestimates AGB in the lower biomass ranges and is not identifying heterogeneity

II. Biomass estimation in tropical forests using the backscatter approach in Indonesia (Chapter I)

Remote Sens. 2018, 10, 831

12 of 22

in forests in detail. In contrast, the map of [30] underestimates high biomass ranges, but captures disturbances in forested areas. Avitabile et al. [36] combine the pantropical biomass maps of [7] and [30] and additional data in order to create an improved pan-tropical biomass map. The final product of [36] with a resolution of 1 km has a lower RMSE and bias than the two previous studies. Comparing maps (a) and (e), a similar trend of the biomass distribution is visible. The estimated AGB map based on the MLR model has a much finer resolution (100 m) which allows visualizing AGB variability more precisely and detects even small-scaled changes for carbon modelling, as well as forest monitoring or risk managing systems. Moreover, the modelled maps show a better accordance to the LiDAR-derived AGB in the subset.

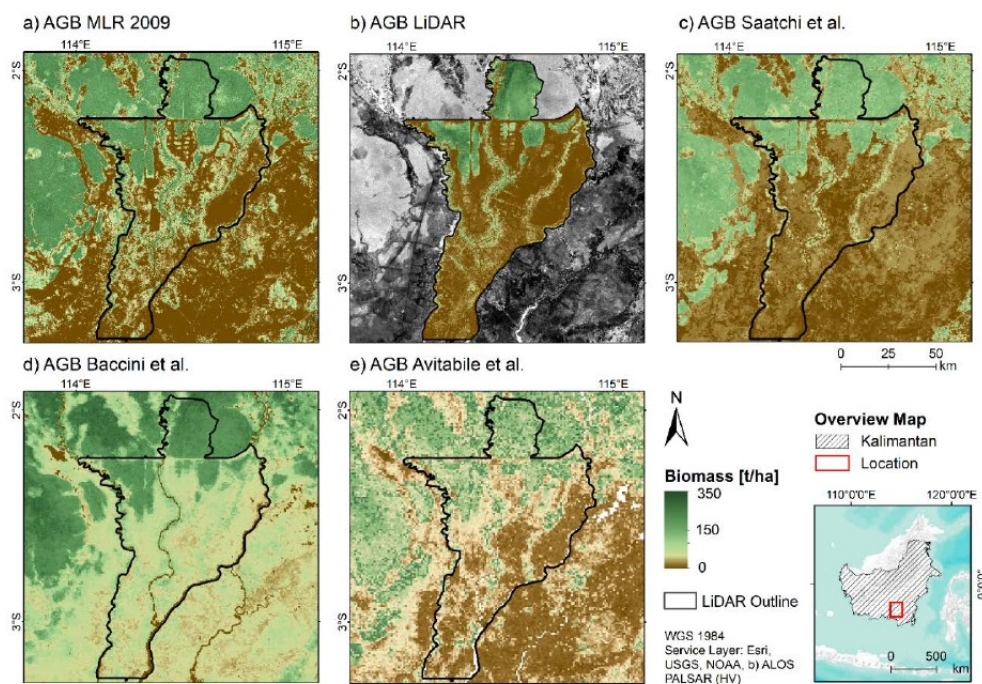


Figure 5. Comparison between different AGB maps (a) AGB MLR model result for 2009; (b) LiDAR; (c) Saatchi et al. (2011); (d) Baccini et al. (2012); and (e) Avitabile et al. (2016) in a range of 0–350 t/ha for a subset in the south of Kalimantan. The resolution of AGB maps of the MLR model and the LiDAR data is 100 m; the map of Saatchi et al., 1 km; the map of Baccini et al., 500 m; and the map of Avitabile et al., 1 km.

4.4. Validation and Uncertainty

Various validation statistics of the estimated AGB in Kalimantan, calculated using approximately 500 points per map, are listed in Table 3. The sample points were randomly distributed over areas, where reference data was available (training sites, Figure 1). Average AGB estimates are consistently higher than those obtained from the reference biomass, except to the AGB range >200 t/ha. Higher averages indicate a positive bias, while the magnitude of the bias is variable across the AGB ranges and points to the highest values in the biomass classes of 50–100 t/ha and 100–150 t/ha. In contrast, AGB ranges >200 t/ha display a negative bias. The root mean square error (RMSE) is similar in all years, with the highest relative errors exceeding 100% in the lower AGB ranges and low relative errors of around 22% in the highest AGB ranges. The distribution of the relative RMSE is similar in all three years. The relative overall RMSE ranges between 31% (2016), 36% (2009), and 38% (2007).

II. Biomass estimation in tropical forests using the backscatter approach in Indonesia (Chapter I)

The scatterplots of AGB estimates against the reference AGB display a similar distribution in all years (Figure 6). AGB values up to 250 t/ha show an overestimation of the models, especially in 2007, while AGB ranges higher than 250 t/ha indicate an underestimation. The coefficient of determination (R^2) varies in a range of 0.69 in 2016 to 0.77 in 2007 and the standard deviation (SD) is 53 t/ha in 2009 and 2016 to 56 t/ha in 2007. The NSE, indicating the efficiency of a model in a range from $-\infty$ to 1, shows a good model performance for all years, reaching values between 0.70 and 0.76.

Table 3. Overview of validation statistics per AGB ranges and year.

Year	AGB (t/ha)	# of Points	\overline{AGB}_{est} (t/ha)	\overline{AGB}_{ref} (t/ha)	RMSE (t/ha)	SD (t/ha)	Bias (t/ha)	Rel. RMSE	R^2	NSE
2007	0–50	134	27	7	41	36	20	5.86	0.77	0.76
	50–100	19	151	68	90	35	84	1.32		
	100–150	34	179	128	68	45	52	0.53		
	150–200	78	219	176	55	35	43	0.31		
	>200	154	239	273	62	52	−34	0.23		
	Overall	419	159	149	57	56	10	0.38		
2009	0–50	139	48	13	52	38	35	4.00	0.71	0.71
	50–100	21	130	78	71	50	52	0.91		
	100–150	37	175	132	64	49	42	0.48		
	150–200	115	194	178	40	35	18	0.22		
	>200	180	207	247	57	41	−39	0.23		
	Overall	492	154	149	53	53	5	0.36		
2016	0–50	82	19	9	27	37	10	3.00	0.70	0.70
	50–100	24	130	72	75	48	58	1.04		
	100–150	37	162	126	54	41	36	0.43		
	150–200	115	196	179	41	30	28	0.23		
	>200	210	252	210	63	46	−42	0.30		
	Overall	468	168	173	54	53	−5	0.31		

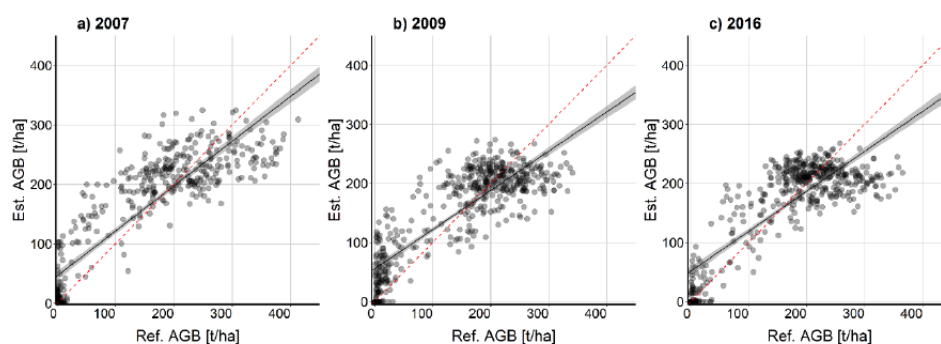


Figure 6. Linear regression of estimated above-ground biomass and reference above-ground biomass using approximately 500 randomly-generated points across the reference layer for each year (red dashed line = 1:1 line; black line = linear trend including confidence bounds).

Figure 7 shows the number of sample points (frequency) of the reference AGB in contrast to the estimated AGB in each biomass range. The distribution of the frequency for the reference and the modelled biomass per range are similar, showing just small discrepancies in each year. The histogram of 2007 is affected by a smaller frequency of estimated biomass in each range, except the range >200 t/ha with a relative error of about 25%. In contrast, the histogram of 2009 is dominated by a lower sum of observations per range for all ranges except the smallest biomass range (0–50 t/ha) with a relative error of 42%. 2016 shows only little differences in each biomass range.

II. Biomass estimation in tropical forests using the backscatter approach in Indonesia (Chapter I)

Remote Sens. 2018, 10, 831

14 of 22

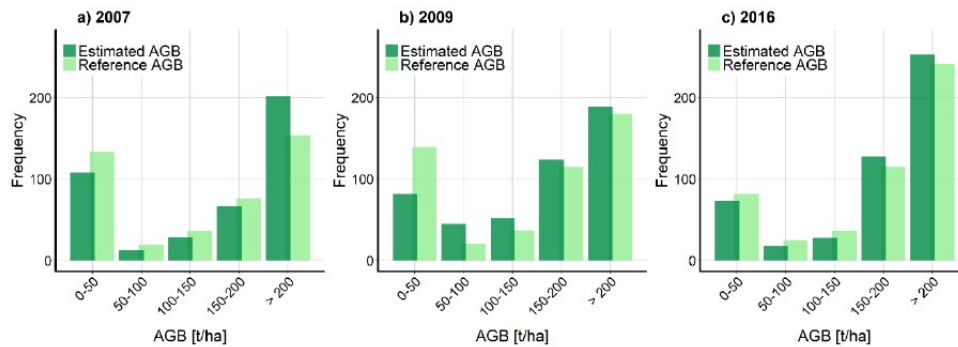


Figure 7. Histograms of reference above-ground biomass and estimated above-ground biomass per biomass range for each year. Frequency refers to the number of observations per range.

The uncertainty per AGB range (Figure 8), computed as a percentage of the AGB estimates, shows the highest relative errors in areas with low AGB estimates (Table 4). The relative errors in the biomass range 0–50 t/ha vary between 61.3% to 117.9%, in which the lowest values were obtained in 2009 and the highest in 2007. Areas with high biomass estimates show low relative errors of about 6% in each year. Additionally, the overall relative error per year show similar values varying in a range from 7.8% to 9.1%.

Table 4. Uncertainty per AGB range and year in percentage.

AGB (t/ha)	2007	2009	2016
0–50	117.9	61.3	103.6
50–100	20.4	17.5	19.3
100–150	9.8	9.3	8.2
150–200	5.8	4.8	4.8
>200	6.0	6.4	5.8
Overall	9.1	8.5	7.8

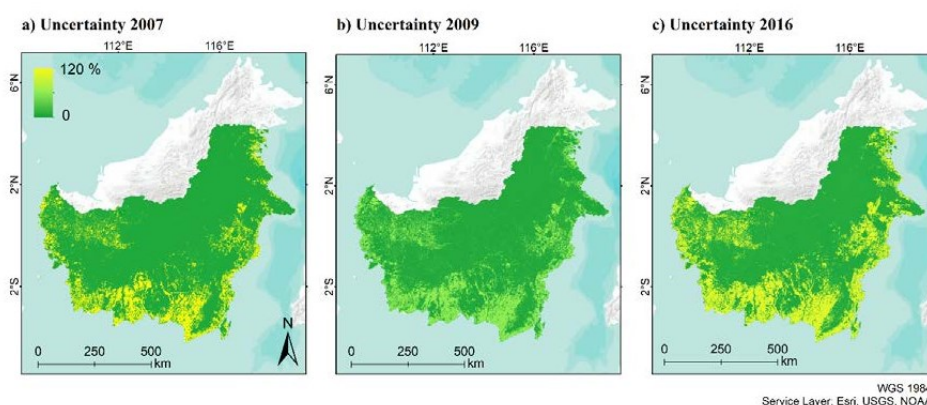


Figure 8. Uncertainty maps per AGB range for each year showing highest errors in low biomass ranges.

II. Biomass estimation in tropical forests using the backscatter approach in Indonesia (Chapter I)

5. Discussion

5.1. Biomass Estimation

The results suggest that a MLR using backscatter values in combination with ratios and textures of ALOS PALSAR-1/2 L-band and Sentinel-1 C-band data is eligible to model AGB in tropical forests. Englhart et al. [53], the authors found that in terms of biomass variability and saturation in tropical forest ecosystems MLR models are superior to ANN and SVR models. Since Kalimantan is dominated by high biomass values, a MLR was, therefore, used to model the AGB.

The use of highly accurate field inventory plots in combination with extensive LiDAR surveys as reference datasets improved the SAR-based biomass modelling. These datasets were collected in different ecosystems across Kalimantan, covering a wide range of ecosystems, vegetation types, forest structures and, thus, biomass ranges, for which reason they provide more precise biomass estimates than other sensors or the exclusive use of field inventory data [40]. Nevertheless, uncertainties between field data and the modelled reference AGB can originate from different factors. First of all, the lag time between field data and LiDAR data acquisitions can introduce uncertainties due to regrowing or deforestation. For the reason that LiDAR data was not available for 2016, LiDAR data from 2011/2012 was adjusted as the reference layer for 2016. In order to minimize the effect of this temporal shift additional MODIS hotspot data (MCD14DL) was used to eliminate burned areas between 2011 and 2016. Certainly, forest cover changes resulting from logging or regrowing is not captured and can cause inaccuracies. Second, extrapolating field inventory data can introduce errors, since the spatial variability cannot be covered. In addition, the accuracy and precision of AGB extrapolated from field plots are affected by plot size and shape [59]. Previous studies showed that errors in LiDAR-estimated AGB decrease exponentially with increasing field plot size, resulting from a smaller effect of co-registration errors and a spatial averaging of errors [58–61]. In contrast, smaller plots have less overlap with the LiDAR data, cannot capture the variability of a forest, and are more sensitive to individual trees [13,62]. For lack of data, differing field plot sizes and shapes were used to estimate the reference AGB. However, most of the used field plots exceed an area of 1000 m², which is sufficiently large to be more robust against boundary effects [59,63,64]. In contrast, Mauya et al. [65] show improvements of the model accuracy with increasing plot sizes in a range from 200–3000 m². In addition to the size, the shape affects the precision and accuracy of the extrapolated biomass. Circular plots are less influenced by the circumference to area ratio than rectangular ones [65]. As the number of rectangular plots in this study is limited and only within regrowing forest areas, their influence in AGB estimation is marginal. The uncertainty resulting from different sampling strategies are considered as the error of sampling size in the overall uncertainty of the SAR model with 20% [58]. Finally, uncertainties may also be introduced by reason that a universal AGB model was applied for different forest types [66]. Since tropical forests consist of hundreds of different tree species species-specific regression models cannot be applied [39].

After creating a reference biomass layer from LiDAR and field inventory data, AGB can be estimated for large-scaled areas using remote sensing data. The applied SAR backscatter approach is well known for radar-based forest cover and biomass mapping. It is computationally less intensive than alternative approaches and transferable to other regions, but also limited by some factors like backscatter saturation and backscatter variations due to terrain and wetness [19,67]. The resulting maps point that the biomass variability due to different degradation stages in the forest, as well as disturbances in contrast to non-disturbed areas or clear-cuts that can be captured very well. The R^2 varies in a range of 0.69 in 2016 to 0.77 in 2007 and the NSE shows good model performance for all years, reaching values between 0.70 and 0.76. Studies modelling biomass and carbon based on ALOS PALSAR HV backscatter values in tropical forests found similar correlations, varying from 0.407 to 0.76 [68–70]. Nevertheless, all maps show an underestimation at higher AGB levels compared to reference AGB. In addition to the underestimation in higher biomass ranges, biomass in lower AGB ranges is overestimated. Similar distributions of estimated biomass are shown in other regional studies

II. Biomass estimation in tropical forests using the backscatter approach in Indonesia (Chapter I)

estimating biomass from SAR backscatter values for different forest ecosystems, as a characteristic of SAR data for high biomass levels [17,66,71,72].

One of the general limitations of the applied approach is that SAR-based AGB retrieval suffers from saturation of the backscatter signal in the higher biomass range. The saturation level varies amongst others with the sensor wavelength and polarization, as well as the forest structure [20]. AGB studies in tropical forests, such as in Kalimantan, were mostly conducted on the basis of L-band SAR data, being the most suitable operational data for biomass estimation [24–28]. The saturation level in tropical forests, using the L-band, varies around 50 t/ha to 200 t/ha [25,30,72]. Comparable to Thapa et al. [51], the present study uses backscatter values and, additionally, backscatter ratios and textures, which increases the saturation level to approximately 200–250 t/ha. A higher amount of ratios and textures based on backscatter values of different polarizations could further improve the model results, as shown in [51]. With an increasing model complexity, the correlation and the NSE also increase in a range from 0.62 to 0.84 and from 0.54 to 0.83, respectively.

Another limiting factor of the backscatter approach are the moisture conditions of soil and vegetation [73]. Especially in tropical forests, located in areas with a high amount of annual precipitation, the estimation of biomass based on backscatter can cause errors. To reduce humidity effects, scenes acquired during different periods of the year were averaged. Furthermore, images with a high influence of precipitation were excluded from the mosaics by incorporating TRMM data as selection criteria. Analogous to literature, variables based on HV backscatter were found as less influenced by changes in moisture and topography conditions at longer wavelengths and more sensitive to biomass than co-polarized data [21,25,30,34,70,72]. However, even with the use of variables based on HV polarization, moisture effects can cause differences in the biomass estimation for the different years [74]. The very dry conditions in 2007 may be an explanation for the higher backscatter saturation in 2007 and, thus, a better overall correlation. The lower R^2 of 2016 may not only result from the higher amount of precipitation in 2016, but also from the distribution of the validation samples. In contrast to the other years, the biomass range >200 t/ha contains 45% of all samples, which makes this class the most influential. The distinct underestimation of this AGB range is reflected in the overall R^2 of 2016. The given distribution of sample points originated because of the fire catastrophe in 2015, where a lot of areas within the reference biomass layer were burned. In order to reduce errors in the later modelling, those areas were excluded from the reference layer with the use of a MODIS hotspot product. The fires primarily occurred in areas that were already stressed by former burning or logging activities, accordingly in the lower biomass ranges, which leads to a lack of validation data in this class.

Furthermore, topography influences biomass estimation based on SAR data. To reduce possible errors caused by the effect of slope on radar backscatter, Mitchard et al. [26] suggested the use of a DEM, which is why we excluded AGB estimations in steep terrain with slopes $>10^\circ$, an area of 27% of the study area. Since the mountainous areas are barely affected by degradation and human activity, those regions were manually set to a biomass level of a healthy natural forest, 350 t/ha, as derived from LiDAR data. Additionally, settlement areas are not reliable in the final AGB maps. The high backscatter values due to double bounce effects result in backscatter values similar to those of forests. The use of an additional urban layer allows to flag settlements in a quality assurance layer, which we provided for each map.

Since models are minimizing the bias and overall error in order to get the best fit, the overestimation in lower biomass ranges results from the model adjustment due to the inability of estimating higher biomass ranges correctly [75].

In contrast to [33,76] a combination of C- and L-bands in the model of 2016 shows only minor improvement in comparison to a single-band approach. The C-band is more sensitive to variabilities in surface roughness resulting in improved modelling in burned areas or grass cover, so the combination of the C-band with the L-band slightly improves the correlation of estimated and predicted biomass compared to the use of the L-band alone.

II. Biomass estimation in tropical forests using the backscatter approach in Indonesia (Chapter I)

The final biomass maps have a spatial resolution of 100 m, which is much finer than other existing large-scale biomass maps from Indonesia by [30], yet with a comparable accuracy. Additionally, the model is transferable to other countries and regions, if precise reference data is available. The results have important implications for carbon-related projects, such as UN-REDD, and can help to achieve the objectives through supporting monitoring or risk managing systems. The fine-scaled resolution and the sensitivity to AGB variability of our products allow capturing even small-scale logging activities, and the results can be used as an early warning for more extensive changes of forests due to logging and fire vulnerability. Furthermore, the more accurate biomass maps can lead to more precise carbon estimations when used as input data for carbon-related models.

The results of the biomass estimation in tropical forests could be further improved using biomass estimation approaches based on coherence or phase instead of backscatter, but these methods are limited by data availability. A combined data approach using optical data/vegetation indices and SAR data could also enhance biomass estimation. The launch of new P-band satellites, like ESA's Earth Explorer Biomass in 2021, will allow a more accurate estimation of biomass in tropical forests.

5.2. Temporal Change Estimation

To perform a change analysis a comparability of the three biomass maps is required. This is best accomplished using the same processing steps, model, reference, and radar data type for each map in order to avoid differences resulting from the methods and data. The three biomass maps of this study were generated using the same processing steps and model, but included Sentinel-1 as an additional sensor in the calculations for 2016. Differences between the three maps could also occur since different reference layers for each year were used. Nevertheless, the use of contemporaneous reference layers is essential, because of rapid changes in the landscape (e.g., fires and logging) and allows a more accurate calibration of the model. The use of two MLR models in 2016 may also cause discrepancies, since two variables were excluded from the second model. Using a confidence interval of 95% to identify changes allows a reduction of errors during the change mapping.

The resulting change maps show a significant loss of forest and, thus, biomass during 2007–2009, 2009–2016, and for the overall period 2007–2016. In addition to fires, changes can result due to illegal logging activities. The maps provide a helpful tool for REDD+, as well as national projects, since small-scaled deforestation is detected in an accurate and low-cost way for the entirety of Kalimantan over a period of approximately ten years using three time steps for the first time.

6. Conclusions

It was shown that a multivariate linear regression model using C- and L-band SAR-derived ratios and textures is able to model biomass more precisely and at a better resolution than existing models in this region. Nevertheless, the applied backscatter approach is limited by the fact that SAR-based AGB estimation is defined by saturation effects of the backscatter signal in higher biomass ranges. Due to the use of textures and the large amount of reference data, the saturation level could be increased to approximately 250 t/ha. Accordingly, the estimated AGB maps show an underestimation in higher AGB ranges, but also an overestimation in lower biomass ranges. The correlation of field biomass and estimated biomass varies in a span between 0.69 and 0.77. The model is able to capture biomass variability due to different degradation stages in forested areas. Additionally, different disturbances in contrast to non-disturbed area or clear-cuts can be identified. A biomass overestimation in urban areas and a reduced accuracy because of relief effects (layover, radar shadow) in steep slopes are known issues using SAR data and have been corrected via additional data. Sentinel-1 data, which was additionally used in 2016, did slightly improve the results. Modelling AGB for three different time steps allowed the estimation of change products. The change maps detected, for the first time, deforestation in an accurate and low-cost way for the entirety of Kalimantan over a period of approximately ten years based on three different time steps. The much higher spatial resolution of all products (100 m) allows capturing even small-scaled variabilities in forested areas, with the layer providing important

II. Biomass estimation in tropical forests using the backscatter approach in Indonesia (Chapter I)

Remote Sens. 2018, 10, 831

18 of 22

assistance for recent UN-REDD projects and can help to achieve the objectives, as well as support monitoring and risk managing systems. Furthermore, the fine-scaled biomass maps can be used to estimate carbon stocks and carbon emission due to fires. The AGB estimation approach is transferable and allows modeling of biomass in other tropical forests with similar conditions in an accurate and less computationally intensive manner.

Author Contributions: S.L. and M.S. conceived and designed the experiments; A.B. and M.S. performed the experiments; A.B. and S.L. analyzed the data; F.S. supervised the project and commented on the manuscript; A.B., S.L. and F.S. discussed the results. A.B. wrote the paper.

Acknowledgments: The authors would like to thank the Japan Aerospace Agency for supplying ALOS PALSAR mosaics within the Kyoto and Carbon Initiative and the European Space Agency for providing Sentinel-1 data and for funding the study within the Globbiomass project (ESA contract no. 4000113100). We gratefully acknowledge Suwido Limin and his team from the Centre for International Co-operation in Management of Tropical Peatland (CIMTROP) as well as Hendrik Segah and his team from the University of Palangka Raya for the logistical support during the field surveys. The LiDAR dataset of 2007 was acquired by Kalteng Consultants. We would like to thank the Kalimantan Forests and Climate Partnership (KFCP) and AusAID (Australian Agency for International Development) for providing the 2011 LiDAR data. The Forests and Climate Change Programme (Forclime) lead by GIZ (Deutsche Gesellschaft für Internationale Zusammenarbeit) is highly acknowledged for providing field inventory and LiDAR data.

Conflicts of Interest: The authors declare no conflict of interest. The founding sponsors had no role in the design of the study; in the collection, analyses, or interpretation of data; in the writing of the manuscript; or in the decision to publish the results.

References

1. World Bank Group. Forest Area (% of Land Area): Indonesia. Available online: <https://data.worldbank.org/indicator/AG.LND.FRST.ZS?end=2015&locations=ID&type=shaded&view=map&year=2010> (accessed on 2 February 2018).
2. Page, S.E.; Hoscilo, A.; Langner, A.; Tansey, K.; Siegert, F.; Limin, S.; Rieley, J.O. Tropical peatland fires in Southeast Asia. In *Tropical Fire Ecology*; Springer Praxis Books: Berlin/Heidelberg, Germany, 2009.
3. Tyrrell, M.L.; Ashton, M.S.; Spalding, D.; Gentry, B. *Forests and Carbon: A Synthesis of Science, Management, and Policy for Carbon Sequestration in Forests*; Yale School Forestry & Environmental Studies: New Haven, CT, USA, 2009. Available online: <http://environment.yale.edu/publication-series/5947.html> (accessed on 7 March 2018).
4. Van der Werf, G.R.; Morton, D.C.; DeFries, R.S.; Olivier, J.G.J.; Kasibhatla, P.S.; Jackson, R.B.; Collatz, G.J.; Randerson, J.T. CO₂ emissions from forest loss. *Nat. Geosci.* **2009**, *2*, 737–738. [CrossRef]
5. IPCC 2014. *Climate Change 2014. Synthesis Report*; Contribution of Working Groups I, II and III to the Fifth Assessment Report of the Intergovernmental Panel on Climate Change; Core Writing Team, Pachauri, R.K., Meyer, L.A., Eds.; Intergovernmental Panel on Climate Change: Geneva, Switzerland, 2015.
6. MacKinnon, K.; Hatta, G.; Halim, H.; Mangalik, A. *The Ecology of Kalimantan: Indonesian Borneo*; Tuttle Publishing: New York, NY, USA, 2013.
7. Baccini, A.; Goetz, S.J.; Walker, W.S.; Laporte, N.T.; Sun, M.; Sulla-Menashe, D.; Hackler, J.; Beck, P.S.A.; Dubayah, R.; Friedl, M.A.; et al. Estimated carbon dioxide emissions from tropical deforestation improved by carbon-density maps. *Nat. Clim. Chang.* **2012**, *2*, 182–185. [CrossRef]
8. Page, S.E.; Rieley, J.O.; Banks, C.J. Global and regional importance of the tropical peatland carbon pool. *Glob. Chang. Biol.* **2011**, *17*, 798–818. [CrossRef]
9. Jaenicke, J.; Rieley, J.O.; Mott, C.; Kimman, P.; Siegert, F. Determination of the amount of carbon stored in Indonesian peatlands. *Geoderma* **2008**, *147*, 151–158. [CrossRef]
10. Olivier, J.G.J.; Janssens-Maenhout, G.; Muntean, M.; Peters, J.A.H.W. *Trends in Global CO₂ Emissions: 2016 Report*; PBL Netherlands Environmental Assessment Agency: Den Haag, The Netherlands, 2015.
11. Edwards, D.P.; Koh, L.P.; Laurance, W.F. Indonesia's REDD+ pact: Saving imperilled forests or business as usual? *Biol. Conserv.* **2012**, *151*, 41–44. [CrossRef]
12. Global Canopy Foundation. The REDD Desk. Available online: https://theredddesk.org/countries/search-countries-database?f%5B0%5D=type%3Aactivity&f%5B1%5D=field_project%3A1 (accessed on 7 February 2018).

II. Biomass estimation in tropical forests using the backscatter approach in Indonesia (Chapter I)

13. Goetz, S.; Dubayah, R. Advances in remote sensing technology and implications for measuring and monitoring forest carbon stocks and change. *Carbon Manag.* **2011**, *2*, 231–244. [[CrossRef](#)]
14. FAO. *Assessment of the Status of the Development of the Standards for the Terrestrial Essential Climate Variables; Biomass (T12)*; FAO: Rome, Italy, 2009.
15. Bojinski, S.; Verstraete, M.; Peterson, T.C.; Richter, C.; Simmons, A.; Zemp, M. The Concept of Essential Climate Variables in Support of Climate Research, Applications, and Policy. *Bull. Am. Meteorol. Soc.* **2014**, *95*, 1431–1443. [[CrossRef](#)]
16. Searle, E.B.; Chen, H.Y.H. Tree size thresholds produce biased estimates of forest biomass dynamics. *For. Ecol. Manag.* **2017**, *400*, 468–474. [[CrossRef](#)]
17. Joshi, N.; Mitchard, E.T.A.; Schumacher, J.; Johannsen, V.K.; Saatchi, S.; Fensholt, R. L-Band SAR Backscatter Related to Forest Cover, Height and Aboveground Biomass at Multiple Spatial Scales across Denmark. *Remote Sens.* **2015**, *7*, 4442–4472. [[CrossRef](#)]
18. Olesk, A.; Praks, J.; Antropov, O.; Zalite, K.; Arumäe, T.; Voormansik, K. Interferometric SAR Coherence Models for Characterization of Hemiboreal Forests Using TanDEM-X Data. *Remote Sens.* **2016**, *8*, 700. [[CrossRef](#)]
19. Koch, B. Status and future of laser scanning, synthetic aperture radar and hyperspectral remote sensing data for forest biomass assessment. *ISPRS J. Photogramm. Remote Sens.* **2010**, *65*, 581–590. [[CrossRef](#)]
20. Joshi, N.; Mitchard, E.T.A.; Brolly, M.; Schumacher, J.; Fernández-Landa, A.; Johannsen, V.K.; Marchamalo, M.; Fensholt, R. Understanding ‘saturation’ of radar signals over forests. *Nat. Sci. Rep.* **2017**, *7*, 3505. [[CrossRef](#)] [[PubMed](#)]
21. Ghasemi, N.; Reza Sahebi, M.; Mohammadzadeh, A. A review on biomass estimation methods using synthetic aperture radar data. *Int. J. Geomat. Geosci.* **2011**, *1*, 776–788.
22. Mermoz, S.; Le Toan, T.; Villard, L.; Réjou-Méchain, M.; Seifert-Granzin, J. Biomass assessment in the Cameroon savanna using ALOS PALSAR data. *Remote Sens. Environ.* **2014**, *155*, 109–119. [[CrossRef](#)]
23. Hamdan, O. Assessment of Alos Palsar L-Band SAR for Estimation of above Ground Biomass in Tropical Forests. Ph.D. Thesis, Univeriti Putra Malaysia, Serdang, Malaysia, 2015.
24. Wijaya, A. Evaluation of ALOS Palsar mosaic data for estimating stem volume and biomass: A case study from tropical rainforest of Central Indonesia. *J. Geogr.* **2009**, *2*, 14–21.
25. Hamdan, O.; Khali Aziz, H.; Rahman, A. Remotely sensed L-band SAR data for tropical forest biomass estimation. *J. Trop. For. Sci.* **2011**, *23*, 318–327.
26. Mitchard, E.T.A.; Saatchi, S.S.; Lewis, S.L.; Feldpausch, T.R.; Woodhouse, I.H.; Sonké, B.; Rowland, C.; Meir, P. Measuring biomass changes due to woody encroachment and deforestation/degradation in a forest–savanna boundary region of central Africa using multi-temporal L-band radar backscatter. *Remote Sens. Environ.* **2011**, *115*, 2861–2873. [[CrossRef](#)]
27. Ryan, C.M.; Hill, T.; Woollen, E.; Ghee, C.; Mitchard, E.; Cassells, G.; Grace, J.; Woodhouse, I.H.; Williams, M. Quantifying small-scale deforestation and forest degradation in African woodlands using radar imagery. *Glob. Chang. Biol.* **2012**, *18*, 243–257. [[CrossRef](#)]
28. Wijaya, A.; Liesenberg, V.; Susanti, A.; Karyanto, O.; Verchot, L.V. Estimation of Biomass Carbon Stocks over Peat Swamp Forests using Multi-Temporal and Multi-Polarizations SAR Data. *Int. Arch. Photogramm. Remote Sens. Spat. Inf. Sci.* **2015**, *XL-7/W3*, 551–556. [[CrossRef](#)]
29. Englhart, S.; Keuck, V.; Siegert, F. Aboveground biomass retrieval in tropical forests—The potential of combined X- and L-band SAR data use. *Remote Sens. Environ.* **2011**, *115*, 1260–1271. [[CrossRef](#)]
30. Saatchi, S.S.; Harris, N.L.; Brown, S.; Lefsky, M.; Mitchard, E.T.A.; Salas, W.; Zutta, B.R.; Buermann, W.; Lewis, S.L.; Hagen, S.; et al. Benchmark map of forest carbon stocks in tropical regions across three continents. *Proc. Natl. Acad. Sci. USA* **2011**, *108*, 9899–9904. [[CrossRef](#)] [[PubMed](#)]
31. Watanabe, M.; Motohka, T.; Shiraishi, T.; Thapa, R.B.; Kawano, N.; Shimada, M. Dependency of forest biomass on full Polarimetric parameters obtained from L-band SAR data for a natural forest in Indonesia. In Proceedings of the 2013 IEEE International Geoscience and Remote Sensing Symposium (IGARSS), Melbourne, Australia, 21–26 July 2013; pp. 3919–3922. [[CrossRef](#)]
32. Kumar, S.; Khati, U.G.; Chandola, S.; Agrawal, S.; Kushwaha, S.P.S. Polarimetric SAR Interferometry based modeling for tree height and aboveground biomass retrieval in a tropical deciduous forest. *Adv. Space Res.* **2017**, *60*, 571–586. [[CrossRef](#)]

II. Biomass estimation in tropical forests using the backscatter approach in Indonesia (Chapter I)

33. Hoekman, D.H.; Quinones, M.J. *Land Cover Type and Forest Biomass Assessment in the Colombian Amazon. 1997 International Geoscience and Remote Sensing Symposium 3–8 August 1997, Singapore International Convention & Exhibition Centre, Singapore Remote Sensing—A Scientific Vision for Sustainable Development*; Institute of Electrical and Electronics Engineers: Piscataway, NJ, USA; IEEE Service Center Distributor: New York, NY, USA, 1997.
34. Pandey, U.; Kushwaha, S.P.S.; Kachhwaha, T.S.; Kunwar, P.; Dadhwal, V.K. Potential of Envisat ASAR data for woody biomass assessment. *Trop. Ecol.* **2010**, *51*, 117–124.
35. Mitchard, E.T.A.; Saatchi, S.S.; Baccini, A.; Asner, G.P.; Goetz, S.J.; Harris, N.L.; Brown, S. Uncertainty in the spatial distribution of tropical forest biomass: A comparison of pan-tropical maps. *Carbon Balance Manag. J.* **2013**, *8*, 1–13. [[CrossRef](#)] [[PubMed](#)]
36. Avitabile, V.; Herold, M.; Heuvelink, G.B.M.; Lewis, S.L.; Phillips, O.L.; Asner, G.P.; Armston, J.; Ashton, P.S.; Banin, L.; Bayol, N.; et al. An integrated pan-tropical biomass map using multiple reference datasets. *Glob. Chang. Biol.* **2016**, *22*, 1406–1420. [[CrossRef](#)] [[PubMed](#)]
37. Posa, M.R.C.; Wijedasa, L.S.; Corlett, R.T. Biodiversity and Conservation of Tropical Peat Swamp Forests. *BioScience* **2011**, *61*, 49–57. [[CrossRef](#)]
38. Pearson, T.; Walker, S.; Brown, S. Sourcebook for Land Use, Land-use Change and Forestry Projects. Available online: <https://theredddesk.org/resources/sourcebook-land-use-land-use-change-and-frestry-projects> (accessed on 1 December 2017).
39. Chave, J.; Andalo, C.; Brown, S.; Cairns, M.A.; Chambers, J.Q.; Eamus, D.; Fölster, H.; Fromard, F.; Higuchi, N.; Kira, T.; et al. Tree allometry and improved estimation of carbon stocks and balance in tropical forests. *Oecologia* **2005**, *145*, 87–99. [[CrossRef](#)] [[PubMed](#)]
40. Englhart, S.; Jubanski, J.; Siegert, F. Quantifying Dynamics in Tropical Peat Swamp Forest Biomass with Multi-Temporal LiDAR Datasets. *Remote Sens.* **2013**, *5*, 2368–2388. [[CrossRef](#)]
41. NASA; JAXA. Tropical Rainfall Measuring Mission. Available online: <https://pmm.nasa.gov/trmm> (accessed on 27 April 2018).
42. NASA. Near Real-Time and MCD14DL MODIS Active Fire Detections (SHP Format): Data Set. Available online: <https://earthdata.nasa.gov/earth-observation-data/near-real-time/firms/c6-mcd14dl> (accessed on 27 April 2018).
43. Giglio, L.; Descloitres, J.; Justice, C.O.; Kaufman, Y.J. An Enhanced Contextual Fire Detection Algorithm for MODIS. *Remote Sens. Environ.* **2003**, *87*, 273–282. [[CrossRef](#)]
44. Esri, Garmin International, Inc. World Water Bodies Layer. Available online: <https://www.arcgis.com/home/item.html?id=e750071279bf450cbd510454a80f2e63> (accessed on 27 April 2018).
45. European Space Agency. CCI Land Cover. Available online: <http://maps.elie.ucl.ac.be/CCI/viewer/download.php> (accessed on 27 April 2018).
46. Hughes, R.F.; Kauffman, J.B.; Jaramillo, V.J. Biomass, Carbon, and Nutrient Dynamics of Secondary Forests in a Humid Tropical Region of Mexico. *Ecology* **1999**, *80*, 1892–1907.
47. Jubanski, J.; Ballhorn, U.; Kronseder, K.; Franke, J.; Siegert, F. Detection of large above-ground biomass variability in lowland forest ecosystems by airborne LiDAR. *Biogeosciences* **2013**, *10*, 3917–3930. [[CrossRef](#)]
48. Solberg, S.; Astrup, R.; Gobakken, T.; Næsset, E.; Weydahl, D.J. Estimating spruce and pine biomass with interferometric X-band SAR. *Remote Sens. Environ.* **2010**, *114*, 2353–2360. [[CrossRef](#)]
49. Ballhorn, U.; Jubanski, J.; Siegert, F. ICESat/GLAS Data as a Measurement Tool for Peatland Topography and Peat Swamp Forest Biomass in Kalimantan, Indonesia. *Remote Sens.* **2011**, *3*, 1957–1982. [[CrossRef](#)]
50. Quegan, S.; Le Toan, T.; Yu, J.J.; Ribbes, F.; Floury, N. Multitemporal ERS SAR analysis applied to forest mapping. *IEEE Trans. Geosci. Remote Sens.* **2000**, *38*, 741–753. [[CrossRef](#)]
51. Thapa, R.B.; Watanabe, M.; Motohka, T.; Shimada, M. Potential of high-resolution ALOS-PALSAR mosaic texture for aboveground forest carbon tracking in tropical region. *Remote Sens. Environ.* **2015**, *160*, 122–133. [[CrossRef](#)]
52. Haralick, R.M. Statistical and structural approaches to texture. *Proc. IEEE* **1979**, *67*, 786–804. [[CrossRef](#)]
53. Englhart, S.; Keuck, V.; Siegert, F.; Englhart, S.; Keuck, V.; Siegert, F. Modeling Aboveground Biomass in Tropical Forests Using Multi-Frequency SAR Data—A Comparison of Methods. *IEEE J. Sel. Top. Appl. Earth Obs. Remote Sens.* **2012**, *5*, 298–306. [[CrossRef](#)]

II. Biomass estimation in tropical forests using the backscatter approach in Indonesia (Chapter I)

54. Asner, G.P.; Powell, G.V.N.; Mascaro, J.; Knapp, D.E.; Clark, J.K.; Jacobson, J.; Kennedy-Bowdoin, T.; Balaji, A.; Paez-Acosta, G.; Victoria, E.; et al. High-resolution forest carbon stocks and emissions in the Amazon. *Proc. Natl. Acad. Sci. USA* **2010**, *107*, 16738–16742. [[CrossRef](#)] [[PubMed](#)]
55. Nash, J.E.; Sutcliffe, J.V. River Flow Forecasting Through Conceptual Models Part I- A Discussion of Principles. *J. Hydrol.* **1970**, *10*, 282–290. [[CrossRef](#)]
56. Holm, S.; Nelson, R.; Ståhl, G. Hybrid three-phase estimators for large-area forest inventory using ground plots, airborne lidar, and space lidar. *Remote Sens. Environ.* **2017**, *197*, 85–97. [[CrossRef](#)]
57. Saarela, S.; Holm, S.; Grafström, A.; Schnell, S.; Næsset, E.; Gregoire, T.G.; Nelson, R.F.; Ståhl, G. Hierarchical model-based inference for forest inventory utilizing three sources of information. *Ann. For. Sci.* **2016**, *73*, 895–910. [[CrossRef](#)]
58. Chave, J.; Condit, R.; Lao, S.; Caspersen, J.P.; Foster, R.B.; Hubbel, S.P. Spatial and temporal variation of biomass in a tropical forest: Results from a large census plot in Panama. *J. Ecol.* **2003**, *91*, 240–252. [[CrossRef](#)]
59. Frazer, G.W.; Magnussen, S.; Wulder, M.A.; Niemann, K.O. Simulated impact of sample plot size and co-registration error on the accuracy and uncertainty of LiDAR-derived estimates of forest stand biomass. *Remote Sens. Environ.* **2011**, *115*, 636–649. [[CrossRef](#)]
60. Levick, S.R.; Hessenmöller, D.; Schulze, E.-D. Scaling wood volume estimates from inventory plots to landscapes with airborne LiDAR in temperate deciduous forest. *Carbon Balance Manag.* **2016**, *11*, 7. [[CrossRef](#)] [[PubMed](#)]
61. Zolkos, S.G.; Goetz, S.J.; Dubayah, R. A meta-analysis of terrestrial aboveground biomass estimation using lidar remote sensing. *Remote Sens. Environ.* **2013**, *128*, 289–298. [[CrossRef](#)]
62. Kachamba, D.; Ørka, H.; Næsset, E.; Eid, T.; Gobakken, T. Influence of Plot Size on Efficiency of Biomass Estimates in Inventories of Dry Tropical Forests Assisted by Photogrammetric Data from an Unmanned Aircraft System. *Remote Sens.* **2017**, *9*, 610. [[CrossRef](#)]
63. Ruiz, L.; Hermosilla, T.; Mauro, F.; Godino, M. Analysis of the Influence of Plot Size and LiDAR Density on Forest Structure Attribute Estimates. *Forests* **2014**, *5*, 936–951. [[CrossRef](#)]
64. Rafael, M.N.-C.; Eduardo, G.-F.; Jorge, G.-G.; Carlos, J.; Ceacero, R.; Rocío, H.-C. Impact of plot size and model selection on forest biomass estimation using airborne LiDAR: A case study of pine plantations in southern Spain. *J. For. Sci.* **2017**, *63*, 88–97. [[CrossRef](#)]
65. Mauya, E.W.; Hansen, E.H.; Gobakken, T.; Bollandsås, O.M.; Malimbwi, R.E.; Næsset, E. Effects of field plot size on prediction accuracy of aboveground biomass in airborne laser scanning-assisted inventories in tropical rain forests of Tanzania. *Carbon Balance Manag.* **2015**, *10*, 10. [[CrossRef](#)] [[PubMed](#)]
66. Urbazaev, M.; Thiel, C.; Cremer, F.; Dubayah, R.; Migliavacca, M.; Reichstein, M.; Schmullius, C. Estimation of forest aboveground biomass and uncertainties by integration of field measurements, airborne LiDAR, and SAR and optical satellite data in Mexico. *Carbon Balance Manag.* **2018**, *13*, 5. [[CrossRef](#)] [[PubMed](#)]
67. Zhou, Y.; Hong, W.; Yirong, W. Analysis of Temporal Decorrelation in Dual-Baseline Polinsar Vegetation Parameter Estimation. In Proceedings of the IGARSS 2008 IEEE International Geoscience and Remote Sensing Symposium, Boston, MA, USA, 7–11 July 2008.
68. Hamdan, O.; Khali Aziz, H.; Mohd Hasmadi, I. L-band ALOS PALSAR for biomass estimation of Matang Mangroves, Malaysia. *Remote Sens. Environ.* **2014**, *155*, 69–78. [[CrossRef](#)]
69. Suresh, M.; Kiran Chand, T.R.; Fararoda, R.; Jha, C.S.; Dadhwal, V.K. Forest above ground biomass estimation and forest/non-forest classification for Odisha, India, using L-band Synthetic Aperture Radar (SAR) data. *Int. Arch. Photogramm. Remote Sens. Spat. Inf. Sci.* **2014**, *XL-8*, 651–658. [[CrossRef](#)]
70. Mitchard, E.T.A.; Saatchi, S.S.; Woodhouse, I.H.; Nangendo, G.; Ribeiro, N.S.; Williams, M.; Ryan, C.M.; Lewis, S.L.; Feldpausch, T.R.; Meir, P. Using satellite radar backscatter to predict above-ground woody biomass: A consistent relationship across four different African landscapes. *Geophys. Res. Lett.* **2009**, *36*, L23401. [[CrossRef](#)]
71. Antropov, O.; Rauste, Y.; Häme, T.; Praks, J. Polarimetric ALOS PALSAR Time Series in Mapping Biomass of Boreal Forests. *Remote Sens.* **2017**, *9*, 999. [[CrossRef](#)]
72. Hamdan, O.; Mohd Hasmadi, I.; Khali Aziz, H.; Norizah, K.; Helmi Zulhaidi, M.S. L-Band saturation level for above-ground Biomass of Dipterocarp forests in Peninsula Malaysia. *J. Trop. For. Sci.* **2015**, *27*, 388–399.
73. Thoma, D.P.; Moran, M.S.; Bryant, R.; Rahman, M.; Holifield-Collins, C.D.; Skirvin, S.; Sano, E.E.; Slocum, K. Comparison of four models to determine surface soil moisture from C-band radar imagery in a sparsely vegetated semiarid landscape. *Water Resour. Res.* **2006**, *42*, 4325. [[CrossRef](#)]

II. Biomass estimation in tropical forests using the backscatter approach in Indonesia (Chapter I)

Remote Sens. **2018**, *10*, 831

22 of 22

74. Lucas, R.; Armston, J.; Fairfax, R.; Fensham, R.; Accad, A.; Carreiras, J.; Kelley, J.; Bunting, P.; Clewley, D.; Bray, S.; et al. An Evaluation of the ALOS PALSAR L-Band Backscatter—Above Ground Biomass Relationship Queensland, Australia: Impacts of Surface Moisture Condition and Vegetation Structure. *IEEE J. Sel. Top. Appl. Earth Obs. Remote Sens.* **2010**, *3*, 576–593. [[CrossRef](#)]
75. Xu, L.; Saatchi, S.S.; Yang, Y.; Yu, Y.; White, L. Performance of non-parametric algorithms for spatial mapping of tropical forest structure. *Carbon Balance Manag.* **2016**, *11*, 18. [[CrossRef](#)] [[PubMed](#)]
76. Naidoo, L.; Mathieu, R.; Main, R.; Kleynhans, W.; Wessels, K.; Asner, G.; Leblon, B. Savannah woody structure modelling and mapping using multi-frequency (X-, C- and L-band) Synthetic Aperture Radar data. *ISPRS J. Photogramm. Remote Sens.* **2015**, *105*, 234–250. [[CrossRef](#)]



© 2018 by the authors. Licensee MDPI, Basel, Switzerland. This article is an open access article distributed under the terms and conditions of the Creative Commons Attribution (CC BY) license (<http://creativecommons.org/licenses/by/4.0/>).

III. Biomass estimation in tropical forests using the backscatter approach in different biomes (Chapter II)

Rodríguez-Veiga, P., Quegan, S., Carreiras, J., Persson H.J., Fransson, J.E.S., Hoscilo A., Ziólkowski D., Stereńczak, K., Lohberger S., Stängel, M., Berninger, A., Siegert, F., Avitabile V., Herold, M. Mermoz, S., Bouvet, A., Le Toan, T., Carvalhais N., Santoro, M., Cartus, O., Rauste, Y., Mathieu, R., Asner, G.P., Thiel, C., Pathe, C., Schmullius, C., Seifert, F.M., Tansey, K., & H. Balzter (2019) Forest biomass retrieval approaches from Earth Observation in different biomes. *International Journal of Applied Earth Observation and Geoinformation*, 77, 53-68.

A PDF of this article is available at:

<https://www.sciencedirect.com/science/article/pii/S0303243418307104>

III. Biomass estimation in tropical forests using the backscatter approach in different biomes (Chapter II)

Int J Appl Earth Obs Geoinformation 77 (2019) 53–68



Contents lists available at ScienceDirect

Int J Appl Earth Obs Geoinformation

journal homepage: www.elsevier.com/locate/jag



Forest biomass retrieval approaches from earth observation in different biomes



Pedro Rodríguez-Veiga^{a,b,*}, Shaun Quegan^{b,c}, Joao Carreiras^{b,c}, Henrik J. Persson^d, Johan E.S. Fransson^d, Agata Hoscilo^e, Dariusz Ziólkowski^e, Krzysztof Stereńczak^f, Sandra Lohberger^g, Matthias Stängel^g, Anna Berninger^g, Florian Siegert^{g,h}, Valerio Avitabileⁱ, Martin Herold^j, Stéphane Mermoz^j, Alexandre Bouvet^j, Thuy Le Toan^j, Nuno Carvalhais^{k,l}, Maurizio Santoro^m, Oliver Cartus^m, Yrjö Rausteⁿ, Renaud Mathieu^{o,p}, Gregory P. Asner^q, Christian Thiel^r, Carsten Pathe^s, Chris Schmullius^s, Frank Martin Seifert^t, Kevin Tansey^u, Heiko Balzter^{a,b}

^a University of Leicester, Centre for Landscape and Climate Research, United Kingdom

^b National Centre for Earth Observation, United Kingdom

^c University of Sheffield, United Kingdom

^d Sveriges Lantbruksuniversitet, Sweden

^e Institute of Geodesy and Cartography, Poland

^f Forest Research Institute, Poland

^g Remote Sensing Solutions, Germany

^h Ludwig-Maximilians-University Munich, Germany

ⁱ Wageningen University & Research, the Netherlands

^j CESBIO, Université de Toulouse, CNES, CNRS, IRD, UPS, France

^k Max Planck Institute for Biogeochemistry, Germany

^l Universidade NOVA de Lisboa, CENSE, Departamento de Ciências e Engenharia do Ambiente, Faculdade de Ciências e Tecnologia, Portugal

^m GAMMA Remote Sensing, Switzerland

ⁿ VTT Technical Research Centre of Finland Ltd, Finland

^o CSIR, South Africa

^p University of Pretoria, Department of Geography, Geomatics and Meteorology, South Africa

^q Carnegie Institution for Science, USA

^r German Aerospace Agency, Germany

^s Friedrich-Schiller-University Jena, Germany

^t European Space Agency ESRIN, Italy

ARTICLE INFO

Keywords:

Aboveground biomass
Forest biomes
Forest plots
Carbon cycle
Optical
SAR
LIDAR

ABSTRACT

The amount and spatial distribution of forest aboveground biomass (AGB) were estimated using a range of regionally developed methods using Earth Observation data for Poland, Sweden and regions in Indonesia (Kalimantan), Mexico (Central Mexico and Yucatan peninsula), and South Africa (Eastern provinces) for the year 2010. These regions are representative of numerous forest biomes and biomass levels globally, from South African woodlands and savannas to the humid tropical forest of Kalimantan. AGB retrieval in each region relied on different sources of reference data, including forest inventory plot data and airborne LiDAR observations, and used a range of retrieval algorithms. This is the widest inter-comparison of regional-to-national AGB maps to date in terms of area, forest types, input datasets, and retrieval methods. The accuracy assessment of all regional maps using independent field data or LiDAR AGB maps resulted in an overall root mean square error (RMSE) ranging from 10 t ha^{-1} to 55 t ha^{-1} (37% to 67% relative RMSE), and an overall bias ranging from -1 t ha^{-1} to $+5 \text{ t ha}^{-1}$ at pixel level. The regional maps showed better agreement with field data than previously developed and widely used pan-tropical or northern hemisphere datasets. The comparison of accuracy assessments showed commonalities in error structures despite the variety of methods, input data, and forest biomes. All regional retrievals resulted in overestimation (up to 63 t ha^{-1}) in the lower AGB classes, and underestimation (up to 85 t ha^{-1}) in the higher AGB classes. Parametric model-based algorithms present advantages due to their low

* Corresponding author at: University of Leicester, United Kingdom.

E-mail address: pedro.rodriguez@leicester.ac.uk (P. Rodríguez-Veiga).

<https://doi.org/10.1016/j.jag.2018.12.008>

Received 24 July 2018; Received in revised form 6 December 2018; Accepted 21 December 2018

Available online 02 January 2019

0303-2434/ © 2019 The Authors. Published by Elsevier B.V. This is an open access article under the CC BY license

(<http://creativecommons.org/licenses/by/4.0/>).

III. Biomass estimation in tropical forests using the backscatter approach in different biomes (Chapter II)

demand on in situ data compared to non-parametric algorithms, but there is a need for datasets and retrieval methods that can overcome the biases at both ends of the AGB range. The outcomes of this study should be considered when developing algorithms to estimate forest biomass at continental to global scale level.

1. Introduction

1.1. Background

Forests cover around one third of the Earth's land surface, are an essential socio-cultural element of modern society, support biodiversity and influence the climate system via coupled carbon-water-energy cycles (Bonan, 2008). Quantifying forest aboveground woody biomass (AGB), i.e. the amount of woody matter within a forest, has profound social and economic importance, since it is a source of materials and energy for direct human use, and its structure and temporal dynamics exert substantial influence on the functioning of terrestrial ecosystems, with direct impacts on biodiversity, as well as on the carbon and energy cycles and consequently the whole Earth system (e.g. Bonan, 2008; Le Quéré et al., 2018; Pan et al., 2011). As such, AGB can be used to evaluate the dynamics of global vegetation and Earth system models (e.g. Thurner et al., 2017; Carvalhais et al., 2014), was recognised by the Global Climate Observing System (GCOS) as an Essential Climate Variable (ECV) (Bojinski et al., 2014), and plays an important role in several essential biodiversity variables (EBV) (Pereira et al., 2013). However, quantification of AGB still presents a scientific challenge with significant implications for our current knowledge about the Earth system (Pan et al., 2011; Le Quéré et al., 2018).

Knowledge of the spatial distribution of forest AGB is typically derived from ground measurements collected by national forest inventories. From these, regional- to national-scale summary data are generated for the FAO's quinquennial Global Forest Resource Assessment (FRA) reports (FAO, 2005, 2010; FAO, 2015), aiming at giving a global portrait of biomass stocks and their changes in time. Vast areas covered by forests mean that ground-based forest inventories need a large amount of resources to provide accurate information on the extent, spatial distribution and dynamics of forest AGB. However, forest inventory data in developing countries can be fairly inaccurate (Saatchi and Moghaddam, 2000) and often many years out of date (Shvidenko and Schepaschenko, 2014). A review of the country FRA reports (FAO, 2010) showed that 45 countries (i.e. around 20%) indicated high quality for the reference data used (mostly located in Europe and North America), while 171 did not report on quality (most African and Asian countries). In addition, forest inventory data are not always comparable and biomass estimates may be biased due to differing national forest definitions and differences in methods used to produce the estimates, such as the choice of the minimum tree diameter sampled (Searle and Chen, 2017) and plot size (Réjou-Méchain et al., 2014). The only practical approach for consistent global or regional woody biomass estimation therefore lies in systematic use of Earth Observation (EO) data, either in parameterised model-based approaches or in combination with high-quality reference data. Satellite data have long been used for forest cover mapping, clear-cut or burnt area monitoring and detection of disturbances (Hansen et al., 2013; Healey et al., 2005; Fraser and Li, 2002; Rignot et al., 1997). However, without biomass information this is insufficient to quantify the role of forests in the global carbon and energy cycles and other biogeochemical cycles. In addition, financial mechanisms aiming to reduce emissions and enhance carbon stocks, such as the Reducing Emissions from Deforestation and Forest Degradation (REDD+) initiative and carbon trading schemes, require credible and consistent measurement, reporting and verification (MRV) systems that are spatially explicit with a wall-to-wall extension and provide a full carbon account of forest ecosystems (Steffen et al., 1998).

1.2. Current status of biomass estimation from space

Studies aiming at wall-to-wall estimation of AGB at regional and global scale have used passive optical, active or passive microwave, and LIDAR data obtained from Earth Observation space platforms either stand-alone or in synergy (e.g. Saatchi et al., 2011; Baccini et al., 2012; Thurner et al., 2014; Gallaun et al., 2010; Hu et al., 2016; Liu et al., 2015). Multispectral optical imagery contains information on the photosynthetic parts of vegetation rich in chlorophyll, while microwave active sensors, such as Synthetic Aperture Radar (SAR), contain information on the dielectric (essentially moisture content) and structural properties of objects, soil surface and plants. The main advantage of microwave radar sensors is that, unlike optical imagery, radar images are unaffected by cloud cover, allowing usable image acquisitions even in the cloudiest places on Earth. Spaceborne LiDAR sensors, on the other hand, give a sampled retrieval pattern along the orbit and to measure elapsed time between emitted and received light pulses which can be used to estimate forest canopy height at each footprint location. However, these datasets present different degrees of saturation to AGB, where saturation refers to the AGB level at which the sensitivity of the signal (i.e. backscatter, reflectance) becomes too small to be measurable, or where the signal fails to penetrate the canopy (Fagan and DeFries, 2009). This is particularly relevant for dense tropical forest, which is a key biome where accurate biomass information is needed.

The search for consistent approaches over forested areas in the tropics prompted the use of satellite data calibrated against in situ biomass, with special emphasis on forest height estimates derived from the first spaceborne LiDAR, the Geoscience Laser Altimeter System (GLAS) on board the Ice, Cloud and land Elevation Satellite (ICESat) (Lefsky, 2010). This led to the development of two pan-tropical biomass maps (Saatchi et al., 2011; Baccini et al., 2012) at reporting grid size of 1 km and 500 m respectively. The former reported a relative RMSE at pixel level of approximately 30%, while the latter reported similar figures in terms of RMSE (38–50 t ha⁻¹). These maps exhibited significant regional differences, although these decreased when biomass estimates were aggregated to country or biome scale (Mitchard et al., 2013, 2014; Rodríguez-Veiga et al., 2016).

Avitabile et al. (2016) fused Saatchi et al. (2011), and Baccini et al. (2012) datasets into a 1 km pan-tropical map using a bias-removal approach by incorporating additional field observations and locally-calibrated high-resolution biomass maps. The bias in the overall mean AGB was reduced to + 5 t ha⁻¹, compared with the biases in the input maps of + 21 t ha⁻¹ and + 28 t ha⁻¹ respectively.

Using very long time series of C-band radar data from Envisat ASAR, Santoro et al. (2015a) produced a Growing Stock Volume (GSV) map for the northern hemisphere at 1 km spatial resolution. The relative RMSE of the retrievals at provincial level was between 12% and 45% (average 29%) when compared to National Forest Inventory data from the major forested countries. This map provided the basis for a carbon stock map of the boreal and temperate forests (Thurner et al., 2014).

A first composite global dataset of forest AGB was developed within the European Commission-funded GEO-CARBON project. The product merged, at a pixel size of 0.01°, the Saatchi et al. (2011), and Baccini et al. (2012) pan-tropical datasets with the boreal and temperate dataset (Santoro et al., 2015a; Thurner et al., 2014) and used the IPCC Tier 1 biomass values for the few remaining areas not covered by these datasets (Avitabile et al., 2014, 2016). This exercise, despite being hindered by limitations in the input EO data used by individual biomass maps, approximations in the retrieval approaches and the fact that the individual maps were based on data acquired at different times between

III. Biomass estimation in tropical forests using the backscatter approach in different biomes (Chapter II)

P. Rodríguez-Veiga et al.

Int J Appl Earth Obs Geoinformation 77 (2019) 53–68

2000 and 2010, is still the most consistent global AGB map to date. Hu et al. (2016) also published a global AGB map at 1 km resolution derived using GLAS metrics interpolations, MODIS NDVI and Land Cover products and the SRTM DEM, together with climate data. However, the dataset used to calibrate the map consisted of 3348 forest inventory plots of different sizes (including very small plots of 0.05 ha). The calibration dataset was also geographically biased as the plots were mostly located in continental China (> 55% of plots) and Brazil (23% of plots), while almost no plots were used from Europe, North America, Australia, and Africa. These issues might explain the large differences observed in this map when compared to previous global and pan-tropical maps (Rodríguez-Veiga et al., 2017; Hu et al., 2016).

Liu et al. (2015) used vegetation optical depth (VOD) retrieved from several passive microwave satellite sensors to map time series of AGB for all vegetation types globally over the period 1993–2012 at 27.5 km resolution. Unfortunately, this approach was calibrated using the Saatchi et al. (2011) map, which added the uncertainties from this product to the final map, and make it difficult to validate due to the coarse resolution of the product.

At continental scale, MODIS data and forest inventory plots have been used to map AGB over Europe (Gallaun et al., 2010) at 500 m resolution, and Africa (Baccini et al., 2008) at 1 km resolution. The woodlands and savannas of Africa were also mapped at 25 m spatial resolution using ALOS PALSAR data (Bouvet et al., 2018).

At national and regional scales, several examples have been published, such as for Mexico (Rodríguez-Veiga et al., 2016; Cartus et al., 2014), Canada (Beaudoin et al., 2014), Cameroon (Mermoz et al., 2014), China (Yin et al., 2015; Piao et al., 2005; Liu et al., 2012), the Amazon basin (Saatchi et al., 2007), Russia (Houghton et al., 2007), USA (Kelldorfer et al., 2011) and Colombia (Anaya et al., 2009), with spatial resolutions ranging from 30 m to 1 km and in most cases using a combination of optical and SAR imagery. Regional approaches use field AGB measurements to calibrate the algorithms, often complemented with airborne LIDAR datasets (Asner et al., 2014, 2013; Perrin et al., 2016; Lu et al., 2012). These regionally-calibrated products can use a wider variety of datasets, as well as regional expertise, to provide the best possible estimates of biomass. In contrast, global, pantropical or continental products suffer from limitations in the amount and representativeness of data available for calibration and validation. Pantropical maps from Saatchi et al. (2011), and Baccini et al. (2012) circumvented the paucity of ground data for calibrating their non-parametric machine learning approaches at large scale by using AGB estimated from LiDAR footprints from the space-borne ICESAT-GLAS instrument. However, they still used a fair amount of ground-based values of AGB to calibrate the relationship between AGB and LiDAR footprint metrics. An algorithm that avoids the use of in situ data for model training is the BIOMASAR algorithm (Santoro et al., 2015a, 2011; Cartus et al., 2012); the algorithm is, however, constrained with information on maximum biomass which are derived from inventory data, regional and national statistics, as well as remote sensing-based biomass estimates (Santoro et al., 2015a, 2011; Cartus et al., 2012). Inaccurate data sources ultimately translate into local estimation biases (Santoro et al., 2011).

The long list of AGB datasets presented above highlights that biomass mapping methods are largely driven by data availability and are scale-dependent. National and regional products can be generated by different parametric and non-parametric approaches. Non-parametric methods, such as machine learning techniques, usually out-perform parametric approaches (Evans and Cushman, 2009) and are preferred at national and regional level if enough ground data are available. At global or continental level the lack of representative in situ measurements is the motivation for using physically-based approaches that require few ground data (if any).

This paper describes a diverse set of regional approaches to AGB mapping in different biomes carried out during the European Space Agency (ESA) Data User Element GlobBiomass project (GlobBiomass,

2015; Schullius et al., 2015; Balzter et al., 2016; Schullius, 2017). This study aimed to produce spatially consistent and accurate maps of AGB, using all available EO data and regional knowledge with the objective of supporting the development of global biomass retrieval algorithms and the assessment of thereof resulting estimates. These maps can be used for direct estimation of carbon emission factors or emissions contributing to greenhouse gas inventories. Further aims were: i) to better understand the strengths and weaknesses of existing methods to map AGB using available EO datasets, ii) to establish how differences in forest structure and reference data affect methods to invert EO data to AGB. Five regional AGB maps derived using reference data and EO imagery and various retrieval methods were generated for the year 2010 at 25–100 m spatial resolution. The regions were selected to encompass a wide range of biomes and forest types. Each region was at least 300,000 km² in size; it was either nationwide for Poland (temperate forest) and Sweden (boreal forest), or covered a substantial part of Indonesia (Kalimantan, tropical forest), Mexico (the Yucatan peninsula & Central Mexico, tropical forest-woodland transition), and South Africa (Eastern forest belt, subtropical dry forest). All maps were evaluated quantitatively against an independent dataset, and qualitatively by local experts. They were also compared with existing continental scale AGB maps (Saatchi et al., 2011; Baccini et al., 2012; Thurner et al., 2014) where these overlapped the study areas.

2. Study regions

The study regions cover the most common range of woody AGB from low (< 50 t ha⁻¹) to high (> 300 t ha⁻¹) and are representative of major climates and forested biomes, including boreal, temperate, dry tropical savanna and wet tropics (Fig. 1).

Sweden is mostly situated in the boreal region, while Poland lies in the temperate forest zone. Sweden and Poland occupy approximately 447,000 km² and 313,000 km², of which 60% and 30% are forests, respectively. Coniferous forests predominate, though broadleaved forests occupy a significant area in Poland.

The study areas in Central Mexico, the Yucatan peninsula and Kalimantan represent a wide variety of tropical and subtropical forest

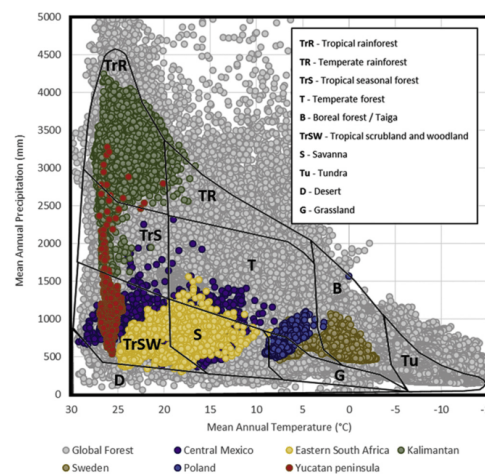


Fig. 1. Mean annual precipitation vs. mean annual temperature (Fick and Hijmans (2017) for global forests and study sites sampled at 0.5° grid scale. The climate space is divided into global terrestrial biomes (Whittaker, 1962, 1970). The global distribution of forests is according to the Global Land Cover (GLC2000) map (Bartholomé and Belward, 2005).

III. Biomass estimation in tropical forests using the backscatter approach in different biomes (Chapter II)

ecosystems. The Yucatan peninsula study area with approximately 160,000 km² comprises a mix of tropical moist, tropical dry forests and mangroves, whilst an area of 353,000 km² in Central Mexico covers subtropical coniferous forest, tropical dry forest, tropical moist forest, xeric shrublands, and includes some of the forests with the highest biomass density in Mexico (the Oyamel forest). The Indonesian part of Borneo (Kalimantan) covers 73% of Borneo's land mass (approximately 540,000 km²). The ecosystems of Kalimantan include different forest types: mangrove forests, peat swamp and freshwater swamp forests, the most extensive extent of heath forests in Southeast Asia, lowland dipterocarp forests, ironwood forests, forests on limestone and ultrabasic soils, hill dipterocarp forests and various montane formations (MacKinnon et al., 1996).

The South African study area of approximately 334,000 km² is situated along a 1300 km North-South transect running to the East of the country next to Zimbabwe, Mozambique, Swaziland, and the Indian Ocean, and is dominated by forested landscape. This area contains various forest types: savanna (68% of the area), commercial plantations, and scattered remnants of indigenous dense forests (Mucina and Rutherford, 2006).

3. Data

Remote sensing imagery from different airborne and satellite sensors (optical, LiDAR and SAR) were utilized in this study (Table 1). Except for Sweden, the main dataset used was the freely available ALOS PALSAR 2009 and 2010 mosaics of gamma nought ($\gamma^0 = \sigma^0 / \cos\theta$, where σ^0 is the radar backscattering coefficient and $\cos\theta$ is the local incidence angle) produced by JAXA at 25 m pixel spacing in HH and HV polarizations (Shimada et al., 2014). The ALOS PALSAR mosaics are processed according to a standard protocol (Shimada et al., 2014) which involves calibration, multi-looking (16 looks), projection, orthorectification and slope correction using the Shuttle Radar Topography Mission (SRTM) Digital Elevation Model (DEM) data. A destriping process (Shimada and Isoguchi, 2002) was also applied to try and equalise intensity differences between neighbouring strips normally attributed to seasonal and daily differences in soil moisture conditions. As part of our methods, if significant strip effects still remained locally, substitution by another year's mosaic or histogram matching of the problematic strip with neighbouring strips was performed. A multi-temporal multichannel filter (Quegan and Yu, 2001) using a 7 × 7 window was also applied to all the annual mosaics. At this point, the remaining speckle effect was considered negligible.

Landsat 5 and 7 ETM + Surface Reflectance (SR) imagery computed by the Landsat Ecosystem Disturbance Adaptive Processing System (LEDAPS) method (<http://ledaps.nascom.nasa.gov/>) (Masek et al., 2006) were used to generate annual (± 1 yr) median value composites from good quality pixels for all spectral bands in Mexico and Poland. Landsat Percent Tree Cover (PTC) products (Hansen et al., 2013; Sexton et al., 2013) for the year 2010 were acquired from USGS Land Cover Institute (<https://landcover.usgs.gov/>), and the Global Land Cover Facility (<http://glcf.umd.edu/>) for Mexico and Eastern South Africa, respectively. Additionally, freely available 30 m spatial resolution elevation data from the Shuttle Radar Topography Mission (void-filled SRTM Plus NASA V3) was obtained for Mexico, Eastern South Africa and Kalimantan from the USGS Earth Explorer repository (<http://earthexplorer.usgs.gov/>). SPOT-4 High Resolution Visible Infrared (HRVIR) and SPOT-5 High Resolution Geometric (HRG) data were acquired between 2008 and 2010 (approximately 80% from 2010) for Sweden; all images were geometrically precision-corrected to the Swedish National Grid, and the pixel size for all bands was resampled to 25 m using cubic convolution.

The accuracies of the resulting maps were evaluated using either AGB forest inventory plots or airborne LiDAR-derived AGB maps, collected and produced according to different protocols (Table 1), and with characteristics specific to each region. Airborne LiDAR-derived

Table 1
Datasets and algorithms used for each 2010 regional map.

Regional Map	Method	Method type	Datasets	Reference data					
				Plot size / LIDAR point density	ALOS PALSAR	Landsat 5/7	Landsat PTC	SPOT 4 & 5	SRTM DEM
Indonesia Kalimantan	Two step LiDAR + SAR multiple linear regression	P	DD	247 field plots & 1245 LiDAR samples calibration / 501 LiDAR samples validation	x			x	
Eastern South Africa	WCM + Bayesian inversion	P	MB	37 field plots calibration / 3188 LiDAR samples validation	x	x			
Sweden	KNN	NP	DD	0.5 - 4 points m ⁻² / 18,401 field plots calibration / 3989 field plots validation	x			x	
Central Mexico & Yucatan peninsula	MaxEnt	NP	DD	5140 field plots calibration / 700 field plots validation	x				x
Poland	Random Forest	NP	DD	285 field plots calibration / 84 field plots validation	x				x

P (parametric), NP (non-parametric), DD (data-driven), MD (model-based).

III. Biomass estimation in tropical forests using the backscatter approach in different biomes (Chapter II)

AGB maps were used in Kalimantan for calibration and validation, but only for validation in Eastern South Africa (Naidoo et al., 2015). A subset of LiDAR-derived AGB maps or the field data (15–30%) was excluded in each region and used as an independent validation dataset. The subset was extracted by stratifying the reference dataset into different AGB classes in order to have a similar distribution of AGB in both the calibration and validation datasets.

4. Methods

4.1. Biomass estimation methods

Both parametric and non-parametric methods were used to predict AGB. These can be further grouped into data-driven and model-based methods. The method for each region was selected based on data availability and the expertise of each regional research group. Teams working in areas with forest inventory and other in situ data of sufficient number and quality for calibration purposes used non-parametric machine learning algorithms, while areas with insufficient in situ data used parametric models, such as model-based regression, and when available, complemented the ground observations with airborne LiDAR biomass predictions (Table 1).

The probabilistic outputs from the non-parametric MaxEnt algorithm (Phillips et al., 2006, 2004) were used for Mexico (Rodríguez-Veiga et al., 2016). Machine learning algorithms Random Forest (Breiman, 2001; Cartus et al., 2014) and a k-Nearest Neighbours (kNN) (Tomppo et al., 2008; Reese et al., 2003) were applied in Poland and Sweden respectively, both requiring large amounts of field plots for calibration. The parametric method used in Kalimantan used a two-step calibration approach where field plots are first used to calibrate airborne LiDAR measurements covering a larger area, and these were then used to calibrate a multivariate linear regression model with backscatter intensity and texture parameters from the SAR imagery as predictors (Englhart et al., 2011, 2012). Bayesian inversion of a semi-

empirical model (the water cloud model - WCM) was used to relate PALSAR backscatter to AGB in South Africa (Bouvet et al., 2018). This method relies on a small number of at least 1 ha in situ AGB plots, ancillary data and simulations from the Multi-static Interferometric and Polarimetric Electromagnetic model for Remote Sensing (MIPERS) (Villard and Borderies, 2007; Villard, 2009) for parameterization.

4.2. Accuracy assessment methods

A standardised accuracy assessment was carried out for all regional AGB maps by making use of the independent reference data. The assessment was based on stratifying the reference AGB into contiguous ranges of values and quantifying the estimation bias, the standard deviation of the error and the Root Mean Square Error (RMSE) within each range. The selected ranges varied with test site, depending on the maximum value of biomass for the site and the need to have a sufficient number of reference data within each range.

In more detail, we have a set of reference AGB values, $B_{ref}^{(i)}$ (from in situ or LiDAR data), and their estimates, $B_{est}^{(i)}$, where the reference values are restricted to a given range, $B_1 < B_{ref}^{(i)} < B_2$. For this range we define the bias, b , as the average value of the error $B_{est}^{(i)} - B_{ref}^{(i)}$, and we also calculate the standard deviation (SD) of the errors, σ . The RMSE in the given range is then given by $\sqrt{\sigma^2 + b^2}$, and the relative RMSE as $Rel. RMSE = RMSE / B_{ref} \times 100$. Also of interest is the Coefficient of Variation (CV) of the error, given by σ/b . When the CV exceeds 1, the RMSE is dominated by random error, but when it is less than 1 the dominant error source is bias in the estimator. In particular, if $CV = 10$, then bias makes up 10% of the RMSE, while if $CV = 0.48$ it contributes 90%.

5. Results

The constructed AGB maps for the year 2010 were generated with a pixel size of 25 m for Mexico-Yucatan Peninsula, Central Mexico,

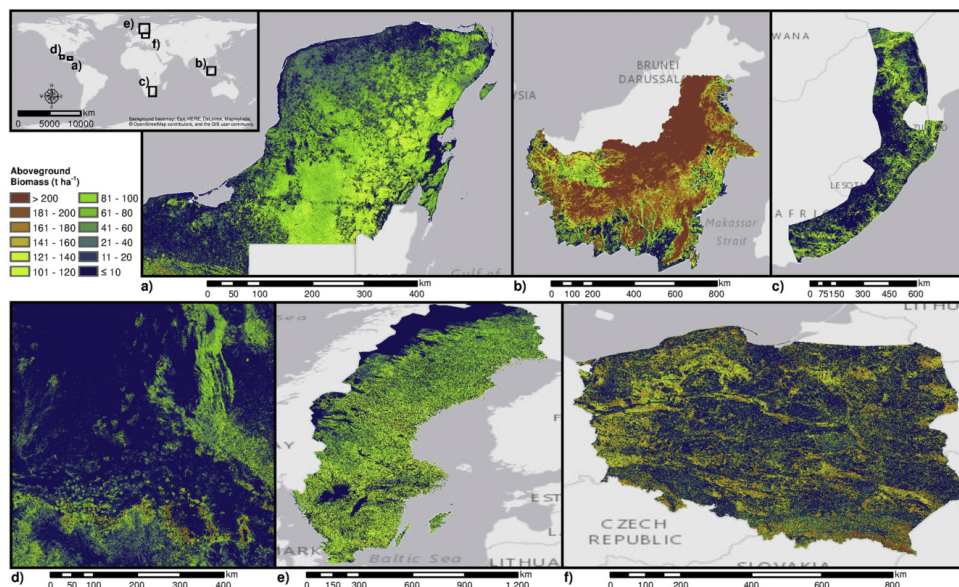


Fig. 2. Above-ground biomass (AGB) maps for a) the Mexico-Yucatan Peninsula, b) Indonesia-Kalimantan, c) Eastern South Africa, d) Central Mexico, e) Sweden, and f) Poland. Warmer colours indicate higher AGB.

III. Biomass estimation in tropical forests using the backscatter approach in different biomes (Chapter II)

P. Rodríguez-Veiga et al.

Int J Appl Earth Obs Geoinformation 77 (2019) 53–68

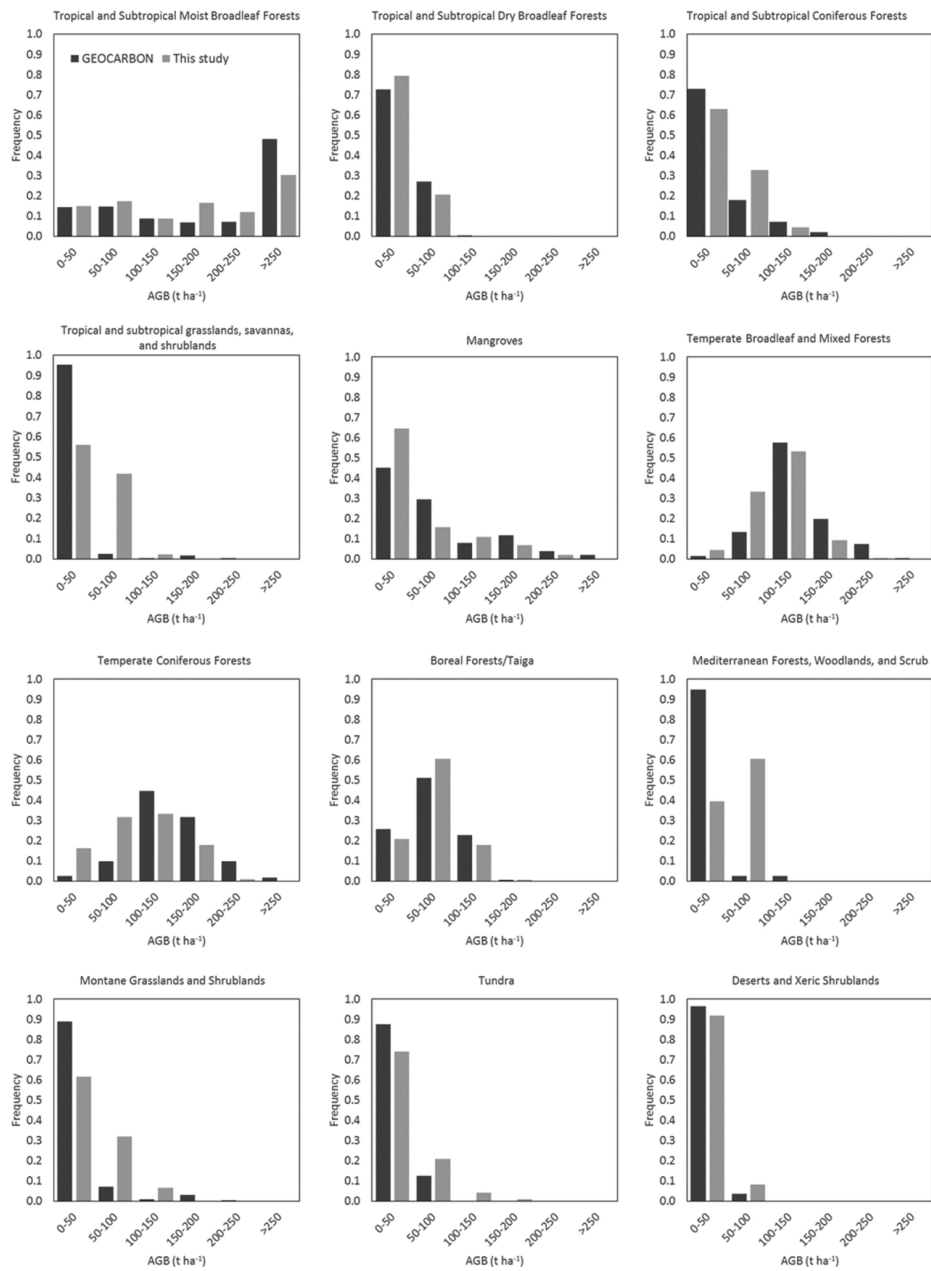


Fig. 3. AGB histograms per forest biome (Olson et al., 2001) derived from the combined regional maps in this study (light grey) aggregated to 1 km spatial resolution compared to the AGB histogram from the GEO-CARBON global map (dark grey) within the study areas. Flooded grasslands and savannas biome is not included in this analysis due to the small amount of data available from the study regions, while the temperate grasslands, savannas, and shrublands biome was not encountered in the study regions.

III. Biomass estimation in tropical forests using the backscatter approach in different biomes (Chapter II)

Eastern South Africa, Sweden, and Poland, and 100 m for Indonesia-Kalimantan (Fig. 2).

The regional maps cover the whole range of expected woody AGB densities from low to high biomass. The histogram of the combined regional maps was comparable to the histogram of AGB extracted from the global AGB map of the GEO-CARBON project in the different forest biomes (Olson et al., 2001) covered by this study (Fig. 3). The most substantial differences are on the tropical and subtropical grasslands, savannas and shrublands, and in the montane grasslands and shrublands biomes, where the GEO-CARBON map showed a strongly skewed histogram towards low AGB (< 50 t ha⁻¹) and very low frequency of higher AGB classes, while this study showed a more distributed declining trend from low to high AGB classes in those biomes. Additionally, the GEO-CARBON map shows the same skewed histogram towards low AGB in the Mediterranean forests, woodlands, and scrub biome, while this study's histogram showed to be slightly skewed towards higher AGB (50-100 t ha⁻¹). In the tropical and subtropical moist broadleaf forests biome histograms are similarly skewed towards high AGB, but GEO-CARBON's histogram showed higher frequency at the highest AGB range (> 250 t ha⁻¹).

The accuracies of the regional AGB maps were assessed using the independent validation datasets (Table 2, Figs. 4 and Fig. 5). LiDAR AGB datasets were aggregated to the corresponding satellite map resolution for validation, while plot datasets used the average value of the pixels within the plot boundaries.

The accuracy analysis reveals several commonalities but also some important differences between study regions. All regions over-estimate AGB for the lower AGB ranges and, with the exception of Eastern S. Africa which covers a very limited biomass range, under-estimate in the upper ranges, especially in the highest AGB class. The bias in the lowest AGB class is substantial in absolute terms for all regions except Central Mexico and Eastern S. Africa, but even in these regions it has values that are 47% and 40% of the mid-range values (i.e., 15 and 10 t ha⁻¹), respectively. For most regions the bias decreases in absolute value before increasing again. This is expected for regression-based approaches, which ensure that the regression curve passes through the point defined by mean of the reference and estimated data, but occurs for all methods.

There are striking differences in the balance between bias and random error in the RMSE, as is clear from Table 2 and Fig. 4. In Kalimantan, bias and random error are of similar magnitude except in the middle AGB ranges, where random error dominates. For Central Mexico and Eastern S. Africa, random error is dominant except for the highest AGB class in Central Mexico, where it is comparable to bias. Note that in these two regions the bias is roughly constant across all ranges (except for the highest range in Central Mexico) so it decreases sharply relative to the mid-range values. In the Yucatan Peninsula and Sweden, bias and random error are comparable in the lower biomass ranges, the middle ranges are dominated by random error, while bias is the largest component of error in the highest AGB ranges. For Poland, bias is by the

Table 2

Accuracy assessment of the regional AGB maps stratified by reference AGB range: Sample size (N), Root Mean Square Error (RMSE), Relative RMSE (Rel. RMSE), Standard Deviation of the error (SD), Bias, and Coefficient of Variation (CV) of the error (when CV > 1 the random error dominates, when CV < 1 the bias does).

Study region	Reference AGB range (t ha ⁻¹)	N	RMSE (t ha ⁻¹)	Rel. RMSE (%)	Bias (t ha ⁻¹)	SD (t ha ⁻¹)	CV
Indonesia Kalimantan	0-50	141	54	415	37	39	1.1
	50-100	21	71	91	52	50	1.0
	100-150	38	66	50	39	54	1.4
	150-200	117	42	24	16	39	2.4
	> 200	184	60	24	-40	44	1.1
	Overall	501	55	37	4	55	13.8
Central Mexico	0-30	83	21	159	7	19	2.7
	30-60	48	30	69	8	29	3.6
	60-90	25	34	47	-3	34	11.3
	90-120	12	42	40	2	42	21.0
	120-150	6	24	19	4	24	6.0
	> 150	2	64	32	-41	49	1.2
	Overall	176	28	67	5	28	5.6
Mexico Yucatan peninsula	0-30	130	33	237	21	26	1.2
	30-60	109	33	75	15	30	2.0
	60-90	111	23	31	6	22	3.7
	90-120	85	25	24	-14	21	1.5
	120-150	54	46	34	-42	17	0.4
	> 150	35	67	40	-65	16	0.2
	Overall	524	35	50	-1	35	35.0
Eastern South Africa	0-20	2,216	8	100	4	8	2.0
	20-40	734	14	48	7	11	1.6
	40-60	233	15	33	7	11	1.6
	> 80	5	7	11	3	5	1.7
	Overall	3188	10	63	5	9	1.8
Sweden	0-30	901	38	271	30	23	0.8
	30-60	871	35	76	24	25	1.0
	60-90	850	29	39	12	26	2.2
	90-120	606	29	28	-6	29	4.8
	120-150	361	43	32	-29	32	1.1
	150-180	245	61	37	-50	35	0.7
	> 180	155	82	42	-74	36	0.5
	Overall	3989	32	39	-13	29	2.2
Poland	0-50	13	67	258	63	23	0.4
	50-100	19	54	67	49	24	0.5
	100-150	17	26	20	8	25	3.1
	150-200	16	32	18	-21	25	1.2
	200-250	11	73	30	-70	20	0.3
	> 250	8	86	32	-85	16	0.2
	Overall	84	54	39	3	54	18.0

III. Biomass estimation in tropical forests using the backscatter approach in different biomes (Chapter II)

P. Rodríguez-Veiga et al.

Int J Appl Earth Obs Geoinformation 77 (2019) 53–68

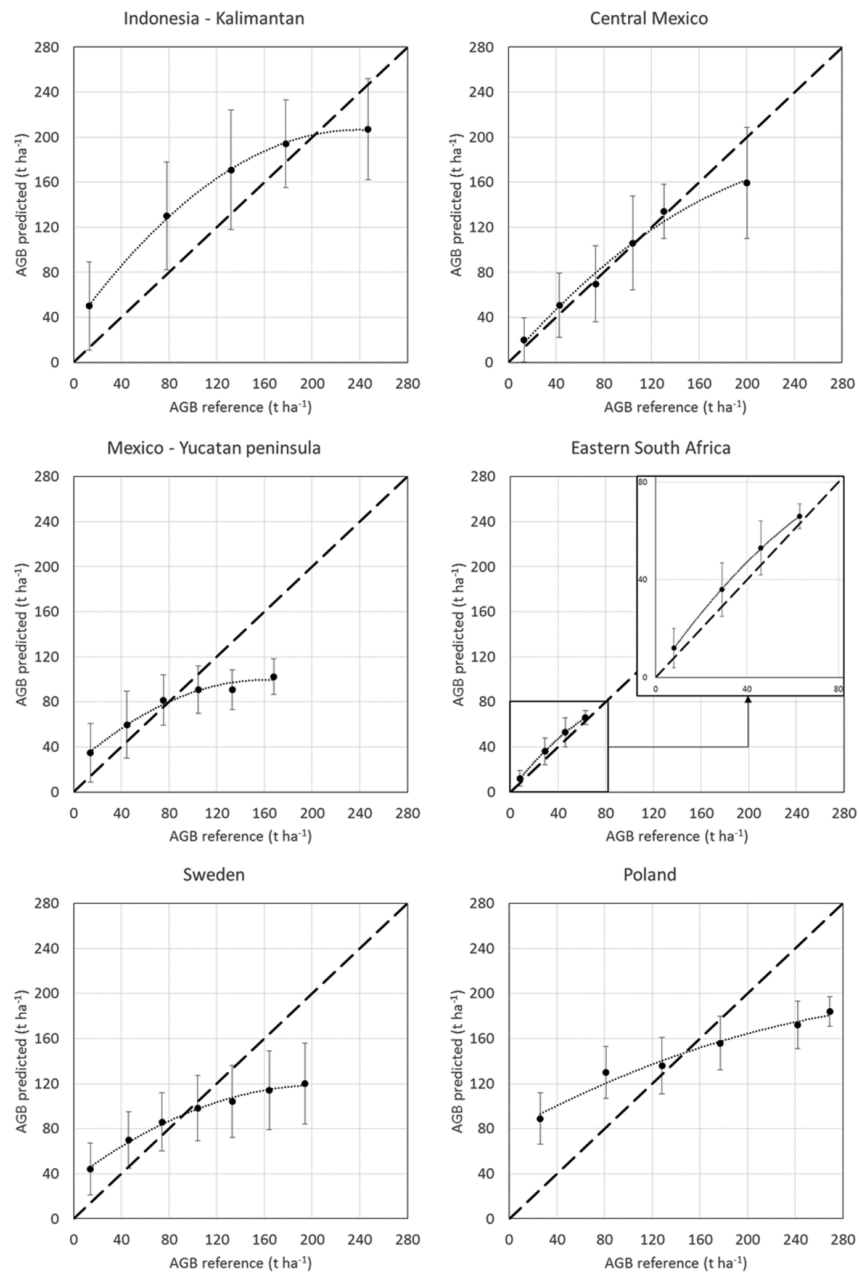


Fig. 4. Scatterplots of average predicted AGB versus average reference AGB per reference AGB range. Error bars indicate the standard deviation (random error) of the predicted AGB per reference AGB range. The dotted line indicates a fitting curve to the calculated points (second order polynomial) and the dashed line corresponds to the $y = x$ line. If the error bars do not overlap the $y = x$ line then bias is the dominant error in that AGB range.

III. Biomass estimation in tropical forests using the backscatter approach in different biomes (Chapter II)

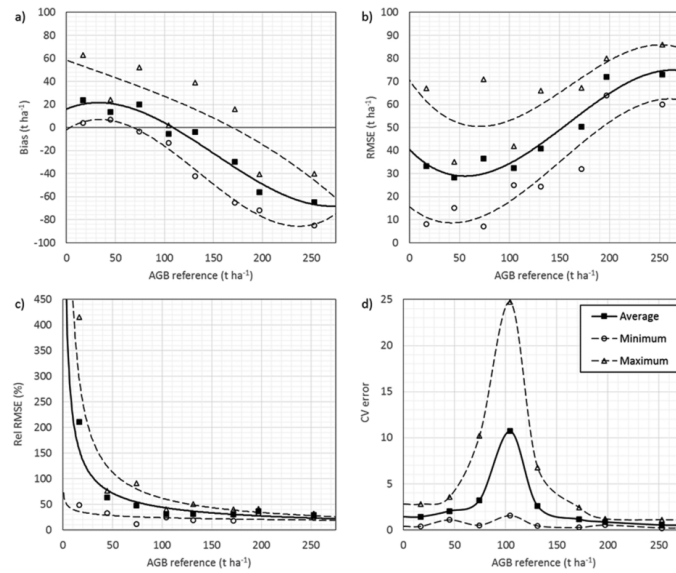


Fig. 5. Distribution of a) bias, b) relative root mean square error, c) relative RMSE, and d) coefficient of variation of the error across the reference AGB range for all regional maps.

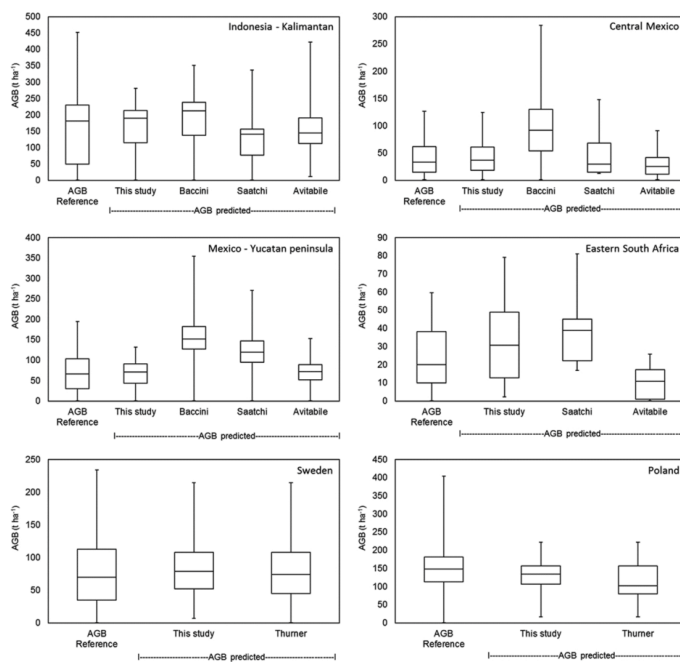


Fig. 6. Boxplots by region of reference and predicted AGB in this study, Baccini et al. (2012); Saatchi et al. (2011); Avitabile et al. (2016) and Thurner et al. (2014). The central mark of each box represents the median of the distribution, while the lower and upper limits of the box represent the 25th and 75th percentiles. The whiskers cover the range of extreme values. Outliers are not included. All the maps were aggregated to 1 km spatial resolution.

III. Biomass estimation in tropical forests using the backscatter approach in different biomes (Chapter II)

far the dominant error source apart from the two middle ranges of AGB.

It is also noticeable that the SD of the error does not vary greatly across the different AGB ranges for each region, though is markedly different between regions (see Table 2 and Fig. 4). Hence, roughly speaking, the random error is not strongly dependent on the true AGB, and its value relative to the true AGB decreases as AGB increases (Fig. 5). It can also be seen that the contribution of the random error to the RMSE increases as AGB increases up to approximately 100 t ha^{-1} , then reduces sharply with increasing AGB (Fig. 5).

The values given for the overall bias in each region are close to zero (Table 2). This implies that all the methods cause the fitting curve (or its equivalent) to go through the point defined by the averages of the reference and estimated data, in common with normal regression methods which force this to happen. This explains why the overall RMSE and SD are nearly the same, since $\text{SD}^2 = (\text{RMSE})^2 - (\text{overall bias})^2$ and the overall bias is constrained to be nearly zero (Table 2).

Previously published pan-tropical (Saatchi et al., 2011; Baccini et al., 2012; Avitabile et al., 2016) and northern hemisphere (Thurner et al., 2014) mapping studies show AGB distributions and spatial patterns that are different from those for the regional maps from this study and the independent validation data (Figs. 6 and 7). In particular, in Mexico the distributions from Baccini et al. (2012) are shifted towards much higher values than is found in the present study and the validation data.

Similar estimates can be found in areas with high AGB levels such as Kalimantan, but they deviate from the reference AGB in areas of lower AGB such as Eastern South Africa, Yucatan and Central Mexico. In Central Mexico, the Saatchi et al. (2011) AGB distribution is similar to those in our study and the validation data, but for the Yucatan peninsula and Eastern South Africa it is shifted towards higher values while for Kalimantan is shifted towards lower values. In Avitabile et al. (2016) and this study, the AGB distribution is similar to that obtained from the validation data in Yucatan and Central Mexico but in Eastern South Africa the Avitabile et al. (2016) data are shifted toward lower values while this study is shifted towards higher values. In Kalimantan, the distributions of the validation data and all the maps, except for Avitabile et al. (2016), are highly skewed towards high values. Only the Avitabile et al. (2016) AGB map provides estimates similar to the true

AGB in the Mexican sites. In Sweden, the AGB distributions estimated in this study and in Thurner et al. (2014) largely agree with the validation data. In Poland, the AGB distribution from Thurner et al. (2014) looks highly skewed and shifted towards lower values than the estimates from this study and in the validation subset.

6. Discussion

6.1. Evaluation of the maps

The analysis of the regional maps affirms important properties of AGB estimation methods, some of which have been previously reported in the literature (e.g. Cartus et al., 2014; Carreiras et al., 2012; Englhart et al., 2012; Baccini et al., 2008; Sandberg et al., 2011; Rauste, 2005; Avitabile et al., 2016; Avitabile and Camia, 2018). The accuracy assessment shows underestimation in the upper AGB ranges in which the major error component of the RMSE originates from bias (Table 2). The exception is in Eastern South Africa, where the reference values of AGB are below 80 t ha^{-1} . Additionally, although less apparent in Eastern South Africa and Central Mexico, AGB values below 100 t ha^{-1} are overestimated, regardless of the choices of data and method used to retrieve AGB (Table 2 & Fig. 4). Fig. 4 is derived from an independent dataset not used in model fitting, but similar behaviour is seen for data used in model fitting. This means that, although direct linear regression is not being used, all model fits used to predict AGB have an intercept at zero AGB that is too high, and/or the gradient of the model is too large for lower AGB values.

A major problem with the observed biases is that they depend on the true value of the AGB. If not, the data could easily be calibrated to remove them. Even though the analysis quantifies how the bias depends on the true AGB in each region, this does not lead to any way to correct the estimated values. Although some of the methods incorporate bias reduction measures, e.g. MaxEnt (Xu et al., 2016; Saatchi et al., 2011), and post-processing bias reduction techniques are also available, there is a risk of undesirable effects such as inflation of the overall mean square error due to an increase of the variance (Kosmidis, 2014; Xu et al., 2016). Addressing this problem requires new algorithms that intrinsically remove the bias (if this is possible), new data that do not

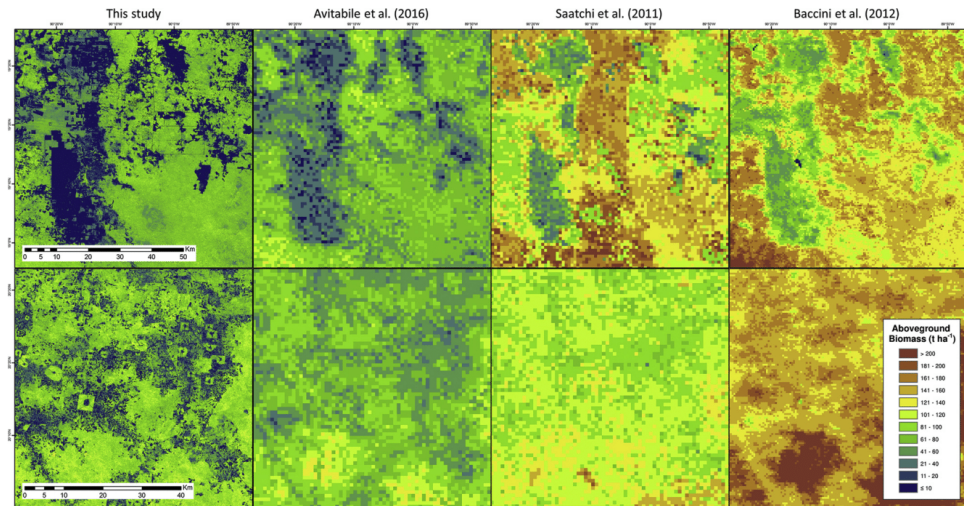


Fig. 7. Comparison of four AGB maps over two sites in the Yucatan peninsula (Mexico), showing the regional AGB map presented in this study, and the maps by Avitabile et al. (2016); Saatchi et al. (2011), and Baccini et al. (2012).

III. Biomass estimation in tropical forests using the backscatter approach in different biomes (Chapter II)

suffer saturation of the signal for higher biomass (assuming this is the primary cause of the observed underestimation in this range of biomass), or accepting that such bias will occur because AGB is only indirectly related to the remote sensing observables considered in these studies.

However, as has been shown, for some regions and methods bias is not the dominant effect (i.e. Kalimantan and Central Mexico); instead, the most important type of error is random scatter of the data points in the model inversions, i.e., the model inversions are noisy. Some of this scatter may be reducible if its source can be identified, e.g., there may be errors due to inaccuracies in the ground data, geolocation errors (so that the reference data and inversions are spatially mismatched), radar speckle may have been insufficiently reduced (though our methodology ensures this should be of negligible importance in our analysis), or the remote sensing signal may be weakly correlated to AGB due to the limited sensitivity to biomass of the sensor. Moreover, if the dominant error term comes from scatter, it can be reduced by spatial averaging (whereas bias cannot) at the expense of reduced spatial resolution and aggregation to coarser spatial units.

Pan-tropical (Saatchi et al., 2011; Baccini et al., 2012; Avitabile et al., 2016) and northern hemisphere maps (Turner et al., 2014) were compared to in situ data and the estimates from this study. Some similarities were found between our study and Avitabile et al. (2016) in the Mexico sites and Turner et al. (2014) in Sweden. Even though Avitabile's map is a fusion of Saatchi's and Baccini's data, the fusion method used additional ground measurements and higher resolution regional maps to correct for the bias of the original estimates. This is the case in Mexico, where the Avitabile et al. (2016) product was calibrated with another regional AGB product (i.e. Cartus et al., 2014). However, in Eastern South Africa, Avitabile's map does not have calibration data and systematically underestimates AGB with maximum predicted AGB values just above 20 t ha^{-1} , close to a factor of three less than the higher AGB values reported in the validation dataset (60 t ha^{-1}). In general, the distributions of the AGB estimates from this study are closer to those of the independent validation data than those of the published AGB global maps.

6.2. Strengths and weaknesses of proposed retrieval methods and available datasets

Several methods were used to predict AGB and showed specific strengths and weaknesses (The requirement for only a limited number of ground data points is an advantage of semi-empirical methods, such as the Water Cloud Model (WCM) + Bayesian inversion used in Eastern South Africa where only one parameter of the regression needs to be derived from in situ biomass data. However, the formulation of the WCM for this region does not produce estimates for AGB above $\sim 100 \text{ t ha}^{-1}$

ha-1, and it is tuned for regions such as savannas with biomass below the saturation level at L-band (Mermoz et al., 2015). A method for global mapping, BIOMASAR (Santoro et al., 2011), is also based on the WCM and does not need in situ data to fit the model parameters. However, the BIOMASAR algorithm is understood to estimate growing stock volume (GSV), so a further step is needed to estimate AGB, which requires spatial information on specific wood density and biomass expansion factors, or similar proxies.

Table 3). A key factor in the performance of regional methods was the amount and quality of available in situ data. In regions with abundant in situ data from a forest inventory, non-parametric data-driven methods, such as k-NN and MaxEnt were chosen, but in regions where data were scarce a model-based parametric approach was selected. Large numbers of forest plots were available in Sweden (22,548 plots) and Mexico (5140 plots). Poland (285 plots) and Kalimantan (247 forest plots) had fewer, but in Kalimantan airborne LiDAR biomass maps were developed to increase the size of the training and validation dataset. In the data-scarce region of the South Africa savannas only 37 1-ha AGB plots were available, but they were complemented with airborne LiDAR-based biomass maps derived from locally developed LiDAR models calibrated against field data (Naidoo et al., 2015) for validation. LiDAR airborne data was used for calibration and validation in Kalimantan, while only as validation in Eastern South Africa. This study assumed the AGB predicted by the LiDAR airborne to be error-free. However, the use of LiDAR data might introduce substantial errors in the AGB prediction originated from the ground-to-LiDAR model used (Saarela et al., 2016; Holm et al., 2017), which are not accounted for in this study.

The requirement for only a limited number of ground data points is an advantage of semi-empirical methods, such as the Water Cloud Model (WCM) + Bayesian inversion used in Eastern South Africa where only one parameter of the regression needs to be derived from in situ biomass data. However, the formulation of the WCM for this region does not produce estimates for AGB above $\sim 100 \text{ t ha}^{-1}$, and it is tuned for regions such as savannas with biomass below the saturation level at L-band (Mermoz et al., 2015). A method for global mapping, BIOMASAR (Santoro et al., 2011), is also based on the WCM and does not need in situ data to fit the model parameters. However, the BIOMASAR algorithm is understood to estimate growing stock volume (GSV), so a further step is needed to estimate AGB, which requires spatial information on specific wood density and biomass expansion factors, or similar proxies.

The most used dataset in this study was the L-band SAR ALOS PALSAR annual mosaics (Shimada et al., 2014; Shimada and Ohtaki, 2010), which were used in all regional methods except for Sweden. The saturation level of L-band SAR was found in previous studies to vary between 40 t ha^{-1} and 150 t ha^{-1} (Balzter et al., 2002a, b; Tansey et al.,

Table 3
Strengths and weaknesses of proposed methods/datasets when considering global implementation.

METHOD	STRENGTHS	WEAKNESSES
Two step LiDAR + SAR multiple linear regression	<ul style="list-style-type: none"> • Low demand on <i>in situ</i> data • Can combine different EO datasets 	<ul style="list-style-type: none"> • Requires airborne LiDAR (costly and not always available) • Overestimation at low AGB • Underestimation at high AGB
WCM + Bayesian inversion	<ul style="list-style-type: none"> • Low demand on <i>in situ</i> data 	<ul style="list-style-type: none"> • Requires large <i>in situ</i> plots (1 ha) (not always available) • Assumes saturation of L-band SAR above 100 t ha^{-1} (i.e., only applicable on low AGB areas)
Random Forests	<ul style="list-style-type: none"> • Can combine different EO datasets 	<ul style="list-style-type: none"> • Medium / high demand on <i>in situ</i> data • Overestimation at low AGB • Underestimation at high AGB
MaxEnt	<ul style="list-style-type: none"> • Can combine different EO datasets 	<ul style="list-style-type: none"> • High demand on <i>in situ</i> data • Overestimation at low AGB • Underestimation at high AGB
kNN	<ul style="list-style-type: none"> • Can combine different EO datasets 	<ul style="list-style-type: none"> • SPOT data not freely available • High demand on <i>in situ</i> data • Overestimation at low AGB • Underestimation at high AGB

III. Biomass estimation in tropical forests using the backscatter approach in different biomes (Chapter II)

P. Rodríguez-Veiga et al.

Int J Appl Earth Obs Geoinformation 77 (2019) 53–68

2004, Lucas et al., 2010; Hame et al., 2013) and generally HV gave higher saturation levels than HH polarization (Le Toan et al., 1992; Saatchi et al., 2007; Mitchard et al., 2009; Hamdan et al., 2011; Mitchard et al., 2012; Saatchi et al., 2011; Englhart et al., 2011; Hamdan et al., 2014). The saturation level at i -band depends on the geometry of the radar measurements, and therefore on forest type and environmental effects (Yu and Saatchi, 2016), as it can be observed in the different relationships found in the Yucatan peninsula and Central Mexico (Fig. 8). Use of the annual mosaics was also a limitation, as better results have been obtained with the use of multi-temporal SAR datasets due to the decrease in the retrieval error in AGB ranges to which the sensitivity of the SAR signal is weak (Antropov et al., 2013; Santoro et al., 2015b, 2006; Thiel and Schmulius, 2016; Antropov et al., 2017; Cartus et al., 2012). However, this was necessary due to the cost of acquiring the multiple ALOS PALSAR images used to generate the mosaics over large areas and for a given year.

For the model-based approaches, information provided by optical sensors, such as Landsat Percent Tree Cover (e.g. in Eastern South Africa), was needed for parameterisation (Bouvet et al., 2018). Such datasets were also used in the non-parametric machine learning methods, where they contributed towards improving model performance. Three out of the five regional methods used optical data as predictor variables. DEM data from SRTM were also used in Mexico and Poland as a predictor variable and in South Africa and Kalimantan for correcting or masking terrain effects, respectively. The use of topographic information by machine learning approaches for forests located in mountainous areas contributed to the estimation of AGB in Central Mexico.

The evaluation of the maps showed that a crucial limitation of the retrievals is that underestimation occurs at high AGB ranges, and overestimation at low AGB ranges. Remote sensing of AGB (using either reflectance or radar backscatter) is subject to decreasing sensitivity to AGB as biomass increases. Hence changes in AGB above a saturation level result in changes in the remotely sensed variable that are small compared to the variability in the signal. In these circumstances it is readily understood how linear regression would lead to these effects. The regression line always passes through the point defined by the mean of the reference data and the mean of the estimates, and the fitting effectively rotates the line about this point in order to reduce the sum of squared differences between the linear estimates and the reference data. For a concave curve, such as is produced by saturation, it is then inevitable that over-estimation will occur for low biomass and under-estimation for high biomass: getting a good fit for low biomass tends to steepen the line, while for high biomass it reduces the slope, and the regression line trades one against the other. In the case just discussed the model does not properly capture the relationship between the signal and the reference AGB, either due to insufficient calibration

data in the upper AGB range, or by fitting an inappropriate model to the AGB observations. However, if instead a fitting curve is used that correctly represents the saturation, bias is still to be expected for higher values of biomass. This occurs because, by definition, the backscatter values in the saturation zone are the result of random variation around the saturation level, with at most a weak dependence on biomass. Hence, although it is possible to use an estimator that assigns values of biomass above the saturation level, these represent the scatter in the data and the estimator will be biased towards the saturation level.

However, for correctly fitted data the overestimation at low AGB ranges is more difficult to explain. For SAR datasets, it could be connected to the high variability of the signal under soil moisture changes, as well as soil roughness (Mattia et al., 2009), but these do not apply to an optical-based method or to methods using SAR and optical data in synergy. Alternatively, it could be linked to the underestimation at high AGB ranges, as models provide the best fit by minimising an overall error term or cost function. The overestimation in the lower reference AGB ranges may stem from the model compensating for its inability to predict high AGB values accurately. In Kalimantan, the estimations were the highest, above 300 t ha^{-1} , and underestimation can only be observed above 200 t ha^{-1} . That underestimation occurs at such a high AGB level might be due to the large number of reference data points at high AGB levels compared to all other regions, which resulted in a fitted model with the largest errors and biases in the mid AGB ranges, between 50 and 150 t ha^{-1} , for which fewer calibration data were available (Table 2 and Fig. 4).

Avitabile et al. (2016) also found overestimations in the low AGB range and underestimations in the high AGB range when validating pan-tropical datasets (Saatchi et al., 2011; Baccini et al., 2012) against reference data. Several studies using the Random Forests regression algorithm have found similar behaviour at both ends of the AGB range, and report it as an effect of the averaging of tree-based algorithms (Baccini, 2004; Baccini et al., 2008; Avitabile et al., 2011; Urbazaev et al., 2018). Blackard et al. (2008) reported the same using a tree-based method (i.e. recursive partitioning regression), but suggested that saturation of optical data could explain the underestimation for high AGB densities, and scaling issues between plot and pixel could explain the underestimations at low AGB. This effect, characteristic of tree-based algorithms, could also explain the results in Poland, but cannot explain them in the other regions. Additionally other studies, such as Tsui et al. (2013) which used Kriging, Chopping et al. (2011) which used a geometric-optical canopy reflectance model, Del Frate and Solimini (2004) which used Neural Networks, or Sun et al. (2011), and Chi et al. (2015) which used multiple linear regression methods showed the same effects. Kattenborn et al. (2015) also reported the same effect for four semi- or non-parametric regression models (Random Forest, Generalized Additive Model, Generalized Boosted Regression Models

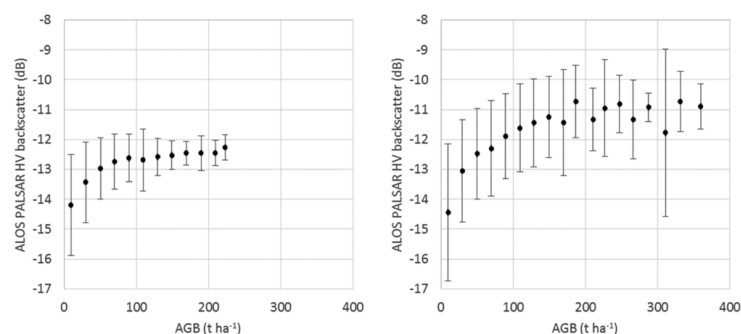


Fig. 8. Scatterplots of average ALOS PALSAR HV backscatter versus average reference AGB by reference AGB range. Error bars indicate the standard deviation of the ALOS PALSAR HV backscatter per reference AGB range for the Yucatan peninsula (left) and Central Mexico (right).

III. Biomass estimation in tropical forests using the backscatter approach in different biomes (Chapter II)

P. Rodríguez-Veiga et al.

Int J Appl Earth Obs Geoinformation 77 (2019) 53–68

and Boosted Generalized Additive Model), and suggested insufficient calibration data at the low and high AGB ends as the main cause. However, the consistency across all these studies suggests that there is a fundamental problem in retrieving biomass from the available data, which may only be solved by the use of SAR data with higher sensitivity to small scattering elements such as C-band (e.g. Sentinel-1) on the lower AGB range, and data with greater sensitivity to large scattering objects (i.e. high biomass) such as the P-band (Villard and Le Toan, 2015) to be exploited by the ESA BIOMASS mission.

7. Conclusions

The regional forest AGB mapping methods presented here reflect both the variety of training data available in different regions and the diverse range of algorithmic choices of each regional team. However, the retrieved AGB values agree better with independent in situ data than those published recently (Saatchi et al., 2011; Baccini et al., 2012; Avitabile et al., 2016; Thurner et al., 2014). As the different methods were not compared on the same site, we cannot comment on relative performance. However, we can form conclusions based on the commonalities observed from the comparison of standardized accuracy assessments.

The key EO dataset used in most methods was the L-band ALOS PALSAR mosaics, which provides the highest sensitivity to AGB of the currently available spaceborne sensors. However, it is clear that all current spaceborne sensors (SAR and optical) are inadequate for accurately estimating AGB beyond 100–150 t ha⁻¹. The case studies presented here highlight challenges of using sub-optimal datasets for this task. Any estimation beyond this range was dominated by negative bias or presented large errors for any of the given study sites. The assessment indicates, however, that one could push this limit in certain conditions, as seen in Kalimantan or Central Mexico. This could be linked to the use of large amounts of in situ data in the case of Kalimantan. In Central Mexico, a forest structure which leads to a higher L-band saturation level, or the contribution of additional datasets (i.e. the DEM) could be the cause.

There is also a general problem with overestimation at low AGB densities which cannot be entirely explained by the datasets used, but rather as an intrinsic problem of the proposed algorithms to correctly capture the relationship between EO data and AGB in the low AGB range. This means that we might have to consider alternative regression schemes, or accept the biases at both ends of the biomass range, provided that the modelling framework captures the relationship between observations and biomass.

This aspect shall deserve substantial attention in future studies as currently existing models for large-scale biomass estimation rely on simplifying assumptions that may not fully encompass the complex interaction of the remote sensing signal with vegetation.

The amount and type of reference data is also very relevant in terms of achieving the most reasonable AGB prediction model. Eastern South Africa used large plots (i.e. 1 ha), more suitable for calibration of EO methods (Réjou-Méchain et al., 2014), which might explain the good results for the low AGB ranges in this study area. Mexico, Sweden, Poland and Kalimantan relied on datasets of numerous small plots for calibration, supplemented with LiDAR in the case of Kalimantan. In the future, similar research should be based on homogeneous field-based datasets to avoid possible discrepancies resulting from the training data.

Better quality and more abundant large plots for calibration of the algorithms (Réjou-Méchain et al., 2014), the use of SAR time series (from Sentinel-1, ALOS 2 PALSAR 2, or future NovaSAR and NISAR) (Santoro et al., 2011; Antropov et al., 2017), the increasing availability of airborne or spaceborne LiDAR sensors like GEDI (Dubayah et al., 2014; Goetz et al., 2015) and MOLI (Kimura et al., 2017), satellites specifically designed for biomass estimation such as NISAR (Rosen et al., 2016, 2015), TanDEM-L (Moreira et al., 2015), and the P-band

BIOMASS SAR mission (Le Toan et al., 2011), and algorithms capable of reducing the errors in the low and high AGB ranges, are a promising way forward to improve global biomass estimates and reduce biases and errors in the map products in all biomass ranges.

Author contributions

P. Rodríguez-Veiga drafted the manuscript, and made the overall analysis and interpretation of the data. P. Rodríguez-Veiga and Heiko Balzter made the study conception and design. S. Quegan did the accuracy analysis, supervised the teams, and interpreted the results. Data acquisition, field work, mapping, and accuracy analysis, in each region was performed by the different teams organized as follows: Yucatan peninsula and central Mexico (P. Rodríguez-Veiga, K. Tansey, and H. Balzter), Eastern South Africa (S. Mermoz, A. Bouvet, T. Le Toan, R. Mathieu, and G. P. Asner), Sweden (H. J. Persson, and J.E.S. Fransson), Poland (A. Hoscilo, D. Ziolkowski, and K. Stereńczak), and Kalimantan (S. Lohberger, M. Stängel, Anna Berninger, and F. Siegert). V. Avitabile and M. Herold provided support for the teams on standardized definitions, and characterization of the uncertainties. C. Thiel, C. Pathe, and C. Schullius were responsible for the conceptual design of the GlobBiomass project proposal, as well as for the overall coordination of the project. Moreover, C. Pathe assisted in SAR data acquisition and pre-processing. S. Quegan, H. Balzter, C. Schullius, and F. M. Seifert supervised the project, and provided science advice on the work of the regional teams. S. Quegan, J. Carreiras, Y. Rauste, M. Santoro, N. Carvalhais, V. Avitabile, and R. Mathieu made critical revisions of the paper. All authors discussed the results, provided critical feedback, and helped shape the research, analysis and manuscript.

Acknowledgements

The authors would like to thank the following people and organizations for making the data freely available: JAXA, NASA, USGS, University of Maryland, ESKOM (South Africa), Southern Mapping Company (South Africa), CONAFOR (Mexico), Deutsche Gesellschaft für Internationale Zusammenarbeit (GIZ) GmbH (Indonesia), Martin Thurner, Alessandro Baccini, and Sassan Saatchi. The GlobBiomass project was funded by the European Space Agency under its Data User Element - ITT AO/1-7822/14/I-NB. P. Rodríguez-Veiga, H. Balzter, J. Carreiras, and S. Quegan were supported by the UK's National Centre for Earth Observation (NCEO). H. Balzter was also supported by the Royal Society Wolfson Research Merit Award, 2011/R3.

References

- Anaya, J.A., Chuvieco, E., Palacios-Orueta, A., 2009. Aboveground biomass assessment in Colombia: a remote sensing approach. *For. Ecol. Manage.* 257, 1237–1246.
- Antropov, O., Rauste, Y., Ahola, H., Hame, T., 2013. Stand-level stem volume of boreal forests from spaceborne SAR imagery at L-band. *IEEE J. Sel. Top. Appl. Earth Obs. Remote. Sens.* 6, 35–44.
- Antropov, O., Rauste, Y., Hame, T., Praks, J., 2017. Polarimetric ALOS PALSAR time series in mapping biomass of boreal forests. *Remote Sens. (Basel)* 9, 999.
- Asner, G.P., Mascaro, J., Anderson, C., Knapp, D.E., Martin, R.E., Kennedy-Bowdoin, T., Van Breugel, M., Davies, S., Hall, J.S., Muller-Landau, H.C., 2013. High-fidelity national carbon mapping for resource management and REDD+. *Carbon Balance Manag.* 8, 7.
- Asner, G.P., Knapp, D.E., Martin, R.E., Tupayachi, R., Anderson, C.B., Mascaro, J., Sinca, F., Chadwick, K.D., Higgins, M., Farfan, W., 2014. Targeted carbon conservation at national scales with high-resolution monitoring. *Proc. Natl. Acad. Sci.* 111, E5016–E5022.
- Avitabile, V., Camia, A., 2018. An assessment of forest biomass maps in Europe using harmonized national statistics and inventory plots. *For. Ecol. Manage.* 409, 489–498.
- Avitabile, V., Herold, M., Henry, M., Schullius, C., 2011. Mapping biomass with remote sensing: a comparison of methods for the case study of Uganda. *Carbon Balance Manag.* 6, 7.
- Avitabile, V., Herold, M., Heuvelink, G.B.M., Lewis, S.L., Phillips, O.L., Asner, G.P., Armston, J., Ashton, P.S., Banin, L., Bayol, N., Berry, N.J., Boeckx, P., Jong, B.H.J., Devries, B., Girardin, C.A.J., Kearsley, E., Lindsell, J.A., Lopez-Gonzalez, G., Lucas, R., Malhi, Y., Morel, A., Mitchard, E.T.A., Nagy, L., Qie, L., Quinones, M.J., Ryan, C.M., Ferry, S.J.W., Sunderland, T., Laurin, G.V., Gatti, R.C., Valentini, R., Verbeek,

III. Biomass estimation in tropical forests using the backscatter approach in different biomes (Chapter II)

- H., Wijaya, A., Willcock, S., 2016. An integrated pan-tropical biomass map using multiple reference datasets. *Glob. Chang. Biol.* 22, 1406–1420.
- Avitabile, V., Herold, M., Lewis, S., Phillips, O., Aguilar-Amuchastegui, N., Asner, G., Brienen, R., Devries, B., Gatti, R.G., Feldpausch, T., 2014. Comparative analysis and fusion for improved global biomass mapping. *Book of Abstracts of the International Conference Global Vegetation Monitoring and Modeling (GV2M)*. pp. 251–252.
- Baccini, A., 2004. Forest biomass estimation over regional scales using multisource data. *Geophys. Res. Lett.* 31.
- Baccini, A., Laporte, N., Goetz, S.J., Sun, M., Dong, H., 2008. A first map of tropical Africa's above-ground biomass derived from satellite imagery. *Environ. Res. Lett.* 3.
- Baccini, A., Goetz, S.J., Walker, W.S., Laporte, N.T., Sun, M., Sulla-Menashe, D., Hackler, J., Beck, P.S.A., Dubayah, R., Friedl, M.A., Samanta, S., Houghton, R.A., 2012. Estimated carbon dioxide emissions from tropical deforestation improved by carbon-density maps. *Nat. Clim. Change* 2, 182–185.
- Balster, H., Baker, J.R., Hallikainen, M., Tomppo, E., 2002a. Retrieval of timber volume and snow water equivalent over a Finnish boreal forest from airborne polarimetric synthetic aperture radar. *Int. J. Remote Sens.* 23, 3185–3208.
- Balster, H., Talmon, E., Wagner, W., Gaveau, D., Plummer, S., Yu, J.J., Quegan, S., Davidson, M., Toan, T.L., Gluck, M., 2002b. Accuracy assessment of a large-scale forest cover map of central Siberia from synthetic aperture radar. *Can. J. Remote Sens.* 28, 719–737.
- Balster, H., Rodríguez-Veiga, P., Tansey, K., Quegan, S., Carreiras, J., Persson, H.J., Fransson, J.E.S., Hosco, A., Ziolkowski, D., Dabrowska-Zielinska, K., Stereńczak, K., Englhart, S., Stängel, M., Siegfert, F., Avitabile, V., Mermoz, S., Bouvet, A., Le Toan, T., Carvalhais, N., Soja, M., Eriksson, L., Santoro, M., Pathe, C., Schmillius, C., 2016. GLOBBIOMASS regional case studies - preparing the ground for global forest biomass mapping. *ESA Living Planet Symposium*. Prague.
- Bartholomé, E., Belward, A., 2005. *Glc2000: a new approach to global land cover mapping from Earth observation data*. *Int. J. Remote Sens.* 26, 1959–1977.
- Beaudoin, A., Bernier, P., Guilford, L., Villemain, P., Guo, X., Stinson, G., Bergeron, T., Magnussen, S., Hall, R., 2014. Mapping attributes of Canada's forests at moderate resolution through k NN and MODIS imagery. *Can. J. For. Res.* 44, 521–532.
- Blackard, J.A., Finco, M.V., Helmer, E.H., Holden, G.R., Hoppus, M.L., Jacobs, D.M., Lister, A.J., Moisen, G.G., Nelson, M.D., Riemann, R., Ruefenacht, B., Salajana, D., Weyerermann, D.L., Winterberger, K.C., Brandeis, T.J., Czaplewski, R.L., Mroberts, R.E., Patterson, P.L., Tymcio, R.P., 2008. Mapping U.S. forest biomass using nationwide forest inventory data and moderate resolution information. *Remote Sens. Environ.* 112, 1658–1677.
- Bojinski, S., Verstraete, M., Peterson, T.C., Richter, C., Simmons, A., Zemp, M., 2014. The concept of essential climate variables in support of climate research, applications, and policy. *Bull. Am. Meteorol. Soc.* 95, 1431–1443.
- Bonan, G.B., 2008. Forests and climate change: forcings, feedbacks, and the climate benefits of forests. *Science* 320, 1444–1449.
- Bouvet, A., Mermoz, S., Le Toan, T., Villard, L., Mathieu, R., Naidoo, L., Asner, G.P., 2018. An above-ground biomass map of African savannahs and woodlands at 25m resolution derived from ALOS PALSAR. *Remote Sens. Environ.* 206, 156–173.
- Breiman, L., 2001. *Statistical Modeling: the two cultures (with comments and a rejoinder by the author)*. *Stat. Sci.* 16, 199–231.
- Carreiras, J.M.B., Vasconcelos, M.J., Lucas, R.M., 2012. Understanding the relationship between aboveground biomass and ALOS PALSAR data in the forests of Guinea-Bissau (West Africa). *Remote Sens. Environ.* 121, 426–442.
- Cartus, O., Santoro, M., Kellindorfer, J., 2012. Mapping forest aboveground biomass in the Northeastern United States with ALOS PALSAR dual-polarization L-band. *Remote Sens. Environ.* 124, 466–478.
- Cartus, O., Kellindorfer, J., Walker, W., Franco, C., Bishop, J., Santos, L., Fuentes, J., 2014. A national detailed map of forest aboveground carbon stocks in Mexico. *Remote Sens.* 6, 5559–5588.
- Carvalhais, N., Forkel, M., Khomik, M., Bellarby, J., Jung, M., Migliavacca, M.U.M., Saatchi, S., Santoro, M., Thurner, M., Weber, U., Ahrens, B., Beer, C., Cescaati, A., Randerson, J.T., Reichstein, M., 2014. Global covariation of carbon turnover times with climate in terrestrial ecosystems. *Nature* 514, 213–217.
- Chi, H., Sun, G., Huang, J., Guo, Z., Ni, W., Fu, A., 2015. National forest aboveground biomass mapping from icesat/GLAS data and MODIS imagery in China. *Remote Sens.* 7, 5534–5564.
- Chopping, M., Schaaf, C.B., Zhao, F., Wang, Z., Nolin, A.W., Moisen, G.G., Martonchik, J.V., Bull, M., 2011. Forest structure and aboveground biomass in the southwestern United States from MODIS and MISR. *Remote Sens. Environ.* 115, 2943–2953.
- Del Frate, F., Solimini, D., 2004. On neural network algorithms for retrieving forest biomass from SAR Data. *Geosci. Remote Sens. IEEE Trans.* On 42, 24–34.
- Dubayah, R., Goetz, S., Blair, J., Fatoyinbo, T., Hansen, M., Healey, S., Hofton, M., Hurr, G., Kellner, J., Luthcke, S., 2014. The global ecosystem dynamics investigation. *AGU Fall Meet. Abs.* 07.
- Englhart, S., Keuck, V., Siegfert, F., 2011. Aboveground biomass retrieval in tropical forests — the potential of combined X- and L-band SAR data use. *Remote Sens. Environ.* 115, 1260–1271.
- Englhart, S., Keuck, V., Siegfert, F., 2012. Modeling aboveground biomass in tropical forests using multi-frequency SAR Data - a comparison of methods. *Selected topics in applied earth observations and remote sensing*. *IEEE J. S.* 298–306.
- Evans, J.S., Cushman, S.A., 2009. Gradient modeling of conifer species using random forests. *Landscape Ecol.* 24, 673–683.
- Fagan, M., Defries, R., 2009. Measurement and monitoring of the world's forests: a review and summary of remote sensing technical capability, 2009–2015. *Resour. Future*.
- Fao, 2005. *Global forest resources assessment 2005*. *FAO Forestry Paper*. Food and Agriculture Organization of the United Nations.
- Fao, 2010. *Global forest resources assessment 2010*. *FAO Forestry Paper*. Food and Agriculture Organization of the United Nations.
- Fao, 2015. *Global Forest Resources Assessment 2015*. Food and Agriculture Organization of the United Nations, Rome.
- Fick, S.E., Hijmans, R.J., 2017. *Worldclim 2: new 1-km spatial resolution climate surfaces for global land areas*. *Int. J. Climatol.*
- Fraser, R.H., Li, Z., 2002. Estimating fire-related parameters in boreal forest using SPOT VEGETATION. *Remote Sens. Environ.* 82, 95–110.
- Gaillard, H., Zanchi, G., Nabuurs, G.-J., Hengeveld, G., Schardt, M., Verkerk, P.J., 2010. Eu-wide maps of growing stock and above-ground biomass in forests based on remote sensing and field measurements. *For. Ecol. Manage.* 260, 252–261.
- GLOBBIOMASS, 2015. *Globbiomass Project Website* [Online]. Available: Friedrich-Schiller-University Jena, Institute of Geography, Department Of Earth Observation, Jena, Germany. <http://Globbiomass.Org/2016>.
- Goetz, S.J., Hansen, M., Houghton, R.A., Walker, W., Laporte, N., Busch, J., 2015. Measurement and monitoring needs, capabilities and potential for addressing reduced emissions from deforestation and forest degradation under REDD+. *Environ. Res. Lett.* 10, 123001.
- Hamdan, O., Aziz, H.K., Rahman, K.A., 2011. Remote sensed L-band SAR data for tropical forest biomass estimation. *J. Trop. For. Sci.* 318–327.
- Hamdan, O., Hasmadi, I.M., Aziz, H.K., 2014. Combination of SPOT-5 and ALOS PALSAR images in estimating aboveground biomass of lowland dipterocarp forest. *IOP Conference Series: Earth And Environmental Science*. IOP Publishing, 012016.
- Hame, T., Rauste, Y., Antropov, O., Ahola, H.A., Kilpi, J., 2013. Improved Mapping of Tropical Forests With Optical and SAR Imagery, Part II: Above Ground Biomass Estimation. *Ieee J. Sel. Top. Appl. Earth Obs. Remote Sens.* 6, 92–101.
- Hansen, M.C., Potapov, P.V., Moore, R., Hancher, M., Turubanova, S.A., Tyukavina, A., Thau, D., Stehman, S.V., Goetz, S.J., Loveland, T.R., Kommareddy, A., Egorov, A., Chini, L., Justice, C.O., Townshend, J.R.G., 2013. High-resolution global maps of 21st-century forest cover change. *Science* 342, 850–853.
- Healey, S.P., Cohen, W.B., Yang, Z.Q., Krankina, O.N., 2005. Comparison of tasseled cap-based Landsat data structures for use in forest disturbance detection. *Remote Sens. Environ.* 97, 301–310.
- Holm, S., Nelson, R., Ståhl, G., 2017. Hybrid three-phase estimators for large-area forest inventory using ground plots, airborne lidar, and space lidar. *Remote Sens. Environ.* 197, 85–97.
- Houghton, R., Butman, D., Bunn, A.G., Krankina, O., Schlesinger, P., Stone, T., 2007. Mapping Russian forest biomass with data from satellites and forest inventories. *Environ. Res. Lett.* 2, 045032.
- Hu, T., Su, Y., Xue, B., Liu, J., Zhao, X., Fang, J., Guo, Q., 2016. Mapping global forest aboveground biomass with spaceborne LiDAR, optical imagery, and forest inventory data. *Remote Sens.* 8, 565.
- Kattenborn, T., Maack, J., Faßnacht, F., Enßle, F., Erment, J., Koch, B., 2015. Mapping forest biomass from space-Fusion of hyperspectral E01-hyperion data and Tandem-X and WorldView-2 canopy height models. *Int. J. Appl. Earth Obs. Geoinf.* 35, 359–367.
- Kellindorfer, J., Walker, W., Lapointe, L., Bishop, J., Cormier, T., Fiske, G., Kirsch, K., Westfall, J., 2011. *NACP Aboveground Biomass and Carbon Baseline Data (NBCD 2000), USA, 2000. Data Set*. [Online.] Available at: ORNL DAAC, Oak Ridge, Tennessee. daac.ornl.gov.
- Kimura, T., Imai, T., Sakaizawa, D., Murooka, J., Mitsuhashi, R., 2017. The overview and Status of vegetation lidar Mission, moli. 2017. *Ieee International Geoscience and Remote Sensing Symposium (Igrss)*. pp. 4228–4230.
- Kosmidis, L., 2014. *Bias in parametric estimation: reduction and useful side-effects*. *Wiley Interdiscip. Rev. Comput. Stat.* 6, 185–196.
- Le Quéré, C., Andrew, R.M., Friedlingstein, P., Sitch, S., Pongratz, J., Manning, A.C., Korsbakken, J.I., Peters, G.P., Canadell, J.G., Jackson, R.B., 2018. *Global carbon budget 2017*. *Earth Syst. Sci. Data* 10, 405.
- Le Toan, T., Beaudoin, A., Riou, J., Guyon, D., 1992. Relating forest biomass to SAR data. *Geosci. Remote Sens., IEEE Trans.* On 30, 403–411.
- Le Toan, T., Quegan, S., Davidson, M.W.J., Balster, H., Paillou, P., Papanathanassiou, K., Plummer, S., Rocca, F., Saatchi, S., Shugart, H., Ulander, L., 2011. The BIOMASS mission: mapping global forest biomass to better understand the terrestrial carbon cycle. *Remote Sens. Environ.* 115, 2850–2860.
- Lefsky, M.A., 2010. A Global Forest canopy height map from the moderate resolution imaging spectroradiometer and the geoscience laser altimeter system. *Geophys. Res. Lett.* 37, L15401.
- Liu, S., Zhou, T., Wei, L., Shu, Y., 2012. The spatial distribution of forest carbon sinks and sources in China. *Chin. Sci. Bull.* 57, 1699–1707.
- Liu, Y.Y., Van Dijk, A.I.J.M., De Jeu, R.A.M., Canadell, J.G., McCabe, M.F., Evans, J.P., Wang, G., 2015. Recent reversal in loss of global terrestrial biomass. *Nat. Clim. Change* 5 (5), 470–474.
- Lu, D., Chen, Q., Wang, G., Moran, E., Batistella, M., Zhang, M., Vaglio Laurin, G., Saah, D., 2012. Aboveground forest biomass estimation with Landsat and Lidar data and uncertainty analysis of the estimates. *Int. J. For. Res.* 2012, 16.
- Lucas, R., Armston, J., Fairfax, R., Fensham, R., Accad, A., Carreiras, J., Kelley, J., Bunting, P., Clewley, D., Bray, S., Metcalfe, D., Dwyer, J., Bowen, M., Eyre, T., Laidlaw, M., Shimada, M., 2010. An evaluation of the ALOS PALSAR L-Band backscatter - above ground biomass relationship Queensland, Australia: impacts of surface moisture condition and vegetation structure. *Selected topics in applied earth observations and remote sensing*. *IEEE J. S.* 3, 576–593.
- MacKinnon, Kathy, Gusti, Hatta, Mangalik, Arthur, Halim, Hakimah, 1996. *The Ecology of Kalimantan*, vol. 3 Oxford University Press.
- Masek, J.G., Vermote, E.F., Saleous, N.E., Wolfe, R., Hall, F.G., Huemmrich, K.F., Gao, F., Kutler, J., Lim, T.-K., 2006. A Landsat surface reflectance dataset for North America, 1990–2000. *Geosci. Remote Sens. Lett. IEEE* 3, 68–72.
- Mattia, F., Satalino, G., Pauwels, V., Alexander, L., 2009. Soil moisture retrieval through a merging of multi-temporal L-band SAR data and hydrologic modelling. *Hydrol. Earth Syst. Sci.* 13, 343–356.

III. Biomass estimation in tropical forests using the backscatter approach in different biomes (Chapter II)

P. Rodríguez-Veiga et al.

Int J Appl Earth Obs Geoinformation 77 (2019) 53–68

- Mermoz, S., Le Toan, T., Villard, L., Réjou-Méchain, M., Seifert-Granzin, J., 2014. Biomass assessment in the Cameroonian savanna using ALOS PALSAR data. *Remote Sens. Environ.* 155, 109–119.
- Mermoz, S., Réjou-Méchain, M., Villard, L., Le Toan, T., Rossi, V., Gourlet-Fleury, S., 2015. Decrease of L-band SAR backscatter with biomass of dense forests. *Remote Sens. Environ.* 159, 307–317.
- Mitchard, E., Saatchi, S., Baccini, A., Asner, G., Goetz, S., Harris, N., Brown, S., 2013. Uncertainty in the spatial distribution of tropical forest biomass: a comparison of pan-tropical maps. *Carbon Balance Manag.* 8, 10.
- Mitchard, E.T.A., Saatchi, S.S., Woodhouse, I.H., Nangendo, G., Ribeiro, N.S., Williams, M., Ryan, C.M., Lewis, S.L., Feldpausch, T.R., Meir, P., 2009. Using satellite radar backscatter to predict above-ground woody biomass: a consistent relationship across four different African landscapes. *Geophys. Res. Lett.* 36, L23401.
- Mitchard, E.T.A., Meir, P., Ryan, C.M., Woolen, E.S., Williams, M., Goodman, L.E., Mucavele, J.A., Watts, P., Woodhouse, I.H., Saatchi, S.S., 2012. A novel application of satellite radar data: measuring carbon sequestration and detecting degradation in a Community Forestry Project in Mozambique. *Plant Ecol. Divers.* 6, 159–170.
- Mitchard, E.T.A., Feldpausch, T.R., Brienen, R.J.W., Lopez-Gonzalez, G., Monteagudo, A., Baker, T.R., Lewis, S.L., Lloyd, J., Quesada, C.A., Gloor, M., Ter Steege, H., Meir, P., Alvarez, E., Araujo-Murakami, A., Aragão, L.E.O.C., Arroyo, L., Aymard, G., Banki, O., Bonal, D., Brown, S., Brown, F.I., Cerón, C.E., Chama Moscoso, V., Chave, J., Comiskey, J.A., Cornejo, F., Corrales Medina, M., Da Costa, L., Costa, F.R.C., Di Fiore, A., Domingues, T.F., Erwin, T.L., Frederickson, T., Higuchi, N., Honorio Coronado, E.N., Killen, T.J., Laurance, W.F., Lewis, C., Magnusson, W.E., Marimon, B.S., Marimon Junior, B.H., Mendoza Polo, I., Mishra, P., Nascimento, M.T., Neill, D., Núñez Vargas, M.P., Palacios, W.A., Parada, A., Pardo Molina, G., Peña-Claros, M., Pitman, N., Peres, C.A., Poorter, L., Prieto, A., Ramirez-Angulo, H., Restrepo Correa, Z., Roosind, A., Roucoux, K.H., Rudas, A., Salomão, R.P., Schiatti, J., Silveira, M., De Souza, P.F., Steininger, M.K., Stropp, J., Terborgh, J., Thomas, R., Toledo, M., Torres-Lezama, A., Van Andel, T.R., Van Der Heijden, G.M.F., Vieira, I.C.G., Vieira, S., Vilanova-Torre, E., Vos, V.A., Wang, O., Zartman, C.E., Malhi, Y., Phillips, O.L., 2014. Markedly divergent estimates of Amazon forest carbon density from ground plots and Satellites. *Glob. Ecol. Biogeogr.* 23, 935–946.
- Moreira, A., Krieger, G., Hajnsek, I., Papathanassiou, K., Younis, M., Lopez-Dekker, P., Huber, S., Villano, M., Pardini, M., Eineder, M., 2015. Tandem-L: A highly innovative bistatic SAR mission for global observation of dynamic processes on the Earth's surface. *Ieee Geosci. Remote. Sens. Mag.* 3, 8–23.
- Mucina, L., Rutherford, M.C., 2006. The vegetation of South Africa. *South African National Biodiversity Institute, Lesotho and Swaziland.*
- Naidoo, L., Mathieu, R., Main, R., Kleytnans, W., Wessels, K., Asner, G., Leblon, B., 2015. Savannah woody structure modelling and mapping using multi-frequency (X-, C- and L-band) Synthetic Aperture Radar data. *Isprs J. Photogramm. Remote. Sens.* 105, 234–250.
- Olson, D.M., Dinerstein, E., Wikramanayake, E.D., Burgess, N.D., Powell, G.V.N., Underwood, E.C., D'Amico, J.A., Itoua, I., Strand, H.E., Morrison, J.C., 2001. Terrestrial ecoregions of the world: a new map of life on earth. *BioScience* 51, 933–938.
- Pan, Y., Birdsey, R.A., Fang, J., Houghton, R., Kauppi, P.E., Kurz, W.A., Phillips, O.L., Shvidenko, A., Lewis, S.L., Canadell, J.G., 2011. A large and persistent carbon sink in the World's Forests. *Science* 333, 988–993.
- Pereira, H.M., Ferrier, S., Walters, M., Geller, G.N., Jongman, R., Scholes, R.J., Bruford, M.W., Brummitt, N., Butchart, S., Cardoso, A., 2013. Essential biodiversity variables. *Science* 339, 277–278.
- Perrin, I.F., Nicolas, B., Jean-Stéphane, B., Nicolas, B., Valéry, G., Bruno, N., Mahmoud El, H., Frédéric, F., José, 2016. Regional scale rain-forest height mapping using regression-kriging of space borne and airborne LiDAR data: application on French Guiana. *Remote Sens.* 8, 240.
- Phillips, S.J., Dud, M., Schapire, R.E., 2004. A maximum entropy approach to species distribution modeling. *Proceedings of the Twenty-First International Conference on Machine Learning.* 2004, 1015412: ACM, 83.
- Phillips, S.J., Anderson, R.P., Schapire, R.E., 2006. Maximum entropy modeling of species geographic distributions. *Ecol. Modell.* 190, 231–259.
- Piao, S., Fang, J., Zhu, B., Tan, K., 2005. Forest biomass carbon stocks in China over the past 2 decades: estimation based on integrated inventory and satellite data. *J. Geophys. Res. Biogeosci.* 110.
- Quegan, S., Yu, J.J., 2001. Filtering of multichannel SAR images. *Geosci. Remote Sens. IEEE Trans.* 39, 2373–2379.
- Rauste, Y., 2005. Multi-temporal JERS SAR data in boreal forest biomass mapping. *Remote Sens. Environ.* 97, 263–275.
- Reese, H., Nilsson, M., Pahlén, T.G., Hagner, O., Joyce, S., Tingelöf, U., Egberth, M., Olsson, H., 2003. Countrywide estimates of forest variables using satellite data and field data from the national forest inventory. *Ambio A J Hum. Environ.* 32, 542–548.
- Réjou-Méchain, M., Muller-Landau, H.C., Detto, M., Thomas, S.C., Toan, T., Saatchi, S.S., 2014. Local spatial structure of forest biomass and its consequences for remote sensing of carbon stocks. *Biogeosciences* 11.
- Rignot, E., Salas, W.A., Skole, D.L., 1997. Mapping deforestation and secondary growth in Rondonia, Brazil, using imaging radar and thematic mapper data. *Remote Sens. Environ.* 59, 167–179.
- Rodríguez-Veiga, P., Saatchi, S., Tansey, K., Balzter, H., 2016. Magnitude, spatial distribution and uncertainty of forest biomass stocks in Mexico. *Remote Sens. Environ.* 183, 265–281.
- Rodríguez-Veiga, P., Wheeler, J., Louis, V., Tansey, K., Balzter, H., 2017. Quantifying forest biomass carbon stocks from space. *Curr. For. Rep.* 1–18.
- Rosen, P.A., Hensley, S., Shaffer, S., Veilleux, L., Chakraborty, M., Misra, T., Bhan, R., Sagi, V.R., Satish, R., 2015. The nasa-isro sar mission-an international space partnership for science and societal benefit. *Radar Conference (RadarCon).* IEEE, 2015.
- IEEE, 1610–1613.
- Rosen, P., Hensley, S., Shaffer, S., Edelstein, W., Kim, Y., Kumar, R., Misra, T., Bhan, R., Satish, R., Sagi, R., 2016. An update on the nasa-isro dual-frequency DfB Sar (Nisar) mission. *Geoscience and Remote Sensing Symposium (IGARSS) 2106–2108.*
- Saarela, S., Holm, S., Grafström, A., Schnell, S., Nasset, E., Gregoire, T.G., Nelson, R.F., Ståhl, G., 2016. Hierarchical model-based inference for forest inventory utilizing three sources of information. *Ann. For. Sci.* 73, 895–910.
- Saatchi, S.S., Moghaddam, M., 2000. Estimation of crown and stem water content and biomass of boreal forest using polarimetric Sar imagery. *Ieee Trans. Geosci. Remote. Sens.* 38, 697–709.
- Saatchi, S.S., Houghton, R., Dos Santos Alvares, R., Soares, J., Yu, Y., 2007. Distribution of aboveground live biomass in the Amazon Basin. *Glob. Chang. Biol.* 13, 816–837.
- Saatchi, S.S., Harris, N.L., Brown, S., Lefsky, M., Mitchard, E.T.A., Salas, W., Zutta, B.R., Buermann, W., Lewis, S.L., Hagen, S., Petrova, S., White, L., Silman, M., Morel, A., 2011. Benchmark map of forest carbon stocks in tropical regions across three continents. *Proc. Natl. Acad. Sci.* 108, 9899–9904.
- Sandberg, G., Ulander, L.M.H., Fransson, J.E.S., Holmgren, J., Le Toan, T., 2011. L- and P-Band backscatter intensity for biomass retrieval in hemiboreal forest. *Remote Sens. Environ.* 115, 2874–2886.
- Santoro, M., Eriksson, L., Askne, J., Schmillius, C., 2006. Assessment of stand-wise stem volume retrieval in boreal forest from Jers-1 L-band Sar backscatter. *Int. J. Remote Sens.* 27, 3425–3454.
- Santoro, M., Beer, C., Cartus, O., Schmillius, C., Shvidenko, A., Mccallum, I., Wegmüller, U., Wiesmann, A., 2011. Retrieval of growing stock volume in boreal forest using hyper-temporal series of Envisat ASAR ScanSAR backscatter measurements. *Remote Sens. Environ.* 115, 490–507.
- Santoro, M., Beaudoin, A., Beer, C., Cartus, O., Fransson, J.E., Hall, R.J., Pathe, C., Schmillius, C., Schepaschenko, D., Shvidenko, A., 2015a. Forest growing stock volume of the northern hemisphere: spatially explicit estimates for 2010 derived from Envisat ASAR. *Remote Sens. Environ.* 168, 316–334.
- Santoro, M., Eriksson, L.E., Fransson, J.E., 2015b. Reviewing Alos Palsar backscatter observations for stem volume retrieval in Swedish Forest. *Remote Sens.* 7, 4290–4317.
- Schmillius, C., 2017. Globbiomass – estimates of biomass on global and regional scales. 37th International Symposium On Remote Sensing Of Environment (Irsr-37).
- Schmillius, C., Seifert, F.M., Thiel, C., Pathe, C., Matejka, E., Quegan, S., Carreiras, J., Wegmüller, U., Santoro, M., Balzter, H., Tansey, K., Rodríguez-Veiga, P., Le Toan, T., Mermoz, S., Bouvet, A., Dabrowska-Zielinska, K., Hosco, A., Ziolkowski, D., Siegert, F., Englhart, S., Fransson, J., Herold, M., Avitabile, V., Häme, T., Rauste, Y., Shvidenko, A., Fritz, S., Schepaschenko, D., Sterenczak, K., Eriksson, L., Ulander, L., Reichstein, M., Carvalhais, N., 2015. Due globbiomass - estimates of biomass on a global scale. *Irsr (May)*, 11–15 2015 Berlin.
- Searle, E.B., Chen, H.Y.H., 2017. Tree size thresholds produce biased estimates of forest biomass dynamics. *For. Ecol. Manage.* 400, 468–474.
- Sexton, J.O., Song, X.-P., Feng, M., Noojipady, P., Anand, A., Htuang, C., Kim, D.-H., Collins, K.M., Channan, S., Dimiceli, C., 2013. Global, 30-m resolution continuous fields of tree cover: Landsat-based rescaling of Modis vegetation continuous fields with Lidar-based estimates of error. *Int. J. Digit. Earth* 6, 427–448.
- Shimada, M., Isoguchi, O., 2002. Jers-1 Sar mosaics of Southeast Asia using calibrated path images. *Int. J. Remote Sens.* 23, 1507–1526.
- Shimada, M., Ohtaki, T., 2010. Generating large-scale high-quality Sar Mosaic datasets: application to Palsar data for global monitoring. *Selected topics in applied earth observations and remote sensing.* Ieee J. 3, 637–656.
- Shimada, M., Itoh, T., Motooka, T., Watanabe, M., Shirashi, T., Thapa, R., Lucas, R., 2014. New global forest/non-forest maps from Alos Palsar Data (2007–2010). *Remote Sens. Environ.* 155, 13–31.
- Shvidenko, A.Z., Schepaschenko, D.G., 2014. Carbon budget of Russian Forests. *Siberian J. For. Sci.* 69–92.
- Steffen, W., Noble, I., Canadell, J., 1998. The Terrestrial Carbon Cycle: Implication For The Kyoto Protocol. *Science* 280, 1393–1394.
- Sun, G., Ranson, K.J., Guo, Z., Zhang, Z., Montesano, P., Kimes, D., 2011. Forest biomass mapping from Lidar and radar synergies. *Remote Sens. Environ.* 115, 2906–2916.
- Tansey, K.J., Luckman, A.J., Skinner, L., Balzter, H., Strozzi, T., Wagner, W., 2004. Classification of forest volume resources using Ers Tandem Coherence and Jers Backscatter Data. *Int. J. Remote Sens.* 25, 751–768.
- Thiel, C., Schmillius, C., 2016. The potential of Alos Palsar backscatter and Insar Coherence for Forest growing stock volume estimation in Central Siberia. *Remote Sens. Environ.* 173, 258–273.
- Turner, M., Beer, C., Santoro, M., Carvalhais, N., Wutzler, T., Schepaschenko, D., Shvidenko, A., Komptzer, E., Ahrens, B., Levick, S.R., Schmillius, C., 2014. Carbon stock and density of northern boreal and temperate forests. *Glob. Ecol. Biogeogr.* 23, 297–310.
- Turner, M., Beer, C., Gais, P., Friend, A.D., Ito, A., Kleidon, A., Lomas, M.R., Quegan, S., Rademacher, T.T., Schaphoff, S., Tum, M., Wiltshire, A., Carvalhais, N., 2017. Evaluation of climate-related carbon turnover processes in global vegetation models for boreal and temperate forests. *Glob. Chang. Biol.* 23, 3076–3091.
- Tomppo, E., Olsson, H., Ståhl, G., Nilsson, M., Hagner, O., Katila, M., 2008. Combining national forest inventory field plots and remote sensing data for forest databases. *Remote Sens. Environ.* 112, 1982–1999.
- Tsui, O.W., Coops, N.C., Wulder, M.A., Marshall, P.L., 2013. Integrating Airborne Lidar and Space-Borne Radar via Multivariate Kriging to estimate above-ground biomass. *Remote Sens. Environ.* 139, 340–352.
- Urbaznev, M., Thiel, C., Cremer, F., Dubayah, R., Migliavacca, M., Reichstein, M., Schmillius, C., 2018. Estimation of forest aboveground biomass and uncertainties by integration of field measurements, Airborne Lidar, And Sar and optical satellite data in Mexico. *Carbon Balance Manag.* 13, 5.

III. Biomass estimation in tropical forests using the backscatter approach in different biomes (Chapter II)

P. Rodríguez-Veiga et al.

Int J Appl Earth Obs Geoinformation 77 (2019) 53–68

- Villard, L., 2009. Forward & Inverse Modeling For Synthetic Aperture Radar Observables In Bistatic Configuration. Applications In Forest Remote Sensing. Institut Supérieur De L'aéronautique Et De L'espace.
- Villard, L., Borderies, P., 2007. backscattering border effects for forests At C-band. *Piers Online* 3, 731–735.
- Villard, L., Le Toan, T., 2015. Relating P-band Sar intensity to biomass for tropical dense forests in hilly terrain: T0 Or T0? *IEEE J. Sel. Top. Appl. Earth Obs. Remote. Sens.* 8, 214–223.
- Whittaker, R.H., 1962. Classification of natural communities. *Bot. Rev.* 28, 1–239.
- Whittaker, R.H., 1970. *Communities and Ecosystems*. Communities and Ecosystems.
- Xu, L., Saatchi, S.S., Yang, Y., Yu, Y., White, L., 2016. performance of non-parametric algorithms for spatial mapping of tropical forest structure. *Carbon Balance Manag.* 11, 18.
- Yin, G., Zhang, Y., Sun, Y., Wang, T., Zeng, Z., Piao, S., 2015. Modis based estimation of forest aboveground biomass in China. *PLoS One* 10, E0130143.
- Yu, Y., Saatchi, S., 2016. Sensitivity of L-band sar backscatter to aboveground biomass of global forests. *Remote Sens.* 8, 522.

IV. Biomass estimation in tropical forests based on Pol-InSAR data (Chapter III)

Berninger, A., Lohberger, S., Zhang, D. & F. Siegert (2019) Forest Height and Above-Ground Biomass retrieval in Tropical Forests Using Multi-Pass X- and C-Band Pol-InSAR Data. *Remote Sensing*, 11(18), 2105-2128.



Article

Canopy Height and Above-Ground Biomass Retrieval in Tropical Forests Using Multi-Pass X- and C-Band Pol-InSAR Data

Anna Berninger^{1,2,*}, Sandra Lohberger¹, Devin Zhang³ and Florian Siegert^{1,2}

¹ Remote Sensing Solutions GmbH, Dingolfinger Str. 9, 81673 Munich, Germany

² Department of Biology, Ludwig-Maximilians-University Munich, Großhaderner Str. 2, 82152 Planegg-Martinsried, Germany

³ A.U.G. Signals Ltd. (AUG), 73 Richmond Street West, Suite 103, Toronto, ON M5H 4E8, Canada

* Correspondence: berninger@rsgsgmbh.de

Received: 31 July 2019; Accepted: 6 September 2019; Published: 9 September 2019

Abstract: Indonesia's landscape is strongly characterized by degradation and deforestation, which results in carbon release. This makes Indonesia one of the largest carbon sources worldwide. The study at hand, investigates monitoring of canopy height and above-ground biomass (AGB) from space in Indonesian tropical forests. Using data from 2015, the canopy height and AGB were modelled in Kalimantan based on quad-pol Pol-InSAR data from RADARSAT-2 (RS-2) and dual-pol Pol-InSAR data from TerraSAR-X (TS-X). Novel algorithms utilizing the Random Volume over Ground (RVoG) interferometric model and the Random Motion over Ground (RMoG) interferometric model were tested to obtain a more accurate and robust forest parameter estimation during dry weather conditions. As a reference for modelling canopy height and AGB, extensive field inventory as well as LiDAR and drone data collected in Kalimantan were used.

The RMoG model-based height inversion algorithm led to more accurate results for canopy height than the RVoG model. Using RS-2 imagery, the independent validation displayed a coefficient of determination (R^2) of 0.63 and a slight overestimation for the modelled canopy height. The modelled canopy height from TS-X data achieved an R^2 of up to 0.66 and resulted in underestimated modelled canopy height. The resulting AGB estimation based on the modelled canopy height resulted in an R^2 of 0.83 for RS-2 data and 0.84 for TS-X data. The results of the different tested images varied since the acquisition parameters and the weather conditions changed during acquisitions. It can be concluded, that not all RS-2 and TS-X data is suitable for modelling canopy height from coherence. The parameters that most affect the canopy height model were identified as the baselines (temporal and perpendicular), HoA (height of ambiguity), incident angle and moist weather conditions, as well as the wavelength. Ascending and descending flight directions did not display influence.

Globally available high-resolution information about canopy height and AGB is important for carbon accounting. The present study showed that Pol-InSAR data from TS-X and RS-2 could be used together with field inventories and high-resolution data such as drone or LiDAR data to support the carbon accounting in the context of REDD+ (Reducing Emissions from Deforestation and Forest Degradation) projects.

Keywords: TerraSAR-X; RADARSAT-2 carbon; Pol-InSAR; Random Volume over Ground (RVoG); Random Motion over Ground (RMoG); linear regression modelling; Indonesia; peat swamp forest

1. Introduction

Tropical forests represent an extensive carbon reservoir containing approximately 40% of terrestrial carbon [1]. The unsustainable use of these forests causes large greenhouse gas emissions, which can be accounted for in form of carbon dioxide equivalents (CO₂-e). Deforestation and forest degradation in the tropics account for approximately 11% of global anthropogenic CO₂ emissions each year [2]. Particularly tropical, wooded peat lands form an additional carbon reservoir obtained from the forests growing on top. Indonesia's peatlands approximately store 55–58 Gt of carbon [3,4]. Nevertheless, the tropical forests in Indonesia are affected by severe anthropogenic impacts, resulting in significant carbon emissions. Between 1990 and 2010, Borneo lost about half of its original peatland forest. This is mainly due to legal and illegal logging, extensive expansion of plantations, massive peatland drainage, and significant forest fires caused by extreme El Niño droughts in 1997/98, 2009 and 2015. Due to this anthropogenic destruction, Indonesia has become one of the largest greenhouse gas emitters [5] in the world and a prime target for REDD+ (Reducing Emissions from Deforestation and Forest Degradation) projects [6]. The REDD+ projects require close monitoring of carbon stocks of forests and their spatial distribution [7]. Forest carbon stocks are primarily derived based on the assumption that 50% of above-ground biomass (AGB) is carbon [8]. Biomass itself is defined as the fundamental biophysical parameter quantifying the Earth's living vegetation [9]. It describes the amount of woody matter within a forest and is specified by the Global Climate Observing System (GCOS) as an essential climate variable (ECV) [10]. Thus, the urgency to develop suitable methods for accurate, large-scale detection of canopy height and biomass has increased significantly. Collecting punctual AGB field data is time-consuming and expensive, and only provides limited information about the spatial variability within different forest types.

Remote sensing is able to overcome these limitations. Earth observation approach is able to cover larger areas and in a more cost-effective manner. The inaccessibility of tropical forests is a hindrance for extensive field inventory and highlights the benefits of remote sensing. Radar satellite data has the advantage that it is independent of cloud cover and the time of day [11]. Especially in tropical regions, cloud coverage is a reoccurring issue that aggravates monitoring based on multispectral satellite data. The extrapolating of accurate forest inventories or regional LiDAR-derived biomass estimations with large-scale satellite imagery represents an appropriate compromise [12–15]. Solberg et al. [16] and Englhart et al. [17] investigated the suitability of airborne laser scanning (ALS) for extrapolating biomass reference data from field plots. LiDAR data allows for accurate estimates of canopy closure, tree height and AGB based on point cloud metrics [18,19]. Many studies have demonstrated a great potential of LiDAR to estimate AGB in tropical forests [14,20,21]. Lidar point height distributions, such as the Quadratic Mean Canopy Height ($R^2 = 0.84$) and Centroid Height ($R^2 = 0.75$, RMSE = 20.5 t ha⁻¹) [22,23] were identified as appropriate parameters to estimate AGB from LiDAR data. Kronseder et al. [20] found an $R^2 = 0.83$ for LiDAR based AGB estimates in Indonesia's peat forests. Besides, Englhart et al. [24] derived an R^2 of 0.81 in tropical forests of Kalimantan, Indonesia and presented a robust application of LiDAR derived forest estimates. LiDAR provides accurate AGB estimations and was therefore used to extrapolate field inventory data for large-scale analysis based on Pol-InSAR data.

Other studies have successfully demonstrated the derivation of canopy height and AGB using polarimetric SAR interferometry (Pol-InSAR) techniques. Pol-InSAR is a remote sensing method that enables the investigation of the 3D structure of volume scatterers, such as forests. This results from the fact that the interferometric coherence is directly related to the vertical distribution of the backscattering elements and thus allows an exact 3D localization of the scattering center of an object. Using a coherent combination of single- and multi-baseline interferograms with different polarizations enables the characterization of vertical forest structure. Model based canopy height retrieval using Pol-InSAR data has been widely established and validated. The Random Volume over Ground (RVoG) model is often used for canopy height estimation from Pol-InSAR data as it interprets interferometric coherence as a function of vertical backscatter profiles [25–27]. Different studies have applied this model at various frequencies whereby the results were partly dependent on forest density [28,29]. A comparison of airborne X-, L-, and P-band Pol-InSAR data showed that L- and P-band achieved a lower variance in canopy height estimation than the X-band based canopy height

derivation [30]. The INDREX-II campaign by the German Aerospace Center (DLR) provided airborne X-, C-, L-, and P-band InSAR and Pol-InSAR data in tropical peat swamp forests on Borneo [31]. The authors found a good applicability of the RVoG model in tropical forests for both, L- and P-band, even if P-band estimations are on average higher than L-band estimations. In the context of INDREX-II, Hajnsek et al., [32] showed that canopy height determination is possible in Indonesian forests with L- and P-Band estimates within a 10% accuracy. The L-band estimates showed an R^2 of 0.91, while the P-band estimates were characterized by an R^2 of 0.94. Interferometric X-band data also provided an accurate estimate (R^2 in a range from 0.51 to 0.94) and underlined the high potential of Terra-SAR-X and Tandem-X X-band Pol-InSAR data for canopy height derivation. Kugler et al. [33] successfully derived the canopy height from TandDEM-X Pol-InSAR data in boreal, temperate and tropical forests. The authors achieved correlations between R^2 of 0.86 (boreal forest), R^2 of 0.77 (temperate forest), and R^2 from 0.54 to 0.69 (tropical forest) for dual-pol data. Besides X-, L-, and P-band, C-band Pol-InSAR data has been used only to a very limited extent for the derivation of canopy height [34]. Varekamp et al. [35] concluded in their study that C-band InSAR data are more suitable for canopy simulation than X-band InSAR data. The combination of X- and C-band Pol-InSAR data has only been used to a very limited extent for the determination of canopy heights in tropical forests so far.

This study analyzes the use of TerraSAR-X (X-band) and RADARSAT-2 (C-band) Pol-InSAR datasets for the determination of canopy height in tropical peat forests in Indonesia based on different wavelengths, acquisition parameters, and weather conditions. (i) First, the suitability of two different inversion models, Random Volume over Ground (RVoG) and Random Motion over Ground (RMoG), regarding their performance modelling canopy height from X- and C-band Pol-InSAR data was investigated. (ii) Secondly, regional regression models were set up based on the canopy height in order to model AGB on a high-resolution basis. Canopy height and above-ground biomass (AGB) derived from field inventory and LiDAR data were used as reference data for model calibration and validation. The resulting canopy height and AGB maps ranging in resolution from 3–12 m allows a monitoring of even small-scaled changes in the forests of Indonesia. This higher spatial resolution is important in order to make them a promising alternative building a forest monitoring or risk managing system, but also to achieve the objectives of REDD+, UNEP-WCMC, the Global Canopy Programme, and other programs protecting forests or analyzing carbon release at national and subnational levels.

2. Study Area and Data

2.1. Study Area

The study area is located south of Palangka Raya in Central Kalimantan on the island of Borneo, Indonesia (Figure 1). The predominant vegetation in the area of interest is tropical peat swamp forest. The subterranean peat dome was formed over thousands of years by plant residues under water-saturated conditions [36]. In this area of Kalimantan, they can reach a width of 20 m and form a gigantic carbon reservoir, up to ten times larger than the forests growing on top [3]. Due to severe anthropogenic destruction, the peat domes release enormous emissions. Legal and illegal logging, drainage and fires have degraded the forests and thus the peat domes.

The majority of the area of interest is located in the Sebangau National Park, which was designated as such in 2004. Since this area is protected, a slight change in canopy height and AGB is expected. Peat swamp forests usually have a maximum tree height of 20–30 m and an average AGB of 252–314 t ha⁻¹ in Central Kalimantan, depending on the soil conditions and the forest type [37,13].

2.2. Reference Data

2.2.1. Field Inventory Data

An overview of the reference data within the study area is visible in Figure 1. We collected field inventory data in forest and reforestation areas in 2010 and 2011 ($n = 53$). The inventory plot design was divided into two different recording systems based on the recommendations of the High Carbon

IV. Biomass estimation in tropical forests based on Pol-InSAR data (Chapter III)

Remote Sens. **2019**, *11*, 2105

4 of 24

Stock Science Study [38,24] and Pearson et al. 2005 [39]. In forested areas, with high biomass values, we collected data in concentric circular nested plots ($n = 36$). Within each nest of the circular nested plots, DBH, tree height, and tree species of trees with a certain breast height diameter (DBH) were measured depending on degradation intensity: 2 cm to 10 cm or 5 cm to 20 cm (within the 4 m radius), 10 cm to 20 cm or 20 cm to 50 cm (within 14 m radius), and greater than 20 cm or 50 cm (within 20 m radius) [24]. In regrowing areas, e.g., after a forest fire, data was collected in rectangular plots with a size of 50 m \times 20 m ($n = 17$) in the context of former projects [23,24]. Within the rectangular plots all trees were measured regarding DBH, tree height, and tree species.

2.2.2. LiDAR Data

LiDAR data was recorded during the dry season between August and October 2011. Measurements were acquired using Optech Orion M200 and Optech ALTM 3100 airborne laser scanners (Teledyne Optech, Vaughan, Ontario, Canada) at an altitude of 800 m above-ground. The data was collected using a half scan angle of $\pm 11^\circ$. Point density amounted up to 10.7 points per m^2 . The accuracy of AGB estimations derived from LiDAR metrics increases with a higher point density, which is why a weighting of the plots accordingly to their point density was conducted [24]. In total, 4 340 ha were covered within the study area. The areas covered by LiDAR is depicted in Figure 1.

During a drone flight mission in 2016, 270 ha were flown, covering all inventory plots and other areas. The unmanned aerial vehicle (UAV) used in the mission recorded optical data in RGB with a 1/2.3" CMOS sensor and with a resolution of 4 000 \times 3 000 pixel. A lens with a field of view (FOV) of 94° above ground level (AGL) ensured a constant and terrain independent ground resolution of 5 cm. All images were acquired in nadir and with an 80% forward- and side overlap. Furthermore, the entire flight area was recorded in two directions of flight with perpendicular flight tracks in order to increase data density and to attain a larger amount of matching points during the photogrammetric processing.

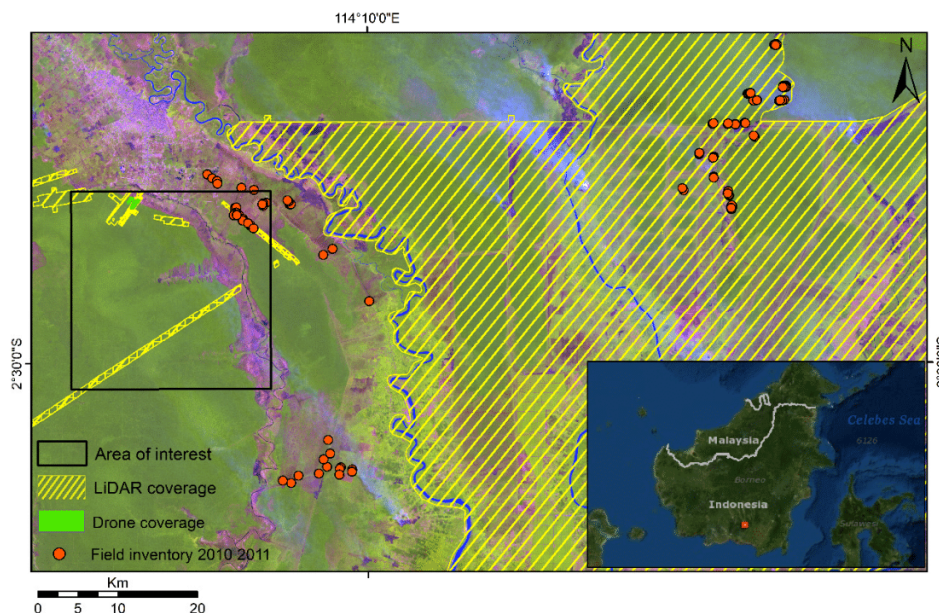


Figure 1. RGB composite of Landsat-8 (short-wave infrared, near-infrared, red) from 2015 showing the location of the area of interest including the field plots from 2010–2011 and the LiDAR (2011) and UAV (2016) coverage.

2.3. SAR Data

RS-2, launched by the Canadian Space Agency (CSA) in 2007, operates at C-band with a wavelength of 5.6 cm and a frequency of 5.3 GHz. For this study, single look complex (SLC) imageries acquired in the fine quad-polarization wide (FQW) mode with a nominal spatial resolution of 8 m was used. Further information about the characteristics of the data are listed in Table 1.

The DLR launched the TS-X satellite in June 2007. TS-X provides different acquisition modes with varying spatial resolutions at X-band wavelength (3 cm) with a frequency of 9.65 GHz. In the study at hand, SLC data acquired in stripmap mode with dual polarization (HH/HV) and a resolution of 6 m in both azimuth and ground range was used. The characteristics of the datasets are summarized in Table 2.

The image parameters for both sensors vary concerning the perpendicular baseline, the height of ambiguity (HoA), beam modes and incidence angles θ in both far range (FR) and near range (NR). Furthermore, the data was acquired in ascending and descending mode during the dry season in 2015.

Table 1. RS-2 data and the different acquisition parameters from 2015 applied in the study. (Date format = DD.MM.2015. Perp. baseline = perpendicular baseline, HoA = height of ambiguity, θ = incidence angle in far range (FR) and near range (NR)).

Ascending					
Dates	Perp. Baseline [m]	HoA [m]	Beam Mode	θ NR [°]	θ FR [°]
18.08.–11.09.	159.27	91.90	FQ14W	32.69	35.66
25.08.–18.09.	46.00	235.00	FQ7W	24.89	28.25
11.09.–05.10.	43.12	339.47	FQ14W	32.69	35.66
18.09.–12.10.	18.63	585.91	FQ7W	24.89	28.25
05.10.–29.10.	59.42	246.37	FQ14W	32.69	35.66
Descending					
Dates	Perp. Baseline [m]	HoA [m]	Beam Mode	θ NR [°]	θ FR [°]
10.08.–03.09.	45.00	193.00	FQ3W	20.06	23.63
03.09.–27.09.	56.55	155.53	FQ3W	20.06	23.63
27.09.–21.10.	34.8	252.83	FQ3W	20.06	23.63

Table 2. TS-X data and the different acquisition parameters from 2015 used in the study. (Date format = DD.MM.2015. Perp. baseline = perpendicular baseline, HoA = height of ambiguity, θ = incidence angle in far range (FR) and near range (NR)).

Ascending					
Dates	Perp. Baseline [m]	HoA [m]	Beam Mode	θ NR [°]	θ FR [°]
13.07.–24.07.	158.39	29.00	stripNear_007R	29.66	31.26
24.07.–04.08.	89.47	51.64	stripNear_007R	29.66	31.26
04.08.–15.08.	152.31	30.33	stripNear_007R	29.66	31.26
15.08.–26.08.	63.14	73.17	stripNear_007R	29.66	31.26
06.09.–17.09.	13.33	361.53	stripFar_007R	30.79	32.32

3. Methods

An overview of this study’s workflow is displayed in Figure 2. The applied steps are described in the following section in detail.

IV. Biomass estimation in tropical forests based on Pol-InSAR data (Chapter III)

Remote Sens. 2019, 11, 2105

6 of 24

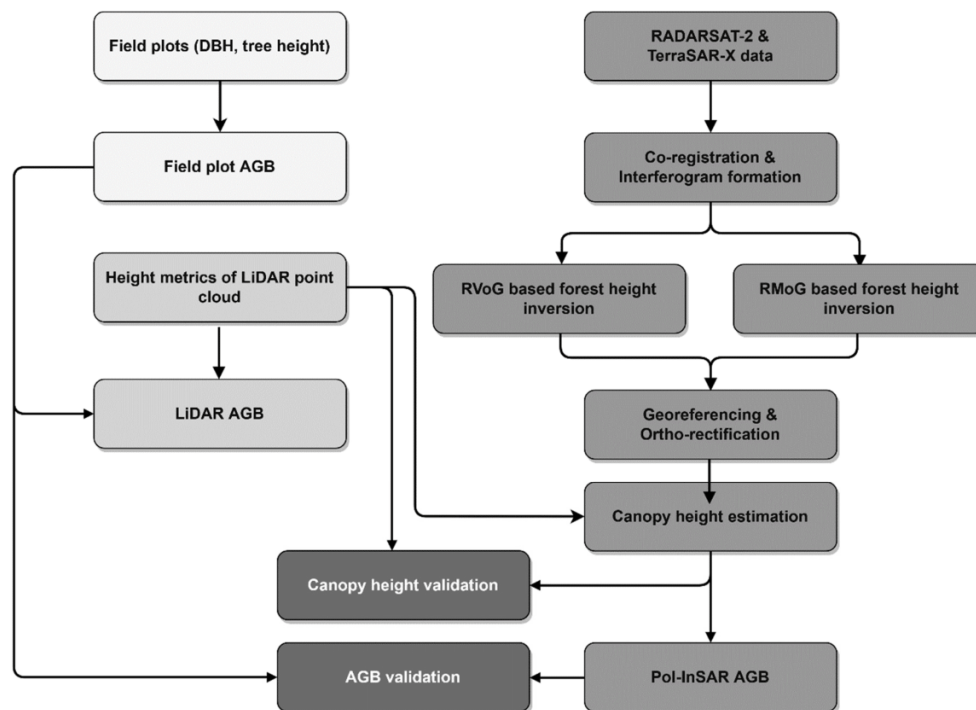


Figure 2. Workflow of the methodology applied in this study (bright grey = field data, grey = LiDAR data, medium dark grey = SAR data, dark grey = validation).

3.1. Extrapolated Reference Data

Canopy height from LiDAR data and AGB based on field inventory and LiDAR height metrics are used as reference data, representing the highest possible accuracy, for model calibration and validation. In a first step, a Digital Surface Model (DSM) was estimated from the hierarchical filtered highest points of the LiDAR point cloud. Besides, the DTM (Digital Terrain Model) with a resolution of 1 m was calculated from the filtered ground points of the 3D LiDAR point cloud [23,40]. By subtracting the DTM from the LiDAR DSM, a very accurate determination of the canopy height became possible. The final Canopy Height Model (CHM) based on LiDAR data has a spatial resolution of 1 m and is resampled to the respective Pol-InSAR data.

The field inventory data enabled the estimation of AGB in $t\ ha^{-1}$ by using the tree height, DBH, and wood specific density of each tree as the input for a combination of different allometric models. We applied allometric models according to [41] for saplings (DBH < 5 cm and height ≤ 1.3 m) and small trees (DBH < 5 cm and height > 1.3 m) and based on [42] for moist tropical forest stands (DBH ≥ 5 cm and height > 1.3 m). The applied models are described in detail in [24]. In a next step this ground-based AGB in $t\ ha^{-1}$ was related to the LiDAR transects in order to estimate AGB reference data based on centroid height derived from LiDAR using previously established regression models [23,24]. For each AGB grid cell, we computed the LiDAR height histograms by normalizing all points within a grid of 20 m (the same radius as the field plots) using the DTMs as ground reference as in [23,24]. The regression models are based on a combination of a power function in the lower biomass range and a linear function in the higher biomass range using the centroid height to calculate a certain threshold [24]. The centroid height is an appropriate height parameter of the LiDAR point cloud. The threshold of the centroid height was determined by increasing the value in steps of 0.001 m by identifying the lowest RMSE. The resolution of the final AGB map is 5 m and is resampled to the respective Pol-InSAR data. This extrapolating from field inventory data to LiDAR transects allows the creation of numerous biomass reference data for the calibration of SAR images.

In addition, inventory plots and surrounding areas were covered during a drone mission, approximately 270 ha. With the use of a Semi-Global Matching (SGM), a dense stereo-matching procedure, a 3D point cloud was created from the captured aerial photos. Similar to the LiDAR point cloud, a DSM was derived from this point cloud, which allowed a very precise determination of the canopy height minus the existing LiDAR DTM. We compared the unmanned aerial vehicle (UAV) derived canopy height to the LiDAR derived canopy height resulting in a correlation of 0.89.

3.2. SAR Processing

We applied a speckle reduction using the Refined Lee filter. Besides filtering, the co-registration of repeat pass SAR data is fundamental for generating an interferogram, as it ensures that a target on the ground corresponds to the same pixel in the master as in the slave image. This step compensates for different sensor attitudes, orbit crossings, along- and across track shifting and different sampling rates. After co-registering the image pairs, we computed an interferogram, also called the phase difference, for each pixel. The interferogram of two registered complex images was calculated by the multiplication of one image with the conjugate of the second image [43].

In a next step, we smoothed the interferogram by using an adaptive filter based on the local fringe spectrum. The goal of the adaptive filter was to reduce phase noise, thereby reducing the number of residues. It read the complex valued interferogram, computed the interferogram power spectrum, designed a filter based on the power spectrum, filtered the interferogram, estimated the phase noise coherence value for the filtered interferogram and finally wrote the filtered interferogram.

3.3. Canopy Height Estimation

We tried two inversion models in order to estimate canopy height, the RVoG and the RMoG model. The RVoG model is a simple two-layer model, in which one layer represents the forest canopy and the other a reflective ground layer below the vegetation layer. It simulates vegetation as a homogeneous layer of thickness (h_v) containing volume scatterers with randomly oriented particles over a ground scatterer positioned at z . The model ignores the even-bounce scattering mechanism as well as higher order interactions. Pol-InSAR data is commonly used as input because it provides a number of independent parameters for modelling [26].

The RVoG presents the interferometric coherence $\tilde{\gamma}$ as

$$\tilde{\gamma} = \exp(i\phi_0) \frac{\tilde{\gamma}_v + m}{1 + m} \tag{1}$$

where ϕ_0 is the phase and refers to the topography of the ground, m is the effective ground-to-volume amplitude ratio. The complex coherence $\tilde{\gamma}_v$ for the volume is given as [44–46]

$$\tilde{\gamma}_v = \frac{I}{I_0} \begin{cases} I = \int_0^{h_v} \exp\left(\frac{2\sigma z'}{\cos\theta_0}\right) \exp(ik_z z') dz' \\ I_0 = \int_0^{h_v} \exp\left(\frac{2\sigma z'}{\cos\theta_0}\right) dz' \end{cases} \tag{2}$$

with θ_0 as the mean incidence angle, the assumption of an exponential distribution of all scatterers is a widely used approach, especially at higher frequencies such as X- and C-band [33]. $\tilde{\gamma}_v$ depends on the extinction coefficient for the random volume σ and its thickness (h_v). The variable dz is defined as an independent distributed random variable that represent the physical displacement of scatterers along z . The effective vertical interferometric wavenumber k_z depends on the wavelength λ and the imaging geometry as the difference of the incidence angle $\Delta\theta$ [44]

$$k_z = \frac{k\Delta\theta}{\sin\theta_0} \quad \text{with} \quad k = \frac{4\pi}{\lambda} \tag{3}$$

The RMoG links the RVoG coherence model with the temporal coherence model and volumetric decorrelation to overcome those limitations [47]. The RMoG model separates temporal and volumetric decorrelations into four structural parameters and two dynamic parameters. The structural parameters are the tree height, wave extinction, ground topography and ground-to-volume ratio. The dynamic parameters are known as ground and canopy motion standard deviations induced by the temporal baseline [47].

The complex coherence γ_M in the RMoG model is defined as

$$\gamma_M = \frac{\int_0^{h_v} p(z) \exp(jk_z z) \left(-\frac{1}{2} \left(\frac{4\pi}{\lambda}\right)^2\right) \sigma_r^2(z) dz}{\int_0^{h_v} p(z) dz} \quad (4)$$

where the scatterer motion function $\sigma_r^2(z)$ is obtained from

$$\sigma_r^2(z) = \sigma_g^2 + (\sigma_v^2 - \sigma_g^2) \frac{z - z_g}{h_r}, \quad (5)$$

with h_r as reference height, which is a constant, λ is the wavelength of the SAR system, and σ_g and σ_v are the ground and vegetation layer motion standard deviation. The term $p(z)$ is the structure function defining the vertical structure of the vegetation layer [47,48]. The structure of trees is assumed as a Gaussian function.

To compare the estimation results with each other as well as with the ground truth, we applied geo-referencing and ortho-rectifications. As a result, each pixel was mapped to a geographical location (longitude and latitude). After modelling the canopy height, an overestimation of the model was identified in the RS-2 results. For minimizing this overestimation, a linear correction factor of -1.4 m was applied on the final canopy height results of the RS-2 datasets.

3.4. SAR Based AGB Modelling

In a next step, we used Pol-InSAR based canopy height and LiDAR AGB as reference to set up a linear regression model for each scene based on 500 randomly selected pixels in the overlapping area. AGB was modelled for each scene based on the respective linear regression equation. Using the Cook's distance (Cook's D), influential outliers were removed from the set of predictor variables [49]. The Cook's D identifies points with large residuals based on the observation's leverage and the residual values, and thus influential outliers. Following this approach points over $4/n$, where n is the number of observations, are removed from the modelling process [49]. The final resolution of the Pol-InSAR AGB maps is 3 and 12 m depending on the used sensor.

3.5. Validation

The validation of the estimated canopy height and modelled AGB is achieved using the reference data of the canopy height estimated from the drone DSM in combination with LiDAR DTM. A random sampling strategy was applied in ArcGIS (ESRI) to collect 475 randomly selected pixel within an overlapping area of the drone, as well as the LiDAR reference data and the modelled canopy height. Our drone data was acquired one year after the SAR data, and the LiDAR data was acquired four years before the SAR data. Nevertheless, the coverage of the drone data with the Pol-InSAR data is just about 270 ha. The LiDAR data on the other hand covers, depending on image, more than 4000 ha of the Pol-InSAR scenes. To overcome the limitations of the small coverage of the UAV data, the validation for canopy height is achieved based on both reference datasets within the respective overlapping areas. Since drone data is only available for canopy height, AGB is validated entirely with LiDAR modelled AGB. The resolution of the AGB validation datasets is resampled to the resolution of the respective SAR based canopy height and AGB map (3–12 m).

4. Results

4.1. RVoG vs. RMoG

For testing RVoG model-based inversion, we used six sets of RS-2 pairs from different beam-modes FQ3W (10.08. and 03.09., 27.09. and 21.10.), FQ7W (18.09. and 25.08., 18.09. and 12.10.) and FQ14W (11.09. and 18.08, 11.09. and 05.10.) as inputs for the RVoG and RMoG algorithms.

The RVoG model shows a strong overestimation in canopy height modelling in comparison to the LiDAR data in all tested datasets. An example for the modelling results using both inversion models is shown in Figure 3. The scatterplots show a strong overestimation of modelled canopy height using the RVoG model. The RMoG model demonstrates its superiority over the RVoG resulting in a more significant p-value and a higher R^2 . As a result, we decided to use the better suitable RMoG model for estimating canopy height based on Pol-InSAR data in the following.

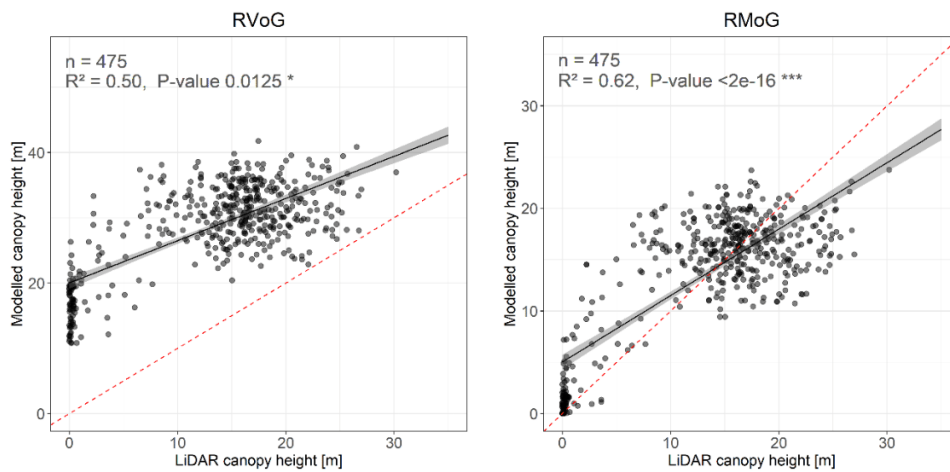


Figure 3. Correlation of reference LiDAR canopy height and modelled RS-2 canopy height for the RVoG (left) and RMoG (right) based on an interferogram from 27.09.-21.10. Dashed line = 1:1 line.

4.2. Canopy Height Estimation

In Figure 4, the canopy height of LiDAR, drone and two examples of RS-2 and TS-X based canopy height are displayed for a transect of approximately 500 m. The general pattern of the canopy height shows an appropriate overlap, but not all peaks match the reference height. The increase of the canopy height at a distance of 175 m results from a transition zone from non-forested area to forested area. The RS-2 based mean canopy height leads to an average overestimation of approximately 0.6 m compared to LiDAR reference and an underestimation of 0.16 m compared to the reference canopy height of the UAV. Mean tree height modelled from TS-X data is underestimated by 1.1 m compared to drone data and underestimated by 0.36 m in comparison to LiDAR canopy height. Both Pol-InSAR datasets tend to overestimate the canopy height in lower heights and underestimate in forested areas.

IV. Biomass estimation in tropical forests based on Pol-InSAR data (Chapter III)

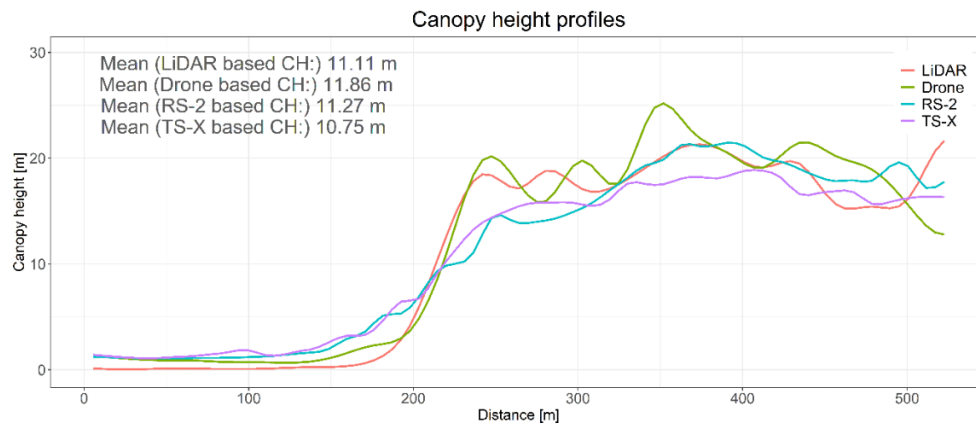


Figure 4. Example height profile of reference LiDAR canopy height, drone canopy height, modelled RS-2 canopy height based on the interferogram from 03.09.-27.09 and modelled canopy height based on TS-X from 06.09.-17.09.

Figure 5 gives an overview of the correlation of the modelled canopy height based on Pol-InSAR data and the reference data based on LiDAR. The coefficient of determination (R^2) for modelled canopy height from RS-2 varies between 0.62–0.63. The canopy height based on Pol-InSAR is overestimating heights ranging from 0–15 m and underestimates trees with heights taller than 15 m.

In Figure 6, the correlation of the reference and modelled canopy height based on TS-X is pointed out. The coefficient of determination varies from 0.58–0.66. Canopy heights modelled based on TS-X data result in an underestimation, whereby the image pair from July/August shows a stronger underestimation and a higher Root Mean Square Error (RMSE) than the interferogram estimated from two September images. A saturation effect can be identified at trees taller than 15 m.

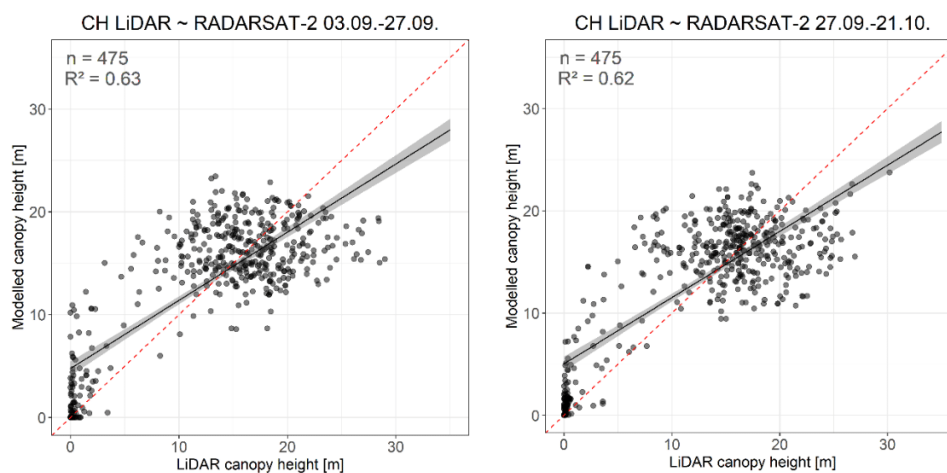


Figure 5. Correlation of reference LiDAR canopy height and modelled RS-2 canopy height using RMoG model based on an interferogram from 03.09.-27.09. (left) and 27.09.-21.10. (right). Red dashed line = 1:1 line; black line = linear trend including confidence bounds.

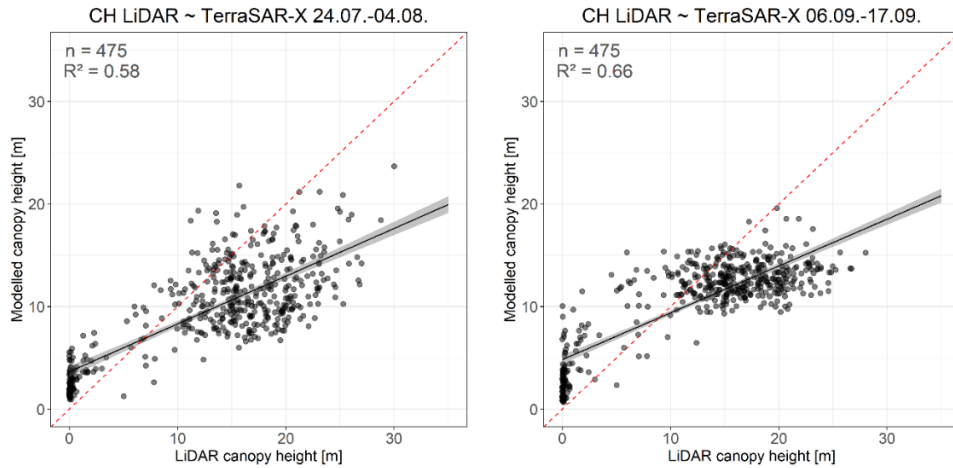


Figure 6. Correlation of reference LiDAR canopy height and modelled TS-X canopy height using RMoG model based on an interferogram from 24.07.–04.08. (left) and 06.09.–17.09. (right). Red dashed line = 1:1 line; black line = linear trend including confidence bounds.

In Figure 7, the differences between the modelling results of TS-X and RS-2 become clear. The correlation of the two sensors is strong until a canopy height of 10 m is reached. With increasing height, a stronger underestimation of TS-X in comparison to RS-2 is visible. At a height of approximately 15 m, a saturation effect in the TS-X data is monitored. For RS-2 the saturation effect can be identified at about 20 m.

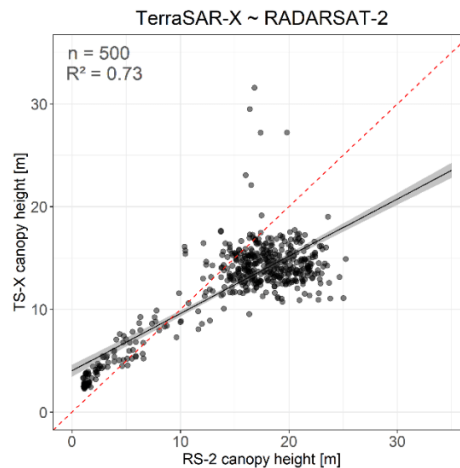


Figure 7. Correlation of modelled TS-X (06.09.–17.09.) canopy height and modelled RS-2 (03.09.–27.09.) canopy height based on the RMoG model. Red dashed line = 1:1 line; black line = linear trend including confidence bounds.

In Table 3 and 4, the validation statistics of the modelled canopy height are listed for both LiDAR and drone data. Each result was validated against the LiDAR and UAV canopy height using 475 collected random points, respectively. The LiDAR bias shows a slight overestimation of approximately 0.30–3.85 m for the modelled canopy height based on RS-2 and an underestimation

IV. Biomass estimation in tropical forests based on Pol-InSAR data (Chapter III)

(−3.5 – −6.07 m) for the TS-X data (Table 3). The coefficient of determination varies in a range from 0.39 – 0.66 for the different results, showing the highest correlation for the TS-X interferogram in the date span of 06.09.–17.09. The standard deviation (SD) shows a higher value for the reference data than for the modelled data, meaning that the model does not adequately capture the canopy height range. The RMSE is about 4.65–6.74 m for RS-2 based canopy height and 5.2–8.44 m for TS-X based canopy height. Two TS-X datasets could not be modelled since the coherence was too low. The four results with the highest coefficient of determination were used to model AGB and to compare with the UAV data from 2016 (Table 4). The drone data has a smaller time lag towards the SAR data than the LiDAR data. Nevertheless, the area covered by drone data is very small. The results are comparable to the LiDAR data, the RMSE is slightly lower, varying from 4.27–4.95. The bias is smaller than for LiDAR data, especially for TS-X. Nevertheless, TS-X still shows an underestimation, while RS-2 is overestimating canopy height in average.

Table 3. Validation statistics of canopy heights per interferogram based on LiDAR data. (\overline{CH}_{Ref} = mean of the reference canopy height, \overline{CH}_{Est} = mean of the estimated canopy height, SD = standard deviation, RMSE = root mean square error)

Sensor	Image Pair	\overline{CH}_{Ref} [m]	\overline{CH}_{Est} [m]	SD_{Ref} [m]	SD_{Est} [m]	Bias [m]	R ²	RMSE [m]	
RS-2	10.08.–03.09.	14.04	15.86	7.09	5.49	1.8	0.54	5.12	
	18.08.–11.09.	13.66	17.51	7.66	5.96	3.85	0.48	6.74	
	25.08.–18.09.	13.51	16.73	7.59	6.68	3.22	0.57	5.99	
	03.09.–27.09.*	13.08	13.43	7.61	6.36	0.35	0.63	4.65	
	11.09.–05.10.	13.45	15.58	7.75	6.93	2.13	0.59	5.43	
	18.09.–12.10.	13.43	13.62	7.69	6.31	0.18	0.60	4.88	
	27.09.–21.10.*	13.36	13.68	7.43	6.13	0.32	0.62	4.62	
	05.10.–29.10.	13.36	14.98	7.80	5.88	1.62	0.41	6.22	
13.07.–24.07.	Coherence too low for modelling								
24.07.–04.08.*	13.38	9.88	7.53	4.59	−3.5	0.58	6.10		
TS-X	04.08.–15.08.	Coherence too low for modelling							
	15.08.–26.08.	12.96	6.89	7.45	3.84	−6.07	0.39	8.44	
	06.09.–17.09.*	13.06	10.79	7.43	4.16	−2.27	0.66	5.21	

*datasets used for AGB modelling.

Table 4. Validation statistics of canopy heights per interferogram based on drone data. (\overline{CH}_{Ref} = mean of the reference canopy height, \overline{CH}_{Est} = mean of the estimated canopy height, SD = standard deviation, RMSE = root mean square error)

Sensor	Image Pair	\overline{CH}_{Ref} [m]	\overline{CH}_{Est} [m]	SD_{Ref} [m]	SD_{Est} [m]	Bias [m]	R ²	RMSE [m]
RS-2	03.09.–27.09.	13.95	15.21	7.36	6.40	1.25	0.69	4.27
	27.09.–21.10.	13.91	15.03	7.34	6.08	1.12	0.65	4.47
TS-X	24.07.–04.08.	13.13	11.81	7.05	4.49	−1.31	0.55	4.95
	06.09.–17.09.	13.50	12.38	7.06	4.17	−1.12	0.68	4.43

4.3. AGB Estimation

For AGB modelling, the datasets with the highest accuracy for the canopy height were used. The statistics of the linear regression models for modelling AGB in t ha^{−1} based on the canopy height are summarized in Table 5. In addition, coefficient of determination and the residual standard error (RSE) are displayed for the different models. The R² varies between 0.66–0.77 and points out the ability of the model to predict AGB based on canopy height. In Figure 8 and 9, the correlation of the reference and modelled AGB based on RS-2 and TS-X are pointed out. The coefficient of determination varies from 0.81–0.85 for RS-2 and from 0.60–0.85 for TS-X. RS-2 shows in general a better fit compared to the 1:1 line than the TS-X datasets. Both sensors tend to overestimate the AGB in lower biomass

IV. Biomass estimation in tropical forests based on Pol-InSAR data (Chapter III)

ranges and underestimate in higher biomass ranges. Estimated AGB from TS-X based on the datasets from 24.07.–04.08 depict a stronger scattering than the other datasets in the higher AGB range.

Table 5. Overview of the model statistics, adjusted R² and Residual Standard Error (RSE) for the linear regression AGB model based on canopy height.

Sensor	Image Pair	B	Std. Error	Beta	P Value	R ²	RSE [t ha ⁻¹]
RS-2	03.09.–27.09.	14.3462	0.4306	33.31	<2e-16 ***	0.74	60.68
	27.09.–21.10.	14.516	0.469	30.952	<2e-16 ***	0.71	58.3
TS-X	24.07.–04.08.	21.2768	0.7791	27.309	<2e-16 ***	0.66	63.67
	06.09.–17.09.	22.6038	0.6227	36.30	<2e-16 ***	0.77	52.16

Signif. codes: 0 '***' 0.001 '**' 0.01 '*' 0.05 '.' 0.1 ' ' 1.

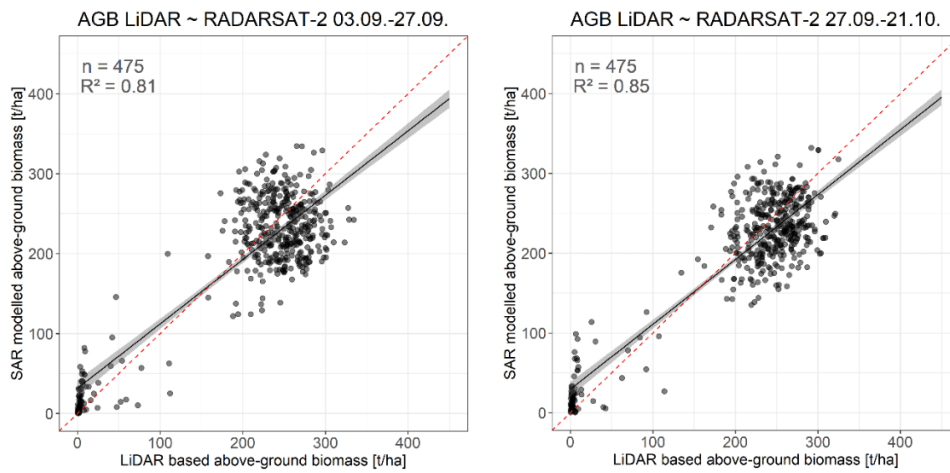


Figure 8. Correlation of reference LiDAR AGB and modelled RS-2 AGB based on an interferogram from 03.09.–27.09. (left) and 27.09.–21.10. (right). Red dashed line = 1:1 line; black line = linear trend including confidence bounds, n = 475.

IV. Biomass estimation in tropical forests based on Pol-InSAR data (Chapter III)

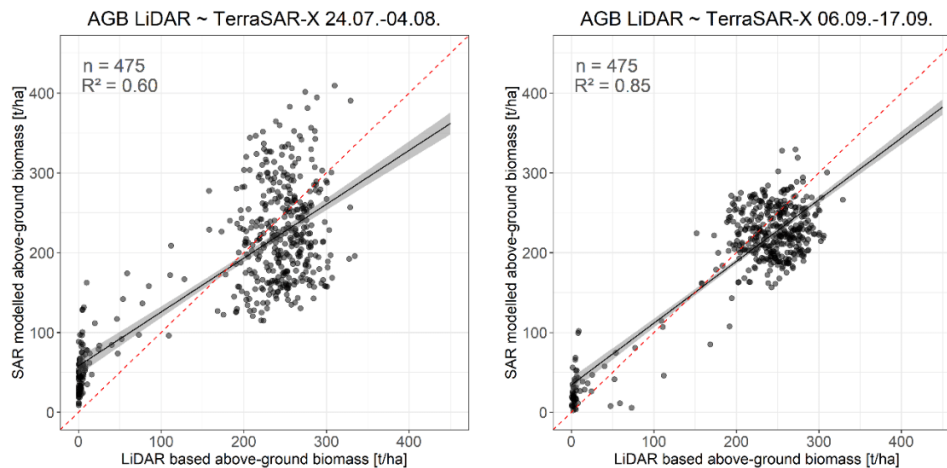


Figure 9. Correlation of reference LiDAR AGB and modelled TS-X AGB based on an interferogram from 24.07.–04.08. (left) and 06.09.–17.09. (right). Red dashed line = 1:1 line; black line = linear trend including confidence bounds.

The validation of the modelled AGB using 475 random points resulted in the statistics summarized in Table 6. R^2 varies from 0.66 to 0.84 showing a good agreement between the modelled AGB based on canopy height and the reference data. Nevertheless, the average AGB estimates are consistently lower than the reference biomass. The bias shows an underestimation of all four datasets and varies between 1.7% and 8.6%. Overall, the RMSE and coefficient of determination are similar in all datasets except for the TS-X data from July/August. This dataset shows higher deviations from the reference AGB than the other images. The relative RMSE varies from 20.2% to 23.3% for RS-2 datasets and from 20.9% to 32.9% for TS-X.

The comparison of different AGB maps shows the advantage of high-resolution images (Figure 10). The displayed wetland in the Sebangau National Park consists of a pattern of linearly vegetated and non-vegetated areas. TS-X with a resolution of 3 m is able to capture the pattern of the vegetation and its AGB better than existing maps. Even small-scaled variabilities and heterogeneities can be detected.

IV. Biomass estimation in tropical forests based on Pol-InSAR data (Chapter III)

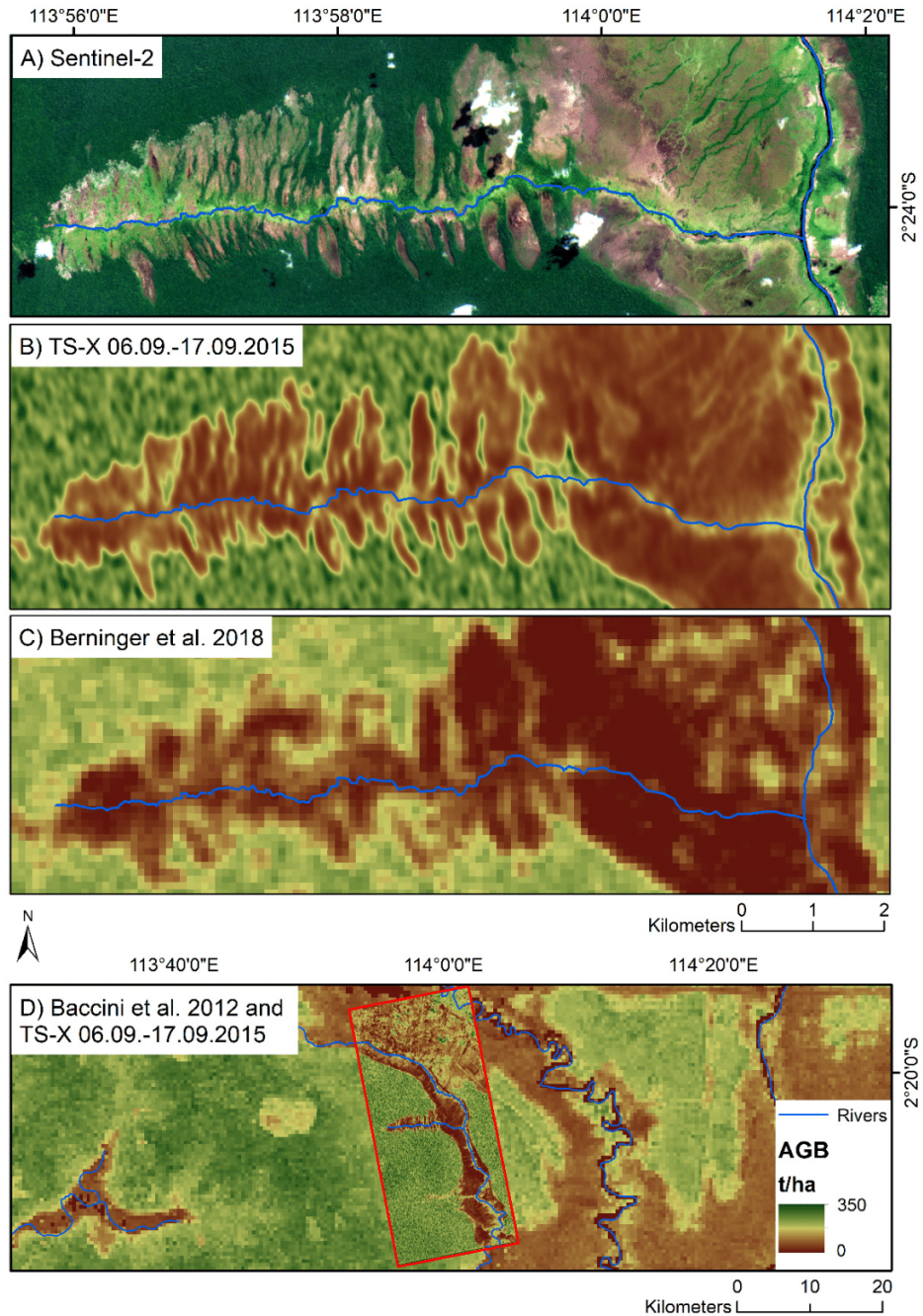


Figure 10. Comparison between different biomass maps. A) True-color image of Sentinel-2 showing a wetland in the Sebangau National Park, Central Kalimantan. B) AGB with a resolution of 3 m modelled based on TerraSAR-X images from 06.09.-17.09.2015. C) AGB with a resolution of 100 m, modelled by Berninger et al. [50] using ALOS PALSAR and Sentinel-1 from 2015. D) AGB with a resolution of 500 m, modelled by Baccini et al. [51] based on ICE-Sat data from 2007 through 2008 and the TS-X based AGB results are from 06.09.-17.09.2015 (framed in red).

Table 6. Validation statistics of AGB per image pair.

Sensor	Image Pair	\overline{AGB}_{Ref} [t ha ⁻¹]	\overline{AGB}_{Est} [t ha ⁻¹]	SD_{Ref} [t ha ⁻¹]	SD_{Est} [t ha ⁻¹]	Bias [t ha ⁻¹]	R ²	RMSE [t ha ⁻¹]
RS-2	03.09.–27.09.	197.30	188.05	100.64	95.83	–9.25	0.81	46.34
	27.09.–21.10.	198.14	188.02	100.10	93.68	–10.12	0.83	40.19
TS-X	24.07.–04.08.	196.94	191.08	100.49	87.82	–5.85	0.60	64.89
	06.09.–17.09.	196.44	181.48	99.19	93.44	–14.96	0.85	41.11

5. Discussion

5.1. Comparison of the RVoG and RMoG Models

The choice of different models has an effect on the resulting estimation result since the models differ in the number of input variables. The number of observables limits the complexity of the model meaning that the inversion process can be deterministic. However, a certain number of parameters is needed to deliver a good simulation of the scattering process. The RVoG model does not take the temporal baseline resulting from repeat-pass Pol-InSAR into consideration. However, the dynamic changes caused by wind, precipitations, seasonal variations and anthropogenic activities also lead to further decorrelation, altering the magnitude and phase of the observed coherence by an amount comparable to volumetric decorrelation.

Comparing the results of the two inversion models, the superiority of the RMoG model was pointed out. This is expected since the RVoG model does not take temporal decorrelation, introduced by the time gaps between acquisition dates, into consideration [48,47]. Especially the motion of scatterers, like wind motion of trees, results in lower coherences and inaccuracies in the canopy height estimation [52]. In addition, during this time period results of the inversion approach are not only affected by the motion of canopies but also by changes of dielectric properties [53]. Since all datasets of this study are multi-pass interferometric, temporal decorrelation is always present. The temporal baseline is about eleven days for TS-X and even 24 days for RS-2. As expected, the RMoG model demonstrates its capability to compensate parts of the temporal decorrelation.

5.2. Canopy Height Estimation

The results of the study indicate a suitability of Pol-InSAR C- and X-band data for canopy height modelling. The results of the different tested Pol-InSAR images against LiDAR and drone data varied since the acquisition parameters and the weather conditions changed during acquisitions. It can be concluded, that not all RS-2 and TS-X data is suitable for modelling canopy height from coherence. The parameters that most affect the canopy height model were identified as the baselines (temporal and perpendicular), the HoA, the incident angle and moist weather conditions, as well as the wavelength. Ascending and descending flight direction was not showing an influence. Nevertheless, our modelling results are comparable with several studies using InSAR and Pol-InSAR data for canopy height and AGB estimation. InSAR images at C-band were used by [54] to estimate stem volume and attained a RMSE value of 27%. Schlund et al. [55] modelled canopy height in boreal and temperate forests based on single-polarized TanDEM-X data. The authors used the RVoG model to estimate tree heights and validated their results with LiDAR data. The R² lied between 0.08–0.64 and the RMSE varied from 4.8 to 13.5 m [55]. Khati et al. [53] analyzed Indian tropical canopy heights based on TS-X/TanDEM-X data and attained RMSEs from 2.71–3.17 m for different seasons using the RVoG inversion approach. Other studies in tropical forests showed an average error between 3–5 m in estimating tree heights using Pol-InSAR likewise [56]. Kugler et al. [33] found an underestimation for tall forest stands and an overestimation for low canopy heights using dual-pol TanDEM-X data in Central Kalimantan, similar to our outcomes. Depending on rainy or dry season, their correlations (R²) varied between 0.55 and 0.69 for modelled canopy height based on the RVoG model [33]. Ghasemi et al. [48] modelled canopy height using P-band Pol-InSAR data and reached correlations of 0.43–0.48.

5.3. Possible Sources of Error

5.3.1. Acquisition Parameters

The quality of the interferogram is a useful parameter for determining the accuracy of the registration procedure. SAR data pairs may not be registered properly, if the resulting interferogram shows very little fringes and many decorrelated areas. However, co-registration of forested areas plays a crucial role within interferogram formation and leads to a low coherence. This low coherence in forests results from temporal decorrelation caused by wind effects in tree crowns. In the case of zero ground contribution, coherence becomes independent of polarization [44]. To overcome this limitation, a coherence optimization algorithm that accomplishes a pure signal-to-noise optimization is applied [57]. The coherence optimization allows selecting ground that gives the highest coherence under a random vegetation layer by maximizing the ground and minimizing the volume return [58].

Apart from the temporal baseline, the critical perpendicular baseline can cause decorrelation within an interferogram. The critical baseline is defined as the perpendicular baseline at which the interferometric correlation becomes zero and thus is completely decorrelated [53]. Longer wavelengths are less sensitive to decorrelation due to the perpendicular baseline as found in the comparison between X-and C-band. In general, the perpendicular baseline is inversely proportional to the HoA. A decreasing perpendicular baseline means an increasing HoA and results in a decreasing height sensitivity as shown in [59]. Nevertheless, for two TS-X datasets, the canopy height could not be estimated since the perpendicular baseline was too long and thus the HoA to low. The inversion process requires a HoA not smaller than the highest measured plot canopy height [53]. Since the HoA of two datasets was approximately 30 m and the tallest trees in the LiDAR reference data are about 35 m, an adequate inversion model performance was not possible.

The general underestimation of TS-X data results from the weak penetration depth, limited by the short wavelength of X-band [60]. Without this penetration capability, it is not possible to capture the canopy volume in the interferogram and the canopy estimation is restricted [33]. This means, the taller and denser the trees, the more saturated the canopy height estimation. The forests in Central Kalimantan are very dense and reach a height of up to 30 m, which limits the canopy height estimation. Alongside the density and height of the forest, the dielectric properties of the canopy also influence the penetration depth. The dataset of July/August were influenced by precipitation, consequently changing the dielectric properties of the forest.

Other studies found that the incidence angle also influences the canopy height inversion since the vertical wavenumber is estimated based on the incidence angle [61,62]. A smaller angle causes a larger vertical wavenumber relative to the effective baseline [61]. Using X-band and C-band with a weak penetration depth, a larger vertical wavelength can be sensitive to canopy height inversion. Additionally, very flat angles can cause radar shadows and introduce noise to the data [62].

With its longer wavelength the RS-2 data is able to penetrate the canopy layer more profoundly to capture the canopy volume in a more accurate way than TS-X. Nevertheless, TS-X has a better spatial resolution than RS-2 data, which enables the identification of small-scaled differences in the forest as e.g. because of logging. The fusion of RS-2 and TS-X was carried out to combine the complementary information of the two sensors in order to achieve better performance. However, due to difficulties in co-registering the two datasets originating from different sensors, and the general underestimation of TS-X X-band data, fusion did not result in enhanced performance.

5.3.2. Validation Datasets

The modelled canopy height was validated using UAV and LiDAR canopy height. Differences between LiDAR and drone data cannot only occur because of a temporal shift between the datasets, but also since estimations of canopy height vary between the different datasets. The performance of the photogrammetric products by drone can be influenced by structural complexity of a forest [63]. Nevertheless, UAV show good potential and derive similar results compared to LiDAR based canopy height $R^2 = 0.89$ which is consistent with results from [63].

Besides differences in acquisition parameters and weather conditions, another possible source of error is the four-year time shift between the LiDAR reference (2011) and the Pol-InSAR data (2015). Due to the offset of four years, differences resulting from deforestation and growing cannot be ruled out and are probable. Nevertheless, major changes during the four years can be excluded since the data was checked for fires and deforestation. Validating the modelled canopy height with drone data (2016) with a time shift of only one year resulted in higher correlations and lower biases and RMSEs for each dataset. However, area covered by the UAV data is very small, leading to the decision to include the LiDAR data for validation purposes to cover the whole range from low to high canopy height. Furthermore, no AGB data is available modelled from drone data, which is why the calibration and validation of AGB is based on LiDAR data.

Field and LiDAR data used as reference AGB also introduces errors, since spatial variability cannot be fully covered. The precision and accuracy of AGB extrapolated from field plot data are affected by the size and shape of the plots [64]. Most of the used field plots in the present study exceed an area of 1000 m², a size large enough to be more robust against boundary effects and less sensitive to individual trees [65–67]. Aside from the size, the shape affects the results of extrapolated AGB. Rectangular plots are more sensitive to the circumference to area ratio than circular plots [68]. As the count of rectangular plots is limited and only within single regrowing forest areas, their influence is marginal in the context of AGB estimation. In addition to the plot shape and size, the applied allometric model for moist tropical forests can introduce inaccuracies since it does not differentiate between different tree species [69]. We expect uncertainties using allometric equations varying from $\pm 5 - \pm 25\%$ as shown in other studies [70,42]. The use of species-specific regression models is not realizable since tropical forests consist of hundreds of tree species. Nevertheless, the used information about wood specific densities and tree species from field plot data helps to overcome those limitations. By using the extrapolating approach from field plot to LiDAR AGB estimation for reference AGB estimation, the advantage is the enormous amount of data, covering all ranges of AGB. Furthermore, the data is representing the spatial variability in a more accurate way [17]. Even after the separation of the data into calibration and validation samples, the use of a large number of samples is guaranteed. The results of the validation are thus more accurate than in studies with a more limited amount of in-situ data.

5.2. AGB Estimation

AGB can be estimated based on the canopy height [48,71,72]. Extrapolating from field inventory data to LiDAR transects allows creating numerous biomass reference data for the calibration of SAR images. Furthermore, it allows estimating AGB across large areas and different ecosystems taking in account the advantage of mapping the spatial variability of AGB. The estimated AGB from Pol-InSAR derived canopy height showed good correlations compared to reference canopy height. For AGB modelling based on canopy height, most studies use a power function regression. The use of linear regression in this context has been confirmed in few studies [73,74]. Nevertheless, testing both regression models with our data resulted in significant p-values for both regressions but higher R² and lower RMSE using a linear regression.

To overcome the inaccuracies introduced by the time gap between the LiDAR and the Pol-InSAR data, the Cook's D was applied. This standard measure of influence allows to remove influential outlier identified by a combination of observation leverages and residual values [75]. Using the Cook's D, we analyzed each dataset of 500 variables regarding outliers that can influence the linear regression AGB model. Per dataset 1–2% of the variables were identified as influential outliers and removed from the linear regression modelling. In most cases, the identified variables were pixel, where forest was degraded within the time gap of four years.

The comparison with pan-tropical biomass maps as seen in [36,50,51,76] with a resolution of 100 m–1 km in general showed a good consistency of the AGB estimates. Baccini et al. [51], using field data from 2007–2008 and LiDAR waveform measurements from NASA's ICESat, showed an overestimation in lower biomass ranges. The map is not able identifying heterogeneity in tropical forests in detail because of its coarse resolution of 500 m. The map of Saatchi et al. [76] also tends to

underestimate high biomass values but represents disturbances better due to its spatial resolution of 250 m. Avitabile et al. [36] used the maps of [76] and [51] with additional data to create an improved biomass map in the pan-tropical region. This final map shows lower RMSE and bias than the previous studies. Nevertheless, the map with its spatial resolution of 1 km does not capture small heterogeneities and disturbances. Berninger et al. [50] produced AGB maps of Kalimantan with a spatial resolution of 100 m, preserving small scale disturbances and regrowing effects for different years. The RMSE varies between 53–57 t ha⁻¹ and relative RMSE from 31–8%. Other studies using L- and P-band, estimated AGB with RMSE values between 30–40% for L-band and between 20–30% for P-band for boreal forests [77,78]. We obtained a relative RMSE for biomass between 20–30% using X- and C-band but with a much finer resolution of 3–12 m. Similar to the results of the present study, all of the pan-tropical and Indonesian maps underestimate higher AGB ranges and overestimate lower AGB values [36].

6. Conclusions

The results of the study show the suitability of Pol-InSAR RS-2 and TS-X data for canopy height estimation in tropical forests of Indonesia using the RMoG model (i). Since all data utilized are multi-pass interferometric data, temporal decorrelation is always present. While the RMoG model demonstrated good potential for compensating temporal decorrelation, this was not addressed in the RVoG model. Regression models were successfully applied for modelling large-scale AGB based on Pol-InSAR canopy height (ii). The validation of all modelled canopy heights and AGB values using the RMoG model was achieved using extensive LiDAR and drone reference data. The results of the different tested images varied since the acquisition parameters and the weather conditions changed during acquisitions. It was shown that canopy height is slightly underestimated by TS-X, whereas RS-2 overestimates the canopy height. Both sensors underestimate AGB, which can be explained with the saturation effect of SAR data regarding biomass. However, a combined canopy height estimation did not provide enhanced performance.

High-resolution information about canopy height and biomass is important for carbon accounting. Since the collection of field data is time-consuming and not practicable in all areas of the world, the use of LiDAR, drone and satellite data are helpful alternatives. Nevertheless, LiDAR and drone data acquisitions are very cost-intensive. The use of earth observation approaches enables a cost-effective way to cover large areas. Moreover, the high data availability and the combination of different sensors enables the reduction of uncertainties in indirect measurement approaches such as canopy height and biomass modelling from SAR data. We showed that the RMoG can help to estimate high-resolution canopy height data and AGB from different sensors and thus allows a support to monitoring and risk managing systems for spacious areas. The resulting outcomes contribute to REDD+ and other carbon related projects. Future missions such as Tandem-L (DLR) and the Earth Explorer Biomass (ESA) help to further improve data availability for biomass estimation.

Author Contributions: S.L. and A.B. conceived and designed the experiments; A.B. and S.L. performed the experiments; D.Z. supported the Pol-InSAR processing. D.Z. implemented the RVoG and RMoG models. A.B. analyzed the data; F.S. supervised the project and commented on the manuscript; A.B., S.L. and F.S. discussed the results. A.B. wrote the paper. S.L. and F.S. reviewed the manuscript.

Funding: This research was funded by the German Aerospace Center (DLR) under 50EE1507, and the Canadian Space Agency (CSA).

Acknowledgments: We would like to thank the World Wildlife Fund (WWF) for providing the 2011 LiDAR data. The authors would like to first and foremost thank Werner Wiedemann for collecting and processing drone data in Kalimantan. Elisabeth Probst provided much appreciated support during drone data processing. The authors would like to thank Suwido Limin, Agung Restu Susanto and the team from the Centre for International Co-operation in Management of Tropical Peatland (CIMTROP) in Palangka Raya for the logistical support during the field surveys. The authors would like to thank the German Aerospace Center (DLR) for supplying TerraSAR-X data and the Canadian Space Agency (CSA) for providing RADARSAT-2 imagery.

Conflicts of Interest: The authors declare no conflict of interest.

References

1. World Bank Group. Forest Area (% of Land Area): Indonesia. Available online: <https://data.worldbank.org/indicator/AG.LND.FRST.ZS?end=2015&locations=ID&start=2015&type=shaded&view=map&year=2010> (accessed on 14 February 2019).
2. Pachauri, R.K.; Meyer, L.A. *IPCC 2014. Climate change 2014. Synthesis report. Contribution of Working Groups I, II and III to the Fifth Assessment Report of the Intergovernmental Panel on Climate Change*; [Core Writing Team, Pachauri, R.K., Meyer, L.A., eds.]; Intergovernmental Panel on Climate Change: Geneva, Switzerland, 2015, ISBN 9291691437.
3. Page, S.E.; Rieley, J.O.; Banks, C.J. Global and regional importance of the tropical peatland carbon pool. *Global Change Biol.* **2011**, *17*, 798–818, doi:10.1111/j.1365-2486.2010.02279.x.
4. Jaenicke, J.; Rieley, J.O.; Mott, C.; Kimman, P.; Siegert, F. Determination of the amount of carbon stored in Indonesian peatlands. *Geoderma* **2008**, *147*, 151–158, doi:10.1016/j.geoderma.2008.08.008.
5. Edwards, D.P.; Koh, L.P.; Laurance, W.F. Indonesia's REDD+ pact: Saving imperilled forests or business as usual? *Biol. Conserv.* **2012**, *151*, 41–44, doi:10.1016/j.biocon.2011.10.028.
6. Olivier, J.G.J.; Janssens-Maenhout, G.; Muntean, M.; Peters, J.A.H.W. *Trends in global CO2 emissions: 2015 Report*; Den Haag, **2015**. Available online: https://edgar.jrc.ec.europa.eu/news_docs/jrc-2015-trends-in-global-co2-emissions-2015-report-98184.pdf (accessed on 26 February 2019).
7. Global Canopy Foundation. The REDD Desk. Available online: https://theredddesk.org/countries/search-countries-database?f%5B0%5D=type%3Aactivity&f%5B1%5D=field_project%3A1 (accessed on 7 February 2018).
8. Goetz, S.; Dubayah, R. Advances in remote sensing technology and implications for measuring and monitoring forest carbon stocks and change. *Carbon Manag.* **2011**, *2*, 231–244, doi:10.4155/cmt.11.18.
9. FAO. *Assessment of the Status of the Development of the Standards for the Terrestrial Essential Climate Variables; Biomass (T12)* **2009**. Available online: <http://www.fao.org/3/i1238e/i1238e00.pdf> (accessed on 6 February 2019).
10. Bojinski, S.; Verstraete, M.; Peterson, T.C.; Richter, C.; Simmons, A.; Zemp, M. The Concept of Essential Climate Variables in Support of Climate Research, Applications, and Policy. *Bull. Am. Meteorol. Soc.* **2014**, *95*, 1431–1443, doi:10.1175/BAMS-D-13-00047.1.
11. Koch, B. Status and future of laser scanning, synthetic aperture radar and hyperspectral remote sensing data for forest biomass assessment. *ISPRS J. Photogramm. Remote Sens.* **2010**, *65*, 581–590, doi:10.1016/j.isprsjprs.2010.09.001.
12. Joshi, N.; Mitchard, E.T.A.; Schumacher, J.; Johannsen, V.K.; Saatchi, S.; Fensholt, R. L-Band SAR Backscatter Related to Forest Cover, Height and Aboveground Biomass at Multiple Spatial Scales across Denmark. *Remote Sens.* **2015**, *7*, 4442–4472, doi:10.3390/rs70404442.
13. Schlund, M.; Poncet, F.; Kuntz, S.; Schmillius, C.; Hoekman, D.H. TanDEM-X data for aboveground biomass retrieval in a tropical peat swamp forest. *Remote Sens. Environ.* **2014**, *158*, 255–266, doi:10.1016/j.rse.2014.11.016.
14. Asner, G.P.; Clark, J.K.; Mascaro, J.; Galindo García, G.A.; Chadwick, K.D.; Navarrete Encinales, D.A.; Paez-Acosta, G.; Cabrera Montenegro, E.; Kennedy-Bowdoin, T.; Duque, Á.; et al. High-resolution mapping of forest carbon stocks in the Colombian Amazon. *Biogeosciences* **2012**, *9*, 2683–2696, doi:10.5194/bg-9-2683-2012.
15. Asner, G.P.; Flint Hughes, R.; Varga, T.A.; Knapp, D.E.; Kennedy-Bowdoin, T. Environmental and Biotic Controls over Aboveground Biomass Throughout a Tropical Rain Forest. *Ecosystems* **2009**, *12*, 261–278, doi:10.1007/s10021-008-9221-5.
16. Solberg, S.; Astrup, R.; Gobakken, T.; Næsset, E.; Weydahl, D.J. Estimating spruce and pine biomass with interferometric X-band SAR. *Remote Sens. Environ.* **2010**, *114*, 2353–2360, doi:10.1016/j.rse.2010.05.011.
17. Englhart, S.; Keuck, V.; Siegert, F. Aboveground biomass retrieval in tropical forests—The potential of combined X- and L-band SAR data use. *Remote Sens. Environ.* **2011**, *115*, 1260–1271, doi:10.1016/j.rse.2011.01.008.
18. Duncanson, L.I.; Niemann, K.O.; Wulder, M.A. Estimating forest canopy height and terrain relief from GLAS waveform metrics. *Remote Sens. Environ.* **2010**, *114*, 138–154, doi:10.1016/j.rse.2009.08.018.
19. Zhao, K.; Popescu, S.; Nelson, R. Lidar remote sensing of forest biomass: A scale-invariant estimation approach using airborne lasers. *Remote Sens. Environ.* **2009**, *113*, 182–196, doi:10.1016/j.rse.2008.09.009.

20. Kronseder, K.; Ballhorn, U.; Böhm, V.; Siegert, F. Above ground biomass estimation across forest types at different degradation levels in Central Kalimantan using LiDAR data. *Int. J. Appl. Earth Obs. Geoinf.* **2012**, *18*, 37–48, doi:10.1016/j.jag.2012.01.010.
21. Asner, G.P.; Powell, G.V.N.; Mascaró, J.; Knapp, D.E.; Clark, J.K.; Jacobson, J.; Kennedy-Bowdoin, T.; Balaji, A.; Paez-Acosta, G.; Victoria, E.; et al. High-resolution forest carbon stocks and emissions in the Amazon. *Proc. Natl. Acad. Sci. USA* **2010**, *107*, 16738–16742, doi:10.1073/pnas.1004875107.
22. Ballhorn, U.; Jubanski, J.; Siegert, F. ICESat/GLAS Data as a Measurement Tool for Peatland Topography and Peat Swamp Forest Biomass in Kalimantan, Indonesia. *Remote Sens.* **2011**, *3*, 1957–1982, doi:10.3390/rs3091957.
23. Jubanski, J.; Ballhorn, U.; Kronseder, K.; Franke, J.; Siegert, F. Detection of large above-ground biomass variability in lowland forest ecosystems by airborne LiDAR. *Biogeosciences* **2013**, *10*, 3917–3930, doi:10.5194/bg-10-3917-2013.
24. Enghart, S.; Jubanski, J.; Siegert, F. Quantifying Dynamics in Tropical Peat Swamp Forest Biomass with Multi-Temporal LiDAR Datasets. *Remote Sens.* **2013**, *5*, 2368–2388, doi:10.3390/rs5052368.
25. Sun, X.; Song, H.J. A New Improved Algorithm Based on Three-Stage Inversion Procedure of Forest Height. *Proceedings of the 2015 14th International Symposium on Distributed Computing and Applications for Business Engineering and Science (DCABES)* Guiyang, China, 18–24 August **2015**. Available online: <https://dl.acm.org/citation.cfm?id=2917944> (accessed on 26 February 2019).
26. Olesk, A.; Praks, J.; Antropov, O.; Zalite, K.; Arumäe, T.; Voormansik, K. Interferometric SAR Coherence Models for Characterization of Hemiboreal Forests Using TanDEM-X Data. *Remote Sens.* **2016**, *8*, 700, doi:10.3390/rs8090700.
27. Lavallo, M.; Simard, M.; Hensley, S. A Temporal Decorrelation Model for Polarimetric Radar Interferometers. *IEEE Trans. Geosci. Remote Sens.* **2012**, *50*, 2880–2888, doi:10.1109/TGRS.2011.2174367.
28. Garestier, F.; Dubois-Fernandez, P.C.; Papathanassiou, K.P. Pine Forest Height Inversion Using Single-Pass X-Band PolInSAR Data. *IEEE Trans. Geosci. Remote Sens.* **2008**, *46*, 59–68, doi:10.1109/TGRS.2007.907602.
29. Neumann, M.; Ferro-Famil, L.; Reigber, A. Multibaseline Polarimetric SAR Interferometry Coherence Optimization. *IEEE Geosci. Remote Sens. Lett.* **2008**, *5*, 93–97, doi:10.1109/LGRS.2007.908885.
30. Kugler, F. Pol-InSAR Forest Height estimation at different Frequencies: Opportunities and Limitations. **2015**. Available online: <https://elib.dlr.de/102764/1/Dissertation-Florian-Kugler.pdf> (accessed on 22 May 2019).
31. Hajnsek, I.; Hoekman, D.H. INDREX-II Indonesian Radar Experiment Campaign over Tropical Forest in L- and P-band. *Proceedings of the 2005 IEEE International Geoscience and Remote Sensing Symposium (IGARSS)* Seoul, South Korea, 29 July **2005**, *6*, 4335–4338. Available online: <https://ieeexplore.ieee.org/document/1525878> (accessed on 30 April 2019).
32. Hajnsek, I.; Kugler, F.; Lee, S.K.; Papathanassiou, K.P. Tropical-Forest-Parameter Estimation by Means of Pol-InSAR: The INDREX-II Campaign. *IEEE Trans. Geosci. Remote Sens.* **2009**, *47*, 481–493, doi:10.1109/TGRS.2008.2009437.
33. Kugler, F.; Schulze, D.; Hajnsek, I.; Pretzsch, H.; Papathanassiou, K.P. TanDEM-X Pol-InSAR Performance for forest height estimation. *IEEE Trans. Geosci. Remote Sens.* **2014**, *52*, 6404–6422, doi:10.1109/TGRS.2013.2296533.
34. Vyjayanthi, N.; Jha, C.S.; Murthy, M.S.R. Forest Biomass Estimation and Forest Structure Analysis from multi-frequency and multi-polarization SAR data. *RISAT-JEP*. **2017**. Available online: <https://www.climatelinks.org/file/4121/download?token=WzORdfr> (accessed on 22 April 2019).
35. Varekamp, C.; Hoekman, D.H. High-resolution InSAR image simulation for forest canopies. *IEEE Trans. Geosci. Remote Sens.* **2002**, *40*, 1648–1655, doi:10.1109/TGRS.2002.801777.
36. Avitabile, V.; Herold, M.; Heuvelink, G.B.M.; Lewis, S.L.; Phillips, O.L.; Asner, G.P.; Armston, J.; Ashton, P.S.; Banin, L.; Bayol, N.; et al. An integrated pan-tropical biomass map using multiple reference datasets. *Global Change Biol.* **2016**, *22*, 1406–1420, doi:10.1111/gcb.13139.
37. Page, S.E.; Rieley, J.O.; Wüst, R. Lowland tropical peatlands of Southeast Asia. *Peatl. Evol. Rec. Environ. Clim. Changes* **2006**, *9*, 145–172, doi:10.1016/S0928-2025(06)09007-9.
38. Raison, J.; Atkinson, P.; Chave, J.; Defries, R.; Joo, G.K.; Joosten, H.; Konecny, K.; Navratil, P.; Siegert, F. The High Carbon Stock Science Study - Independent Report from the Technical Committee: **2015**. Available online: <https://www.tfa2020.org/en/publication/high-carbon-stock-science-study/> (accessed on 23 May 2019).

IV. Biomass estimation in tropical forests based on Pol-InSAR data (Chapter III)

39. Pearson, T.; Walker, S.; Brown, S. Sourcebook for Land Use, Land-Use Change and Forestry Projects. Available online: <https://theredddesk.org/resources/sourcebook-land-use-land-use-change-and-frestry-projects> (accessed on 1 December 2017)
40. Pfeifer, N.; Stadler, P.; Briese, C. Derivation of digital terrain models in SCOP++ environment. In Proceedings of the OEEPE Workshop on Airborne Laserscanning and Interferometric SAR for Digital Elevation Models, Stockholm, Sweden, 2001; pp. 1–13. Available online: <http://citeseerx.ist.psu.edu/viewdoc/download?doi=10.1.1.589.8666&rep=rep1&type=pdf> (accessed on 19 April 2019).
41. Hughes, R.F.; Kauffman, J.B.; Jaramillo, V.J.; Biomass, Carbon, and Nutrient Dynamics of Secondary Forests in a Humid Tropical Region of Mexico. *Ecology* **1999**, *80*, 1892–1907, doi:10.2307/176667.
42. Chave, J.; Andalo, C.; Brown, S.; Cairns, M.A.; Chambers, J.Q.; Eamus, D.; Fölster, H.; Fromard, F.; Higuchi, N.; Kira, T.; et al. Tree allometry and improved estimation of carbon stocks and balance in tropical forests. *Oecologia* **2005**, *145*, 87–99, doi:10.1007/s00442-005-0100-x.
43. Moreira, A.; Prats-Iraola, P.; Younis, M.; Krieger, G.; Hajnsek, I.; Papathanassiou, K.P. A tutorial on synthetic aperture radar. *IEEE Geosci. Remote Sens. Mag.* **2013**, *1*, 6–43, doi:10.1109/MGRS.2013.2248301.
44. Papathanassiou, K.P.; Cloude, S.R. Single-baseline polarimetric SAR interferometry—Geoscience and Remote Sensing, IEEE Transactions on. *IEEE Trans. Geosci. Remote Sens.* **2001**, *39*, 2352–2363, doi:10.1109/36.964971.
45. Treuhaft, R.N.; Madsen, S.N.; Moghaddam, M.; van Zyl, J.J. Vegetation characteristics and underlying topography from interferometric radar. *Radio Sci.* **1996**, *31*, 1449–1485, doi:10.1029/96RS01763.
46. Treuhaft, R.N.; Siqueira, P.R. Vertical structure of vegetated land surfaces from interferometric and polarimetric radar. *Radio Sci.* **2000**, *35*, 141–177, doi:10.1029/1999RS900108.
47. Lavalle, M.; Hensley, S. Extraction of Structural and Dynamic Properties of Forests From Polarimetric-Interferometric SAR Data Affected by Temporal Decorrelation. *IEEE Trans. Geosci. Remote Sens.* **2015**, *53*, 4752–4767, doi:10.1109/TGRS.2015.2409066.
48. Ghasemi, N.; Tolpekin, V.; Stein, A. Assessment of Forest Above-Ground Biomass Estimation from PolInSAR in the Presence of Temporal Decorrelation. *Remote Sens.* **2018**, *10*, 815, doi:10.3390/rs10060815.
49. Cook, R.D. Detection of Influential Observation in Linear Regression. *Technometrics* **1977**, *19*, 15–18.
50. Berninger, A.; Lohberger, S.; Stängel, M.; Siegert, F. SAR-Based Estimation of Above-Ground Biomass and Its Changes in Tropical Forests of Kalimantan Using L- and C-Band. *Remote Sens.* **2018**, *10*, 831, doi:10.3390/rs10060831.
51. Baccini, A.; Goetz, S.J.; Walker, W.S.; Laporte, N.T.; Sun, M.; Sulla-Menashe, D.; Hackler, J.; Beck, P.S.A.; Dubayah, R.; Friedl, M.A.; et al. Estimated carbon dioxide emissions from tropical deforestation improved by carbon-density maps. *Nat. Clim. Change* **2012**, *2*, 182–185, doi:10.1038/nclimate1354.
52. Lee, S.K.; Kugler, F.; Papathanassiou, K.P.; Moreira, A. *Forest Height Estimation by Means of Pol-InSAR. Limitations Posed by Temporal Decorrelation*. K&C Science Report—Phase 1, **2017**, available online: <https://www.semanticscholar.org/paper/Forest-Height-Estimation-by-means-of-Pol-InSAR-by-Lee-Kugler/a7efde9c825e84e6cd927faab417425fccef9840> (accessed on 24 May 2017).
53. Khati, U.; Singh, G.; Ferro-Famil, L. Analysis of seasonal effects on forest parameter estimation of Indian deciduous forest using TerraSAR-X PolInSAR acquisitions. *Remote Sens. Environ.* **2017**, *199*, 265–276, doi:10.1016/j.rse.2017.07.019.
54. Askne, J.; Santoro, M. Experiences in Boreal Forest Stem Volume Estimation from Multitemporal C-Band InSAR. *Recent Interferometry Applications in Topography and Astronomy*; Padron, I., Ed.; IntechOpen, **2012**, ISBN 978-953-51-0404-9. Available online: <https://pdfs.semanticscholar.org/2bc3/54b863ecf3a7b6cb6f250bf2a5c63bd8f051.pdf> (accessed on 10 April 2019).
55. Schlund, M.; Magdon, P.; Eaton, B.; Aumann, C.; Erasmi, S. Canopy height estimation with TanDEM-X in temperate and boreal forests. *Int. J. Appl. Earth Obs. Geoinf.* **2019**, *82*, 101904, doi:10.1016/j.jag.2019.101904.
56. Arnaubec, A.; Dubois-Fernandez, P.C. Analysis of PolInSAR Precision for Forest and Ground Parameters Estimation in Tropical Context, *Proceedings of the 2012 IEEE International Geoscience and Remote Sensing Symposium (IGARSS)*, Munich, Germany, 22–27 July **2012**; pp. 7585–7588.
57. Fomena, R.T.; Cloude, S.R. On The Role of Coherence Optimization in Polarimetric SAR Interferometry. *CEOS 05* **2005**, *22*, 9.

58. Tharaoui, S.; Ouarzeddine, M.; Souissi, B. Interferometric coherence optimization: A comparative Study. *Eighth International Conference on Broadband and Wireless Computing, Communication and Applications (BWCCA)*, 28–30 Oct. 2013, Compiègne, France; IEEE: Piscataway, NJ. Available online: <https://ieeexplore.ieee.org/xpl/conhome/6689793/proceeding> (accessed on 15 April 2019).
59. Soja, M.; Ulander, L. Digital Canopy Model Estimation from TanDEM-X Interferometry using High-Resolution Lidar DEM, Melbourne, VIC, Australia, 21–26 July 2013. Available online: <https://ieeexplore.ieee.org/document/6721117> (accessed on 11 April 2019).
60. Schlund, M.; Erasmi, S.; Scipal, K. Comparison of Aboveground Biomass Estimation From InSAR and LiDAR Canopy Height Models in Tropical Forests. *IEEE Geosci. Remote Sens. Lett.* **2019**, 1–5, doi:10.1109/LGRS.2019.2925901.
61. Sun, X.; Wang, B.; Xiang, M.; Jiang, S.; Fu, X. Forest Height Estimation Based on Constrained Gaussian Vertical Backscatter Model Using Multi-Baseline P-Band Pol-InSAR Data. *Remote Sens.* **2018**, *11*, 42, doi:10.3390/rs11010042.
62. Hajnsek, I.; Scheiber, R.; Keller, M.; Horn, R.; Lee, S.; Ulander, L.; Gustavson, A.; Sandberg, G.; Le Toan, T.; Tebaldini, S.; et al. *BIOSAR 2008 Technical Assistance for the Development of Airborne SAR and Geophysical Measurements during the BioSAR 2008 Experiment. Final Report*, 2008. Available online: https://earth.esa.int/c/document_library/get_file?folderId=21020&name=DLFE-903.pdf (accessed on 21 June 2019).
63. Jayathunga, S.; Owari, T.; Tsuyuki, S. Evaluating the Performance of Photogrammetric Products Using Fixed-Wing UAV Imagery over a Mixed Conifer–Broadleaf Forest: Comparison with Airborne Laser Scanning. *Remote Sens.* **2018**, *10*, 187, doi:10.3390/rs10020187.
64. Frazer, G.W.; Magnussen, S.; Wulder, M.A.; Niemann, K.O. Simulated impact of sample plot size and co-registration error on the accuracy and uncertainty of LiDAR-derived estimates of forest stand biomass. *Remote Sens. Environ.* **2011**, *115*, 636–649, doi:10.1016/j.rse.2010.10.008.
65. Ruiz, L.; Hermosilla, T.; Mauro, F.; Godino, M. Analysis of the Influence of Plot Size and LiDAR Density on Forest Structure Attribute Estimates. *Forests* **2014**, *5*, 936–951, doi:10.3390/f5050936.
66. Rafael, M.N.C.; Eduardo, G.F.; Jorge, G.G.; Carlos, J.; Ceacero, R.; Rocío, H.C. Impact of plot size and model selection on forest biomass estimation using airborne LiDAR: A case study of pine plantations in southern Spain. *J. For. Sci.* **2017**, *63*, 88–97, doi:10.17221/86/2016-JFS.
67. Kachamba, D.; Ørka, H.; Næsset, E.; Eid, T.; Gobakken, T. Influence of Plot Size on Efficiency of Biomass Estimates in Inventories of Dry Tropical Forests Assisted by Photogrammetric Data from an Unmanned Aircraft System. *Remote Sens.* **2017**, *9*, 610, doi:10.3390/rs9060610.
68. Mauya, E.W.; Hansen, E.H.; Gobakken, T.; Bollandasås, O.M.; Malimbwi, R.E.; Næsset, E. Effects of field plot size on prediction accuracy of aboveground biomass in airborne laser scanning-assisted inventories in tropical rain forests of Tanzania. *Carbon Balanc. Manag.* **2015**, *10*, 10, doi:10.1186/s13021-015-0021-x.
69. Urbazaev, M.; Thiel, C.; Cremer, F.; Dubayah, R.; Migliavacca, M.; Reichstein, M.; Schimmlius, C. Estimation of forest aboveground biomass and uncertainties by integration of field measurements, airborne LiDAR, and SAR and optical satellite data in Mexico. *Carbon Balanc. Manag.* **2018**, *13*, 5, doi:10.1186/s13021-018-0093-5.
70. Saatchi, S.; Marlier, M.; Chazdon, R.L.; Clark, D.B.; Russell, A.E. Impact of spatial variability of tropical forest structure on radar estimation of aboveground biomass. *Remote Sens. Environ.* **2011**, *115*, 2836–2849, doi:10.1016/j.rse.2010.07.015.
71. Lefsky, M.A.; Harding, D.J.; Keller, M.; Cohen, W.B.; Carabajal, C.C.; Del Bom Espirito-Santo, F.; Hunter, M.O.; Oliveira, R. de. Estimates of forest canopy height and aboveground biomass using ICESat. *Geophys. Res. Lett.* **2005**, *32*, doi:10.1029/2005GL023971.
72. Feliciano, E.A.; Wdowski, S.; Potts, M.D.; Lee, S.K.; Fatoyinbo, T.E. Estimating Mangrove Canopy Height and Above-Ground Biomass in the Everglades National Park with Airborne LiDAR and TanDEM-X Data. *Remote Sens.* **2017**, *9*, 702, doi:10.3390/rs9070702.
73. Odipo, V.; Nickless, A.; Berger, C.; Baade, J.; Urbazaev, M.; Walther, C.; Schimmlius, C. Assessment of Aboveground Woody Biomass Dynamics Using Terrestrial Laser Scanner and L-Band ALOS PALSAR Data in South African Savanna. *Forests* **2016**, *7*, 294, doi:10.3390/f7120294.
74. Köhler, P.; Huth, A. Towards ground-truthing of spaceborne estimates of above-ground life biomass and leaf area index in tropical rain forests. *Biogeosciences* **2010**, *7*, 2531–2543, doi:10.5194/bg-7-2531-2010.

IV. Biomass estimation in tropical forests based on Pol-InSAR data (Chapter III)

Remote Sens. **2019**, *11*, 2105

24 of 24

75. Zakaria, A. On the Detection of Influential Outliers in Linear Regression Analysis. *AJTAS* **2014**, *3*, 100, doi:10.11648/j.ajtas.20140304.14.
76. Saatchi, S.S.; Harris, N.L.; Brown, S.; Lefsky, M.; Mitchard, E.T.A.; Salas, W.; Zutta, B.R.; Buermann, W.; Lewis, S.L.; Hagen, S.; et al. Benchmark map of forest carbon stocks in tropical regions across three continents. *Proc. Natl. Acad. Sci. USA* **2011**, *108*, 9899–9904, doi:10.1073/pnas.1019576108.
77. Soja, M.J.; Sandberg, G.; Ulander, L.M.H. Regression-Based Retrieval of Boreal Forest Biomass in Sloping Terrain Using P-Band SAR Backscatter Intensity Data. *IEEE Trans. Geosci. Remote Sens.* **2013**, *51*, 2646–2665, doi:10.1109/TGRS.2012.2219538.
78. Sandberg, G.; Ulander, L.M.H.; Fransson, J.E.S.; Holmgren, J.; Le Toan, T. L- and P-band backscatter intensity for biomass retrieval in hemiboreal forest. *Remote Sens. Environ.* **2011**, *115*, 2874–2886, doi:10.1016/j.rse.2010.03.018.



© 2019 by the authors. Licensee MDPI, Basel, Switzerland. This article is an open access article distributed under the terms and conditions of the Creative Commons Attribution (CC BY) license (<http://creativecommons.org/licenses/by/4.0/>).

V. Peat dome surface modeling using space borne LiDAR
(Chapter IV)

Berninger, A. & F. Siegert (2020) The potential of ICESat-2 to identify carbon-rich peatlands in Indonesia.



1 Article

2 The potential of ICESat-2 to identify carbon-rich 3 peatlands in Indonesia

4 Anna Berninger ^{1,2,*} and Florian Siegert ^{1,2}

5 ¹ RSS - Remote Sensing Solutions GmbH, Dingolfinger Str. 9, 81673 Munich, Germany

6 ² Department of Biology, Ludwig-Maximilians-University Munich, Großhaderner Str. 2, 82152 Planegg-
7 Martinsried, Germany

8 * Correspondence: berninger@rssgmbh.de; Tel.: +49 89 9699 4391 (A.B.)

9 Received: date; Accepted: date; Published: date

10 **Abstract:** Peatlands in Indonesia are one of the primary global storages for terrestrial organic
11 carbon. Poor land management, drainage, recurrent fires and logging lead to the release of huge
12 amounts of carbon dioxide. Field measurements of peatlands and their vegetation are difficult, as
13 these areas are covered by dense forests or, if destroyed, are inaccessible swamps. In the present
14 study, we investigated whether data from the new ICESat-2/ATLAS LiDAR satellite can contribute
15 to identifying and mapping ombrogenous carbon-rich peatlands as well as assessing the tree height
16 of the vegetation covering the peat layer. The spaceborne ICESat-2 LiDAR data was compared and
17 correlated with highly accurate field validated airborne LiDAR data as well as a global WorldDEM
18 DTM. When compared to the airborne DTM, the data produced an R^2 of 0.89 and an RMSE of 0.83
19 m. For the comparison with the WorldDEM DTM, the resulting R^2 lay at 0.94 and the RMSE at 0.86
20 m. Moreover, we modelled the surfaces of three peat hydrological units (PHU) based on ICESat-2
21 terrain height measurements with kriging interpolation in Kalimantan, Indonesia. These three
22 ICESat-2 based peatland models, compared to a comprehensive WorldDEM DTM, produced an R^2
23 of 0.78, 0.84, and 0.94. The RMSE ranged from 0.68 m (relative RMSE 14.3%) to 2.68 (relative RMSE
24 22.5%). These results demonstrate the potential of ICESat-2 in assessing peat surface topography
25 and canopy heights of the forest vegetation growing on tropical peat in Indonesia. Since ICESat-2
26 will collect more data all over the globe in the years to come, it can be used to survey existing and
27 map yet unknown carbon-rich tropical peatlands. Accurate information about peatland extents,
28 canopy heights, and thus below-ground and above-ground biomass is crucial for assessing and
29 quantifying this globally relevant carbon store. ICESat-2 can thus be used as a tool to support carbon
30 accounting in the context of REDD+ (Reducing Emissions from Deforestation and Forest
31 Degradation) and other carbon-related projects.

32 **Keywords:** Light Detection and Ranging (LiDAR), WorldDEM, ICESat-2, ATLAS, tropical peat,
33 canopy height, Indonesia, carbon

34 1. Introduction

35 In the context of global warming and recurrent large scale fire disasters, the accurate
36 determination of carbon contents of vegetation and soil in terrestrial ecosystems is becoming
37 increasingly important. Tropical rainforests account for 40% of the earth's terrestrial carbon storage
38 [1]. However, these forests are continuously damaged and degraded by fire, land clearing, and
39 unsustainable management. Indonesia's forests are globally considered to be one of the most species-
40 rich tropical rainforests [2], storing about 18.6 Gt of carbon [3]. From 2001 – 2018, Indonesia lost 25.6
41 million ha of tree coverage [4]. This loss does not only result in decreased greenhouse gas storage
42 capacities but also in a release of millions of tons of CO₂ into the atmosphere and the carbon sink,
43 consequently becoming a carbon source.

44 Furthermore, the country contains some of the largest known tropical peat reservoirs on the
45 globe. While peatlands only cover 3 – 5% of the earth's surface, they store about 30% of all terrestrial

V. Peat dome surface modeling using space borne LiDAR (Chapter IV)

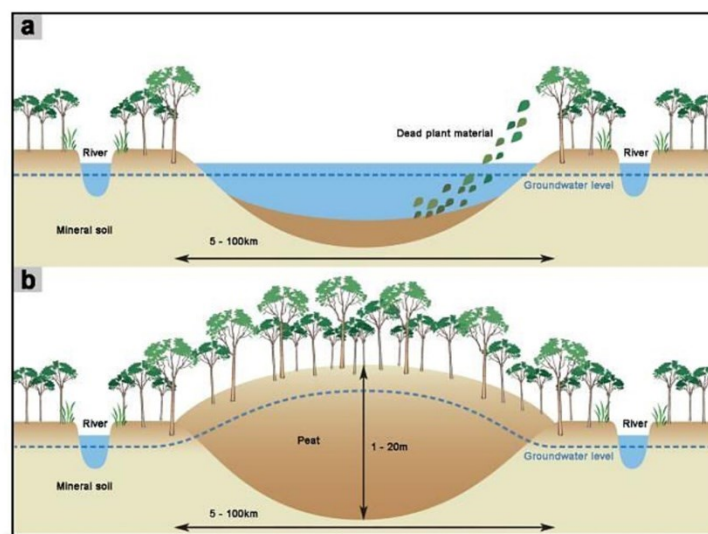
Remote Sens. 2020, 12, x FOR PEER REVIEW

2 of 19

46 soil carbon [5]. With an amount of about 16.8 – 27.0 million ha of peat, Indonesia has the largest
47 known reservoirs of Asia [6,7]. The Indonesian peatlands developed over the past thousands of years
48 when the sea level rose to today's level. Plant debris accumulated under waterlogged conditions in
49 natural sinks such as lakes or alluvial floodplains and formed convex domes of up to 20 m depth and
50 up to 100 km width (see Figure 1) [8]. This ombrogenous type of peat results carries extremely high
51 carbon contents. It was estimated that Indonesian peatlands alone store about 55 – 75 Gt of carbon
52 [9–11]. Peat swamp forests that grow on top of the peatlands, form and protect the peat layer. The
53 biomass of these peatland forests can reach up to 600 t/ha, but on average, it ranges between 150 –
54 300 t/ha [6]. Peatland forests, therefore, contain up to ten times less carbon than their underlying peat
55 layer [12].

56 Due to deforestation, logging, and drainage, between 1990 – 2010, Southeast Asia lost about 40%
57 of its peatland forests [5]. From 2000 to 2010 alone, the isle of Borneo lost approximately 25% of its
58 peat swamp forest while Sumatra lost more than 40% [13].

59



60

61 **Figure 1:** Schematic overview of the formation of peat domes in Indonesia and other tropical countries
62 (WWF, 2009).

63 Drainage lowers the water level within the peat layer, which was found to be positively
64 correlated with CO₂ emissions [14,15]. A low layer of water exposes the top of the peat layer to
65 oxygen. Subsequently, this leads to decomposition and, thus, carbon dioxide emissions [15]. When
66 peatlands are drained and peat swamp forests are logged, the ecosystem becomes extremely
67 vulnerable to massive long-lasting fire events.

68 Fires sweeping across the country often affect Indonesian tropical forest ecosystems. This is
69 especially true during strong El Niño Southern Oscillation (ENSO) periods, as in the years 1982/83,
70 1997/98, 2003, 2006, 2015, and 2019 [12]. The fire disasters have increased in frequency and severity
71 over the past two decades. In 2019 alone, 942,000 ha were burned [16], which constitutes the most
72 substantial fire-related loss since 2015, when 4.6 million ha burned [17]. Economic costs for 2015 were
73 estimated at 16 billion USD, not including hard to quantify costs such as the loss of biodiversity [18].
74 The vast amount of aerosols emitted by fires did affect public health in Indonesia, as well as adjacent
75 countries such as Thailand, Malaysia, and Singapore [19]. From the perspective of climate change,

76 the fires in 2015 released 0.89 – 1.75 Gt CO₂ [17,20,21]. The extreme fire disaster of 1997/1998 was the
77 first to be analyzed by remote sensing. It was estimated that 2.4 – 6.8 million ha of peatlands burned
78 and up to 9.43 Gt CO₂ were released into the atmosphere [17,20,22]. The economic costs were
79 estimated at 9.3 billion USD [22].

80 The total area of peatlands in Indonesia and Southeast Asia is still not precisely known. Even
81 less is known about the peat layers' thickness and carbon stock, which are highly challenging to
82 determine. The most accurate method for measuring the peat thickness and corresponding carbon
83 content is by collecting field data with peat corings. Nevertheless, coring is time-consuming and
84 expensive, especially in remote areas with poor accessibility, such as in intact peat swamp forests.

85 Multiple studies have shown that carbon-rich ombrogenous peatlands can be located by remote
86 sensing technologies. This time-saving indirect approach identifies raised peat domes beneath the
87 forest vegetation with airborne and spaceborne LiDAR instruments and radar satellites. LiDAR and
88 SAR instruments take measurements over vast areas in a short time. Jeanicke et al. [12] identified a
89 strong correlation between the convex peat dome surface derived from a digital terrain model (DTM)
90 and the thickness of the dome-shaped peat layer. This correlation allowed calculation of a 3-
91 dimensional model of the peat layer and thus, in combination with field data, an estimation of the
92 contained carbon stock. Measurements with airborne LiDAR are more accurate than spaceborne data,
93 but at the same time, it is extremely costly to cover large and remote areas. A satellite-based approach
94 would allow screening the whole country. The ability of satellite-based LiDAR datasets (e.g.,
95 ICESat/GLAS) to serve as an alternative measurement tool for forest structure and topography was
96 already shown by [23–28]. It was also mentioned that terrain analyses in areas with medium to high
97 reliefs result in higher errors [26,27], making the satellite-based LiDAR data more applicable for
98 flatter terrain.

99 In this study, we investigate the applicability of the new ICESat-2/ATLAS instruments and
100 compare the results to highly accurate airborne LiDAR DTMs. Since peatlands have an extremely
101 smooth topography, ICESat-2 could be a useful tool to identify dome-shaped ombrogenous
102 peatlands. In contrast to other LiDAR systems, ATLAS detects laser reflections at a single-photon
103 level, which reduces the laser power requirements and thus the payload. The repetition rate, on the
104 other hand, is operated at a higher level than in other sensors. Most other LiDAR systems record
105 thousands of photons for triggering a detection. The constellation allows for surfaces of low as well
106 as high reflectivity to be detected. The nominal diameter footprint for each beam is about 17 m, and
107 the received ranging precision is 25 – 35 cm in flat terrain [29,30].

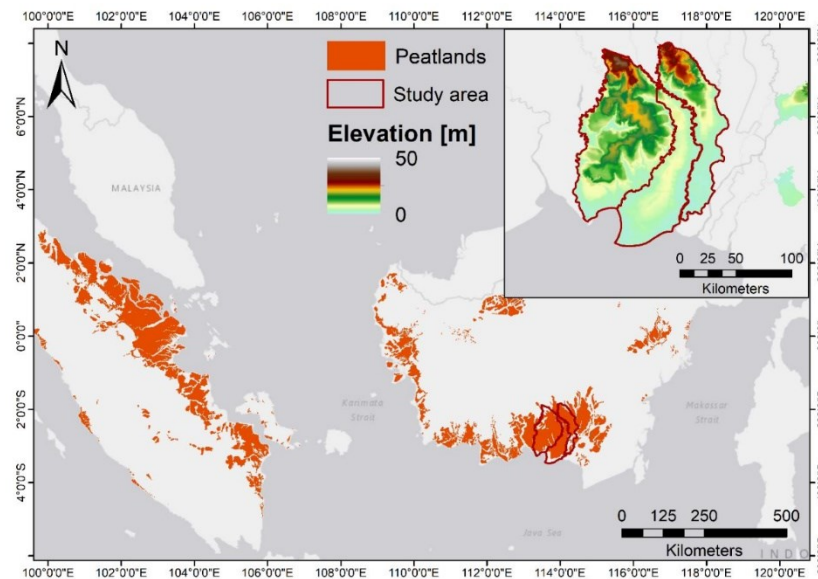
108 We use the ATLAS derived DTM information as a tool for the indirect identification of carbon-
109 rich dome-shaped peatlands in Indonesia. A DTM is defined as a model of the elevation surface and
110 represents the bare earth referenced to a common vertical datum. Precise airborne LiDAR data,
111 validated with field data, is used as a reference for mapping the surface. In a second step, we use the
112 ICESat-2 footprints to generate a wall-to-wall model of the peat dome surface. This step is achieved
113 by interpolating the ICESat-2 footprints using the geostatistical interpolation method Kriging.
114 Kriging is considered to be one of the best methods for interpolating non-uniform and irregularly
115 spaced spatial data [31,32]. The resulting peat dome surface model is validated with an airborne
116 derived DTM and complemented with the Airbus WorldDEM DTM at a spatial resolution of 12 × 12
117 m in areas with no available airborne data. Knowledge about the peat dome surface permits
118 conclusions about its volume and thus its carbon content, which consequently shows ICESat-2 to be
119 an essential tool for carbon-related projects.

120 2. Materials and Methods

121 2.1 Study area

122 Indonesia's climate is mainly characterized by a wet northwest monsoon from November to
123 April and a dry southeast monsoon from May to October. Additionally, it is influenced by frequent
124 rainfall and high temperatures throughout the year. These conditions are ideal for plant growth,
125 which is why Indonesia's land cover is dominated by tropical forests covering 94,432,000 km² and,

126 thus, more than 52% of the country [33]. The main forest ecosystems are mangrove forests, peat
127 swamp and freshwater swamp forests, lowland dipterocarp forests, and various montane formations
128 [2]. All forests store significant amounts of carbon [9]. Nevertheless, the most significant carbon
129 storages in Indonesia are the peat soils. Literature quantification of the area covered by peatlands in
130 Indonesia varies between 17 and 27 million ha [7,12]. The peat depths are estimated from very
131 shallow (less than 0.5 m) to very deep peat with up to 20 m of depth [12]. Figure 1 shows the coastal
132 peatlands of Sumatra and Kalimantan, Indonesia, including the study area in Central Kalimantan.
133 Peatlands often cover areas wider than 10,000 ha with a complex structure of different soils,
134 transecting canals and rivers as well as different forest types. They can be divided into different peat
135 hydrological units (PHUs), depending on the connected river systems. Within the hydrological units,
136 convex-shaped peat domes are commonly found.
137



138
139 **Figure 2:** Overview of the peatlands of Kalimantan and Sumatra, Indonesia. Three PHUs Sungai
140 Katingan Sebangau, Sungai Kahayan Sebangau and Sungai Kahayan Kapuas (from west to east)
141 within Central Kalimantan represent the study area.

142 We investigated one of the largest and less disturbed peat swamp forest complexes in Central
143 Kalimantan, which included the three PHUs Sungai Katingan Sebangau, Sungai Kahayan Sebangau
144 and Sungai Kahayan Kapuas (from west to east). The peat domes are ombrogenous and have a peat
145 depth varying from 0.5 – 12 m [34]. The peat swamp ecosystem of Central Kalimantan, including
146 Sungai Kahayan Sebangau and Sungai Kahayan Kapuas, have been extensively logged and drained
147 during the former Mega Rice Project, a resettlement project by the Indonesian Government in the
148 1990s [12]. The damaged and dried peatlands became susceptible to fire and burned more than once
149 [35]. Today, the area is mainly dominated by oil palm plantations and smallholder agriculture, as
150 well as burned areas covered by ferns and lianas. Sungai Katingan Sebangau contains the Sebangau
151 National Park, a peat swamp national park located between the rivers Kahayan and Katingan [36].
152 This area is characterized by dense low pole forest with a canopy height of about 20 m and tall peat
153 swamp forest trees of up to 45 m.

154 2.2 Data

155 2.2.1 Airborne LiDAR Data

156 Airborne LiDAR data was collected during the dry season (May to October) in 2011 to avoid any
157 influence of standing water during the DTM generation. The acquisition was flown 800 m
158 aboveground with an Optech Orion M200. The discrete return airborne LiDAR sensor uses a
159 wavelength of 1.064 μm . The data was recorded with a half scan angle of $\pm 22^\circ$, a point density of 2.8
160 points/m², and a side overlap of 30% [37]. The LiDAR campaign covered an area of 700,000 ha and
161 diverse landcover, including peat swamp forests partly affected by former or recent selective logging,
162 old burn scars, fern, grassland, bushes, and agricultural land [38]. The vertical accuracy lies at 0.14 m
163 for the DSM and 0.18 m for the DTM [38]. The modelled DTM surface was within the 95% confidence
164 interval of the ground truth data.

165 2.2.2 WorldDEM data

166 For comparisons, we used the WorldDEM DTM produced by Airbus DS Geo GmbH. The
167 WorldDEM DTM is based on the WorldDEM product, a DSM provided by Airbus Defence and Space.
168 All WorldDEM products are generated based on X-band radar data acquired from the TanDEM-X
169 mission (2010 – 2014) operated by Airbus and the German Aerospace Center (DLR). Both radar
170 satellites of this mission operate as a single-pass Synthetic Aperture Radar Interferometer (InSAR).
171 Data is acquired with the bi-static InSAR StripMap mode [39].

172 The DTM contains information about the bare earth elevation, excluding surface features such
173 as vegetation and buildings [39]. With a resolution of 12 x 12 m, the data offers more details than the
174 SRTM (30 m or 90 m spatial resolution) or the ASTER Global Digital Elevation Map (GDEM, 30 m
175 spatial resolution). The vertical relative accuracy of the WorldDEM DTM is 5 m, and the absolute
176 vertical accuracy 10 m. Within flat terrain, the vertical accuracy is improved. The absolute horizontal
177 accuracy lies below 6 m [39].

178 2.2.3 ICESat-2 data

179 ICESat-2 was launched in September 2018, carrying a single instrument, the Advanced
180 Topographic Laser Altimeter System (ATLAS). This system is a photon-counting LiDAR that detects
181 sensitivities at the photon level. The sensor operates at a wavelength of 532 nm (green) and a pulse
182 repetition rate of 10 kHz [29]. It uses six beams arranged in three pairs containing a low-energy and
183 a high-energy beam, separated by 90 m in across-track direction. This constellation permits surfaces
184 of low and high reflectivity to be detected [29]. The nominal diameter footprint for each beam is about
185 17 m [29].

186 Within the ICESat-2 ATL08 product, photons collected by ATLAS are classified as terrain or
187 canopy and used for computing the final ATL08 parameters. To guarantee continuity, a fixed
188 segment size of 100 m was selected for all parameter calculations (mean, minimum, maximum, etc.)
189 in along-track direction [29]. Each 100 m segment is calculated using five sequential 20 m segments
190 from the ATL03 Product [30]. All derived terrain and canopy height values are defined as absolute
191 heights above the WGS84 ellipsoid [30].

192 In the study at hand, we analyzed the ATL08 parameters 'lat', 'lon', 'h_te_best_fit', 'h_te_interp',
193 and 'h_te_median', and 'h_canopy'. 'Lat' and 'lon' define the center latitude and longitude information
194 within each 100 m segment [30]. The parameter 'h_te_interp' contains the ground height interpolated
195 from the surface at the center of each 100 m step. This parameter is calculated in case less than 5% of
196 the photons are classified as ground [29]. The height, calculated based on the ground photons, is
197 called 'h_te_best_fit' [30]. This parameter is adjusted according to the specific topography [29].
198 Moreover, the parameter 'h_te_median' represents the median terrain height above the ellipsoid and
199 is derived from photons labeled as ground. The ATL08 product also provides the relative canopy
200 height ('h_canopy'), defined as the height above an estimated ground representing the 98th percentile

V. Peat dome surface modeling using space borne LiDAR (Chapter IV)

201 from the relative heights [29,30]. For the analysis, we used all available data from September 2018
202 through December 2019.

203 2.2.4 EGM2008

204 The Earth Gravitational Model 2008 (EGM2008) is a spherical harmonic model of the
205 gravitational potential of the earth [40] published by the National Geospatial-Intelligence Agency
206 (NGA). It can be downloaded at [41] for free. We used the EGM2008 to correct the ATLAS terrain
207 height for a potential geoid deviation.

208 2.3 Methods

209 2.3.1 ICESat-2/ATLAS Data

210 We downloaded the product ATL08 (land/vegetation) of ICESat-2 ATLAS and read the .h5
211 datasets in a jupyter notebook using python. The parameters 'lat', 'lon', 'h_te_best_fit', 'h_te_interp',
212 and 'h_te_median' were used to create a new data file including the earth's location and the different
213 height values identified and derived from ICESat-2/ATLAS. The values from the extracted
214 parameters were stored into a newly created shapefile using the entries' latitude and longitude
215 information to generate a geolocated product. This process resulted in a point layer with spatially
216 correctly located information about the terrain and canopy height derived by ICESat-2.

217 The EGM2008 was then subtracted from the ICESat-2 terrain height information pointwise to
218 correct for potential geoid deviations [34,42]. The relative canopy height was added to the terrain
219 height to obtain the absolute canopy height.

220 2.3.2 WorldDEM Data

221 The WorldDEM DTM has a spatial resolution of 12 x 12 m, whereas the ICESat-2/ATLAS covers
222 footprints with a diameter of approximately 20 m [43]. Five of these 20 m footprints were combined
223 to a ~100 m segment. Using the function "zonal statistics" in ArcGIS by ESRI, all WorldDEM pixels
224 covered by the specific ICESat-2 segment are identified. Afterwards, the mean of all pixels within this
225 ATLAS footprint is calculated and used for further data comparison and evaluation.

226 2.3.3 Peat Dome Surface Interpolation

227 To create a surface model from the ICESat-2 point data within the PHUs, we used the
228 geostatistical interpolation method Kriging, developed by Matheron [44]. Before applying the
229 interpolation to all ICESat-2 elevation measurements, the dataset was verified for errors resulting
230 from dense vegetation. On the basis of the dataset's canopy height information, points strongly
231 influenced by vegetation were identified. Consequently, we excluded those points before
232 interpolating the surface of the area to avoid overestimations. In addition, the data's characteristics
233 were analyzed regarding a normal distribution, stationarity, and trends before the interpolation [45].
234 Since a normal distribution was not inherent to the data, we transformed it within Rcran using the
235 package *bestNormalize*. Since the dataset did not show any trends or stationarity, spherical kriging
236 interpolation can be applied. To model the surface topography of the PHUs, we used a peatland map,
237 which had been derived from historical and recent satellite data for delineating the unit. After the
238 Kriging, the data was retransformed to elevation values.

239 2.3.4 Validation

240 For the validation, we generated a random point layer using the software ArcGIS. The values of
241 the modelled and reference elevations at the random points were extracted and compared in the next
242 step. For this comparison, the coefficient of determination (R^2), standard deviation, Root Mean Square
243 Error (RMSE), relative RMSE, also called the coefficient of variation (calculated as the ratio of the
244 RMSE to the mean of the observed variable), and the mean of the terrain heights in m were calculated.

245 3. Results

246 3.1 Peat surface topography and forest canopy height

247 In the analysis of the different terrain height parameters provided by ICESat-2, all three
248 parameters ($h_{te_best_fit}$, h_{te_med} , h_{te_interp}) showed very similar values with a mean at
249 approximately 6.15 m. For the following analyses, we only used $h_{te_best_fit}$.

250 The study area lies in the coastal flatlands of Kalimantan, where the terrain heights vary between
251 0–40 m over a distance of more than 100 km from the shore towards the inland. The highest terrain
252 values were identified in the North of the study area, displayed in white on the map in Figure 3.
253 When comparing ICESat-2 with the airborne derived terrain elevation heights, overlapping datasets
254 showed a strong correlation as showed in the scatterplot in Figure 3. However, ICESat-2 tends to
255 overestimate the terrain heights slightly. The mean elevation of the ICESat-2 values lies at 4.00 m,
256 which is lower than for the airborne derived elevations (5.28 m). The coefficient of determination (R^2)
257 reached a value of 0.94, while the RMSE is ± 1.61 m. Areas with a vegetation cover below 2 m showed
258 an RMSE of ± 1.38 m.
259

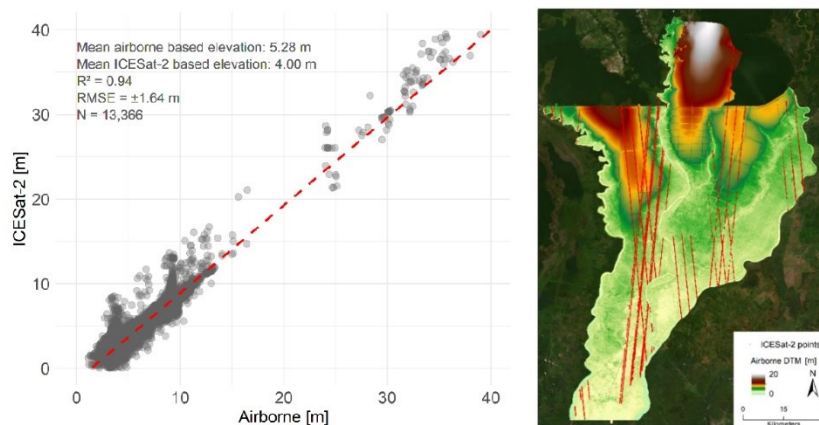


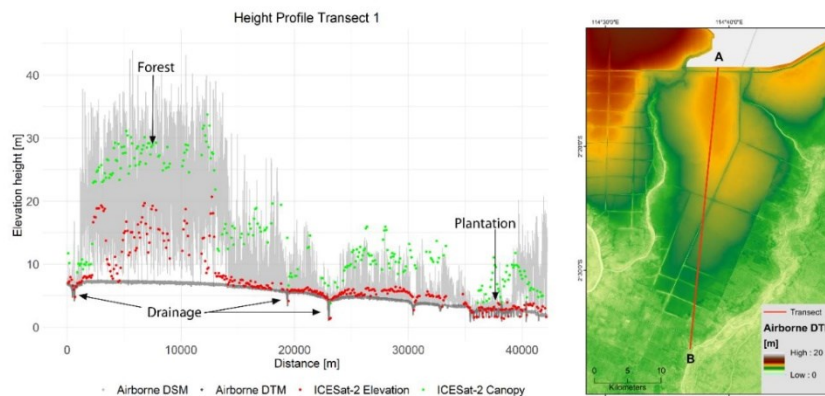
Figure 3: Scatterplot displaying the correlation between airborne and ICESat-2 derived terrain height values ($R^2 = 0.94$, left side) and the location of the used point information within the study area in Indonesia (red dots at the map, right side).

260 Extracting and plotting elevation values under different transects in peatland areas allowed a
261 detailed comparison of the two data sources. Figures 4 to 6 display three different transects and
262 corresponding estimated height values of ICESat-2 and airborne data. The transects have a length
263 between 40–52 km and pass over dome-shaped ombrogenous peatlands that are covered by tall peat
264 swamp forests, palm oil plantations, frequently burned areas covered by grasses, ferns and vines,
265 rivers, and drainage canals. All figures show the location of the specific transect in a map on the right
266 side of the corresponding height profiles. Peat domes are characterized by a smooth topography that
267 ranges from 0 m (displayed in green) to 20 m (dark brown). Figure 4 shows a small section of the
268 dome that reaches heights up to 10 m, while the dome displayed in Figures 5 and 6 ranges from 0 m
269 in the South to 20 m in the North. A transect of the highest section of the dome is illustrated in Figure
270 5, whereas Figure 6 presents the lower part of the dome. The whole area is influenced by rivers and
271 manmade drainage canals cutting into the peat. The airborne LiDAR DTM (dark grey) and DSM
272 (light grey) serve as a reference. The ICESat-2 elevations for terrain (red) and forest canopy (green)
273 are superimposed.

V. Peat dome surface modeling using space borne LiDAR (Chapter IV)

274 All ICESat-2 derived DTM measurements show a strong correlation with the airborne DTM data,
275 especially in non-forested areas. Even drainage canals can be detected, which are approximately 10
276 m wide and only 2 m deep. Plantations show a heterogeneous height pattern, which results from the
277 linear planting. However, in densely forested areas, as in Figure 4 (200 – 13,000 m), the ICESat-2 DTM
278 shows significant errors. The ground measurements for transect 1 exceed the ground reference by \pm
279 6.42 m. In areas with low vegetation (< 2 m), the accuracy of the ICESat-2 data lies in the range of \pm
280 0.55 cm. It is clear that the mean deviation of the ground correlates with the vegetation height. In
281 Figure 5, displaying transect 2, the discrepancy between the airborne and the satellite-derived
282 elevation for non-vegetated areas is ± 0.34 m, whereas the forested areas with trees taller than 10 m
283 show differences at about ± 2.00 m. The third transect (Figure 6) shows similar deviations with ± 2.02
284 m for forested areas and ± 1.05 m in non-vegetated areas.

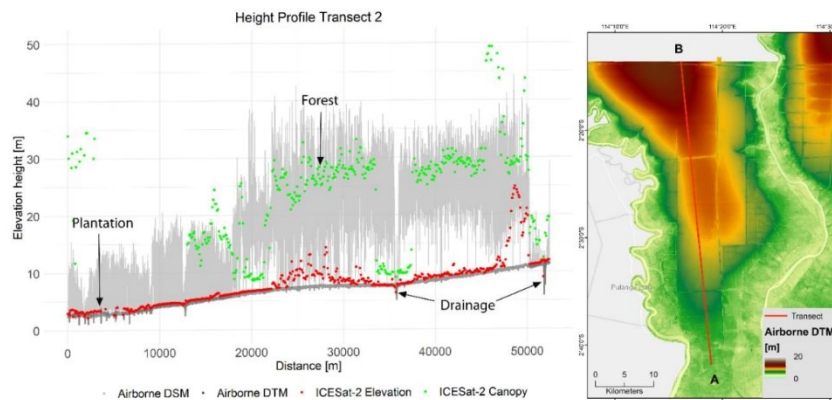
285 The DSM describes a digital surface model and thus the top of the canopy. The comparison of
286 the airborne DSM with the ICESat-2 DSM shows, in general, a good agreement of both datasets.
287 However, the satellite-based canopy height is lower than the airborne one. The RMSE of the canopy
288 height is ± 6.85 m for transect 1, ± 9.49 m for transect 2, and ± 6.66 m for transect 3. ICESat-2 exceeds
289 the airborne-based canopy heights by 5 – 20 m in the beginning and end of the transect, as shown in
290 Figure 5. A similar observation can be made in Figure 6 between 5,000 – 15,000 m. This variation can
291 be attributed to forest growth or growing plantations, which was identified with optical satellite data
292 from Sentinel-2 (25.07.2019). Furthermore, Figure 6 shows a distinct discrepancy between the
293 airborne and the ICESat-2 derived DSM at 25,000 – 35,000 m. Comparisons with optical data showed
294 that those differences occur because of the temporal shift of seven years and significant land cover
295 changes between the acquisitions.
296



297

298 **Figure 4:** Transect of 40 km covering one peat dome from A to B, left to right in the plot, in Kalimantan,
299 Indonesia.

V. Peat dome surface modeling using space borne LiDAR (Chapter IV)

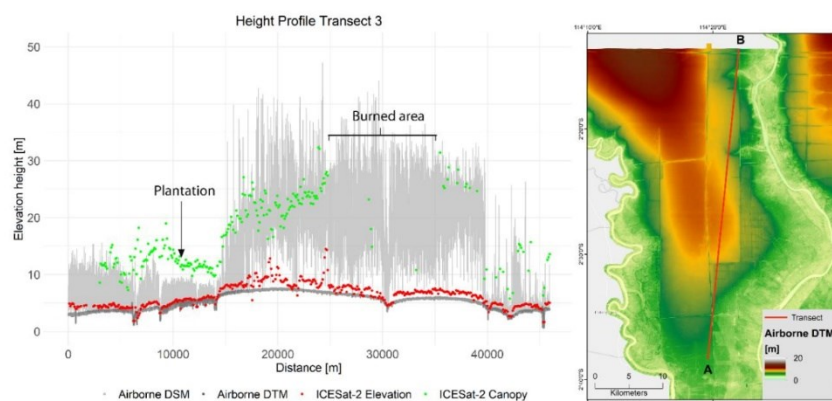


300

301

302

Figure 5: Transect of 52 km covering one peat dome from A to B, left to right in the plot, in Kalimantan, Indonesia.



303

304

305

Figure 6: Transect of 46 km covering the edge of one peat dome from A to B, left to right in the plot, in Kalimantan, Indonesia.

306

307

308

309

310

311

312

313

314

315

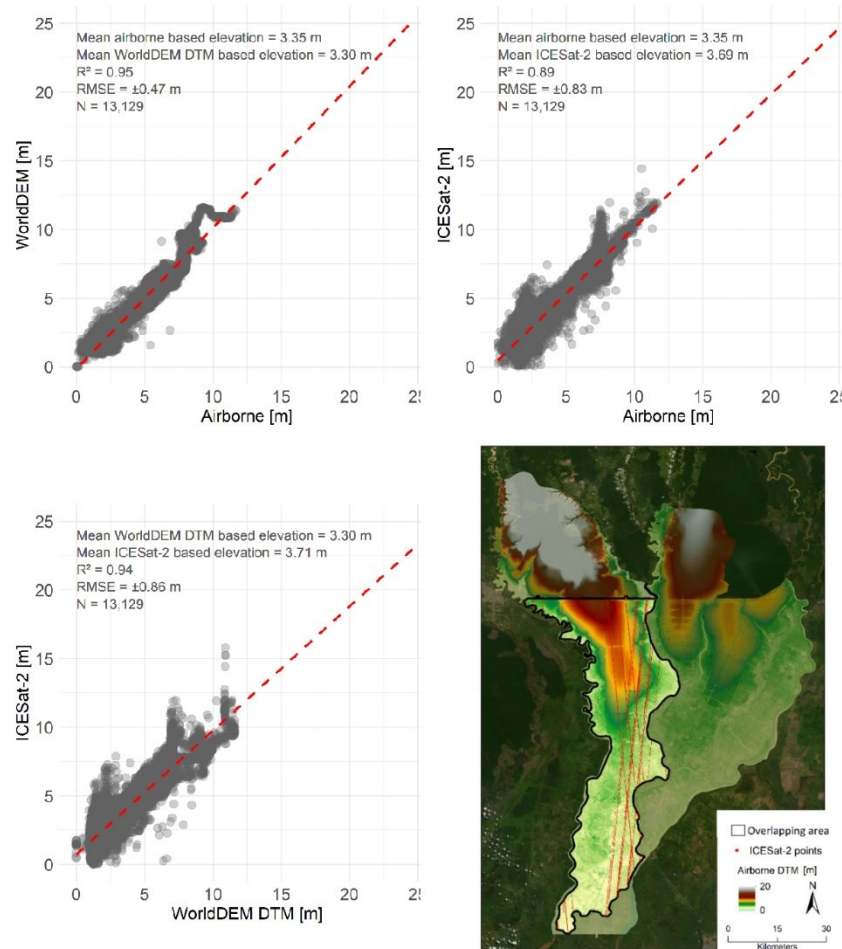
316

317

318

Since the airborne data is only available for a limited area, we furthermore validated ICESat-2 data with globally available WorldDEM DTM data. The first analysis is based on the overlapping part of all three data sets to provide an accurate overview of the satellite-based DTMs compared to the high-precision airborne DTM estimations. Figure 7 displays the scatterplots and the statistics for each the ICESat-2 and WorldDEM DTM compared to the reference DTM of airborne data. Altogether, 13,129 pixels were analyzed. Within the overlapping area (254,055 ha), the elevation ranges from 0 – 13 m. The mean elevation of the airborne data is 3.35 m, which is similar to the WorldDEM DTM (3.30 m) and is slightly exceeded by ICESat-2 (3.69 m). With an RMSE of ± 0.47 m and an R^2 of 0.95, low deviations from the WorldDEM DTM to the airborne derived DTM are expected. The strong agreement between the two datasets justifies the usage of the WorldDEM DTM as a reference dataset for areas without available airborne data. Regarding the same area but comparing the ICESat-2 data to the airborne elevations results in an R^2 of 0.89 and an RMSE of ± 0.83 . Besides, ICESat-2 shows a strong correlation to the WorldDEM DTM ($R^2 = 0.94$), with an RMSE at about ± 0.86 m.

319



320
321
322

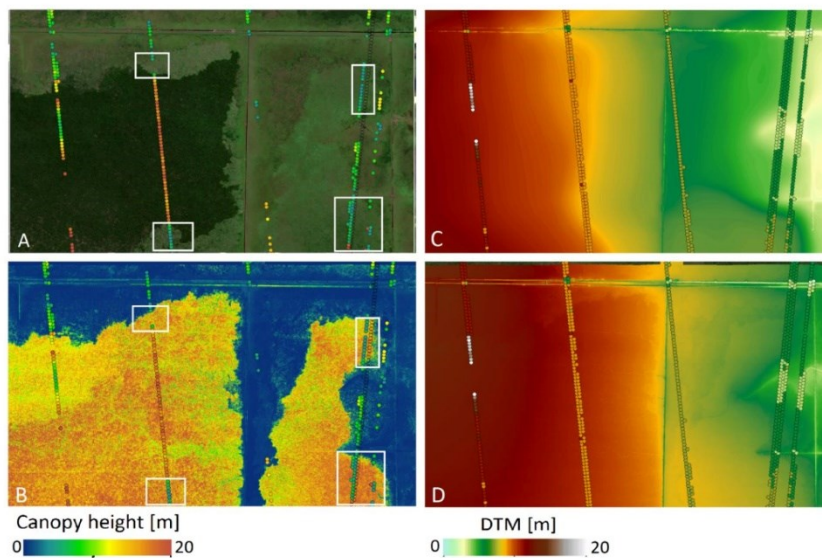
Figure 7: Scatterplot displaying the correlation between airborne, WorldDEM, and ICESat-2 derived terrain height values within the overlapping areas of all three data sets and the location of the used point information within the study area in Indonesia (red dots on the map, right side).

323
324
325
326
327
328
329
330

Figure 8 contains a subset of the overlapping area of the three analyzed data sets. Figure 8 A displays a Sentinel-2 true-color image from 25.07.2019 with superimposed ICESat-2 canopy height values from 2018 – 2019. The area is dominated by forest (dark green) and former burned areas with young grass (lighter green). Drainage canals, in the form of linear structures, can also be identified. Figure 8 B shows the airborne LiDAR canopy heights from 2011 in a color range from 0 – 20 m and superimposed with ICESat-2 canopy height values derived in 2018 – 2019. Within the forested areas, ICESat-2 canopy heights reach a maximum of 18.67 m, whereas airborne LiDAR canopy heights have a maximum of 19.73 m. One can see height differences within the white rectangles in Figure 8 A and

331 B. In these areas, ICESat-2 has significant lower canopy height values than the airborne LiDAR data.
332 The Sentinel-2 image from 25.07.2019 shows new and old burned areas within these regions. Thus, it
333 can be concluded that substantial canopy height differences indicate forest losses during the study
334 period.

335 When comparing the WorldDEM DTM data in Figure 8 C and the airborne LiDAR DTM in
336 Figure 8 D, a strong correlation within the overlapping area becomes apparent. The mean height is
337 3.35 m for the airborne LiDAR-derived DTM and 3.3 m for the WorldDEM DTM. The airborne LiDAR
338 DTM has a finer spatial resolution (1 x 1 m) in contrast to the WorldDEM DTM (12 x 12 m), which
339 allows the identification of more details, for example, canals. Furthermore, both datasets show a
340 strong agreement with the ICESat-2 derived DTM values that were plotted on top of the DTMs within
341 the overlapping area of the airborne and the WorldDEM data. With a mean height of 3.69 m, the
342 ICESat-2 derived DTM is slightly higher than the reference datasets. Compared with the optical
343 image and the canopy height, outliers are found entirely within forested regions.
344



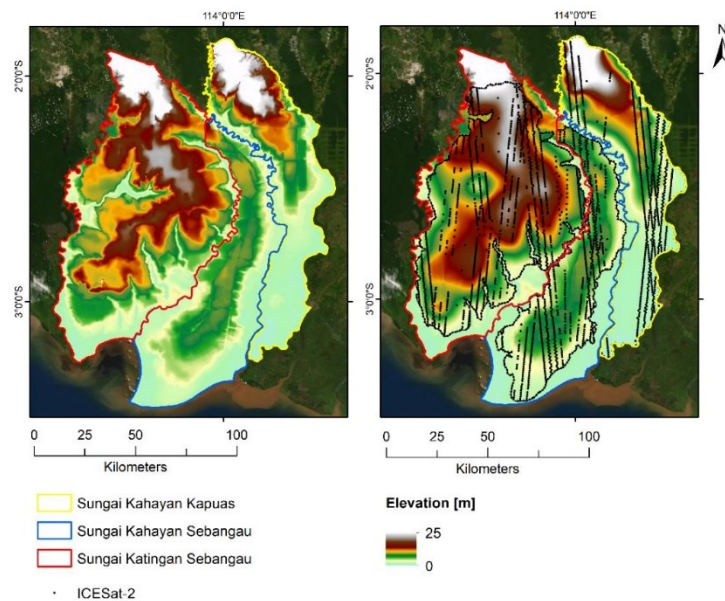
345

346 **Figure 8:** Subset of a peat dome, all images show the same area. A) Sentinel-2 imagery from 25.07.2019,
347 including ICESat-2 canopy height values from 2019. B) Airborne LiDAR canopy height from 2011,
348 including ICESat-2 canopy height values from 2019. C) WorldDEM DTM including ICESat-2 DTM
349 values from 2019. D) Airborne Lidar DTM from 2011 including ICESat-2 DTM values. White
350 rectangles show areas with land cover change.

351 3.2 Peat Dome Surface Interpolation

352 To model the entire peat dome surface, a comprehensive DTM is generated, which is achieved
353 by interpolating the point ground information derived from the ICESat-2 footprints. Using the
354 geostatistical interpolation method Kriging, we modelled the peat surfaces of the three PHUs Sungai
355 Katingan Sebangau (western dome), Sungai Kahayan Sebangau (middle dome) and Sungai Kahayan
356 Kapuas (eastern dome) in Kalimantan, Indonesia. Since no airborne data is available for this area, we
357 used WorldDEM DTM data as a reference. Sungai Katingan Sebangau covers an area of 828,596 ha
358 (red), while Sungai Kahayan Sebangau and Sungai Kahayan Kapuas are smaller, covering 454,542 ha
359 (blue) and 403,000 ha (yellow), respectively (Figure 9). The highest elevations are found in the

360 Northern part of Sungai Katingan Sebangau and Sungai Kahayan Kapuas, with altitudes of
 361 approximately 30 m and 32 m, accordingly. In the South, on the coast, the elevation is about 1 m.
 362 Sungai Kahayan Sebangau is characterized by lower altitudes that range from 1 – 9 m. The pattern of
 363 the interpolated terrain elevation is visibly consistent with the WorldDEM DTM's. With 12 x 12 m,
 364 the spatial resolution of the WorldDEM is fine enough to detect larger rivers and canals, whereas the
 365 interpolated data set gives a good overview of the general terrain. However, small-scaled details
 366 cannot be identified. Nevertheless, the dome shape of the peat dome is apparent. Only the southern
 367 part of Sungai Katingan Sebangau shows noticeable differences in altitude. In this area, the
 368 WorldDEM DTM displays lower values than ICESat-2 while being surrounded by higher values. This
 369 indicates an error due to the manual correction of the WorldDEM DTM data.
 370



371
 372 **Figure 9:** Comparison of the surface elevation of three peat hydrological units. The image on the left
 373 displays the WorldDEM DTM; the one on the right shows the Kriging result based on ICESat-2 points,
 374 including the points used for the interpolation.

375 For validation purposes, we used random points spread throughout the PHUs. The values per
 376 dataset under all random points were extracted and plotted, the result of which is displayed in Figure
 377 10. It shows scatterplots comparing the elevation values of both datasets, the WorldDEM DTM and
 378 ICESat-2. The coefficient of determination for Sungai Katingan Sebangau reaches a value of 0.78 using
 379 1,300 random points. In the smaller Sungai Kahayan Sebangau, the R^2 value is 0.84, based on 700
 380 random points, which underlines a strong correlation between the two datasets. With an R^2 of 0.94
 381 for 950 randomly selected points, the less forested Sungai Kahayan Kapuas produced the strongest
 382 correlation. The RMSE is ± 2.67 m for Sungai Katingan Sebangau, ± 1.47 m for Sungai Kahayan
 383 Kapuas, and ± 0.68 m for Sungai Kahayan Sebangau. These result in a relative RMSE (coefficient of
 384 variation) of 22.5%, 19.09%, and 14.3%, respectively, indicating the lowest deviations in the areas with
 385 the lowest vegetation cover.
 386

V. Peat dome surface modeling using space borne LiDAR (Chapter IV)

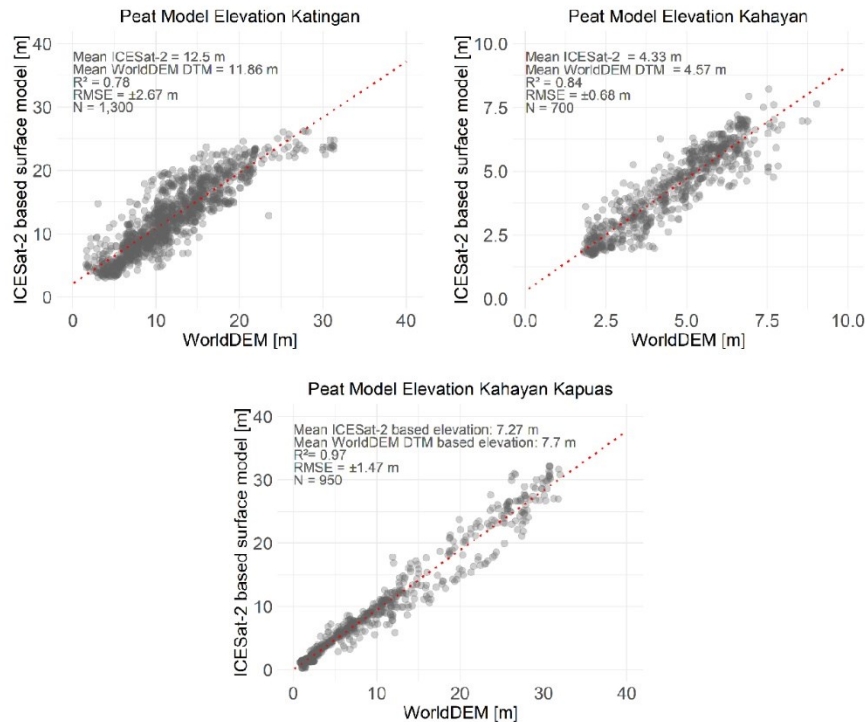


Figure 10: Scatterplot and trendline of the ICESat-2 based interpolated peat model elevation in comparison to the WorldDEM DTM elevation for the three peat domes Sungai Katingan and Sungai Kahayan.

387 4. Discussion

388 Identifying tropical peatlands in Indonesia by field-based methods at a large scale is not feasible
389 due to the large extent of potential peatlands (> 25 Million ha), poor accessibility, and remoteness. Up
390 to date, only a limited number of field measurements have been collected for selected areas in
391 Sumatra and Kalimantan to assess their carbon pools. Furthermore, pristine peatlands are covered
392 by dense tropical forests and shrubs and are thus highly inaccessible for ground surveys. Remote
393 sensing enables a countrywide data collection in a short period of time. Since peatlands have a
394 smooth, dome-shaped topography, the indirect detection of peatlands using the topography from
395 remote sensing data is possible [12,23]. The most accurate DTM can be derived from airborne LiDAR
396 [23]. Since airborne data acquisition is associated with high costs, it is not a solution for wall-to-wall
397 assessments in large countries like Indonesia. The first global topography was mapped by the SRTM.
398 Since the X-band SAR data of this product cannot penetrate the vegetation entirely, especially in
399 dense tropical forests, terrain heights cannot be assessed with sufficient accuracy on forested
400 peatlands [12]. A newer global DTM is the WorldDEM DTM derived from the TerraSAR-X Tandem
401 mission, which is corrected explicitly for vegetation artefacts. Space-born LiDAR (ICESat/GLAS) was
402 successfully tested for the identification of peatland topography by Ballhorn et al. (2011) [23] and
403 Hayashi et al. (2015) [46]. In a recent study, Vernimmen et al. (2020) demonstrated the great potential
404 of mapping peatlands from an airborne LiDAR-derived DTM in eastern Sumatra [47]. The authors

405 visually compared an airborne derived DTM with an ICESat-2 derived DTM. The comparison
406 showed that ICESat-2 data reveals peat dome shapes in eastern Sumatra similar compared to high
407 precise airborne DTM.

408 4.1 Ground Height Results derived from ICESat-2

409 We investigated whether the space-born ICESat-2 LiDAR instrument, with its improved spatial
410 resolution and photon counting system, is suitable for identifying dome-shaped peatlands. This was
411 achieved by relating ICESat-2 measurements to highly accurate wall-to-wall airborne LiDAR
412 measurements. We compared the ICESat-2 'h_te_best_fit' data with an airborne LiDAR DTM
413 acquired in 2011, and the more comprehensive WorldDEM DTM data acquired in 2014. ICESat-2
414 elevation was derived with a vertical accuracy in three different transects in a range of $\pm 0.34 - 1.09$
415 m compared to the airborne data. A coefficient of determination of 0.90 showed a strong correlation
416 between the airborne and the ICESat-2 data. Testing the suitability of the WorldDEM DTM for
417 extensive reference purposes equally resulted in a strong correlation of the data compared to highly
418 accurate airborne data ($R^2 = 0.95$, RMSE = ± 0.47), making the WorldDEM DTM a good alternative for
419 areas with no available airborne data.

420 Within the overlapping area of the three datasets, the analysis of the ICESat-2 derived terrain
421 elevations in comparison to airborne data ($R^2 = 0.89$) and the WorldDEM DTM data ($R^2 = 0.86$)
422 resulted in strong correlations. The smooth shape of the peat domes was identified in multiple
423 different transects. Our results are comparable with those of Ballhorn et al. (2011) [34], who analyzed
424 ICESat/GLAS point cloud data as a measurement tool for peatlands in Indonesia. The authors
425 achieved an R^2 of 0.92 and 0.90, correlating the ICESat/GLAS data with the SRTM derived elevation
426 and the 3D peatland elevation models based on the SRTM. Besides, the ICESat/GLAS data was
427 compared to airborne LiDAR data and also displayed a strong correlation of $R^2 = 0.91$ [34].

428 However, in this study, we showed that in individual areas, terrain heights are overestimated
429 by ICESat-2. A more detailed investigation showed that this incidence proved accurate, especially
430 within densely forested areas, in which measurements labeled as ground are most likely dense
431 underwood or ground vegetation. This occurs because the canopy height values, as well as the
432 airborne DSM, are strongly influenced by vegetation. Neuenschwander et al. (2019) [29] identified a
433 decreasing accuracy for ground detection with an increasing canopy cover. This is expected due to
434 the sensitivity of LiDAR towards vegetation. Especially in dense tropical forests with several
435 vegetation layers and dense underwood, too few photons are reflected from the ground.
436 Furthermore, in Neuenschwander and Magruder (2016), the authors investigate the potential impact
437 of vertical sampling uncertainty on ICESat-2/ATLAS in different forest ecosystems [48]. The study
438 evaluates simulated ICESat-2 canopy and terrain heights with airborne LiDAR ground truth data.
439 The results show small mean bias errors and an error uncertainty of 0.06 m (± 0.24 m RMSE) and -
440 0.13 m (± 0.77 m RMSE) in wooded savannas and boreal forests, respectively. In ecosystems with
441 dense vegetation, terrain errors lay at about 1.93 m (± 1.66 m RMSE) and 2.52 m (± 2.63 m RMSE). The
442 authors explained the higher errors are due to reduced ground returns in dense forests.
443 Neuenschwander and Pitts (2019) mentioned that ICESat-2/ATLAS can lose its ground signal for
444 canopy closure of $> 95\%$ but also when cloud cover obscures the terrestrial signal [30]. In the tropical
445 forest of Indonesia, both restrictions are probable. Nevertheless, the forest within the study area is
446 affected by human activity and has a density below 95%. In conclusion, it can be stated that peat
447 domes with their smooth topography and convex shape can be identified from ICESat-2/ATLAS data.
448 However, the accuracy might be impaired in areas with dense vegetation.

449 4.2 Canopy Height Results derived from ICESat-2

450 We showed that the relative canopy height measurements provided by ICESat-2 are comparable
451 to the airborne LiDAR data. However, on average, the vegetation heights derived from ICESat-2 are
452 5 – 20 m lower than the airborne LiDAR heights. Similarly, Neuenschwander et al. 2016 found that
453 simulated ICESat-2 underestimates the top of the canopy for all tested ecosystems [48]. The errors
454 ranged from 0.28 m (± 1.39 m RMSE) to 1.25 m (± 2.63 m RMSE) when analyzing wooden savanna,

455 boreal forest, deciduous forest, and tropical forest with dense vegetation delivering the highest errors.
456 The general underestimation of vegetation heights in comparison to airborne measurements can be
457 attributed to the different signal sampling resolutions. Furthermore, the penetration depth of the
458 sensor plays a decisive role in deriving the vegetation height. Besides, the relative canopy height is
459 defined as the height between the absolute canopy height and the interpolated ground height [29].
460 Since the ground height is underestimated due to dense vegetation, the relative tree height is also
461 underestimated in the subsequent calculation. To mitigate this problem, the ICESat-2 derived
462 absolute canopy height could be used in combination with an external DTM to calculate the relative
463 canopy height [48].

464 4.3 Creating a continuous DTM model from ICESat-2

465 To model the surface topography of ombrogenous peatlands, we used a peatland classification
466 based on historical and recent satellite data. The modelled surface of the three peatlands based on
467 ICESat-2 measurements correlates well with the WorldDEM DTM data ($R^2 = 0.78, 0.84, \text{ and } 0.94$). In
468 addition, the interpolated surface shows a similar value distribution as the WorldDEM DTM.
469 However, cuts from rivers or channels within the PHUs can only be mapped to a limited extent
470 because of the limited availability of measuring points for the modelling. The relative RMSE of 14.3%
471 for Sungai Kahayan Sebangau shows a slightly better result than for Sungai Katingan Sebangau
472 (22.5%) and Sungai Kahayan Kapuas (19.09%). This can be explained by the variable numbers of
473 measurements (700 – 1,300) for each peatland.

474 Since the WorldDEM is recorded with an X-band radar, the wavelength is about 3 cm [49]. Such
475 short wavelengths are known to interact with the upper vegetation layer [50,51]. Penetrating the
476 vegetation to reach the ground is hardly possible, especially in dense tropical rainforests [52]. As a
477 result, the elevation measurements are overestimated, and vegetation artifacts in the results are
478 clearly visible.

479 4.4 Error Sources

480 Differences in resolution and extent also mean that different areas on the ground influence the
481 derived pixel value [53]. For an accurate comparison of the three datasets; airborne LiDAR,
482 WorldDEM, and ICESat-2; we overcame the problem of different resolutions by using the mean of all
483 pixels per dataset covered by the 100 m segment of ICESat-2. However, there may still be negligible
484 deviations because of edge effects.

485 Furthermore, different sensor accuracies should be considered. The utilized airborne LiDAR
486 product has a vertical accuracy of 0.14 m (DSM) and 0.18 m (DTM) [38]. ICESat-2 has a ranging
487 precision of 25 – 35 cm in flat terrain [29,30]. In steeper terrain, the sloping topography is incorporated
488 as a function of the "geolocation knowledge of the pointing multiplied by the tangent of the surface
489 slope" [30]. Since the study area is in an extremely flat region of Indonesia, we assume a ranging
490 precision no higher than 35 cm on bare ground. The global model of the WorldDEM DTM has a
491 relative vertical accuracy of < 5 m, while for flat terrain, as for the study area, the vertical accuracy in
492 comparison with the airborne DTM lies at ± 0.47 m. Regarding the size of the investigated area, the
493 inaccuracies of the individual sensors are negligibly small [12].

494 In addition to the different spatial resolutions, acquisition geometries, and sensor accuracies, the
495 different acquisition times of the sensors can lead to potential errors. During the acquisitions, peat
496 loss due to oxidation can result in subsidence. The subsidence rate for peatlands in Sumatra and
497 Kalimantan ranges from 2 cm*year⁻¹ to 4 cm*year⁻¹ depending on the distance to draining canals
498 and the unaffected forest cover of the respective peatland [47]. Furthermore, the vegetation height
499 can change from natural growth or fires and thus indirectly influence the terrain measurements.

500 5. Conclusions

501 We showed that carbon-rich ombrogenous peatlands could be identified based on terrain
502 heights derived from the freely available ICESat-2 data comparably fast and robustly. This

503 identification becomes possible because of the peat domes' smooth convex topography, which is
504 visible in the transects of the ICESat-2 data.

505 Furthermore, we demonstrated the benefits of the ICESat-2 flight tracks for the first time in terms
506 of interpolating seamless peat dome surfaces robustly. By improving the knowledge of the surface
507 structure of a peat area, conclusions about the volume of this endangered ecosystem become possible.
508 Since it has already been proven that the surface and depth of a peat dome are related, the precise
509 topography estimates based on ICESat-2 also allow the determination of the peat domes' volume.
510 Based on estimated peat volumes, the below-ground carbon content can then be calculated for large
511 areas. By 2022, ICESat-2 will reach almost global coverage, providing flight lines with a distance of
512 less than 2 km at the equator. These dense measurements will further enhance interpolations of the
513 peat dome surface topography and thus the estimation of the carbon content.

514 Besides accurate terrain height measurements, the canopy height provided by ICESat-2 showed
515 great potential for gaining information about tropical forests, such as the canopy height, which
516 enables the modelling of above-ground biomass - another essential parameter for deriving the carbon
517 content. Those highly accurate estimations of both above-ground and below-ground carbon contents
518 are significant input variables for global climate models and thus provide a crucial contribution to
519 emission reduction projects, such as REDD+.

520 In the near future, the new mission Global Ecosystem Dynamics Investigation (GEDI), a high-
521 powered laser system operating from the ISS, will provide additional information between 52° North
522 and South. The distance of GEDI's flight tracks is approximately 600 m, which further improves the
523 global coverage of publicly accessible LiDAR data. A combination of ICESat-2 and GEDI data offers
524 enhanced possibilities to derive below-ground and above-ground biomass from peatland
525 topographies as well as the forest structure of tropical forests.

526 **Author Contributions:** A.B. and F.S. conceived and designed the experiments, A.B. collected, prepared
527 and analyzed the data, A.B. wrote the manuscript, and F.S. reviewed and commented on the
528 manuscript.

529 **Conflicts of Interest:** The authors declare no conflict of interest.

530 References

- 531 1. Tyrrell, M.L.; Ashton, M.S.; Spalding, D.; Gentry, B. Forests and Carbon. A Synthesis of Science,
532 Management, and Policy for Carbon Sequestration in Forests; 23, New Haven, 2009. Available online:
533 <http://environment.yale.edu/publication-series/5947.html> (accessed on 7 March 2018).
- 534 2. MacKinnon, K.; Hatta, G.; Halim, H.; Mangalik, A. Indonesian Borneo; Tuttle Publishing: New York,
535 1996, ISBN 0-945971-73-7.
- 536 3. Baccini, A.; Goetz, S.J.; Walker, W.S.; Laporte, N.T.; Sun, M.; Sulla-Menashe, D.; Hackler, J.; Beck,
537 P.S.A.; Dubayah, R.; Friedl, M.A.; et al. Estimated carbon dioxide emissions from tropical deforestation
538 improved by carbon-density maps. *Nature Climate change* 2012, 2, 182–185, doi:10.1038/nclimate1354.
- 539 4. Global Forest Watch. Tree cover Loss in Indonesia. Available online:
540 <https://www.globalforestwatch.org>.
- 541 5. Murdiyarto, D.; Saragi-Sasmito, M.F.; Rustini, A. Greenhouse gas emissions in restored secondary
542 tropical peat swamp forests. *Mitig Adapt Strateg Glob Change* 2019, 24, 507–520, doi:10.1007/s11027-017-
543 9776-6.
- 544 6. Page, S.E.; Rieley, J.O.; Wüst, R. Lowland tropical peatlands of Southeast Asia. *Peatlands: Evolution*
545 *and Records of Environmental and Climate Changes* 2006, 9, 145–172, doi:10.1016/S0928-2025(06)09007-9.
- 546 7. Page, S.E.; Banks, C.J.; Rieley, J.O. Tropical peatlands: distribution, extent and carbon storage —
547 uncertainties and knowledge gaps. *Peatlands International* 2007, 2, 1–7.
- 548 8. Posa, M.R.C.; Wijedasa, L.S.; Corlett, R.T. Biodiversity and Conservation of Tropical Peat Swamp
549 Forests. *BioScience* 2011, 61, 49–57, doi:10.1525/bio.2011.61.1.10.
- 550 9. Page, S.E.; Rieley, J.O.; Banks, C.J. Global and regional importance of the tropical peatland carbon
551 pool. *Global Change Biology* 2011, 17, 798–818, doi:10.1111/j.1365-2486.2010.02279.x.

V. Peat dome surface modeling using space borne LiDAR (Chapter IV)

- 552 10. Warren, M.; Hergoualc'h, K.; Kauffman, J.B.; Murdiyarso, D.; Kolka, R. An appraisal of Indonesia's
553 immense peat carbon stock using national peatland maps: Uncertainties and potential losses from
554 conversion. *Carbon Balance Manag.* 2017, 12, 12, doi:10.1186/s13021-017-0080-2.
- 555 11. Page, S.E.; Wüst, R.A.J.; Weiss, D.; Rieley, J.O.; Shoty, W.; Limin, S.H. A record of Late Pleistocene
556 and Holocene carbon accumulation and climate change from an equatorial peat bog (Kalimantan,
557 Indonesia): Implications for past, present and future carbon dynamics. *J. Quaternary Sci.* 2004, 19, 625–635,
558 doi:10.1002/jqs.884.
- 559 12. Jaenicke, J.; Rieley, J.O.; Mott, C.; Kimman, P.; Siegert, F. Determination of the amount of carbon stored
560 in Indonesian peatlands. *Geoderma* 2008, 147, 151–158, doi:10.1016/j.geoderma.2008.08.008.
- 561 13. Miettinen, J.; Shi, C.; Liew, S.C. Deforestation rates in insular Southeast Asia between 2000 and 2010.
562 *Global Change Biology* 2011, 17, 2261–2270, doi:10.1111/j.1365-2486.2011.02398.x.
- 563 14. Dinsmore, K.J.; Skiba, U.M.; Billett, M.F.; Rees, R.M. Effect of water table on greenhouse gas emissions
564 from peatland mesocosms. *Plant Soil* 2009, 318, 229–242, doi:10.1007/s11104-008-9832-9.
- 565 15. Carlson, K.M.; Goodman, L.K.; Calen C. M. T. Modeling relationships between water table depth and
566 peat soil carbon loss in Southeast Asian plantations. *Environ. Res. Lett.* 2015, 10, 74006, doi:10.1088/1748-
567 9326/10/7/074006.
- 568 16. Suroyo, G.; Diela, T. World Bank says Indonesia forest fires cost \$5.2 billion in economic losses;
569 Jakarta, 2019.
- 570 17. Lohberger, S.; Stängel, M.; Atwood, E.C.; Siegert, F. Spatial evaluation of Indonesia's 2015 fire-affected
571 area and estimated carbon emissions using Sentinel-1. *Global Change Biology* 2018, 24, 644–654,
572 doi:10.1111/gcb.13841.
- 573 18. World Bank Group. Indonesia Economic Quarterly. Reforming amid uncertainty, 2015. Available
574 online: <http://pubdocs.worldbank.org/en/844171450085661051/IEQ-DEC-2015-ENG.pdf> (accessed on 20
575 January 2020).
- 576 19. Blunden, J.; Arndt, D.S. State of the Climate in 2015: Special Supplement to the Bulletin of the
577 American Meteorological Society. *American Meteorological Society* 2016, 97.
- 578 20. Huijnen, V.; Wooster, M.J.; Kaiser, J.W.; Gaveau, D.L.A.; Flemming, J.; Parrington, M.; Inness, A.;
579 Murdiyarso, D.; Main, B.; van Weele, M. Fire carbon emissions over maritime southeast Asia in 2015 largest
580 since 1997. *Sci. Rep.* 2016, 6, 26886, doi:10.1038/srep26886.
- 581 21. Jayarathne, T.; Stockwell, C.E.; Gilbert, A.A.; Daugherty, K.; Cochrane, M.A.; Ryan, K.C.; Putra, E.I.;
582 Saharjo, B.H.; Nurhayati, A.D.; Albar, I.; et al. Chemical characterization of fine particulate matter emitted
583 by peat fires in Central Kalimantan, Indonesia, during the 2015 El Niño. *Atmos. Chem. Phys.* 2018, 18, 2585–
584 2600, doi:10.5194/acp-18-2585-2018.
- 585 22. Tacconi, L. Fires in Indonesia: causes, costs and policy implications, Bogor, 2003.
- 586 23. Ballhorn, U.; Jubanski, J.; Siegert, F. ICESat/GLAS Data as a Measurement Tool for Peatland
587 Topography and Peat Swamp Forest Biomass in Kalimantan, Indonesia. *Remote Sensing* 2011, 3, 1957–1982,
588 doi:10.3390/rs3091957.
- 589 24. Ballhorn, U. Airborne and spaceborne LiDAR data as a measurement tool for peatland topography,
590 peat fires burn depth, and forest above ground biomass in Central Kalimantan, Indonesia. Dissertation;
591 Ludwig-Maximilian University, Munich, 2012.
- 592 25. Bourdeau, J.; Nelson, R.F.; Margolis, H.A.; Beaudion, A.; Guidon, L.; Kimes, D. Regional aboveground
593 forest biomass using airborne and spaceborne LiDAR in Québec. *Remote Sensing of Environment* 2008, 112,
594 3876–3890, doi:10.1016/j.rse.2008.06.003.
- 595 26. Carabajal, C.C.; Harding, D. SRTM C-Band and ICESat Laser Altimetry Elevation Comparisons as a
596 Function of Tree Cover and Relief. *Photogrammetric Engineering & Remote Sensing* 2006, 72, 287–298.
- 597 27. Harding, D.J.; Carabajal, C.C. ICESat waveform measurements of within-footprint topographic relief
598 and vegetation vertical structure. *Geophys. Res. Lett.* 2005, 32, 2509, doi:10.1029/2005GL023471.
- 599 28. Liu, M.; Popescu, S.; Malambo, L. Feasibility of Burned Area Mapping Based on ICESAT-2 Photon
600 Counting Data. *Remote Sensing* 2020, 12, 24, doi:10.3390/rs12010024.
- 601 29. Neuenschwander, A.; Pitts, K. The ATL08 land and vegetation product for the ICESat-2 Mission.
602 *Remote Sensing of Environment* 2019, 221, 247–259, doi:10.1016/j.rse.2018.11.005.
- 603 30. Neuenschwander, A.; Pitts, K. Ice, Cloud, and Land Elevation Satellite 2 (ICESat-2) Algorithm
604 Theoretical Basis Document (ATBD) for Land - Vegetation Along-Track Products (ATL08), 2019.

V. Peat dome surface modeling using space borne LiDAR (Chapter IV)

- 605 31. Wojciech, M. Kriging Method Optimization for the Process of DTM Creation Based on Huge Data Sets
606 Obtained from MBESs. *Geosciences* 2018, 8, 433, doi:10.3390/geosciences8120433.
- 607 32. Yilmaz, M.; Uysal, M. Comparing uniform and random data reduction methods for DTM accuracy.
608 *International Journal of Engineering and Geosciences* 2017, 2, 9–16, doi:10.26833/ijeg.286003.
- 609 33. Global Forest Watch. Land Cover Indonesia. Available online:
610 <http://data.globalforestwatch.org/datasets/land-cover-indonesia>.
- 611 34. Ballhorn, U.; Jubanski, J.; Siegert, F. ICESat/GLAS Data as a Measurement Tool for Peatland
612 Topography and Peat Swamp Forest Biomass in Kalimantan, Indonesia. *Remote Sensing* 2011, 3, 1957–1982,
613 doi:10.3390/rs3091957.
- 614 35. Siegert, F.; Ruecker, G.; Hinrichs, A.; Hoffmann, A.A. Increased damage from fires in logged forests
615 during droughts caused by El Niño. *Nature* 2001, 437–440.
- 616 36. Ballhorn, U.; Siegert, F.; Mason, M.; Limin, S. Derivation of burn scar depths and estimation of carbon
617 emissions with LIDAR in Indonesian peatlands. *Proc. Natl. Acad. Sci. U. S. A.* 2009, 106, 21213–21218,
618 doi:10.1073/pnas.0906457106.
- 619 37. Ballhorn, U.; Navratil, P.; Jubanski, J.; Siegert, F. LiDAR survey of the Kalimantan Forests and Climate
620 Partnership (KFCP) project site and EMRP area in Central Kalimantan. Technical Working Paper, Munich,
621 2014.
- 622 38. Konecny, K.; Ballhorn, U.; Navratil, P.; Jubanski, J.; Page, S.E.; Tansey, K.; Hooijer, A.; Vernimmen, R.;
623 Siegert, F. Variable carbon losses from recurrent fires in drained tropical peatlands. *Global Change Biology*
624 2016, 22, 1469–1480, doi:10.1111/gcb.13186.
- 625 39. Suppa, M. WorldDEM™ Technical Product Specification. Digital Surface Model, Digital Terrain
626 Model Version 2.0, 2015.
- 627 40. Pavlis, N.K.; Holmes, S.A.; Kenyon, S.C.; Factor, J.K. The development and evaluation of the Earth
628 Gravitational Model 2008 (EGM2008). *J. Geophys. Res.* 2012, 117, n/a–n/a, doi:10.1029/2011JB008916.
- 629 41. Geographic Lib. Geoid height. Available online:
630 <https://geographiclib.sourceforge.io/html/geoid.html#geoidinst>.
- 631 42. Markus, T.; Neumann, T.; Martino, A.; Abdalati, W.; Brunt, K.; Csatho, B.; Farrell, S.; Fricker, H.;
632 Gardner, A.; Harding, D.; et al. The Ice, Cloud, and land Elevation Satellite-2 (ICESat-2): Science
633 requirements, concept, and implementation. *Remote Sensing of Environment* 2017, 190, 260–273,
634 doi:10.1016/j.rse.2016.12.029.
- 635 43. Neuenschwander, A.L.; Magruder, L.A. Canopy and Terrain Height Retrievals with ICESat-2: A First
636 Look. *Remote Sensing* 2019, 11, 1721, doi:10.3390/rs11141721.
- 637 44. Matheron, G. The theory of regionalized variables and its applications; École Nationale Supérieure
638 des Mines: Fontainebleau, Paris, 1971.
- 639 45. Ferreira, I.O.; Rodrigues, D.D.; Santos, G.R.d.; Rosa, L.M.F. IN BATHYMETRIC SURFACES: IDW OR
640 KRIGING? *Bol. Ciênc. Geod.* 2017, 23, 493–508, doi:10.1590/s1982-21702017000300033.
- 641 46. Hayashi, M.; Saigusa, N.; Yamagata, Y.; Hirano, T. Regional forest biomass estimation using
642 ICESat/GLAS spaceborne LiDAR over Borneo. *Carbon Management* 2015, 6, 19–33,
643 doi:10.1080/17583004.2015.1066638.
- 644 47. Vernimmen, R.; Hooijer, A.; Akmalia, R.; Fitriatanegara, N.; Mulyadi, D.; Yuherdha, A.; Andreas,
645 H.; Page, S. Mapping deep peat carbon stock from a LiDAR based DTM and field measurements, with
646 application to eastern Sumatra. *Carbon Balance Manag.* 2020, 15, 4, doi:10.1186/s13021-020-00139-2.
- 647 48. Neuenschwander, A.; Magruder, L. The Potential Impact of Vertical Sampling Uncertainty on ICESat-
648 2/ATLAS Terrain and Canopy Height Retrievals for Multiple Ecosystems. *Remote Sensing* 2016, 8, 1039,
649 doi:10.3390/rs8121039.
- 650 49. Kugler, F.; Koudogobo, F.N.; Gutjahr, K.; Papathanassiou, K.P. Frequency Effects in Pol-InSAR Forest
651 Height Estimation. Available online: <https://mediatum.ub.tum.de/doc/1256389/1256389.pdf>.
- 652 50. Berninger; Lohberger; Zhang; Siegert. Canopy Height and Above-Ground Biomass Retrieval in
653 Tropical Forests Using Multi-Pass X- and C-Band Pol-InSAR Data. *Remote Sensing* 2019, 11, 2105,
654 doi:10.3390/rs11182105.
- 655 51. Schlund, M.; Magdon, P.; Eaton, B.; Aumann, C.; Erasmi, S. Canopy height estimation with TanDEM-
656 X in temperate and boreal forests. *International Journal of Applied Earth Observation and Geoinformation*
657 2019, 82, 101904, doi:10.1016/j.jag.2019.101904.

V. Peat dome surface modeling using space borne LiDAR (Chapter IV)

Remote Sens. **2020**, *12*, x FOR PEER REVIEW

19 of 19

- 658 52. Schlund, M.; Poncet, F. von; Kuntz, S.; Boehm, H.-D.V.; Hoekman, D.H.; Schullius, C. TanDEM-X
659 elevation model data for canopy height and aboveground biomass retrieval in a tropical peat swamp forest.
660 *International Journal of Remote Sensing* 2016, *37*, 5021–5044, doi:10.1080/01431161.2016.1226001.
661 53. Frazer, G.W.; Magnussen, S.; Wulder, M.A.; Niemann, K.O. Simulated impact of sample plot size and
662 co-registration error on the accuracy and uncertainty of LiDAR-derived estimates of forest stand biomass.
663 *Remote Sensing of Environment* 2011, *115*, 636–649, doi:10.1016/j.rse.2010.10.008.
664



© 2020 by the authors. Submitted for possible open access publication under the terms and conditions of the Creative Commons Attribution (CC BY) license (<http://creativecommons.org/licenses/by/4.0/>).

665

VI. Synthesis

1. General discussion

Fossil fuel and industrial processes are responsible for 32 Gt CO₂-eq/y, which equal 65 % of the overall emissions for 2010. A further 5 Gt CO₂-eq (11 %) originates from forestry and other land-use changes (IPCC 2015). However, other studies, such as, van der Werf et al. (2009) mentioned high uncertainties for estimating deforestation and degradation. They prefer to specify the contribution of the total anthropogenic CO₂ emissions due to forestry at about 6 – 17 %. The total anthropogenic greenhouse gas emissions for 2010 are estimated at 49 Gt CO₂-eq, while 24 % of these emissions are connected to the agricultural, forestry and other land-use sectors. These include the effects of forest and peat fires as well as peat decay (IPCC 2015).

Deforestation and forest degradation in the tropics due to illegal logging and the establishment of oil palm plantations account for a significant proportion of the estimated numbers. Indonesia, especially Sumatra and Kalimantan, does not merely have the world's highest rates of deforestation, but additionally is characterized by peat fires and peat degradation (Warren et al. 2017; Enrici and Hubacek 2019). These circumstances and processes release vast amounts of CO₂ and other greenhouse gases, which is why Indonesia became one of the main objectives of REDD+ (Edwards et al. 2012; Enrici and Hubacek 2018; Irawan et al. 2019; Enrici and Hubacek 2019). REDD+ involves industrialized countries in the protection of tropical forests in order to compensate for the excess of their greenhouse gas emissions quota (Enrici and Hubacek 2018; Enrici and Hubacek 2019). In addition to the Indonesian government's commitment to REDD+ and the establishment of REDD+ projects, the government is trying to improve the country's sustainability with projects such as the “Peat Prize” competition and a moratorium on the issuing of new concession licenses (Atwood 2018; Enrici and Hubacek 2019). The quantification and monitoring of carbon stocks is a central task for REDD+ projects. In order to estimate greenhouse gas emissions accurately, information on the extent of forest and peatland loss and damage, is indispensable.

This thesis demonstrates the capability of active remote sensing systems (radar and LiDAR) to serve as a tool for estimating above- and below-ground biomass and emissions by burning and deforestation in tropical forest ecosystems.

In the first study of this thesis (Chapter I), Sentinel-1 C-band and ALOS PALSAR L-band backscatter signals, ratios and textures were used to robustly estimate accurate and high-resolution AGB maps of Kalimantan for three years using a multivariate linear regression model. High-accurate AGB derived from the extrapolation of field- to airborne LiDAR- data functioned as a reliable reference for calibrating and validating the SAR data. The SAR backscatter approach was already well tested for radar-based forest cover and biomass mapping (Joshi et al. 2015; Yu and Saatchi 2016; Cartus and Santoro 2019). This approach is computationally less intensive than other approaches and transferable to different ecosystems. Nevertheless the method is limited by some factors, such as backscatter saturation and backscatter variations due to terrain and wetness (Koch 2010; Cartus and Santoro 2019). The results of the analysis showed a correlation (R^2) between the reference biomass and the estimated biomass between 0.69 (2016) to 0.77 (2007). The Nash-Sutcliffe efficiency for model performance ranged between 0.70 (2016) to 0.76 (2007). However, all maps show underestimations at higher AGB levels and an overestimation in lower ranges compared to reference AGB. Similar results are shown in other regional studies estimating biomass from SAR backscatter values (Joshi et al. 2015; Hamdan 2015; Antropov et al. 2017; Urbazaev et al. 2018). One of the main limitations of the backscatter approach is that SAR-based AGB estimations suffer from saturation of the backscatter signal in the higher biomass range. The saturation level varies depending on the sensor wavelength and polarization, as well as the forest structure (Joshi et al. 2017). AGB studies in tropical forests were mostly conducted based on L-band SAR data, being the most suitable operational data for biomass estimation (Wijaya 2009; Wijaya et al. 2015; Avitabile et al. 2016; Urbazaev et al. 2018). The saturation level in tropical forests, using L-band, ranges about 50 t/ha to 200 t/ha (Hamdan et al. 2011; Englhart et al. 2011; Hamdan et al. 2015; Urbazaev et al. 2018). Comparable to Thapa et al. (2015), the saturation level could be increased to approximately 200 – 250 t/ha using backscatter values and, additionally, backscatter ratios and textures. Besides the saturation effect, another limiting factor of the backscatter approach are the moisture conditions of soil and vegetation (Thoma et al. 2006; Lu et al. 2015). Especially for tropical forests, located in

areas with a high amount of annual precipitation, the estimation of biomass based on backscatter can introduce errors. Humidity effects in the Sentinel-1 imageries were reduced using the average of scenes acquired during different periods of the year. The use of the annual mosaic of ALOS PALSAR is furthermore compensating for humidity within the L-band. Analogous to literature, variables based on cross-polarized backscatter were found as less influenced by changes in moisture and topography conditions and more sensitive to biomass than co-polarized data (Mitchard et al. 2009; Saatchi et al. 2011; Hamdan 2015).

In addition to the biomass estimation, for a period of ten years, a change analysis was carried out, identifying areas of forest and thus biomass loss and gain. Modeling the years with a consistent method allows a more accurate estimation of the change than relying on available biomass maps derived from different models. With the limitations in mind these methods can be used for more improved carbon modeling, as well as forest monitoring or risk managing systems under REDD+.

The second study (Chapter II) investigates the amount and spatial distribution of forest AGB using a range of regionally developed methods based on Earth Observation data for Poland, Sweden and regions in Indonesia (Kalimantan), Mexico (Central Mexico and Yucatan peninsula), and South Africa (Eastern provinces) for the year 2010. The AGB map of Kalimantan from the first study was used in this comparison of different biomes. Applying an accuracy assessment for all regional maps using independent field data or LiDAR AGB maps resulted in an overall RMSE ranging from 10 t/ha to 55 t/ha (37 % to 67 % relative RMSE), and an overall bias ranging from -1 t/ha to +5 t/ha at pixel level. All regional estimates showcased in an overestimation (up to 63 t/ha) in the lower AGB ranges, and an underestimation (up to 85 t/ha) in higher AGB ranges. The outcomes of this study can be used as a support when developing algorithms to estimate AGB at continental to global scale level. Chapter I and II fulfil the Task A1 of the objectives of the thesis (The robust mapping of high-resolution AGB for extensive areas including reduced uncertainties). Both studies were carried out as part of the DUE Globbiomass, a comprehensive international project funded from the European Space Agency (ESA) in order to improve existing biomass estimations with reduced uncertainties for different forest ecosystems.

The third study (Chapter III) analyzed the possibility to overcome the limitations of AGB estimations due to the saturation effect (Task A2). Canopy heights of the tropical forest were derived from TerraSAR-X and Radarsat-2 X- and C-band Pol-InSAR data for 2015 in a subset of Kalimantan. Consequently, based on the canopy height, AGB in a 3 m and 12 m spatial resolution was modelled. Algorithms utilizing the RVoG and the RMoG interferometric model were tested to obtain a more accurate and robust forest parameter estimation during dry weather conditions. The novel RMoG model-based height inversion algorithm resulted in more accurate canopy height estimations than the RVoG model. The RVoG model does not take the temporal baseline resulting from repeat-pass Pol-InSAR into consideration and is influenced by decorrelation effects due to dynamic changes (wind, precipitations, seasonal variations and anthropogenic activities). Using Radarsat-2 imagery, the independent validation displayed an R^2 of 0.63, while the modelled canopy heights from TS-X data achieved an R^2 of up to 0.66, which is comparable to other studies within the tropical forests, but based on other models (Schlund et al. 2014; Khati et al. 2017; Ghasemi et al. 2018; Schlund et al. 2019). It was shown, that not all RS-2 and TS-X data were suitable for modeling canopy height from coherence. The parameters that most affect the accuracy of the canopy height model were identified as the baselines (temporal and perpendicular), the HoA, the incident angle and moist weather conditions since they introduce a stronger decorrelation and thus a low coherence. Furthermore, the wavelength affects the results. The general underestimation of TS-X data results from the weak penetration depth, limited by the short wavelength of X-band. Besides, the penetration depth is dependent from the density of the forest. Since forests in Central Kalimantan are very dense and reach a height of up to 30 m, canopy height estimation based on short wavelengths is limited. Alongside the density and height of the forest, the dielectric properties of the canopy influence the penetration depth, why images acquired in the wet season are not suitable for canopy height estimation (Schlund et al. 2019). For AGB modeling based on canopy height, most studies use a power function regression. The use of linear regression in this context has been confirmed in few studies (Köhler and Huth 2010; Odipo et al. 2016). Testing both regression models with our data resulted in significant p-values for both regressions but higher R^2 and lower RMSE using a linear regression, why this model was implemented for AGB estimations. The derived AGB showed good correlations compared to reference canopy height ($R^2 = 0.83$ for RS-2, $R^2 = 0.84$ for TS-X). Similar to the results, all of the pan-tropical and

Indonesian maps underestimate higher AGB ranges and overestimate lower AGB values (Saatchi et al. 2011; Avitabile et al. 2016). The present study showed that X- and C-band Pol-InSAR data could be used together with field inventories and high-resolution data such as drone or LiDAR data to support carbon accounting.

To answer Task B Chapter IV investigated the identification of carbon-rich peatlands in Central Kalimantan using the novel LiDAR satellite ICESat-2. ICESat-2 terrain height transects were compared with a highly-precise but cost-intensive airborne LiDAR digital terrain model (DTM) and the radar-based WorldDEM DTM by Airbus. The results show a strong correlation when compared to the DTM ($R^2 = 0.89$, $RMSE = \pm 0.83$ m) and the WorldDEM DTM ($R^2 = 0.94$, $RMSE = \pm 0.86$ m). However, terrain height is overestimated by ICESat-2 in few areas. A more detailed investigation showed that this incidence proved accurate especially within densely forested areas. Neuenschwander and Pitts (2019b) found a decreasing accuracy for ground detection as canopy cover increases. This is expected since LiDAR is sensitive to vegetation. Especially in dense tropical forests with a complex forest structure and dense underwood, too few photons are reflected from the ground (Neuenschwander and Magruder 2016). Neuenschwander and Pitts (2019a) found that ICESat-2/ATLAS can lose its ground signal for canopy closure of higher than 95 % but also when strong cloud cover obscures the terrestrial signal. In the tropical forest of Indonesia, both restrictions are probable. Because of the positive correlation analyses, an interpolation (kriging) of comprehensive DTMs based on ICESat-2 transects was implemented to model the surface topography of three peat domes within the study area. The comparison of the interpolated terrain heights of the peatland area showed an R^2 of 0.78, 0.84, and 0.94 compared to WorldDEM DTM. The RMSE ranged from 0.68 m to 2.68 (relative RMSE 14.3 % and 22.5 %). However, cuts by rivers or channels within the peatlands can only be mapped to a limited extent because of the limited availability of measuring points available for the modeling. In addition, inaccuracies can be introduced by different spatial resolutions, acquisition geometries, sensor accuracies, and the different acquisition times. The methodology represents a cost-effective and robust alternative to derive the topography of peatlands. Knowing the surface topography of typically curved peat domes allows conclusions to be drawn about the volume of the peat dome and the associated estimation of the stored carbon and is thus a contribution to carbon-related projects.

In summary, the studies showed the capability of remote sensing instruments and novel methodologies in order to improve current estimations of above-ground biomass and below-ground carbon stocks in tropical forest ecosystems. The results demonstrate that more robust AGB estimations, with a reduced uncertainty and in a higher spatial resolution can be achieved and consequently contribute to REDD+ monitoring projects and others.

2. Benefits and constraints

The stand-alone publications in the frame of this thesis showed benefits and constraints for using active remote sensing data for biomass estimations in the tropical forests of Indonesia.

The extrapolation from field measurements to LiDAR data results in a highly accurate biomass estimation covering almost all biomass value ranges but is very time- (field data) and cost- (airborne LiDAR data) intensive. Nevertheless, this dataset serves as a strong basis for the calibration and validation of large-scale SAR data. The extrapolation from this highly-accurate AGB reference dataset to SAR data allows a more accurate AGB estimation for large areas in South-East Asia. In addition to the L-band SAR systems ALOS PALSAR and ALOS PALSAR-2, the ability of the relatively new C-band SAR satellite Sentinel-1 was regarded to estimate AGB. Unfortunately, due to the short wavelength, the C-band SAR could only contribute minimally to the results. The use of textures combined with backscatter and polarization ratios enables to shift the saturation effect in tropical rainforests to a higher level. Nevertheless, the saturation effect is a limitation of SAR data for AGB estimations.

The final biomass products of Chapter I have a resolution of 100 m, which is much more detailed than other existing maps of this region (>500 m) why they are more sensitive for small-scaled biomass variability and changes.

The comparison of different forest biomes in Chapter II is the widest inter-comparison of regional-to-national AGB maps in terms of area, forest types, input datasets, and retrieval methods to date. The outcomes of this chapter should be considered when developing novel algorithms for estimating forest biomass at continental or even global scale level.

In order to overcome the constraints of the saturation effect, a study based on more complex Pol-InSAR data were carried out. In the course of analyzing the performance of X- and C-band dual-pol and quad-pol data as inputs for the RVoG and RMoG interferometric coherence models, the RMoG demonstrated good potential for estimating AGB in tropical forests. Limitations of this approach could be found in the temporal decorrelation, but also the perpendicular baseline, the height of ambiguity, the incident angle and moist weather conditions, as well as the wavelength and the forest structure itself. The analysis may be used as a guideline for further analyses on this topic since it extensively discusses the constraints for coherence-based AGB estimations in tropical forests.

The last study developed a scientifically novel approach to identify and derive the surface area of carbon rich ombrogenous peat domes in Indonesia with a new LiDAR satellite (ICESat-2). Furthermore, a secondary result of the analysis is that the sensor, in combination with older remote sensing data, can identify burned areas. Very dense vegetation with a canopy closure of above 95 % was recognized as a limitation to derive accurate terrain height information from ICESat-2 data. The approach still needs to be tested for transferability to other tropical regions (e.g. Congo or Brazil). It is assumed that mountainous areas might produce limitations. However, for peatlands in flat terrain, the transferability of the approach to other regions and countries seems feasible.

In conclusion, improved methods for AGB estimations in tropical forest ecosystems were presented in this thesis. This is a crucial matter in order to obtain more accurate biomass estimated with a better spatial resolution as a basis for carbon content analyses.

3. Future research

Within this thesis, it was demonstrated that remote sensing systems can be used as an efficient tool for estimating and monitoring global carbon pools in tropical forest ecosystems.

For an adequate derivation of AGB from remote sensing data the correct choice of the allometric equation for the calculation of AGB from field data is necessary. Although there are several allometric equations for species-rich tropical forests, there is still no allometric equation for tropical peat swamp forests. Since tropical forests are

characterized by very high biodiversity, general allometric models for tropical forests do not necessarily provide a suitable representation of the actual biomass contribution. Besides, the quality, frequency and spatial resolution of remote sensing data can cause limitations for AGB estimations based on Earth Observation data. New and improved technologies and satellites, such as the LiDAR satellite GEDI (NASA), Tandem-L (DLR) or the BIOMASS mission (ESA) with a higher spatial resolution and more suitable wavelengths, will provide opportunities for even more accurate AGB estimations in the future.

In addition to new satellites, growing data availability from existing satellites enables extensive time series to understand the global carbon cycle more accurately. With the increasing amount of ICESat-2 data over the next years, but also with the new satellite GEDI, it may become possible to investigate the annual accumulation rate, the subsidence of peatlands, or the identification of peat domes threatened by drainage.

Other tropical countries, besides Indonesia, may have also extensive peatland areas not yet known. The methods for estimating the topography of peatlands presented in this study will be tested for the Republic of Congo or Amazonia.

REFERENCES

Aghabalaei, A.; Ebadi, H.; Maghsoudi, Y. (2020): Forest height estimation based on the RVoG inversion model and the PolInSAR decomposition technique. In *International Journal of Remote Sensing* 41 (7), pp. 2684–2703. DOI: 10.1080/01431161.2019.1694726.

Agrawal, N.; Kumar, S.; Tolpekin, V. A. (2019): POLINSAR based scattering information retrieval for forest aboveground biomass estimation. In *Int. Arch. Photogramm. Remote Sens. Spatial Inf. Sci.* XLII-2/W13, pp. 1913–1920. DOI: 10.5194/isprs-archives-XLII-2-W13-1913-2019.

Agus, F.; Gunarso, P.; Saharjo, B. H.; Harris, N.; van Noordwijk, M.; Killeen, T. J. (2013): Historical CO₂ emissions from land use and land use change from the oil palm industry in Indonesia, Malaysia and Papua New Guinea. Edited by Roundtable on Sustainable Palm Oil. Reports from the Technical Panels of the 2nd Greenhouse Gas. Jakarta.

Agus, F.; Hairiah, K.; Mulyani, A. (2011): Measuring carbon stock in peat soils. Practical guidelines. Bogor Jawa Barat Indonesia: World Agroforestry Centre (ICRAF); Southeast Asia Regional Program, Indonesian Centre for Agricultural Land Resources Research and Development.

Anshari, G.; Kershaw, A. P.; van der Kaars, S.; Jacobsen, G. (2004): Environmental change and peatland forest dynamics in the Lake Sentarum area, West Kalimantan, Indonesia. In *J. Quaternary Sci.* 19 (7), pp. 637–655. DOI: 10.1002/jqs.879.

Antropov, O.; Rauste, Y.; Häme, T.; Praks, J. (2017): Polarimetric ALOS PALSAR time series in mapping biomass of boreal forests. In *Remote Sensing* 9 (12), p. 999. DOI: 10.3390/rs9100999.

Askne, J. I. H.; Soja, M. J.; Ulander, L. M. H. (2017): Biomass estimation in a boreal forest from TanDEM-X data, lidar DTM, and the interferometric water cloud model. In *Remote Sensing of Environment* 196, pp. 265–278. DOI: 10.1016/j.rse.2017.05.010.

Asner, G. P. (2010): Cloud cover in Landsat observations of the Brazilian Amazon. In *International Journal of Remote Sensing* 22 (18), pp. 3855–3862. DOI: 10.1080/01431160010006926.

REFERENCES

- Asner, G. P.; Brodrick, P. G.; Philipson, C.; Vaughn, N. R.; Martin, R. E.; Knapp, D. E. et al. (2018): Mapped aboveground carbon stocks to advance forest conservation and recovery in Malaysian Borneo. In *Biological Conservation* 217, pp. 289–310. DOI: 10.1016/j.biocon.2017.10.020.
- Asner, G. P.; Clark, J. K.; Mascaro, J.; Galindo García, G. A.; Chadwick, K. D.; Navarrete Encinales, D. A. et al. (2012a): High-resolution mapping of forest carbon stocks in the Colombian Amazon. In *Biogeosciences* 9 (7), pp. 2683–2696. DOI: 10.5194/bg-9-2683-2012.
- Asner, G. P.; Mascaro, J.; Muller-Landau, H. C.; Vieilledent, G.; Vaudry, R.; Rasamoelina, M. et al. (2012b): A universal airborne LiDAR approach for tropical forest carbon mapping. In *Oecologia* 168 (4), pp. 1147–1160. DOI: 10.1007/s00442-011-2165-z.
- Asner, G. P.; Powell, G. V. N.; Mascaro, J.; Knapp, D. E.; Clark, J. K.; Jacobson, J. et al. (2010): High-resolution forest carbon stocks and emissions in the Amazon. In *Proceedings of the National Academy of Sciences of the United States of America* 107 (38), pp. 16738–16742. DOI: 10.1073/pnas.1004875107.
- Attema, E. P. W.; Ulaby, F. T. (1978): Vegetation modeled as a water cloud. In *Radio Sci.* 13 (2), pp. 357–364. DOI: 10.1029/rs013i002p00357.
- Atwood, E. C. (2018): Remote sensing data as a tool to monitor and mitigate natural catastrophes resulting from anthropogenic activities: Case studies over land and water. Dissertation. Ludwig-Maximilian University, Munich. Biology.
- Avitabile, V.; Baccini, A.; Friedl, M. A.; Schmullius, C. (2012): Capabilities and limitations of Landsat and land cover data for aboveground woody biomass estimation of Uganda. In *Remote Sensing of Environment* 117, pp. 366–380. DOI: 10.1016/j.rse.2011.10.012.
- Avitabile, V.; Herold, M.; Heuvelink, G. B. M.; Lewis, S. L.; Phillips, O. L.; Asner, G. P. et al. (2016): An integrated pan-tropical biomass map using multiple reference datasets. In *Global Change Biology* 22 (4), pp. 1406–1420. DOI: 10.1111/gcb.13139.

REFERENCES

- Babu, A.; Kumar, S. (2018): Tree canopy height estimation using multi-baseline RVoG inversion technique. In *Int. Arch. Photogramm. Remote Sens. Spatial Inf. Sci.* XLII-5, pp. 605–611. DOI: 10.5194/isprs-archives-XLII-5-605-2018.
- Baccini, A.; Goetz, S. J.; Walker, W. S.; Laporte, N. T.; Sun, M.; Sulla-Menashe, D. et al. (2012): Estimated carbon dioxide emissions from tropical deforestation improved by carbon-density maps. In *Nature Climate change* 2 (3), pp. 182–185. DOI: 10.1038/nclimate1354.
- Baccini, A.; Laporte, N.; Goetz, S. J.; Sun, M.; Dong, H. (2008): A first map of tropical Africa's above-ground biomass derived from satellite imagery. In *Environ. Res. Lett.* 3 (4), p. 45011. DOI: 10.1088/1748-9326/3/4/045011.
- Ballhorn, U. (2012): Airborne and spaceborne LiDAR data as a measurement tool for peatland topography, peat fires burn depth, and forest above ground biomass in Central Kalimantan, Indonesia. Dissertation. Ludwig-Maximilian-University, Munich.
- Ballhorn, U.; Jubanski, J.; Siegert, F. (2011): ICESat/GLAS data as a measurement tool for peatland topography and peat swamp forest biomass in Kalimantan, Indonesia. In *Remote Sensing* 3 (12), pp. 1957–1982. DOI: 10.3390/rs3091957.
- Ballhorn, U.; Siegert, F.; Mason, M.; Limin, S. (2009): Derivation of burn scar depths and estimation of carbon emissions with LIDAR in Indonesian peatlands. In *Proceedings of the National Academy of Sciences of the United States of America* 106 (50), pp. 21213–21218. DOI: 10.1073/pnas.0906457106.
- Baltzer, H.; Rowland, C.; Saich, P. (2007): Forest canopy height and carbon estimation at Monks Wood National Nature Reserve, UK, using dual-wavelength SAR interferometry. In *Remote Sensing of Environment* 108 (3), pp. 224–239. DOI: 10.1016/j.rse.2006.11.014.
- Barton, J. M. H.; Buchberger, S. G.; Lange, M. L. (1999): Estimation of error and compliance in surveys by kriging. In *Journal of Surveying Engineering* (125), pp. 87–108.
- Basuki, T. M.; Skidmore, A. K.; van Laake, P. E.; van Duren, I.; Hussin, Y. A. (2012): The potential of spectral mixture analysis to improve the estimation accuracy of tropical

REFERENCES

- forest biomass. In *Geocarto International* 27 (4), pp. 329–345. DOI: 10.1080/10106049.2011.634928.
- Beaudoin, A.; Le Toan, T.; Goze, S.; Nezry, E.; Lopes, A.; Mougin, E. et al. (1994): Retrieval of forest biomass from SAR data. In *International Journal of Remote Sensing* 15 (14), pp. 2777–2796. DOI: 10.1080/01431169408954284.
- Borengasser, M.; Hungate, W. S.; Watkins, R. (2008): *Hyperspectral Remote Sensing. Principles and Applications*. Boca Raton: CRC Press, Taylor and Francis Group.
- Bourdeau, J.; Nelson, R. F.; Margolis, H. A.; Beaudion, A.; Guidon, L.; Kimes, D. (2008): Regional aboveground forest biomass using airborne and spaceborne LiDAR in Québec. In *Remote Sensing of Environment* 112 (10), pp. 3876–3890. DOI: 10.1016/j.rse.2008.06.003.
- Campbell, J. B.; Wynne, R. H. (2011): *Introduction to Remote Sensing*. 5th. New York: The Guilford Press.
- Carabajal, C. C.; Harding, D. (2006): SRTM C-band and ICESat laser altimetry elevation comparisons as a function of tree cover and relief. In *Photogrammetric Engineering & Remote Sensing* 72 (3), pp. 287–298.
- Carlson, K. M.; Goodman, L. K.; Calen C. M. T. (2015): Modeling relationships between water table depth and peat soil carbon loss in Southeast Asian plantations. In *Environ. Res. Lett.* 10 (7), p. 74006. DOI: 10.1088/1748-9326/10/7/074006.
- Cartus, O.; Santoro, M. (2019): Exploring combinations of multi-temporal and multi-frequency radar backscatter observations to estimate above-ground biomass of tropical forest. In *Remote Sensing of Environment* 232, p. 111313. DOI: 10.1016/j.rse.2019.111313.
- Chaparro, D.; Duveiller, G.; Piles, M.; Cescatti, A.; Vall-llossera, M.; Camps, A.; Entekhabi, D. (2019): Sensitivity of L-band vegetation optical depth to carbon stocks in tropical forests. A comparison to higher frequencies and optical indices. In *Remote Sensing of Environment* 232, p. 111303. DOI: 10.1016/j.rse.2019.111303.
- Chave, J.; Andalo, C.; Brown, S.; Cairns, M. A.; Chambers, J. Q.; Eamus, D. et al. (2005): Tree allometry and improved estimation of carbon stocks and balance in tropical forests. In *Oecologia* 145 (1), pp. 87–99. DOI: 10.1007/s00442-005-0100-x.

REFERENCES

- Chave, J.; Condit, R.; Lao, S.; Caspersen, J. P.; Foster, R. B.; Hubbel, S. P. (2003): Spatial and temporal variation of biomass in a tropical forest: results from a large census plot in Panama. In *Journal of Ecology* (91), pp. 240–252, checked on 12/4/2017.
- Chave, J.; Réjou-Méchain, M.; Búrquez, A.; Chidumayo, E.; Colgan, M. S.; Delitti, W. B. C. et al. (2014): Improved allometric models to estimate the aboveground biomass of tropical trees. In *Global Change Biology* 20 (10), pp. 3177–3190. DOI: 10.1111/gcb.12629.
- Chemura, A.; Mutanga, O.; Dube, T. (2017): Remote sensing leaf water stress in coffee (*Coffea arabica*) using secondary effects of water absorption and random forests. In *Physics and Chemistry of the Earth, Parts A/B/C* 100, pp. 317–324. DOI: 10.1016/j.pce.2017.02.011.
- Chen, H.; Cloude, S. R.; Goodenough, D. G. (2016): Forest canopy height estimation using Tandem-X coherence data. In *IEEE J. Sel. Top. Appl. Earth Observations Remote Sensing* 9 (7), pp. 3177–3188. DOI: 10.1109/JSTARS.2016.2582722.
- Chi, H.; Sun, G.; Huang, J.; Li, R.; Ren, X.; Ni, W.; Fu, A. (2017): Estimation of forest aboveground biomass in Changbai mountain region using ICESat/GLAS and Landsat/TM data. In *Remote Sensing* 9 (7), p. 707. DOI: 10.3390/rs9070707.
- Cloude, S. R. (2010): *Polarisation - Applications in remote sensing*. New York: Oxford University Press.
- Cloude, S. R.; Papathanassiou, K. P. (2003): Three-stage inversion process for polarimetric SAR interferometry. In *IEE Proc., Radar Sonar Navig.* 150 (3), p. 125. DOI: 10.1049/ip-rsn:20030449.
- Cloude, S. R.; Papathanassiou, K. P. (2008): Forest vertical structure estimating using coherence tomography. IGARSS 2008; 7 - 11 July 2008, John B. Hynes Veterans Memorial Convention Center, Boston, Massachusetts, U.S.A. ; proceedings. Piscataway, NJ: IEEE. Available online at <http://ieeexplore.ieee.org/servlet/opac?punumber=4757194>.
- Curran, P. J.; Dungan, J. L.; Macler, B. A.; Plummer, S. E. (1991): The effect of a red leaf pigment on relationship between red edge and chlorophyll concentration. In *Remote Sensing of Environment* 1 (35), pp. 69–75. DOI: 10.1016/0034-4257(91)90066-F.

REFERENCES

- Dong, L.; Tang, S.; Min, M.; Veroustraete, F. (2019): Estimation of forest canopy height in hilly areas using lidar waveform data. In *IEEE J. Sel. Top. Appl. Earth Observations Remote Sensing* 12 (5), pp. 1559–1571. DOI: 10.1109/JSTARS.2019.2908682.
- Drake, J. B.; Knox, R. G.; Dubayah, R. O.; Clark, D. B.; Condit, R.; Blair, B.; Hofton, M. (2003): Above-ground biomass estimation in closed canopy Neotropical forests using lidar remote sensing: factors affecting the generality of relationships. In *Global Ecology & Biogeography* (12), pp. 147–159.
- Edwards, D. P.; Koh, L. P.; Laurance, W. F. (2012): Indonesia’s REDD+ pact. Saving imperilled forests or business as usual? In *Biological Conservation* 151 (1), pp. 41–44. DOI: 10.1016/j.biocon.2011.10.028.
- Ellis, P.; Griscom, B.; Walker, W.; Gonçalves, F.; Cormier, T. (2016): Mapping selective logging impacts in Borneo with GPS and airborne lidar. In *Forest Ecology and Management* 365, pp. 184–196. DOI: 10.1016/j.foreco.2016.01.020.
- Englhart, S. (2012): Monitoring restoration and aboveground biomass in tropical peat swamp forests on Borneo using multi-sensoral remote sensing data. Dissertation. Ludwig-Maximilian University, Munich. Biology.
- Englhart, S.; Jubanski, J.; Siegert, F. (2013): Quantifying dynamics in tropical peat swamp forest biomass with multi-temporal LiDAR datasets. In *Remote Sensing* 5 (5), pp. 2368–2388. DOI: 10.3390/rs5052368.
- Englhart, S.; Keuck, V.; Siegert, F. (2011): Aboveground biomass retrieval in tropical forests - The potential of combined X- and L-band SAR data use. In *Remote Sensing of Environment* 115 (5), pp. 1260–1271. DOI: 10.1016/j.rse.2011.01.008.
- Englhart, S.; Keuck, V.; Siegert, F. (2012): Modeling aboveground biomass in tropical forests using multi-frequency SAR data - A comparison of methods. In *IEEE J. Sel. Top. Appl. Earth Observations Remote Sensing* 5 (1), pp. 298–306. DOI: 10.1109/JSTARS.2011.2176720.
- Enrici, A.; Hubacek, K. (2019): A crisis of confidence. Stakeholder experiences of REDD+ in Indonesia. In *Human Ecology* 47 (1), pp. 39–50. DOI: 10.1007/s10745-019-0045-z.

REFERENCES

- Enrici, A. M.; Hubacek, K. (2018): Challenges for REDD+ in Indonesia. A case study of three project sites. In *E&S* 23 (2). DOI: 10.5751/ES-09805-230207.
- ESA / AOES Medialab (2012): The electromagnetic spectrum. A scheme of the electromagnetic spectrum with indication of wavelengths, frequencies and energies. Edited by European Space Agency. Available online at <https://sci.esa.int/web/education/-/50368-the-electromagnetic-spectrum>, updated on 2019, checked on 3/23/2020.
- Eumetrain (2017): Physical background. Distinguishing cloud-free areas with different green vegetation fractions. Typical reflectivity functions of green vegetation and bare soil (green and brown curves) in the shortwave spectral region, checked on 4/20/2020.
- European Space Agency (2020): Radar course 3. Electromagnetic spectrum. Edited by ESA / AOES Medialab, checked on 4/15/2020.
- Evans, C. D.; Williamson, J. M.; Kacaribu, F.; Irawan, D.; Suardiwerianto, Y.; Hidayat, M. Fikky et al. (2019): Rates and spatial variability of peat subsidence in Acacia plantation and forest landscapes in Sumatra, Indonesia. In *Geoderma* 338, pp. 410–421. DOI: 10.1016/j.geoderma.2018.12.028.
- FAO (2009): State of the world's forests. Food and Agriculture Organization. Rome.
- FAO (2013): Statistical yearbook of the Food and Agricultural Organization for the United Nations 2013. World food and agriculture. Food and Agriculture Organization. Rome.
- Ferraz, A.; Saatchi, S.; Xu, L.; Hagen, S.; Chave, J.; Yu, Y. et al. (2018): Carbon storage potential in degraded forests of Kalimantan, Indonesia. In *Environ. Res. Lett.* 13 (9), p. 95001. DOI: 10.1088/1748-9326/aad782.
- Ferreira, I. O.; Rodrigues, D. D.; Santos, G. R. dos; Ferraz Rosa, L. M. (2017): In bathymetric surfaces: IDW or kriging? In *Bol. Ciênc. Geod.* 23 (3), pp. 493–508. DOI: 10.1590/s1982-21702017000300033.
- Foody, G. M.; Boyd, D. S.; Cutler, M. E. J. (2003): Predictive relations of tropical forest biomass from Landsat TM data and their transferability between regions. In *Remote Sensing of Environment* 85 (4), pp. 463–474. DOI: 10.1016/S0034-4257(03)00039-7.

REFERENCES

- Foody, G. M.; Green, R. M.; Lucas, R. M.; Curran, P. J.; Honzak, M.; Do Amaral, I. (1997): Observations on the relationship between SIR-C radar backscatter and the biomass of regenerating tropical forests. In *International Journal of Remote Sensing* 18 (3), pp. 687–694. DOI: 10.1080/014311697219024.
- Fransson, J. E. S.; Smith, G.; Askne, J.; Olsson, H. (2010): Stem volume estimation in boreal forests using ERS-1/2 coherence and SPOT XS optical data. In *International Journal of Remote Sensing* 22 (14), pp. 2777–2791. DOI: 10.1080/01431160010006872.
- Frazer, G. W.; Magnussen, S.; Wulder, M. A.; Niemann, K. O. (2011): Simulated impact of sample plot size and co-registration error on the accuracy and uncertainty of LiDAR-derived estimates of forest stand biomass. In *Remote Sensing of Environment* 115 (2), pp. 636–649. DOI: 10.1016/j.rse.2010.10.008.
- Friedlingstein, P.; Jones, M. W.; Oaapos; Sullivan, M.; Andrew, R. M.; Hauck, J. et al. (2019): Global carbon budget 2019. In *Earth Syst. Sci. Data* 11 (4), pp. 1783–1838. DOI: 10.5194/essd-11-1783-2019.
- Garestier, F.; Dubois-Fernandez, P. C.; Papathanassiou, K. P. (2008): Pine forest height inversion using single-pass X-band PolInSAR data. In *IEEE Trans. Geosci. Remote Sensing* 46 (1), pp. 59–68. DOI: 10.1109/TGRS.2007.907602.
- Ghasemi, N.; Sahebi, M. R.; Mohammadzadeh, A. (2011): A review on biomass estimation methods using synthetic aperture radar data. In *International Journal of Geomatics and Geosciences* 1 (4), pp. 776–788.
- Ghasemi, N.; Tolpekin, V.; Stein, A. (2018): Assessment of forest above-ground biomass estimation from PolInSAR in the presence of temporal decorrelation. In *Remote Sensing* 10 (6), p. 815. DOI: 10.3390/rs10060815.
- Gitelson, A. A.; Merzlyak, M. N.; Lichtenthaler, H. K. (1996): Detection of red edge position and chlorophyll content by reflectance measurements near 700 nm. In *Journal of Plant Physiology* 148 (3-4), pp. 501–508. DOI: 10.1016/S0176-1617(96)80285-9.
- Goetz, S.; Baccini, A.; Laporte, N. T.; Johns, T.; Walker, W.; Kellndorfer, J. et al. (2009): Mapping and monitoring carbon stocks with satellite observations. A

REFERENCES

- comparison of methods. In *Carbon balance and management* 4, p. 2. DOI: 10.1186/1750-0680-4-2.
- Goetz, S.; Dubayah, R. (2011): Advances in remote sensing technology and implications for measuring and monitoring forest carbon stocks and change. In *Carbon Management* 2 (3), pp. 231–244. DOI: 10.4155/cmt.11.18.
- Hamdan, O. (2015): Assessment of Alos Palsar L-band SAR for estimation of above ground biomass in tropical forests. Dissertation. Univeriti Putra Malaysia, Serdang. Forestry, checked on 12/19/2017.
- Hamdan, O.; Khali Aziz, H.; Mohd Hasmadi, I. (2014): L-band ALOS PALSAR for biomass estimation of Matang Mangroves, Malaysia. In *Remote Sensing of Environment* 155, pp. 69–78. DOI: 10.1016/j.rse.2014.04.029.
- Hamdan, O.; Khali Aziz, H.; Rahman A. (2011): Remotely sensed L-band SAR data for tropical forest biomass estimation. In *Journal of Tropical Forest Science* 23 (3), pp. 318–327, checked on 12/19/2017.
- Hamdan, O.; Mohd Hasmadi, I.; Khali Aziz, H.; Norizah, K.; Helmi Zulhaidi, M. S. (2015): L-Band saturation level for above-ground biomass of Dipterocarp forests in peninsular Malaysia. In *Journal of Tropical Forest Science* 27 (3), pp. 388–399, checked on 1/8/2018.
- Harding, D. J.; Carabajal, C. C. (2005): ICESat waveform measurements of within-footprint topographic relief and vegetation vertical structure. In *Geophys. Res. Lett.* 32 (21), p. 2509. DOI: 10.1029/2005GL023471.
- Harrison, M. E.; Capliia, B. R.; Thorton, S. A.; Cattau, M. E.; Page, S. E. (2016): Impacts of the 2015 fire season on peat-swamp forest biodiversity in Indonesian Borneo. In *15th International Peat Congress 2016*, pp. 713–717.
- Harrison, M. E.; Ottay, J. B.; D’Arcy, L. J.; Cheyne, S. M.; Anggodo; Belcher, C. et al. (2020): Tropical forest and peatland conservation in Indonesia. Challenges and directions. In *People and Nature* 2 (1), pp. 4–28. DOI: 10.1002/pan3.10060.
- Horler, D. N. H.; Dockray, M.; Barber, J. (1983): The red edge of plant leaf reflectance. In *International Journal of Remote Sensing* 4 (2), pp. 273–288. DOI: 10.1080/01431168308948546.

REFERENCES

- Hosseini, S.; Ebadi, H.; Maghsoudi, Y.; Garestier, F. (2019): Pol-InSAR for forest biomass estimation with the transformation of the polarization basis. In *J Indian Soc Remote Sens* 47 (7), pp. 1097–1109. DOI: 10.1007/s12524-019-00972-0.
- Huang, J.; Chen, D.; Cosh, M. H. (2009): Sub-pixel reflectance unmixing in estimating vegetation water content and dry biomass of corn and soybeans cropland using normalized difference water index (NDWI) from satellites. In *International Journal of Remote Sensing* 30 (8), pp. 2075–2104. DOI: 10.1080/01431160802549245.
- Huijnen, V.; Wooster, M. J.; Kaiser, J. W.; Gaveau, D. L. A.; Flemming, J.; Parrington, M. et al. (2016): Fire carbon emissions over maritime southeast Asia in 2015 largest since 1997. In *Scientific reports* 6, p. 26886. DOI: 10.1038/srep26886.
- Hulme, P. E. (2005): Adapting to climate change: Is there scope for ecological management in the face of a global threat? In *Journal of Applied Ecology* (42), pp. 784–794.
- Ioki, K.; Tsuyuki, S.; Hirata, Y.; Phua, M.-H.; Wong, W. Vun C.; Ling, Z.-Y. et al. (2014): Estimating above-ground biomass of tropical rainforest of different degradation levels in Northern Borneo using airborne LiDAR. In *Forest Ecology and Management* 328, pp. 335–341. DOI: 10.1016/j.foreco.2014.06.003.
- IPCC (2015): Climate change 2014. Synthesis report. Contribution of Working Groups I, II and III to the Fifth Assessment Report of the Intergovernmental Panel on Climate Change [Core Writing Team, R.K. Pachauri and L.A. Meyer (eds.)]. With assistance of R. K. Pachauri, L. Mayer. Geneva, Switzerland: Intergovernmental Panel on Climate Change.
- Irawan, S.; Widiastomo, T.; Tacconi, L.; Watts, J. D.; Steni, B. (2019): Exploring the design of jurisdictional REDD+. The case of Central Kalimantan, Indonesia. In *Forest Policy and Economics* 108, p. 101853. DOI: 10.1016/j.forpol.2018.12.009.
- Jaenicke, J.; Rieley, J. O.; Mott, C.; Kimman, P.; Siegert, F. (2008): Determination of the amount of carbon stored in Indonesian peatlands. In *Geoderma* 147 (3-4), pp. 151–158. DOI: 10.1016/j.geoderma.2008.08.008.

REFERENCES

- Jassim, F. A.; Altaany, F. (2013): Image interpolation using kriging technique for spatial data. In *Canadian Journal on Image Processing and Computer Vision* 4 (2), pp. 16–21.
- Joosten, H.; Sirin, A.; Couwenberg, J.; Laine, J.; Smith, P. (2016): The role of peatlands in climate regulation. In Aletta Bonn, Tim Allott, Martin Evans, Hans Joosten, Rob Stoneman (Eds.): *Peatland restoration and ecosystem services*. Cambridge: Cambridge University Press, pp. 63–76.
- Joshi, N.; Mitchard, E. T. A.; Brolly, M.; Schumacher, J.; Fernández-Landa, A.; Johannsen, V. K. et al. (2017): Understanding 'saturation' of radar signals over forests. In *Nature Scientific reports* 7 (1), p. 3505. DOI: 10.1038/s41598-017-03469-3.
- Joshi, N.; Mitchard, E. T. A.; Schumacher, J.; Johannsen, V. K.; Saatchi, S.; Fensholt, R. (2015): L-Band SAR backscatter related to forest cover, height and aboveground biomass at multiple spatial scales across Denmark. In *Remote Sensing* 7 (4), pp. 4442–4472. DOI: 10.3390/rs70404442.
- Jubanski, J.; Ballhorn, U.; Kronseder, K.; Franke, J.; Siegert, F. (2013): Detection of large above-ground biomass variability in lowland forest ecosystems by airborne LiDAR. In *Biogeosciences* 10 (6), pp. 3917–3930. DOI: 10.5194/bg-10-3917-2013.
- Jung, J.; Yun, S.-H.; Kim, D.-J; Lavallo, M. (2018): Damage-mapping algorithm based on coherence model using multitemporal polarimetric–interferometric SAR data. In *IEEE Trans. Geosci. Remote Sensing* 56 (3), pp. 1520–1532. DOI: 10.1109/TGRS.2017.2764748.
- Jurasinski, G.; Ahmad, S.; Anadon-Rosell, A.; Berendt, J.; Beyer, F.; Bill, R. et al. (2020): From understanding to sustainable use of peatlands. The WETSCAPES Approach. In *Soil Syst.* 4 (1), p. 14. DOI: 10.3390/soilsystems4010014.
- Khati, U.; Singh, G.; Ferro-Famil, L. (2017): Analysis of seasonal effects on forest parameter estimation of Indian deciduous forest using TerraSAR-X PolInSAR acquisitions. In *Remote Sensing of Environment* 199, pp. 265–276. DOI: 10.1016/j.rse.2017.07.019.
- King, D. (2005): Climate change: The science and the policy. In *Journal of Applied Ecology* (42), pp. 779–783.

REFERENCES

- Klinge, H.; Rodrigues W. A.; Brunig, E.; Fittkau, E. J. (Eds.) (1975): Biomass and structure in a central Amazonian rain forest. *Tropical Ecological Systems: Trends in Terrestrial and Aquatic Research*. With assistance of F. B. Golley, E. Medina. New York: Springer.
- Koch, B. (2010): Status and future of laser scanning, synthetic aperture radar and hyperspectral remote sensing data for forest biomass assessment. In *ISPRS Journal of Photogrammetry and Remote Sensing* 65 (6), pp. 581–590. DOI: 10.1016/j.isprsjprs.2010.09.001.
- Köhler, P.; Huth, A. (2010): Towards ground-truthing of spaceborne estimates of above-ground life biomass and leaf area index in tropical rain forests. In *Biogeosciences* 7 (8), pp. 2531–2543. DOI: 10.5194/bg-7-2531-2010.
- Konecny, K.; Ballhorn, U.; Navratil, P.; Jubanski, J.; Page, S. E.; Tansey, K. et al. (2016): Variable carbon losses from recurrent fires in drained tropical peatlands. In *Global Change Biology* 22 (4), pp. 1469–1480. DOI: 10.1111/gcb.13186.
- Koyama, C. N.; Watanabe, M.; Hayashi, M.; Ogawa, T.; Shimada, M. (2019): Mapping the spatial-temporal variability of tropical forests by ALOS-2 L-band SAR big data analysis. In *Remote Sensing of Environment* 233, p. 111372. DOI: 10.1016/j.rse.2019.111372.
- Kronstedter, K.; Ballhorn, U.; Böhm, V.; Siegert, F. (2012): Above ground biomass estimation across forest types at different degradation levels in Central Kalimantan using LiDAR data. In *International Journal of Applied Earth Observation and Geoinformation* 18, pp. 37–48. DOI: 10.1016/j.jag.2012.01.010.
- Kumar, Y.; Singh, S.; Chatterjee, R. S. (2017): The spectral modelling of above ground forest biomass in Jhajra forest range of Dehradun forest Division using Microwave Data. In *Journal of Plant Development Sciences* 9 (10), pp. 917–923.
- Kuplich, T. M.; Curran, P. J.; Atkinson, P. M. (2011): Relating SAR image texture to the biomass of regenerating tropical forests. In *International Journal of Remote Sensing* 26 (21), pp. 4829–4854. DOI: 10.1080/01431160500239107.
- Lavalle, M.; Hensley, S. (2015): Extraction of structural and dynamic properties of forests from polarimetric-interferometric SAR data affected by temporal decorrelation.

REFERENCES

- In *IEEE Trans. Geosci. Remote Sensing* 53 (9), pp. 4752–4767. DOI: 10.1109/TGRS.2015.2409066.
- Lavalle, M.; Simard, M.; Hensley, S. (2012): A temporal decorrelation model for polarimetric radar interferometers. In *IEEE Trans. Geosci. Remote Sensing* 50 (7), pp. 2880–2888. DOI: 10.1109/TGRS.2011.2174367.
- Le Toan, T.; Beaudion, A.; Riom, J.; Guyon, D. (1992): Relating forest biomass to SAR data - Geoscience and Remote Sensing, IEEE Transactions on. In *IEEE Trans. Geosci. Remote Sensing* 30 (2), pp. 403–411.
- Lefsky, M.; Cohen, W. B.; Parker, G. G.; Harding, D. J. (2002): Lidar Remote Sensing for ecosystem studies. In *BioScience* 52 (1), pp. 19–30.
- Lefsky, M. A. (2010): A global forest canopy height map from the Moderate Resolution Imaging Spectroradiometer and the Geoscience Laser Altimeter System. In *Geophys. Res. Lett.* 37 (15), n/a-n/a. DOI: 10.1029/2010GL043622.
- Lefsky, M. A.; Harding, D. J.; Keller, M.; Cohen, W. B.; Carabajal, C. C.; Del Bom Espirito-Santo, F. et al. (2005): Estimates of forest canopy height and aboveground biomass using ICESat. In *Geophys. Res. Lett.* 32 (22), n/a-n/a. DOI: 10.1029/2005GL023971.
- Levick, S. R.; Hessenmöller, D.; Schulze, E.-D. (2016): Scaling wood volume estimates from inventory plots to landscapes with airborne LiDAR in temperate deciduous forest. In *Carbon balance and management* 11 (1), p. 7. DOI: 10.1186/s13021-016-0048-7.
- Levin, K.; Lebing, K. (2019): CO₂ emissions climb to an all-time high (again) in 2019: six takeaways from the latest climate data. World Resources Institute. Washington. Available online at <https://www.wri.org/blog/2019/12/co2-emissions-climb-all-time-high-again-2019-6-takeaways-latest-climate-data>.
- Li, C.; Li, M.; Liu, J.; Li, Y.; Dai, Q. (2020): Comparative analysis of seasonal Landsat 8 images for forest aboveground biomass estimation in a subtropical forest. In *Forests* 11 (1), p. 45. DOI: 10.3390/f11010045.
- Li, H.; Mausel, P.; Brondizio, E.; Deardorff, D. (2010): A framework for creating and validating a non-linear spectrum-biomass model to estimate the secondary succession

REFERENCES

- biomass in moist tropical forests. In *ISPRS Journal of Photogrammetry and Remote Sensing* 65 (2), pp. 241–254. DOI: 10.1016/j.isprsjprs.2010.01.002.
- Li, W.; Chen, E.; Li, Z.; Ke, Y.; Zhan, W. (2015): Forest aboveground biomass estimation using polarization coherence tomography and PolSAR segmentation. In *International Journal of Remote Sensing* 36 (2), pp. 530–550. DOI: 10.1080/01431161.2014.999383.
- Liao, Z.; He, B.; Quan, X.; van Dijk, A. I. J. M.; Qiu, S.; Yin, C. (2019): Biomass estimation in dense tropical forest using multiple information from single-baseline P-band PolInSAR data. In *Remote Sensing of Environment* 221, pp. 489–507. DOI: 10.1016/j.rse.2018.11.027.
- Liao, Z.; He, B.; van Dijk, A. I. J. M.; Bai, X.; Quan, X. (2018): The impacts of spatial baseline on forest canopy height model and digital terrain model retrieval using P-band PolInSAR data. In *Remote Sensing of Environment* 210, pp. 403–421. DOI: 10.1016/j.rse.2018.03.033.
- Lillesand, T. M.; Kiefer, R. W.; Chipman, J. W. (2015): Remote sensing and image interpretation. 7. ed. Hoboken, NJ: Wiley.
- Liu, M.; Popescu, S.; Malambo, L. (2020): Feasibility of burned area mapping based on ICESAT-2 photon counting data. In *Remote Sensing* 12 (1), p. 24. DOI: 10.3390/rs12010024.
- Lohberger, S.; Stängel, M.; Atwood, E. C.; Siegert, F. (2018): Spatial evaluation of Indonesia's 2015 fire-affected area and estimated carbon emissions using Sentinel-1. In *Global Change Biology* 24 (2), pp. 644–654. DOI: 10.1111/gcb.13841.
- Lu, D. (2006): The potential and challenge of remote sensing-based biomass estimation. In *International Journal of Remote Sensing* 27 (7), pp. 1297–1328. DOI: 10.1080/01431160500486732.
- Lu, D.; Batistella, M. (2005): Exploring TM image texture and its relationships with biomass estimation in Rondônia, Brazilian Amazon. In *Acta Amazonica* 35 (2), pp. 249–257.

REFERENCES

- Lu, D.; Batistella, M.; Moran, E. (2005): Satellite estimation of aboveground biomass and impacts of forest stand structure. In *Photogrammetric Engineering & Remote Sensing* 71 (8), pp. 967–974.
- Lu, D.; Chen, Q.; Wang, G.; Liu, L.; Li, G.; Moran, E. (2015): A survey of remote sensing-based aboveground biomass estimation methods in forest ecosystems. In *International Journal of Digital Earth* 9 (1), pp. 63–105. DOI: 10.1080/17538947.2014.990526.
- Luo, H.; Chen, E.; Li, Z.; Cao, C. (2011): Forest above ground biomass estimation methodology based on polarization coherence tomography. In *Journal of Remote Sensing* 6, pp. 1138–1146.
- MacKinnon, K.; Hatta, G.; Halim, H.; Mangalik, A. (2013): The ecology of Kalimantan. Indonesian Borneo. New York: Tuttle Publishing. Available online at <http://gbv.ebib.com/patron/FullRecord.aspx?p=1139313>.
- Makinano-Santillan, M.; Bolastig, C. G.; Santillan, J. R. (2019): Aboveground biomass estimation of mangroves in Siargao Island, Phillippines using Sentinel-1 image. In *The 40th Asian Conference on Remote Sensing*, pp. 1–10.
- Mallet, C.; Bretar, F. (2009): Full-waveform topographic lidar. State-of-the-art. In *ISPRS Journal of Photogrammetry and Remote Sensing* 64 (1), pp. 1–16. DOI: 10.1016/j.isprsjprs.2008.09.007.
- Mascaro, J.; Detto, M.; Asner, G. P.; Muller-Landau, H. C. (2011): Evaluating uncertainty in mapping forest carbon with airborne LiDAR. In *Remote Sensing of Environment* 115 (12), pp. 3770–3774. DOI: 10.1016/j.rse.2011.07.019.
- Matheron, G. (1971): The theory of regionalized variables and its applications. Fontainebleau, Paris: École Nationale Supérieure des Mines (Les Cahiers du Centre de Morphologie Mathématique, 5).
- McRoberts, R. E.; Næsset, E.; Gobakken, T. (2013): Inference for lidar-assisted estimation of forest growing stock volume. In *Remote Sensing of Environment* 128, pp. 268–275. DOI: 10.1016/j.rse.2012.10.007.
- McRoberts, R. E.; Næsset, E.; Gobakken, T.; Bollandsås, O. M. (2015): Indirect and direct estimation of forest biomass change using forest inventory and airborne laser

REFERENCES

- scanning data. In *Remote Sensing of Environment* 164, pp. 36–42. DOI: 10.1016/j.rse.2015.02.018.
- Mermoz, S.; Le Toan, T. (2016): Forest disturbances and regrowth assessment using ALOS PALSAR data from 2007 to 2010 in Vietnam, Cambodia and Lao PDR. In *Remote Sensing* 8 (3), p. 217. DOI: 10.3390/rs8030217.
- Mermoz, S.; Le Toan, T.; Villard, L.; Réjou-Méchain, M.; Seifert-Granzin, J. (2014): Biomass assessment in the Cameroon savanna using ALOS PALSAR data. In *Remote Sensing of Environment* 155, pp. 109–119. DOI: 10.1016/j.rse.2014.01.029.
- Mette, T.; Papathanassiou, K. P.; Hajnsek, I.; Zimmermann, R. (2012): Forest biomass estimation using polarimetric SAR interferometry. In *IGARSS 2012, IEEE Xplore*, pp. 817–819. DOI: 10.1109/IGARSS.2002.1025695.
- Meyer, V.; Saatchi, S. S.; Chave, J.; Dalling, J. W.; Bohlman, S.; Fricker, G. A. et al. (2013): Detecting tropical forest biomass dynamics from repeated airborne lidar measurements. In *Biogeosciences* 10 (8), pp. 5421–5438. DOI: 10.5194/bg-10-5421-2013.
- Mitchard, E. T. A. (2018): The tropical forest carbon cycle and climate change. In *Nature* 559 (7715), pp. 527–534. DOI: 10.1038/s41586-018-0300-2.
- Mitchard, E. T. A.; Saatchi, S. S.; Woodhouse, I. H.; Nangendo, G.; Ribeiro, N. S.; Williams, M. et al. (2009): Using satellite radar backscatter to predict above-ground woody biomass. A consistent relationship across four different African landscapes. In *Geophys. Res. Lett.* 36 (23), p. 409. DOI: 10.1029/2009GL040692.
- Mitchard, E.T.A.; Saatchi, S. S.; Lewis, S. L.; Feldpausch, T. R.; Woodhouse, I. H.; Sonké, B. et al. (2011): Measuring biomass changes due to woody encroachment and deforestation/degradation in a forest–savanna boundary region of central Africa using multi-temporal L-band radar backscatter. In *Remote Sensing of Environment* 115 (11), pp. 2861–2873. DOI: 10.1016/j.rse.2010.02.022.
- Næsset, E.; Gobakken, T.; Solberg, S.; Gregoire, T. G.; Nelson, R.; Ståhl, G.; Weydahl, D. (2011): Model-assisted regional forest biomass estimation using LiDAR and InSAR as auxiliary data. A case study from a boreal forest area. In *Remote Sensing of Environment* 115 (12), pp. 3599–3614. DOI: 10.1016/j.rse.2011.08.021.

REFERENCES

- Narine, L. L.; Popescu, S. C.; Zhou, T.; Srinivasan, S.; Harbeck, K. (2019): Mapping forest aboveground biomass with a simulated ICESat-2 vegetation canopy product and Landsat data. In *Annals of Forest Research* 62 (1), pp. 1–17.
- Neuenschwander, A.; Magruder, L. (2016): The potential impact of vertical sampling uncertainty on ICESat-2/ATLAS terrain and canopy height Retrievals for Multiple Ecosystems. In *Remote Sensing* 8 (12), p. 1039. DOI: 10.3390/rs8121039.
- Neuenschwander, A.; Pitts, K. (2019a): Ice, Cloud, and Land Elevation Satellite 2 (ICESat-2) algorithm theoretical basis document (ATBD) for land - vegetation along-track products (ATL08).
- Neuenschwander, A.; Pitts, K. (2019b): The ATL08 land and vegetation product for the ICESat-2 Mission. In *Remote Sensing of Environment* 221, pp. 247–259. DOI: 10.1016/j.rse.2018.11.005.
- Neumann, M.; Ferro-Famil, L.; Reigber, A. (2010): Estimation of forest structure, ground, and canopy layer characteristics from multibaseline polarimetric interferometric SAR data. In *IEEE Trans. Geosci. Remote Sensing* 48 (3), pp. 1086–1104. DOI: 10.1109/TGRS.2009.2031101.
- Nie, S.; Wang, C.; Zeng, H.; Xi, X.; Li, G. (2017): Above-ground biomass estimation using airborne discrete-return and full-waveform LiDAR data in a coniferous forest. In *Ecological Indicators* 78, pp. 221–228. DOI: 10.1016/j.ecolind.2017.02.045.
- Odipo, V.; Nickless, A.; Berger, C.; Baade, J.; Urbazaev, M.; Walther, C.; Schmillius, C. (2016): Assessment of aboveground woody biomass dynamics using terrestrial laser scanner and L-band ALOS PALSAR data in South African savanna. In *Forests* 7 (12), p. 294. DOI: 10.3390/f7120294.
- Olesk, A.; Praks, J.; Antropov, O.; Zalite, K.; Arumäe, T.; Voormansik, K. (2016): Interferometric SAR coherence models for characterization of hemiboreal forests using TanDEM-X data. In *Remote Sensing* 8 (9), p. 700. DOI: 10.3390/rs8090700.
- Oliver, M. A.; Webster, R. (1990): Kriging: A method of interpolation for geographical information systems. In *International journal of geographical information systems* 4 (3), pp. 313–332. DOI: 10.1080/02693799008941549.

REFERENCES

- Page, S. E.; Banks, C. J.; Rieley, J. O. (2007): Tropical peatlands: distribution, extent and carbon storage - Uncertainties and knowledge gaps. In *Peatlands International 2*, pp. 1–7.
- Page, S. E.; Hooijer, A. (2016): In the line of fire. The peatlands of Southeast Asia. In *Philosophical transactions of the Royal Society of London. Series B, Biological sciences* 371 (1696). DOI: 10.1098/rstb.2015.0176.
- Page, S. E.; Hoscilo, A.; Tansey, K.; Siegert, F.; Limin, S.; Rieley, J. O.; Langner, A. (2009): Tropical fire ecology. Tropical peatland fires in Southeast Asia. Berlin, Heidelberg: Springer Praxis Books.
- Page, S. E.; Rieley, J. O.; Banks, C. J. (2011): Global and regional importance of the tropical peatland carbon pool. In *Global Change Biology* 17 (2), pp. 798–818. DOI: 10.1111/j.1365-2486.2010.02279.x.
- Page, S. E.; Rieley, J. O.; Wüst, R. (2006): Lowland tropical peatlands of Southeast Asia. In *Peatlands: Evolution and Records of Environmental and Climate Changes 9*, pp. 145–172. DOI: 10.1016/S0928-2025(06)09007-9.
- Pagel, M. D.; Harvey, P. H.; Godfrey, H. C. J. (1991): Species-abundance, biomass, and resource-use distributions. In *The American Naturalist* 138 (4), pp. 836–850.
- Palamba, P.; Ramadhan, M. L.; Pamitran, A. S.; Prayogo, G.; Kosasih, E. A.; Nugroho, Y. S. (2018): Drying kinetics of Indonesian peat. In *IJTech* 9 (5), p. 1006. DOI: 10.14716/ijtech.v9i5.805.
- Pandit, S.; Tsuyuki, S.; Dube, T. (2018): Estimating above-ground biomass in sub-tropical buffer zone community forests, Nepal, using Sentinel 2 data. In *Remote Sensing* 10 (4), p. 601. DOI: 10.3390/rs10040601.
- Paoli, G. D.; Wells, P. E.; Meijaard, E.; Struebig, M. J.; Marshall, A. M.; Obidzinski, K. et al. (2010): Biodiversity conservation in the REDD. In *Carbon balance and management* 5 (7), pp. 1–9. DOI: 10.1186/1750-0680-5-7.
- Papathanassiou, K. P.; Cloude, S. R. (2001): Single-baseline polarimetric SAR interferometry - Geoscience and Remote Sensing, IEEE Transactions on. In *IEEE Trans. Geosci. Remote Sensing* 39 (11), pp. 2352–2363. DOI: 10.1109/36.964971.

REFERENCES

- Parish, F.; Sirin, A.; Charman, D.; Joosten, H.; Minayeva, T.; Silvius, M.; Stringer, L. (2008): Assessment on peatlands, biodiversity, and climate change. Kuala Lumpur: Global Environment Centre & Wetlands International Wageningen.
- Pearson, T. R. H.; Brown, S.; Murray, L.; Sidman, G. (2017): Greenhouse gas emissions from tropical forest degradation. An underestimated source. In *Carbon balance and management* 12 (1), p. 3. DOI: 10.1186/s13021-017-0072-2.
- Pereira, F. R. de Souza; Kampel, M.; Gomes Soares M. L.; Estrada, G.; Bentz, C.; Vincent, G. (2018): Reducing uncertainty in mapping of mangrove aboveground biomass using airborne discrete return lidar data. In *Remote Sensing* 10 (4), p. 637. DOI: 10.3390/rs10040637.
- Peroni Venancio, L.; Chartuni Mantovani, E.; do Amaral, C. H.; Usher Neale, C. M.; Zution Gonçalves, I.; Filgueiras, R.; Coelho Eugenio, F. (2020): Potential of using spectral vegetation indices for corn green biomass estimation based on their relationship with the photosynthetic vegetation sub-pixel fraction. In *Agricultural Water Management* 236, p. 106155. DOI: 10.1016/j.agwat.2020.106155.
- Phua, M.-H.; Johari, S. A.; Wong, O. C.; Ioki, K.; Mahali, M.; Nilus, R. et al. (2017): Synergistic use of Landsat 8 OLI image and airborne LiDAR data for above-ground biomass estimation in tropical lowland rainforests. In *Forest Ecology and Management* 406, pp. 163–171. DOI: 10.1016/j.foreco.2017.10.007.
- Posa, M. R. C.; Wijedasa, L. S.; Corlett, R. T. (2011): Biodiversity and conservation of tropical peat swamp forests. In *BioScience* 61 (1), pp. 49–57. DOI: 10.1525/bio.2011.61.1.10.
- Qi Z.; Linlin G.; Zheyuan D. (2019): A modified RMoG model for forest height inversion using L-band repeat-pass Pol-InSAR data. In *IEEE International Geoscience and Remote Sensing Symposium*, pp. 3217–3220.
- Richards, J. A. (2009): Signals and communication technology - remote sensing with imaging radar. Heidelberg: Springer.
- Rodríguez-Veiga, P.; Quegan, S.; Carreiras, J.; Persson, H. J.; Fransson, J. E. S.; Hoscilo, A. et al. (2019): Forest biomass retrieval approaches from earth observation in

REFERENCES

- different biomes. In *International Journal of Applied Earth Observation and Geoinformation* 77, pp. 53–68. DOI: 10.1016/j.jag.2018.12.008.
- Saatchi, S.; Halligan, K.; Despain, D. G.; Crabtree, R. L. (2007): Estimation of forest fuel load from radar remote sensing. In *IEEE Trans. Geosci. Remote Sensing* 45 (6), pp. 1726–1740. DOI: 10.1109/TGRS.2006.887002.
- Saatchi, S.; Ramachandran, N.; Tebaldini, S.; Quegan, S.; Le Toan, T.; Papathanassiou, K. P. et al. (2019): Estimation of tropical forest structure and biomass from airborne P-band backscatter and TomoSAR Measurements. IGARSS 2019. In *IEEE International Geoscience and Remote Sensing Symposium*, pp. 6007–6009. DOI: 10.1109/igarss.2019.8898797.
- Saatchi, S. S.; Harris, N. L.; Brown, S.; Lefsky, M.; Mitchard, E. T. A.; Salas, W. et al. (2011): Benchmark map of forest carbon stocks in tropical regions across three continents. In *Proceedings of the National Academy of Sciences of the United States of America* 108 (24), pp. 9899–9904. DOI: 10.1073/pnas.1019576108.
- Sandberg, G.; Ulander, L. M. H.; Fransson, J. E. S.; Holmgren, J.; Le Toan, T. (2011): L- and P-band backscatter intensity for biomass retrieval in hemiboreal forest. In *Remote Sensing of Environment* 115 (11), pp. 2874–2886. DOI: 10.1016/j.rse.2010.03.018.
- Sandberg, G.; Ulander, L. M. H.; Wallerman, J.; Fransson, J. E. S. (2014): Measurements of forest biomass change using P-band synthetic aperture radar backscatter. In *IEEE Trans. Geosci. Remote Sensing* 52 (10), pp. 6047–6061. DOI: 10.1109/TGRS.2013.2294684.
- Santoro, M.; Wegmüller, U.; Askne, J. (2018): Forest stem volume estimation using C-band interferometric SAR coherence data of the ERS-1 mission 3-days repeat-interval phase. In *Remote Sensing of Environment* 216, pp. 684–696. DOI: 10.1016/j.rse.2018.07.032.
- Santos, J.; Freitas, C. C.; Araujo, L. S.; Dutra, V. L.; Mura, J. C.; Gama, F. F. et al. (2003): Airborne P-band SAR applied to the aboveground biomass studies in the Brazilian tropical rainforest. In *Remote Sensing of Environment* 87 (4), pp. 482–493. DOI: 10.1016/j.rse.2002.12.001.

REFERENCES

- Sarker, L. R.; Nichol, J. E. (2011): Improved forest biomass estimates using ALOS AVNIR-2 texture indices. In *Remote Sensing of Environment* 115 (4), pp. 968–977. DOI: 10.1016/j.rse.2010.11.010.
- Schlund, M.; Erasmi, S.; Scipal, K. (2019): Comparison of aboveground biomass estimation from InSAR and LiDAR canopy height models in tropical forests. In *IEEE Geosci. Remote Sensing Lett.*, pp. 1–5. DOI: 10.1109/LGRS.2019.2925901.
- Schlund, M.; Poncet, F.; Kuntz, S.; Schmullius, C.; Hoekman, D. H. (2014): TanDEM-X data for aboveground biomass retrieval in a tropical peat swamp forest. In *Remote Sensing of Environment* 158, pp. 255–266. DOI: 10.1016/j.rse.2014.11.016.
- Schowengerdt, R. A. (2007): Remote sensing: models and methods for image processing. 3rd ed. New York: Elsevier.
- Setyawati, W.; Suwarsono (2018): Carbon emission from peat fire in 2015. In *IOP Conf. Ser.: Earth Environ. Sci.* 166, p. 12041. DOI: 10.1088/1755-1315/166/1/012041.
- Simard, M.; Denbina, M. (2018): An assessment of temporal decorrelation compensation methods for forest canopy height estimation using airborne L-band same-day repeat-pass polarimetric SAR interferometry. In *IEEE J. Sel. Top. Appl. Earth Observations Remote Sensing* 11 (1), pp. 95–111. DOI: 10.1109/JSTARS.2017.2761338.
- Singh, M.; Malhi, Y.; Bhagwat, S. (2014): Evaluating land use and aboveground biomass dynamics in an oil palm–dominated landscape in Borneo using optical remote sensing. In *Journal of Applied Remote Sensing* 8 (1). DOI: 10.1117/1.JRS.8.083695.
- Sinha, S.; Jeganathan, C.; Sharma, L. K.; Nathawat, M. S. (2015): A review of radar remote sensing for biomass estimation. In *Int. J. Environ. Sci. Technol.* 12 (5), pp. 1779–1792. DOI: 10.1007/s13762-015-0750-0.
- Soja, M. J.; Askne, J. I. H.; Ulander, L. M. H. (2017): Estimation of boreal forest properties from TanDEM-X data using inversion of the Interferometric Water Cloud Model. In *IEEE Geosci. Remote Sensing Lett.* 14 (7), pp. 997–1001. DOI: 10.1109/LGRS.2017.2691355.

REFERENCES

- Soja, M. J.; Persson, H.; Ulander, L. H. M. (2015): Estimation of forest height and canopy density from a single InSAR correlation coefficient. In *IEEE Geosci. Remote Sensing Lett.* 12 (3), pp. 646–650. DOI: 10.1109/LGRS.2014.2354551.
- Soja, M. J.; Sandberg, G.; Ulander, L. M. H. (2013): Regression-based retrieval of boreal forest biomass in sloping terrain using P-band SAR backscatter intensity data. In *IEEE Trans. Geosci. Remote Sensing* 51 (5), pp. 2646–2665. DOI: 10.1109/TGRS.2012.2219538.
- Solberg, S.; Hansen, E. H.; Gobakken, T.; Næsset, E.; Zahabu, E. (2017): Biomass and InSAR height relationship in a dense tropical forest. In *Remote Sensing of Environment* 192, pp. 166–175. DOI: 10.1016/j.rse.2017.02.010.
- Sousa, A. M. O.; Gonçalves, A. C.; Mesquita, P.; Marques da Silva, J. R. (2015): Biomass estimation with high resolution satellite images. A case study of *Quercus rotundifolia*. In *ISPRS Journal of Photogrammetry and Remote Sensing* 101, pp. 69–79. DOI: 10.1016/j.isprsjprs.2014.12.004.
- Sportouche, H.; Roueff, A.; Dubois-Fernandez, P. C. (2018): Precision of vegetation height estimation using the dual-baseline PolInSAR system and RVoG model with temporal decorrelation. In *IEEE Trans. Geosci. Remote Sensing* 56 (7), pp. 4126–4137. DOI: 10.1109/TGRS.2018.2826054.
- Steininger, M. K. (2010): Satellite estimation of tropical secondary forest above-ground biomass. Data from Brazil and Bolivia. In *International Journal of Remote Sensing* 21 (6-7), pp. 1139–1157. DOI: 10.1080/014311600210119.
- Stelmaszczuk-Górska, M.; Rodriguez-Veiga, P.; Ackermann, N.; Thiel, C.; Balzter, H.; Schmullius, C. (2016): Non-parametric retrieval of aboveground biomass in Siberian boreal forests with ALOS PALSAR Interferometric Coherence and Backscatter Intensity. In *J. Imaging* 2 (1), p. 1. DOI: 10.3390/jimaging2010001.
- Sun, X.; Song, H. J. (2015): New improved algorithm based on three-stage inversion procedure of forest height. In *International Symposium on Distributed Computing and Applications for Business, Engineering and Science; DCABES 2015*, pp. 419–422.
- Takahashi, A.; Kumagai, T.; Kanamori, H.; Fujinami, H.; Hiyama, T.; Hara, M. (2017): Impact of tropical deforestation and forest degradation on precipitation over Borneo

REFERENCES

- Island. In *Journal of Hydrometeorology* 18 (11), pp. 2907–2922. DOI: 10.1175/JHM-D-17-0008.1.
- Thapa, R. B.; Watanabe, M.; Motohka, T.; Shimada, M. (2015): Potential of high-resolution ALOS–PALSAR mosaic texture for aboveground forest carbon tracking in tropical region. In *Remote Sensing of Environment* 160, pp. 122–133. DOI: 10.1016/j.rse.2015.01.007.
- The World Bank (2015): Indonesia economic quarterly. Reforming amid uncertainty. The World Bank.
- Thenkabail, P. S.; Lyon, J. G.; Huete, A. (2012): Hyperspectral remote sensing of vegetation. Boca Raton, Fla.: CRC Press.
- Thiel, C.; Schmullius, C. (2013): Investigating the impact of freezing on the ALOS PALSAR InSAR phase over Siberian forests. In *Remote Sensing Letters* 4 (9), pp. 900–909. DOI: 10.1080/2150704X.2013.810350.
- Thiel, C.; Schmullius, C. (2016): The potential of ALOS PALSAR backscatter and InSAR coherence for forest growing stock volume estimation in Central Siberia. In *Remote Sensing of Environment* 173, pp. 258–273. DOI: 10.1016/j.rse.2015.10.030.
- Thoma, D. P.; Moran, M. S.; Bryant, R.; Rahman, M.; Holifield-Collins, C. D.; Skirvin, S. et al. (2006): Comparison of four models to determine surface soil moisture from C-band radar imagery in a sparsely vegetated semiarid landscape. In *Water Resour. Res.* 42 (1), p. 4325. DOI: 10.1029/2004WR003905.
- Tian, J.; Le W.; Li, X.; Yin, D.; Gong, H.; Nie, S. et al. (2019): Canopy height layering biomass estimation model (CHL-BEM) with full-waveform LiDAR. In *Remote Sensing* 11 (12), p. 1446. DOI: 10.3390/rs11121446.
- United Nations Environment Programme; Global Environment Facility; Asia Pacific Network for Global Change Research; Global Environment Centre (Malaysia); Wetlands International (2008): Assessment on peatlands, biodiversity, and climate change. Kuala Lumpur: Global Environment Centre & Wetlands International Wageningen.
- Urbazaev, M.; Thiel, C.; Cremer, F.; Dubayah, R.; Migliavacca, M.; Reichstein, M.; Schmullius, C. (2018): Estimation of forest aboveground biomass and uncertainties by

REFERENCES

integration of field measurements, airborne LiDAR, and SAR and optical satellite data in Mexico. In *Carbon balance and management* 13 (1), p. 5. DOI: 10.1186/s13021-018-0093-5.

Urbazaev, M.; Thiel, C.; Mathieu, R.; Naidoo, L.; Levick, S. R.; Smit, I. P. J. et al. (2015): Assessment of the mapping of fractional woody cover in southern African savannas using multi-temporal and polarimetric ALOS PALSAR L-band images. In *Remote Sensing of Environment* 166, pp. 138–153. DOI: 10.1016/j.rse.2015.06.013.

van der Werf, G. R.; Morton, D. C.; DeFries, R. S.; Olivier, J. G. J.; Kasibhatla, P. S.; Jackson, R. B. et al. (2009): CO₂ emissions from forest loss. In *Nature Geosci* 2 (11), pp. 737–738. DOI: 10.1038/ngeo671.

Wan-Mohd-Jaafar, W. S.; Woodhouse, I. H.; Silva, C. A.; Omar, H.; Hudak, A. T. (2017): Modelling individual tree aboveground biomass using discrete return LiDAR in lowland dipterocarp forest of Malaysia. In *JTFS* 29 (4), pp. 465–484. DOI: 10.26525/jtfs2017.29.4.465484.

Warren, M.; Hergoualc'h, K.; Kauffman, J. B.; Murdiyarso, D.; Kolka, R. (2017): An appraisal of Indonesia's immense peat carbon stock using national peatland maps. Uncertainties and potential losses from conversion. In *Carbon balance and management* 12 (1), p. 12. DOI: 10.1186/s13021-017-0080-2.

Wijaya, A. (2009): Evaluation of ALOS Palsar mosaic data for estimating stem volume and biomass. A case study from tropical rainforest of Central Indonesia. In *Jurnal Geografi* (2), pp. 14–21, checked on 12/19/2017.

Wijaya, A.; Liesenberg, V.; Susanti, A.; Karyanto, O.; Verchot, L. V. (2015): Estimation of biomass carbon stocks over peat swamp forests using multi-temporal and multi-polarizations SAR data. In *Int. Arch. Photogramm. Remote Sens. Spatial Inf. Sci.* XL-7/W3, pp. 551–556. DOI: 10.5194/isprsarchives-XL-7-W3-551-2015.

Wilhelm, S.; Hüttich, C.; Korets, M.; Schnullius, C. (2014): Large area mapping of boreal growing stock volume on an annual and multi-temporal level using PALSAR L-band backscatter mosaics. In *Forests* 5 (8), pp. 1999–2015. DOI: 10.3390/f5081999.

REFERENCES

Wojciech, M. (2018): Kriging method optimization for the process of DTM creation based on huge data sets obtained from MBESs. In *Geosciences* 8 (12), p. 433. DOI: 10.3390/geosciences8120433.

World Wide Fund for Nature Germany (2009): Die Torfmoorwälder von Sebangau. Besondere Kohlenstoffspeicher und Lebensräume. Project Information Brochure. Edited by WWF Germany. Frankfurt/Main. Available online at https://mobil.wwf.de/fileadmin/fm-wwf/Publikationen-PDF/Kampagne_Projektblatt_Sebangau.pdf.

Yan, E.; Lin, H.; Wang, G.; Sun, H. (2015): Improvement of forest carbon estimation by integration of regression modeling and spectral unmixing of Landsat data. In *IEEE Geosci. Remote Sensing Lett.* 12 (9), pp. 2003–2007. DOI: 10.1109/LGRS.2015.2451091.

Yilmaz, M.; Uysal, M. (2017): Comparing uniform and random data reduction methods for DTM accuracy. In *International Journal of Engineering and Geosciences* 2 (1), pp. 9–16. DOI: 10.26833/ijeg.286003.

Yu, Y.; Saatchi, S. (2016): Sensitivity of L-band SAR backscatter to aboveground biomass of global forests. In *Remote Sensing* 8 (6), p. 522. DOI: 10.3390/rs8060522.

Yule, C. M. (2010): Loss of biodiversity and ecosystem functioning in Indo-Malayan peat swamp forests. In *Biodivers Conserv* 19 (2), pp. 393–409. DOI: 10.1007/s10531-008-9510-5.

Yule, C. M.; Lim, Y. Y.; Lim, T. Y. (2018): Recycling of phenolic compounds in Borneo's tropical peat swamp forests. In *Carbon balance and management* 13 (1), p. 3. DOI: 10.1186/s13021-018-0092-6.

Zhang, H.; Wang, C.; Zhu, J.; Fu, H.; Xie, Q.; Shen, P. (2018): Forest above-ground biomass estimation using single-baseline polarization coherence tomography with P-band PolInSAR data. In *Forests* 9 (4), p. 163. DOI: 10.3390/f9040163.

Zhang, L.; Duan, B.; Zou, B. (2017): Research in inversion models for forest height estimation using polarimetric SAR interferometry. In *Int. Arch. Photogramm. Remote Sens. Spatial Inf. Sci.* XLII-2/W7, pp. 659–663. DOI: 10.5194/isprs-archives-XLII-2-W7-659-2017.

REFERENCES

Zhao, P.; Lu, D.; Wang, G.; Wu, C.; Huang, Y.; Yu, S. (2016): Examining spectral reflectance saturation in Landsat imagery and corresponding solutions to improve forest aboveground biomass estimation. In *Remote Sensing* 8 (6), p. 469. DOI: 10.3390/rs8060469.

STATEMENT AND DECLARATION OF HONOR

Eidesstattliche Erklärung

Ich versichere hiermit an Eides statt, dass die vorgelegte Dissertation von mir selbständig und ohne unerlaubte Hilfe angefertigt ist.

München, den.....5.6.2020.....Anna Luisa Berninger.....

(Unterschrift)

Erklärung

Hiermit erkläre ich, *

- dass die Dissertation nicht ganz oder in wesentlichen Teilen einer anderen Prüfungskommission vorgelegt worden ist.
- dass ich mich anderweitig einer Doktorprüfung ohne Erfolg **nicht** unterzogen habe.
- ~~dass ich mich mit Erfolg der Doktorprüfung im Hauptfach~~
~~und in den Nebenfächern~~
~~..... bei der Fakultät für~~
~~..... der~~
~~(Hochschule/Universität) unterzogen habe.~~
- ~~dass ich ohne Erfolg versucht habe, eine Dissertation einzureichen oder mich der Doktorprüfung zu unterziehen.~~

München, den.....5.6.2020.....Anna Luisa Berninger.....

(Unterschrift)

*) Nichtzutreffendes streichen

CURRICULUM VITAE

Personal Information

Name Anna Luisa Berninger
email berninger@rssgmbh.de

Education

- 2017 - 2020 Doctoral student at the Ludwig-Maximilians-University (LMU), Munich, and research associate and project engineer at the Remote Sensing Solutions GmbH, Munich,
Doctoral thesis title: “*Biomass estimation in tropical forests of Indonesia using active remote sensing systems*”
- 2013 - 2016 Studies of Geoinformatics and Remote Sensing at the Friedrich-Schiller-University Jena,
Graduation: Master of Science,
Master thesis title: “*Spectral unmixing of Landsat 8 OLI data with the use of spectrometer measurements in the Siberian Tundra*”
- 2010 - 2013 Studies of Geography at the Friedrich-Schiller-University Jena,
Graduation: Bachelor of Science,
Bachelor thesis title: “*Daily hydrological modeling with the hydrological model JAMS/J2000 in the catchment of the upper Cueba River in Angola*”

Participation in courses and summer schools:

SAR-EDU Summer School 2018: Angewandte Radarfernerkundung, 24 - 28 September 2018 at Friedrich-Schiller-Universität Jena, Jena, Germany.

SPLIT SPatial LITeracy Remote Sensing Professional Programme 2018, 11 - 16 June 2018 at Czech University of Life Sciences Prague (CULS), Prague, Czech Republic.

ESA 7th Advanced Trainings Course on Land Remote Sensing 2017, 4 - 9 September 2017 at Szent István University Gödöllő, Hungary.

Echoes in Space - Introduction to Radar Remote Sensing by EO College and ESA, date of certificate 26th November 2017.

Publications in peer-reviewed journals:

Migliavacca, M., Priego, O.-P., Rossini, M., El-Madany, T. S., Moreno, G., van der Tol, C., Rascher, U., **Berninger, A.**, Bessenbacher, V., Burkart, A., Carrara, A., Fava, F., Guan, J. H., Hammer, T.-W., Henkel, K., Juarez-Alcalde, E., Julitta, T., Kolle, O., Martin, M. P., Musavi, T., Pacheco-Labrador, J., Perez-Burgueno, A., Wutzler, T., Zaehle, S., Reichstein, M. (2017): Plant functional traits and canopy structure control the relationship between photosynthetic CO₂ uptake and far-red sun-induced fluorescence in a Mediterranean grassland under different nutrient availability. *New Phytologist* 214:1078–1091.

Berninger, A., Lohberger, S., Stängel, M. & F. Siegert (2018) SAR-based Estimation of Above-Ground Biomass and Its Changes in Tropical Forests of Kalimantan using L-Band and C-Band. *Remote Sensing*, 10(6), 831-852.

Rodríguez-Veiga, P., Quegan, S., Carreiras, J. & **A. Berninger** et al. (2019) Forest Biomass Retrieval Approaches from Earth Observation in different Biomes. *International Journal of Applied Earth Observations and Geoinformation*, 77, 53-68.

Berninger, A., Lohberger, S. & F. Siegert (2019) Forest Height and Above-Ground Biomass retrieval in Tropical Forests Using Multi-Pass X- and C-Band Pol-InSAR Data. *Remote Sensing*, 11(18), 2105.

Berninger, A. & F. Siegert (2020): The potential of ICESat-2 to identify carbon-rich peatlands in Indonesia. *Remote Sensing*. 12(24), 4175.

Impact factor of the journals:

Journal	5-year impact factor	2018	2019
Remote Sensing	5.001 (2019)	4.118	4.509
According to the <i>Journal Citation Reports 2019</i> , the journal has a 2016 impact factor of 4.118, ranking it 7 th out of 29 journals in the category "Remote Sensing".			
International Journal of Applied Earth Observations and Geoinformation	5.194 (2018)	4.846	4.846

Oral presentations and posters:

Berninger, A., Lohberger, S. & F. Siegert (2019) Canopy Height and Above-Ground Biomass Retrieval in Tropical Forests Using Multi-Pass X- And C-Band Pol-InSAR Data. *TerraSAR-X / TanDEM-X Science Team Meeting 21st – 24th October 2019 at DLR Oberpfaffenhofen, Germany.*

Berninger, A., Atwood, E. C. & F. Siegert (2019) Detecting Fire Events in West Kalimantan`s Peatlands Using a Combination of Sentinel-1, -2 and -3. *ESA Living Planet Symposium 13 – 17th May 2019 at Milano, Italy.*

Berninger, A., Lohberger, S. & F. Siegert (2018) Biomasseschätzung in tropischen Regenwäldern mittels SAR-Daten. *DLR Symposium "Neue Perspektiven der Erdbeobachtung" 26th June 2018 at Collogne, Germany.*

Berninger, A., Lohberger, S. & F. Siegert (2018) SAR-Based Estimation of Above-Ground Biomass and its Changes in Tropical Forests of Kalimantan Using X- and C-Band. *SPLIT SPatial LITeracy Remote Sensing Professional Programme 2018, 11 - 16 June 2018 at Czech University of Life Sciences Prague (CULS), Prague, Czech Republic.*

Berninger, A., Lohberger, S., Stängel, M. & F. Siegert (2018) Indonesia – Kalimantan Regional Biomass Estimation - Final Results. *GlobBiomass Final Team Meeting 14th December 2017 at ESRIN Frascati, Italy.*

Berninger, A., Lohberger, S. & F. Siegert (2017) Forest Height and Above-Ground Biomass retrieval in Tropical Forests Using Multi-Pass X- and C-Band Pol-InSAR Data. *PolInSAR4AGB Team Meeting 11th November 2017 at RSS Munich, Germany.*

Berninger, A., Lohberger, S., Stängel, M. & F. Siegert (2017) Indonesia – Kalimantan Regional Biomass Estimation Epoch 2015. *Globbiomass Team Meeting 13th September 2017 at Food and Agriculture Organization of the United Nations Rome, Italy.*

Berninger, A., Lohberger, S. & F. Siegert (2017) Tropical Forest and Above-Ground Biomass Estimation in Indonesia with the Use of Pol-InSAR Data – First Results. *ESA 7th Advanced Trainings Course on Land Remote Sensing 2017, 4th - 9th September 2017 at Szent István University Gödöllő, Hungary.*